PHASE CONJUGATE OPTICS:

On the Theory, Observation, and Utilization of Temporally-Reversed Wavefronts as Generated Via Nonlinear Optical Parametric Interactions

Thesis by
David M. Pepper

In Partial Fulfillment of the Requirements

for the Degree of

Doctor of Philosophy

California Institute of Technology

Pasadena, California

1980

(Submitted 9 January 1980)

To my dear father and brother --

In memory of my loving mother ...

Special dedications to

-- *the late Darrell Drickey; for his kindness, support, and guidance ...*

-- *the late Abe Finkelstein; a dear, kind, and loving human being ...*

Thus saith the Lord:

Let not the wise man glory in his wisdom,
Neither let the mighty man glory in his might,
Let not the rich man glory in his riches ...

-- Jeremiah IX, 22

כֹּה־אָמַר יְהוָה׃

אַל־יִתְהַלֵּל חָכָם בְּחָכְמָתוֹ
וְאַל־יִתְהַלֵּל הַגִּבּוֹר בִּגְבוּרָתוֹ
אַל־יִתְהַלֵּל עָשִׁיר בְּעָשְׁרוֹ׃

ירמיה ט

ACKNOWLEDGMENTS

I must say that the last five years have truly been a most rewarding experience for me at Caltech, and especially, being part of the Quantum Electronics group. With all my sincere gratitude and appreciation, I thank my thesis advisor, Professor Amnon Yariv, for his excellent guidance, teachings, and insights that have enabled me to reach this plateau in my academic life. I extend thanks to Dr. Dan Fekete for his kind assistance and expertise during my research efforts. I further acknowledge the fruitful and enlightening interactions with what I consider to be a most enthusiastic and creative group of fellow students, in particular Pochi Yeh and John AuYeung. Thanks also go to Desmond Armstrong and Larry Begay for their technical expertise. Special thanks go to Ruth Stratton for her excellent and meticulous typing of this manuscript as well as past publications.

I would also like to express my appreciation to Professor R. P. Feynman and Professor L. G. DeShazer (of USC) for helpful discussions.

I am very grateful and thankful for the encouragement, kindness and support extended to me by my advisors that I interacted with during my undergraduate studies at UCLA. In particular, I am appreciative of the relationship that I maintained with Professor Charles D. Buchanan and (the late) Professor Darrell J. Drickey.

I am further grateful for the fruitful interactions, technical expertise, and continuous support afforded by the technical staff of the Hughes Research Laboratories. Special thanks go to Drs. George Smith, Art Chester, Richard L. Abrams, and Charles Asawa of the Labs; and Dr. Doug Tanimoto of Hughes, Culver City, for his early support of my interest in quantum electronics.

The financial and academic support granted to me through the Hughes Masters and Doctoral Fellowship Programs are most appreciated. My participation in these programs has played a significant role in my maturing as a physicist. The financial assistance of the Army Research Office, Durham, North Carolina, the National Science Foundation, and of Caltech is gratefully acknowledged.

Finally, to my dearest friends and family go my most sincere thanks. Their constant support, encouragement, love and kindness are most deeply appreciated. Special thanks go to Dee Dee Stewart, Denis Pomeranc, Gary Reiter, Ira Shulman, William Tenenblatt, Rob Drezner, and Lazlo Willinger. The cherished support, guidance and unity provided by my loving parents and dear brother have made my experience a most meaningful one. All my love and appreciation are extended to all. Lastly, in all sincerity, I am proud of myself and my accomplishments; may I continue to grow, learn, love, mature and experience.

ABSTRACT

This thesis describes theoretical and experimental aspects as well as potential applications in the field of coherent optics known as Phase Conjugate Optics (PCO). By utilizing nonlinear optical techniques, real-time phase or wavefront reversal of an arbitrary incident electromagnetic field can be realized. The nonlinear optical interaction gives rise to what is referred to as the "phase conjugate replica" (of the incident monochromatic wave) by performing the operation of complex conjugation upon the incident wave's complex spatial amplitude in real time. This conjugate wave, which is also designated as being a "time-reversed" wavefront, has the property of exactly retracing the path of the incident field. The ability of the conjugate wave to correct for inhomogeneous linear and nonlinear (intensity-dependent) phase aberrations as well as polarization distortions is proved. In particular, the theory of a degenerate four-wave nonlinear optical interaction as providing for the phase conjugator is presented. The effects of linear and nonlinear losses upon this interaction are discussed. The quantum mechanical origin of the third order nonlinear optical susceptibility responsible for the four-wave mixing process is analyzed for both single- and two-photon allowed transitions in an atomic (or molecular) system. The analogies of four-wave mixing with that of real-time holography are discussed. The theory of phase conjugation via four-wave mixing in optical waveguides is presented.

Several of the above characteristics of conjugate fields are verified experimentally where phase conjugate fields via degenerate four-wave

mixing were observed both in the bulk and in waveguide geometries, using carbon disulfide as the nonlinear medium. Amplified time-reversed wavefront generation as well as a mirrorless optical parametric mode of oscillation have been observed, both in agreement with theoretical predictions.

Potential applications of PCO are discussed in three different regimes: spatial-frequency, temporal-frequency, and spatial/temporal frequency domains. In the first category, the ability of PCO to correct for image modal dispersion in optical waveguides as well as the use of PCO to perform real-time coherent image processing and nonlinear microscopy is discussed. Temporal-frequency domain applications of PCO to be analyzed include the use of a nearly degenerate four-wave mixing process as a narrowband, wide field-of-view optical filter, capable of an amplified bandpass. The ability of a PCO interaction to renarrow (transform limited) optical pulses which have been temporally spread due to propagation through (group velocity) dispersive channels is analyzed. A potential application of PCO in the field of nonlinear laser spectroscopy is presented. Specifically, the scattering of a probe photon off a two-photon coherent state (created in a three-level atomic system) is shown to yield a conjugate replica. This conjugate replica is capable of providing sub-Doppler width resolution of the two-photon resonance. Further, in the transient regime, the optical free-induction decay of the conjugate wave is capable of yielding detailed spectral features of the three-level system such as the anharmonic contribution to a (nearly) harmonic potential. This technique, performed in the time domain, is known as α-beat spectroscopy.

Finally, a detailed theoretical and experimental study is presented of a laser resonator in which one (or both) of the mirror(s) comprising the optical cavity is replaced by a phase conjugate mirror (PCM). This novel resonator, which is termed a phase conjugate resonator (PCR), combines many of the spatial- and temporal-frequency aspects of PCO interactions discussed above. The stability criterion, transverse and longitudinal mode spectra, and the PCR output energy, as well as the frequency locking features of the laser modes to the PCM are discussed.

TABLE OF CONTENTS

Chapter I

INTRODUCTION

1.1 General Background

In recent years, a new application area has emerged in the field of quantum electronics, and specifically in the subfield of coherent optics, called "phase conjugate optics." This term has been accepted in the literature to describe a class of nonlinear optical interactions that yield phase conjugate, or "time-reversed" replicas of given (monochromatic) electromagnetic fields. These two terms have been used synonymously in the literature and are in fact formally equivalent in the present context. The phase conjugate replica of an electromagnetic field is, by definition, a second field whose wavefronts at each point in space propagate exactly in the reverse direction relative to that of the original wave. Thus, this backward-going wave retraces the path or trajectory of the original field, and therefore evolves in what one may describe as a "time-reversed" sense. As an example, the conjugate replica of a diverging spherical wave from a given source would be a converging spherical wave that would propagate essentially "backward" to the initial source.

Historically, the requirement for a device that can generate such time-reversed wavefronts emerged in the fields of radar and optics. There was a need to overcome phase distortions that transmitted signals acquired as a result of propagation through aberrating media, for example, the atmosphere. It was recognized that if one can generate a new field whose phase fronts are reversed in sign at each point in space, this new field can now essentially "unravel" the initial distortions as it propagates back through the same aberrating medium.

One device utilized to achieve this is called a "phased array" [1-3]. The phased array consists of an ensemble of (dipole) radiators whose relative phases can be determined externally. Due to the finite number of such radiators (assume N such dipoles), the number of resolution elements, or equivalently, the total spatial information handling capacity of the system, is therefore restricted to $\sim$ N. Since each such element requires its own electronic network, practical devices can easily become expensive and bulky, with restrictive bandwidths, or response times. Such phased arrays have been also employed in the optical regime, with the term "adaptive optics" or "coherent optical adaptive techniques" (COAT) used to categorize the field [4]. These adaptive optics schemes have been recently applied to such diverse fields as laser communications systems, and high power lasers. The COAT systems, which do not use phase conjugation in a formal sense, have the capability of operating in real time, being limited by the bandwidth of the system (which decreases with increasing N).

As a second technique useful in correcting or compensating for optical propagation or imaging through phase distorting media, the optics community has exploited the field of holography [5].

There are well-known techniques by which one can generate what has been called a pseudo-scopic or conjugate field by merely "reconstructing" a hologram with the reference (plane) wave illuminating the hologram from the side opposite to where the original reference wave propagated during formation of the hologram. This results in a diffracted wave that essentially retraces the path of the initial object beam [6]. Drawbacks

of this scheme lie mainly in the fact that it is inherently a multi-step process; that is, one must first construct the hologram, develop the emulsion, then lastly reconstruction follows. Consequently, the successful application of this technique requires that the distorting or aberrating medium be stationary during the entire process.

An additional, less major, problem is the finite number of resolution elements which depends upon the specific film (or thermoplastic) chosen. Finally, since the diffraction efficiency never exceeds 100%, the holographic scheme output intensity is limited.

Another technique recently considered by which backward-going rays can be generated is through the use of an array of retroreflectors, or corner cubes [7,8]. This scheme gives rise to what has been defined to be "approximate phase conjugation" in that a truly time-reversed replica of an input field is not generated in all cases. This is true since the corner cube scheme only works on odd terms in a power series that describes the phase fronts of the incoming wave. In addition, there can be undesirable diffractive effects due to the finite size of each individual retroreflector element.

A further technique is one which involves the generation of phase conjugate wavefronts via nonlinear optical interactions. This class of interactions will be discussed in the next three sections, and constitute the subject matter of the remainder of this work.

1.2 Phase Conjugate Optics

As mentioned in the last section, there exists a coherent optical technique by which real-time processing of electromagnetic fields can

be performed. Specifically, the phase conjugate (or time-reversed) replica of electromagnetic fields may be realized in real time by the use of nonlinear optical interactions. The branch of optics which deals with the generation and utilization of such phase conjugated fields is known as Phase Conjugate Optics (PCO). The major distinguishing features of PCO interactions relative to the above mentioned techniques (COAT, conventional holography, etc.) are as follows:

(i) These interactions occur essentially instantaneously, being limited primarily by the response time, τ, of the atomic or molecular system utilized ($\tau \sim 10^{-3}$ to $< 10^{-12}$ sec at optical frequencies).

(ii) The resolution size of the phase conjugator is essentially limited by the wavelength (λ) of the incoming field.* In cases where the nonlinear medium is rarefied, the resolution size is on the order of $\rho^{-1/3}$, where ρ is the density of the atomic (or molecular) species participating in the interaction (assuming $\lambda < \rho^{-1/3}$). This applies to nonlinear interactions that are phase matched for all input angles.

(iii) The phase conjugate replica intensity can, for the class of time-reversed wavefronts generated by optical parametric interactions (and under the proper conditions), actually <u>exceed</u> the intensity of the input field (which is to be conjugated). Thus, for these cases, the "phase conjugate mirror" is an <u>amplifying</u> device. This amplifying feature of an output field is a common result of general (not necessarily conjugate) parametric interactions.

---

*Diffractive effects due to the conjugator's finite aperture can further limit the spatial frequency bandwidth (see, e.g.,[27]).

(iv) The interaction is purely optical, therefore obviating the use of electromechanical components.

These nonlinear optical (phase conjugating) interactions can be separated into two major classes: stimulated interactions and optical parametric interactions. These two classes will be described briefly below.

1.3 Phase Conjugation via Stimulated Optical Processes

In 1965, Wiggens and coworkers [9] noticed that the backscattered wave produced in stimulated Brillouin scattering (SBS) interactions in N_2 gas possessed divergence angles on the order of that of the forward-going field. This apparently was the first observation of a time-reversed wave; however, it was not discussed in that context. Zel'dovich et al. [10] in 1972 explored this phenomenon in more detail, and were the first to identify (theoretically) the backward-going Stokes wave as being essentially proportional to the phase conjugate of the exciting field. They further proved experimentally that this backward-going wave was capable of correcting for phase aberrations. This was accomplished by passing an input ruby laser plane wave beam through a piece of glass that was etched in hydrofluoric acid (HF). The etched glass represented a phase aberration which increased the divergence of the beam. The output field was then focused into a light pipe (3 mm diameter, 1 m long tube filled with methane) which gave rise to a backward-going field as a result of SBS. The divergence of this wave was measured after it retraversed the same piece of frosted glass, and was seen to be nearly the same as that of the initial forward-going plane

wave. This was the first demonstration of the aberration compensating property of time-reversed waves generated via stimulated optical processes. Nosach et al. [11] showed the ability of the SBS interaction to correct for aberrations within a gain medium by situating a ruby laser amplifier in place of the glass aberrating plate used in Zel'dovich's geometry. Since the appearance of these two papers, a myriad of works, primarily in the Soviet literature, were published that further described theoretically and experimentally the conjugation aspects of stimulated interactions [12]. More recently, Wang and Giuliano [13] measured the divergence of the aberrated and corrected beams in more detail, further verifying the distortion compensating aspects of SBS interactions. Also, the problem of phase conjugation via stimulated optical interactions in optical waveguides has been analyzed [14]. As of this date, work in SBS/phase-conjugate interactions is still being pursued at several research laboratories.

A second class of stimulated optical interactions, namely stimulated Raman scattering (SRS), has also been shown to be capable of yielding time-reversed waves. Phase conjugation via SRS has been treated experimentally and theoretically in the bulk [12], analyzed in optical waveguides [14], and observed using picosecond laser pulses [12].

Stimulated scattering type conjugators have both advantages and disadvantages. The major advantage lies in the fact that only one input optical field is required to effect the desired interaction--that of the field desired to be conjugated. A second feature is that the interaction is capable of yielding a high conjugate return efficiency (defined to be the ratio of the backward to forward field strengths). Conjugate

returns in excess of 80% have been measured [12,13] and are in agreement with theoretical predictions. There are, however, several drawbacks to this class of PCO interactions. First, since SBS and SRS are nonlinear (in terms of the input intensity) processes, the requirement exists for a minimum input optical intensity below which a negligible conjugate return can be obtained. Further, since acoustical phonons (for the case of SBS) or optical phonons (for SRS) are generated, these stimulated interactions correspond to inelastic photon scattering processes. This results in a backward-going (Stokes) wave of lower frequency than the input wave. Hence, a truly time-reversed replica is not strictly generated, which can be a drawback in certain applications. We finally remark that these stimulated processes are not capable of generating an amplified conjugate wave which may also be undesirable.

1.4 Phase Conjugation via Optical Parametric Interactions

The second class of phase conjugate interactions, which will be the major topic of this thesis, involves the generation of time-reversed replicas using nonlinear optical parametric interactions. This approach involves the mixing of several optical fields within a common nonlinear optical medium. If the directions (i.e., $\vec{k}$ vectors) and frequencies of the various optical fields participating in the interaction are properly chosen, the result of the interaction will yield an output field whose complex amplitude is proportional to the complex conjugate of the desired input field. Depending on the specific mixing process and geometry

chosen, the system can either give rise to conjugate replicas for any input field direction, or may be limited in the angular acceptance of this input field (due to phase matching constraints). This latter state of affairs is typically undesirable in that the number of resolution elements or spatial information (of the input field) capable of being time-reversed will be limited.

Apparently the initial experimental efforts were undertaken (independently) by Stepanov and coworkers [15] in the USSR, and by Woerdman [16] in the Netherlands, both in 1970. These initial experiments employed a degenerate four-wave mixing process to generate the backward-going wavefront. Also, Anan'ev [17] recognized the possibility of wavefront correction via this process. Although these experimental results did indeed demonstrate the time-reversed nature of the nonlinearly-generated output field, the theoretical understanding was rather qualitative. The impact of these two early experiments apparently was not fully appreciated by the optics community, as evidenced by the lack of reference to them in the literature. In 1976, Yariv [26] independently described how the specific process of three-wave nonlinear optical mixing can yield phase conjugate replicas of input wavefronts subject to limited angular acceptance ranges. These predictions were verified in experiments by Avizonis, et al. [44,45]. Hellwarth [27] analyzed the degenerate four-wave mixing scheme using a scalar diffraction perturbation approach. He showed rigorously that this mixing scheme overcomes the phase matching limitations inherent in the above three-wave mixing process. Paralleling these efforts was the ongoing work in an area that has been given the name

of real-time, dynamic, or transient holography [18-23]. As evidenced by its title, this area involves the simultaneous formation and reconstruction of a hologram (or diffraction grating) in a myriad of materials. At about the same time, other studies were directed toward understanding the dynamical properties (e.g., diffusion coefficient of the carriers in semiconductors) of the materials responsible in forming the transient hologram, and apparently not (at least initially) aimed at realizing the conjugate nature of the output field so generated. Eichler [25] gives an excellent review (at that time) of the field. Yariv [24] has since discussed the formal operational analogies between four-wave mixing and real-time holography, thus in essence unifying these two fields. Yariv and Pepper [28] applied the formalism of nonlinear optics to the four-wave mixing process and predicted the possibility of amplification of the conjugate wave and also the possibility of oscillation. These predictions were verified in experiments by Bloom et al. [46,56], by Pepper, Fekete, and Yariv [48], and by Jensen and Hellwarth [47]. Since that time numerous theoretical analyses have appeared describing phase conjugation in two-level systems [29], two-photon allowed transitions [30], molecules [31], radiatively cooled vapors [32], plasmas [33], and aerosols [34]. Theoretical problems such as molecular motion [35], pump depletion [36, 37], nonlinear distortions [38], transient four-wave mixing (e.g., photon echoes) [39-41], as well as the use of optical waveguides [42,43] (as opposed to bulk media) as the interaction configuration have been considered. On the experimental side, phase conjugate wavefronts have been observed in waveguide geometries [49,50] using CS_2 as the nonlinear

medium. Using four-wave mixing in the bulk, time-reversed wavefronts have been observed in a myriad of materials by the use of various physical mechanisms such as the generation of free [16,51] and localized electrons [52,53]; saturation-induced nonlinear susceptibility in ruby crystals [54], dyes [20], and vapors such as sodium [22,56-58], Rb [59], and SF_6 [60]; and in liquid crystals [55]. Thus, phase conjugate generation has been observed (both on a pulsed and cw basis) in the visible, the near I.R. and at 10.6 μm. Related to the above techniques in resonant media, phase conjugate fields have been observed via photon echoes [61,62]. Also, conjugate polarization-rotation effects have been observed recently [63], as have atomic motional effects [63]. In addition, phase conjugate fields have been generated from within laser resonators using an additional intracavity nonlinear element as well as the saturation effects of the laser gain medium itself as constituting the nonlinear optical medium [64,65].

There have been a myriad of potential applications discussed using phase-conjugate optical interactions, including Doppler-free spectroscopy [47,30,66,67], optical filtering [68-70], channel dispersion compensation [71,72], phase conjugate resonators [73-76] (i.e., a laser cavity whose conventional mirror is replaced by a phase conjugator), the measurement of the tensor elements of the third order susceptibility ($\chi^{(3)}$) [47], phase correlation measurements [77], spatial diffusion of excitation measurements [78], spatial convolution and correlation [79], and nonlinear microscopy [79]. Also, the use of phase conjugate interactions in the areas of optical gating; temporal convolution, correlation, pulse shaping, and encoding; MOPAs*; and laser fusion have recently received

*Master Oscillator Power Amplifier

much attention. Finally, a recent study [80] has shown that the use of a phase conjugator has the ability to correct for nonlinear refractive index distortions, thus in principle enabling one to compensate for self-induced aberrations [81] such as self-focusing or thermal blooming. Since the field of phase conjugate optics is still in its infancy (although two reviews have already been published [12,82], and several conferences have designated sessions to deal specifically with its recent advances), many promising and exciting applications are yet to be explored.

1.5 Outline of the Thesis

In this work we shall discuss both the theory and several potential applications of phase conjugate optics. We will concentrate almost exclusively on degenerate (and nearly degenerate) four-wave mixing. Properties of phase-conjugated fields in terms of propagation, time-reversal, and polarization will be the topic of Chapter II. We will consider the nature and propagation of phase-conjugate fields through linear, nonlinear, lossless, and lossy (or gain) media. In addition, we will discuss comparisons of phase-conjugators with conventional (ideal) mirrors in terms of both macroscopic (i.e., electromagnetic field) and microscopic (i.e., photon) viewpoints. Thus, Chapter II will essentially treat the phase conjugator as being a "black box."

Chapter III will concentrate on the physics of the optical nonlinearities which lead to phase conjugated wavefronts. Using the formalisms of nonlinear optics, a general description necessary for the generation of phase conjugate fields via three- and four-wave nonlinear interactions will be presented. The remainder of the chapter will concentrate

exclusively on four-wave mixing as the primary scheme to realize phase conjugation. Specifically, a coupled mode (plane wave) approach will be used to describe the interaction. The ability of this process to generate conjugate replicas of arbitrary wavefronts will be established. Next, we will discuss briefly both linear and nonlinear optical competing processes and their effect upon the desired phase conjugate interaction. Next, a quantum mechanical description of the optical nonlinearity within the conjugator for both one- and two-photon transitions will be analyzed. This description will be cast in terms of the time evolution operators with the associated Feynman diagrams as well as in terms of a density matrix formalism using a perturbation approach (this approach neglects limiting mechanisms such as saturation; however, the ease of application of the formalism to the problem of four-wave mixing is well worth the price). The chapter will conclude with a brief description depicting the operational analogs (as well as the differences) of four-wave nonlinear optical mixing with real-time holography.

In Chapter IV we will discuss four-wave mixing experiments that led to the observation of phase conjugate fields. The experiments, which were performed both in the bulk and in waveguide geometries, used carbon disulfide (CS_2), a transparent, isotropic liquid, as the nonlinear medium. Specifically, we have observed amplified phase-conjugate wave generation as well as optical parametric oscillation in the bulk under pulsed (ruby) laser excitation; we have also observed backward-wave generation on a cw basis (using an argon-ion laser as the source) in a CS_2-filled optical waveguide. Each experiment will be prefaced with a brief theoretical description germane to the specific geometry chosen. Results borne out

from the experiments will be compared with the theoretical formalisms discussed in Chapter III. The various diagnostic techniques utilized to verify the nature of the conjugate field as well as to distinguish the observed fields from potential competing effects will be discussed.

Several potential applications of phase conjugate optical interactions will be the topic of the last three chapters. These three chapters will focus upon applications which utilize basically different aspects of PCO: Specifically, several applications that make use of the "spatial-frequency domain" will be considered in Chapter V. Applications in this domain to be discussed will include the restoration of pictorial information due to propagation in optical waveguides, real-time holographic schemes (i.e., spatial convolution, correlation, Van der Lugt filters, etc.) and nonlinear microscopy.

Chapter VI will focus upon several "temporal-frequency domain" applications of PCO. Specifically, the use of a "nearly degenerate" four-wave nonlinear optical interaction will be shown to be capable of yielding a wide field-of-view, narrow bandpass optical filter. Next, a phase conjugator will be shown to be capable of compensating for channel dispersion and hence to be capable of effectively renarrowing optical pulses which were temporally broadened as a result of transmission through a (single mode) dispersive optical channel. The analysis will be extended to investigate general forward- and backward-going phase conjugate interactions. The chapter will conclude with an application of PCO interaction in the field of nonlinear laser spectroscopy. Specifically, using a time-dependent density matrix perturbation

approach, we will analyze the scattering of a probe photon off a transient Doppler-free two-photon coherent state. The resultant free-induction decay signal, which in fact is a conjugate replica of the probe photon, will be shown to yield information regarding the various dephasing rates of the nonlinear medium. Further, the degree of anharmonicity (for a nearly harmonic atomic or molecular potential) will be manifested by examining the amplitude fluctuations of the free-induction decay signal. The latter measurement, which is performed in the time domain, is referred to as α-beat spectroscopy.

The last chapter will describe an application of PCO that utilizes both the spatial- and temporal-frequency domain aspects of PCO interactions. Specifically, we will consider the use of a phase conjugator as forming a "mirror" that replaces a conventional mirror in an optical resonator. We will analyze the stability criterion, as well as the resonator modes of such a "phase conjugate resonator" using the ABCD formalism. The remainder of the chapter will be devoted to describing an experiment we performed where laser oscillation was observed in such a novel resonator. Various aspects of the experiment including the energy output, modal features, temporal output, and oscillation frequency will be described, as well as the experimental diagnostic tests performed to check the theoretical predictions. Finally, the concept of a Gaussian-tapered phase conjugate mirror will be considered in an appendix.

Chapter I - References

1. M. I. Skolnik and D. D. King, "Self-phasing array antennas," IEEE Trans. Antennas and Propagation AP-12, 142 (1964).

2. B. A. Sichelstiel, W. M. Walters, and T. A. Wild, "Self-focusing array research model," IEEE Trans. Antennas and Propagation AP-12, 150 (1964).

3. R. N. Ghose, "Electronically adaptive antenna systems," IEEE Trans. Antennas and Propagation AP-12, 161 (1964).

4. J. Opt. Soc. Amer. 67 (1977). Special issue on adaptive optics.

5. R. J. Collier, C. B. Burckhardt, and L. H. Liu, in Optical Holography (Academic Press, New York, 1971), p. 368.

6. W. Lukosz, "Equivalent-lens theory of holographic imaging," J. Opt. Soc. Amer. 58, 1084 (1968).

7. V. K. Orlov, Ya. Z. Virnik, S. P. Vorotilin, V. B. Gerasinov, Yu. A. Kalinin, and A. Ya. Sagalovich, "Retroreflecting mirror for dynamic compensation of optical inhomogeneities," Kvant. Elektron. (Moscow) 5, 1389 (1978) [Sov. J. Quant. Electron. 8, 799 (1978)]; H. H. Barrett and S. F. Jacobs, "Retroreflective arrays as approximate phase conjugators," Opt. Lett. 4, 190 (1979).

8. A. Yariv, "On the differences between a phase conjugator and a retroreflector array," unpublished.

9. T. A. Wiggens, R. V. Wick, and D. H. Rank, "Stimulated effects in N_2 and CH_4 gases," Appl. Opt. 5, 1069 (1966).

10. B. Ya. Zel'dovich, V. I. Popovichev, V. V. Ragul'skii, and F. S. Faisullov, "Connection between the wavefronts of the reflected and exciting light in stimulated Mandel'stam-Brillouin scattering," Pisma Zh. Eksp. Teor. Fiz. 15, 160 (1972) [JETP Lett. 15, 109 (1972)].

11. O. Y. Nosach, V. I. Popovichev, V. V. Ragul'skii, and F. S. Faisullov, "Cancellation of phase distortion in an amplifying medium with a 'Brillouin mirror,'" Pisma Zh. Eksp. Teor. Fiz. 16, 617 (1972) [JETP Lett. 16, 435 (1972)].

12. B. Ya. Zel'dovich, N. F. Pilipelskii, V. V. Ragul'skii, and V. V. Shkunov, "Wavefront reversal by nonlinear optics methods," Kvant. Elektron. (Moscow) 5, 1800 (1978) [Sov. J. Quant. Electron. 8, 1021 (1978)].

13. V. Wang and C. R. Giuliano, "Correction of phase aberration via stimulated Brillouin scattering," Opt. Lett. 2, 4 (1978).

14. R. W. Hellwarth, "Theory of phase conjugation by stimulated scattering in a waveguide," J. Opt. Soc. Am. 68, 1050 (1978).

15. B. I. Stepanov, E. V. Ivakin, and A. S. Rubanov, "Recording two-dimensional and three-dimensional dynamic holograms in transparent substances," Doklady Akademii Nauk SSSR 196, 567 (1971) [Sov. Phys.-Doklady 16, 46 (1971)].

16. J. P. Woerdman, "Formation of a transient free carrier hologram in Si," Opt. Commun. 2, 212 (1970).

17. Yu. A. Anan'ev, "Possibility of dynamic correction of wave fronts," Kvant. Elektron. 1, 1669 (1974) [Sov. J. Quant. Electron. 4, 929 (1975)].

18. H. J. Gerritsen, "Nonlinear effects in image formation," Appl. Phys. Lett. 10, 239 (1967).

19. D. L. Staebler and J. J. Amodei, "Coupled-wave analysis of holographic storage in $LiNbO_3$," J. Appl. Phys. 43, 1042 (1972).

20. E. V. Ivakin, I. P. Petrovich, and A. S. Rubanov, "Self-diffraction of radiation by light-induced phase gratings," Kvant. Elektron. 1, 96 (1973) [Sov. J. Quant. Electron. 3, 52 (1973)].

21. E. V. Ivakin, I. P. Petrovich, A. S. Rubanov, and B. I. Stepanov, "Dynamic holograms in amplifying medium," Kvant. Elektron. (Moscow) 2, 1556 (1975) [Sov. J. Quant. Electron. 5, 840 (1975)].

22. Yu. I. Ostrovskii, V. G. Sidorovich, D. I. Stasel'ko, and L. V. Tanin, "Dynamic holograms in sodium vapor," Pisma Zh. Tekh. Fiz. 1, 1030 (1975) [Sov. Tech. Phys. Lett. 1, 442 (1975)].

23. J. P. Huignard and F. Micheron, "High-sensitivity real-write volume holographic storage in $Bi_{12}SiO_{20}$ and $Bi_{12}GeO_{20}$ crystals," Appl. Phys. Lett. 29, 591 (1976).

24. A. Yariv, "Four-wave nonlinear mixing as real-time holography," Opt. Commun. 25, 23 (1978).

25. H. J. Eichler, "Laser-induced grating phenomena," Optica Acta 24, 631 (1977).

26. A. Yariv, "Three-dimensional pictorial transmission in optical fibers," Appl. Phys. Lett. 28, 88 (1976); "Compensation of atmospheric degradation of optical beam transmission by nonlinear optical mixing," Opt. Commun. 21, 49 (1977).

27. R. W. Hellwarth, "Generation of time-reversed wavefronts by nonlinear refraction," J. Opt. Soc. Amer. 67, 1 (1977).

28. A. Yariv and D. M. Pepper, "Amplified reflection, phase-conjugation, and oscillation in degenerate four-wave mixing," Opt. Lett. 1, 16 (1977).

29. R. L. Abrams and R. C. Lind, "Degenerate four-wave mixing in absorbing media," Opt. Lett. 2, 94 (1978); ibid 3, 205 (1978).

30. D. C. Haneisen, "Doppler-free two-photon spectroscopy using degenerate four-wave mixing," Opt. Commun. 28, 183 (1979).

31. A. Elci and D. Rogovin, "Phase conjugation in nonlinear molecular gases," Chem. Phys. Lett. 61, 407 (1979).

32. A. J. Palmer, "Nonlinear optics in radiatively cooled vapors," Opt. Commun. 30, 104 (1979).

33. D. G. Steel and J. F. Lam, "Degenerate four-wave mixing in plasmas," Opt. Lett. 4, 363 (1979).

34. A. J. Palmer, "Degenerate four-wave mixing in aerosols," Opt. Lett., to be published in February 1980.

35. S. M. Wandzura, "Effects of atomic motion on wavefront conjugation by resonantly enhanced degenerate four-wave mixing," Opt. Lett. 4, 208 (1979).

36. J. H. Marburger and J. F. Lam, "Nonlinear theory of degenerate four-wave mixing," Appl. Phys. Lett. 34, 389 (1979).

37. H. Hsu, "Large signal theory of phase-conjugate backscatterings," Appl. Phys. Lett. 34, 855 (1979).

38. J. H. Marburger and J. F. Lam, "Effects of nonlinear index changes on degenerate four-wave mixing," Appl. Phys. Lett. 35, 249 (1979).

39. C. V. Heer and P. F. McManamon, "Wavefront correction with photon echoes," Opt. Commun. 23, 49 (1977).

40. N. S. Shiren, "Generation of time-reversed optical wavefronts by backward-wave photon echoes," Appl. Phys. Lett. 33, 299 (1978).

41. A. Yariv and J. AuYeung, "Transient four-wave mixing and real-time holography in atomic systems," IEEE J. Quant. Electron. QE-15, 224 (1979).

42. A. Yariv, J. AuYeung, D. Fekete, and D. M. Pepper, "Image phase compensation and real-time holography by four-wave mixing in optical fibers," Appl. Phys. Lett. 32, 635 (1978).

43. R. W. Hellwarth, "Theory of phase-conjugation by four-wave mixing in a waveguide," IEEE J. Quant. Electron. QE-15, 101 (1979).

44. P. V. Avizonis, F. A. Hopf, W. D. Bamberger, S. F. Jacobs, A. Tomita, and K. H. Womack, "Optical phase conjugation in a lithium formate crystal," Appl. Phys. Lett. 31, 435 (1977).

45. F. A. Hopf, A. Tomita, K. H. Womack, and J. L. Jewell, "Optical distortion in nonlinear phase conjugation by three-wave mixing," J. Opt. Soc. Amer. 69, 968 (1979).

46. D. M. Bloom and G. C. Bjorklund, "Conjugate wavefront generation and image reconstruction by four-wave mixing," Appl. Phys. Lett. 31, 592 (1977).

47. S. M. Jensen and R. W. Hellwarth, "Observation of the time-reversed replica of a monochromatic optical wave," Appl. Phys. Lett. 32, 166 (1978).

48. D. M. Pepper, D. Fekete, and A. Yariv, "Observation of amplified phase-conjugate reflection and optical parametric oscillation by degenerate four-wave mixing in a transparent medium," Appl. Phys. Lett. 33, 41 (1978).

49. S. M. Jensen and R. W. Hellwarth, "Generation of time-reversed waves by nonlinear refraction in a waveguide," Appl. Phys. Lett. 33, 404 (1978).

50. J. AuYeung, D. Fekete, D. M. Pepper, A. Yariv, and R. K. Jain, "Continuous backward-wave generation by degenerate four-wave mixing in optical fibers," Opt. Lett. 4, 42 (1979).

51. R. K. Jain and M. B. Klein, "Degenerate four-wave mixing near the band gap of semiconductors," Appl. Phys. Lett. 35, 454 (1979); R. K. Jain, M. B. Klein, and R. C. Lind, "High-efficiency degenerate four-wave mixing of 1.06 μm radiation in silicon," Opt. Lett. 4, 328 (1979).

52. J. P. Huignard, J. P. Herriau, P. Aubourg, and E. Spitz, "Phase-conjugate wavefront generation via real-time holography in $Bi_{12}SiO_{20}$ crystals," Opt. Lett. 4, 21 (1979).

53. J. Feinberg, D. Heisman, and R. W. Hellwarth, "Phase conjugation in $BaTiO_3$," Paper TuK2, 1978, Annual Meeting Optical Society of America.

54. P. F. Liao and D. M. Bloom, "Continuous-wave backward-wave generation by degenerate four-wave mixing in ruby," Opt. Lett. 3, 4 (1978).

55. D. Fekete, J. AuYeung, and A. Yariv, to be published.

56. D. M. Bloom, P. F. Liao, and N. P. Economou, "Observation of amplified reflection by degenerate four-wave mixing in atomic sodium vapor," Opt. Lett. 2, 58 (1978).

57. P. F. Liao, D. M. Bloom, and N. P. Economou, "cw optical wavefront conjugation by saturated absorption in atomic sodium vapor," Appl. Phys. Lett. 32, 813 (1978).

58. C. V. Heer and N. C. Griffen, "Generation of a phase-conjugate wave in the forward direction with the Na-vapor cells," Opt. Lett. 4, 239 (1979).

59. D. Grischkowsky, N. S. Shiren, and R. J. Bennett, "Generation of time-reversed wavefronts using a resonantly enhanced electronic nonlinearity," Appl. Phys. Lett. 33, 805 (1978).

60. R. C. Lind, D. G. Steel, M. B. Klein, R. C. Abrams, C. R. Giuliano, and R. K. Jain, "Phase conjugation at 10.6 μm by resonantly enhanced degenerate four-wave mixing," Appl. Phys. Lett. 34, 457 (1979).

61. N. C. Griffen and C. V. Heer, "Focusing and phase conjugation of photon echoes in Na vapor," Appl. Phys. Lett. 33, 865 (1978).

62. M. Fujita, H. Nakatsuka, H. Nakanishi, and M. Matsuoka, "Backward echo in two-level systems," Phys. Rev. Lett. 42, 974 (1979).

63. D. G. Steel, R. C. Lind, J. F. Lam, and C. R. Giuliano, "Polarization rotation and thermal motion studies via resonant degenerate four-wave mixing," Appl. Phys. Lett. 35, 376 (1979).

64. E. E. Bergmann, I. J. Bigio, B. J. Feldman, and R. A. Fisher, "High-efficiency pulsed 10.6 μm phase-conjugate reflection via degenerate four-wave mixing," Opt. Lett. 3, 82 (1978).

65. A. Tomita, "Phase conjugation using gain saturation of a Nd:YAG laser," Appl. Phys. Lett. 34, 463 (1979).

66. P. F. Liao, N. P. Economou, and R. R. Freeman, "Two-photon coherent transient measurements of Doppler-free linewidths with broadband excitation," Phys. Rev. Lett. 39, 1473 (1977).

67. D. G. Steel and J. F. Lam, "Two-photon coherent transient measurement of the nonradiative collisionless dephasing rate in SF_6 via Doppler-free degenerate four-wave mixing," Phys. Rev. Lett. 43, 1588 (1979).

68. D. M. Pepper and R. L. Abrams, "Narrow optical bandpass filter via nearly degenerate four-wave mixing," Opt. Lett. 3, 212 (1978).

69. J. Nilsen and A. Yariv, "Nearly degenerate four-wave mixing applied to optical filters," Appl. Opt. 18, 143 (1979).

70. T. Y. Fu and M. Sargent III, "Effects of signal detuning on phase conjugation," Opt. Lett. 4, 366 (1979).

71. J. H. Marburger, "Optical pulse integration and chirp reversal in degenerate four-wave mixing," Appl. Phys. Lett. 32, 392 (1978).

72. A. Yariv, D. Fekete, and D. M. Pepper, "Compensation for channel dispersion by nonlinear optical phase conjugation," Opt. Lett. 4, 52 (1979).

73. I. M. Bel'dyugin, M. G. Galushkin, and E. M. Zemskov, "Properties of resonators with wavefront-reversing mirrors," Kvant. Elektron. (Moscow) 6, 38 (1979) [Sov. J. Quant. Electron. 9, 20 (1979)].

74. J. AuYeung, D. Fekete, D. M. Pepper, and A. Yariv, "A theoretical and experimental investigation of the modes of optical resonators with phase conjugate mirrors," IEEE J. Quant. Electron. QE-15, 1180 (1979).

75. J. F. Lam and W. P. Brown, "Optical resonators with phase conjugate mirrors," submitted to Optics Letters.

76. P. A. Be'langer, A. Hardy, and A. E. Siegman, "Resonant modes of optical cavities with phase-conjugate mirrors," submitted to Applied Optics.

77. G. P. Agrawal, "Phase determination by conjugate wavefront generation," J. Opt. Soc. Amer. 68, 1135 (1978).

78. D. S. Hamilton, D. Heiman, J. Feinberg, and R. W. Hellwarth, "Spatial-diffusion measurements in impurity-doped solids by degenerate four-wave mixng," Opt. Lett. 4, 124 (1979).

79. D. M. Pepper, J. AuYeung, D. Fekete, and A. Yariv, "Spatial convolution and correlation of optical fields via degenerate four-wave mixing," Opt. Lett. 3, 7 (1978).

80. D. M. Pepper and A. Yariv, "Compensation for phase distortions in nonlinear media by phase conjugation," Opt. Lett., to be published in February 1980.

81. A. Yariv, Quantum Electronics, 2nd ed. (John Wiley, New York, 1975).

82. A. Yariv, "Phase conjugate optics and real-time holography," IEEE J. Quant. Electron. QE-14, 650 (1978); ibid, QE-15, 256 and 523 (1979).

Chapter II

PROPERTIES OF PHASE-CONJUGATED WAVEFRONTS

2.1 Introduction

In this chapter we will discuss the basic properties regarding the effect of a phase conjugate interaction upon a given incident electromagnetic field. The specific details pertaining to the mechanism of the conjugator itself will be considered in the next chapter; thus, in the present context, the conjugator is to be regarded as being the proverbial "black box." We will discuss the "time-reversal" properties of the phase conjugator with respect to its ability to "unscramble" undesirable wavefront distortions. To this end, we will discuss the effects of the phase conjugate interaction upon both "phase aberrations" and "polarization aberrations" that can be incurred by an incident field whose time-reversed replica is sought. The latter form of aberration will be shown to be a special case of the more general phase aberration (when considering rotating or vector fields).

The above properties will be discussed from both a macroscopic (i.e., field) and a microscopic (i.e., photon) viewpoint. In terms of the latter description, the helicity, as well as the angular and linear momentum photon aspects of the phase conjugator will be considered. Throughout the discussion, we will compare and contrast the properties of a phase conjugate interaction (which can be viewed as a novel "mirror") with those of an ideal, conventional (i.e., a "real") mirror.

We will conclude this chapter with a discussion of the ability of phase-conjugate mirrors to correct for nonlinear (i.e., intensity-dependent) optical phase distortions. These aberrations which are self-induced and result in undesirable effects such as self-focusing and thermal blooming will be shown to be amenable to compensation via a phase conjugate interaction. Another special case of aberrating media, that of phase and amplitude distortions, will be treated in the Appendix.

2.2 Phase Conjugation as "Time Reversal"

In this section we present arguments that yield the important result that the operation of phase conjugation upon an optical field is equivalent to the generation of a new field that propagates or evolves exactly in the reverse direction (at each point in space) relative to that of the original wave. That is, the phase conjugate replica of a given field can be described as a "time-reversed" replica of this original wave. The causal aspects of "time reversal" will be discussed in Chapter VI.

Consider an electromagnetic field

$$E_1(\vec{r},t) = \mathrm{Re}\{\psi(\vec{r})\ \exp[i(\omega t - kz)]\}$$

$$= \mathrm{Re}\{A_1(\vec{r})\ \exp(i\omega t)\} \qquad (2.2\text{-}1)$$

This field is a monochromatic wave of radian frequency ω, propagating essentially in the positive z-direction. The complex amplitude $\psi(\vec{r})$, can describe any spatial amplitude or phase information imposed

upon E_1. We note that $\psi(\vec{r})$ can also describe the polarization state of the field.

The field conjugate to E_1 is defined to be

$$E_2(\vec{r},t) = \mathrm{Re}\{\psi^*(\vec{r})\ \exp[i(\omega t + kz)]\}$$

$$= \mathrm{Re}\{A_1^*(\vec{r})\ \exp(i\omega t)\} \equiv \mathrm{Re}\{A_2(\vec{r})\ \exp(i\omega t)\} \qquad (2.2\text{-}2)$$

E_2 corresponds to an optical field of radian frequency ω, and has a complex spatial function, $A_2(\vec{r})$, which is equal to the complex conjugate of that corresponding to E_1 (i.e., $A_2 = A_1^*$). It is seen that E_2 evolves in the same manner as if one replaced t with -t in E_1; we thus call E_2 a "time-reversed wavefront," or a "phase conjugate replica" relative to E_1. The "device" that generates E_2 can be described as being a "phase conjugator," or a "phase conjugate mirror" (PCM).

That E_2 is a valid solution of the Maxwell's equations can be shown as follows. We consider the propagation of E_1 and E_2 through a common, lossless, linear dielectric medium, described by a field-independent permittivity, $\varepsilon(\vec{r})$. The field E_1 obeys the scalar wave equation (in cgs)

$$\nabla^2 E - \frac{\mu\varepsilon(\vec{r})}{c^2}\frac{\partial^2 E}{\partial t^2} = 0 \qquad (2.2\text{-}3)$$

Substitution of E_1 given by the first equation in (2.2-1) into (2.2-3) yields

$$\nabla^2\psi + [\omega^2\mu\varepsilon(\vec{r}) - k^2]\psi - 2ik\frac{\partial\psi}{\partial z} = 0 \qquad (2.2\text{-}4)$$

The complex conjugate of (2.2-4) is given by

$$\nabla^2\psi^* + [\omega^2\mu\varepsilon(\vec{r}) - k^2]\psi^* + 2ik\frac{\partial\psi^*}{\partial z} = 0 \qquad (2.2\text{-}5)$$

which is recognized to be the wave equation describing the propagation of E_2. This is easily verified upon substitution of (2.2-2) in (2.2-3). We therefore see that the conjugate replica (E_2) of E_1 satisfies the wave equation, and therefore describes the propagation of a field having the same equiphase surfaces as E_1 at each point in space and propagating opposite to that of the incident wave E_1. If we assume that a PCM is located at the plane $z = z_o$, then the above arguments hold for all $z < z_o$.

We note that the time-reversed replica of the magnetic field vector $\vec{H}_2$ is related to its incident counterpart $\vec{H}_1$ by $\vec{H}_2(t) = -\vec{H}_1(-t)$ for all $z < z_o$. This ensures that $\vec{S}_2(t) = -\vec{S}_1(-t)$ for all $z < z_o$, where $\vec{S}[= c(\vec{E} \times \vec{H})/4\pi]$ is the Poynting's vector.

The treatment of two special yet important classes of distorting mechanisms (and their effect upon conjugate-wave propagation), that of nonlinear optical phase distortions and amplitude distortions, will be the topic of Section 2.5 and the Appendix, respectively.

A frequently quoted application of phase conjugators is their ability to compensate for undesirable phase distortions or aberrations encountered by electromagnetic fields upon propagation through linear, lossless media such as turbulent atmospheres or poor optical quality components. Figure 2.1 shows a typical example. Consider an optical (monochromatic) plane wave propagating from left to right (given by the solid lines) that is incident upon a phase distorting medium. After passage through this medium, the field has acquired a spatially dependent

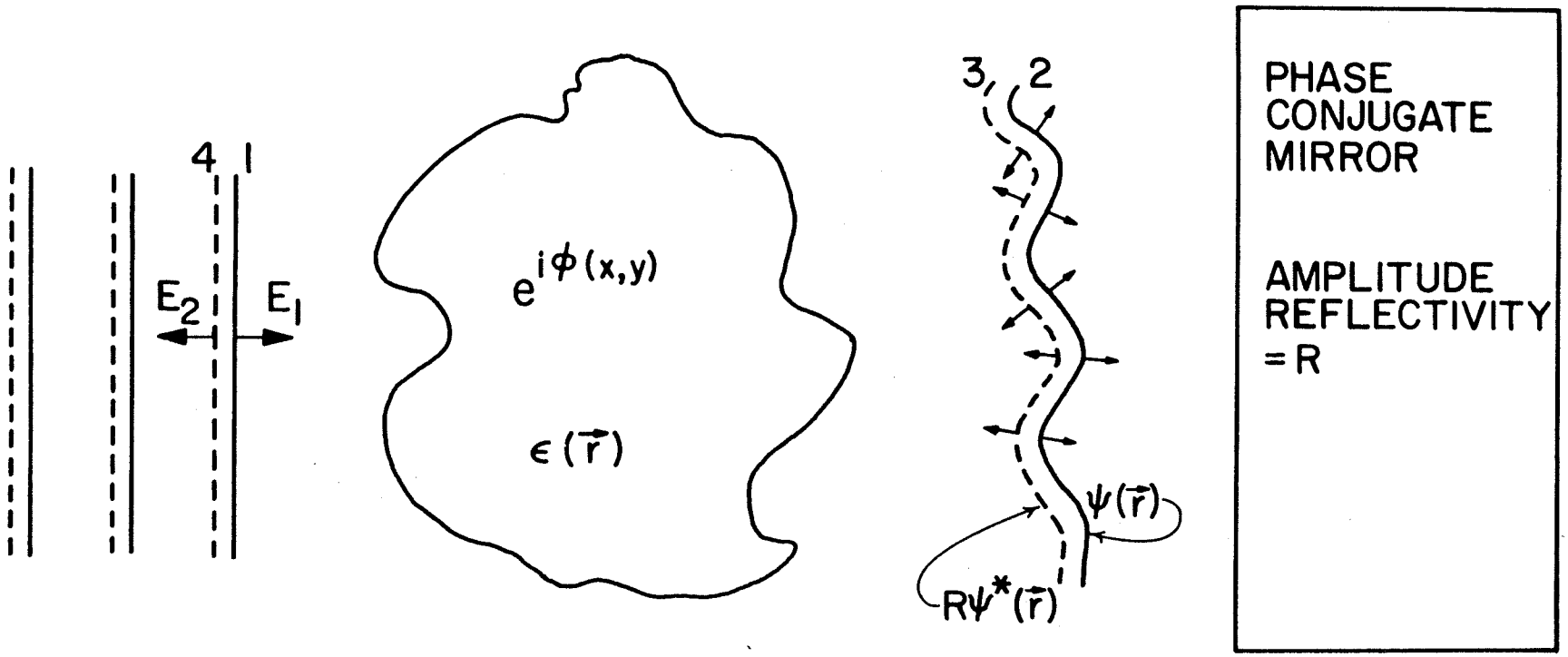

Fig. 2.1 Typical geometry depicting the ability of a PCM to correct for a general spatially dependent phase aberration. A monochromatic plane wave (1) incident from the left encounters a region of nonuniform index, denoted by $\phi(x,y)$. The resultant distorted wavefront (2) is now "time-reversed" (or conjugated) by the PCM (phase conjugate mirror) resulting in (3) which, after retraversing the same medium, emerges (4) having the initial planar wavefronts. The small arrows schematically indicate the (local) spatial plane wave propagation components of the given wavefront.

phase $\phi(x,y)$. The resultant equiphase fronts are no longer planar. This field is now assumed to be incident upon a phase conjugator. The effect of the phase conjugator is to give rise to a new field (dashed curves) which exactly retraces the path of the input wave having a phase term equal to $-\phi(x,y)$. As this wave (which propagates from right to left) retraverses the same distorting medium, the spatially dependent phase distortion exactly cancels. Thus, the original planar wavefronts are recovered.

We now compare pictorially the differences between a conventional mirror and that of a phase conjugate mirror with respect to the propagation of an optical field through a phase distorter. Specifically, we assume a plane wave (again a monochromatic field) to be incident upon a narrow slab of glass of length L, whose phase delay is characterized by its linear index of refraction, n. In Figure 2.2a the effect upon propagation through this glass and a subsequent reflection off of a conventional mirror is shown. For simplicity we do not consider the diffractive effects due to the finite cross section of the glass. After the plane wave propagates (from left to right) through this glass slab, its equiphase surface develops a "bulge" due to the acquired phase delay. After retroreflection from the real, plane mirror and subsequent passage back through the glass slab, an additional (equal) phase delay is again encountered, resulting in a phase "bulge" of twice the size. Thus, the

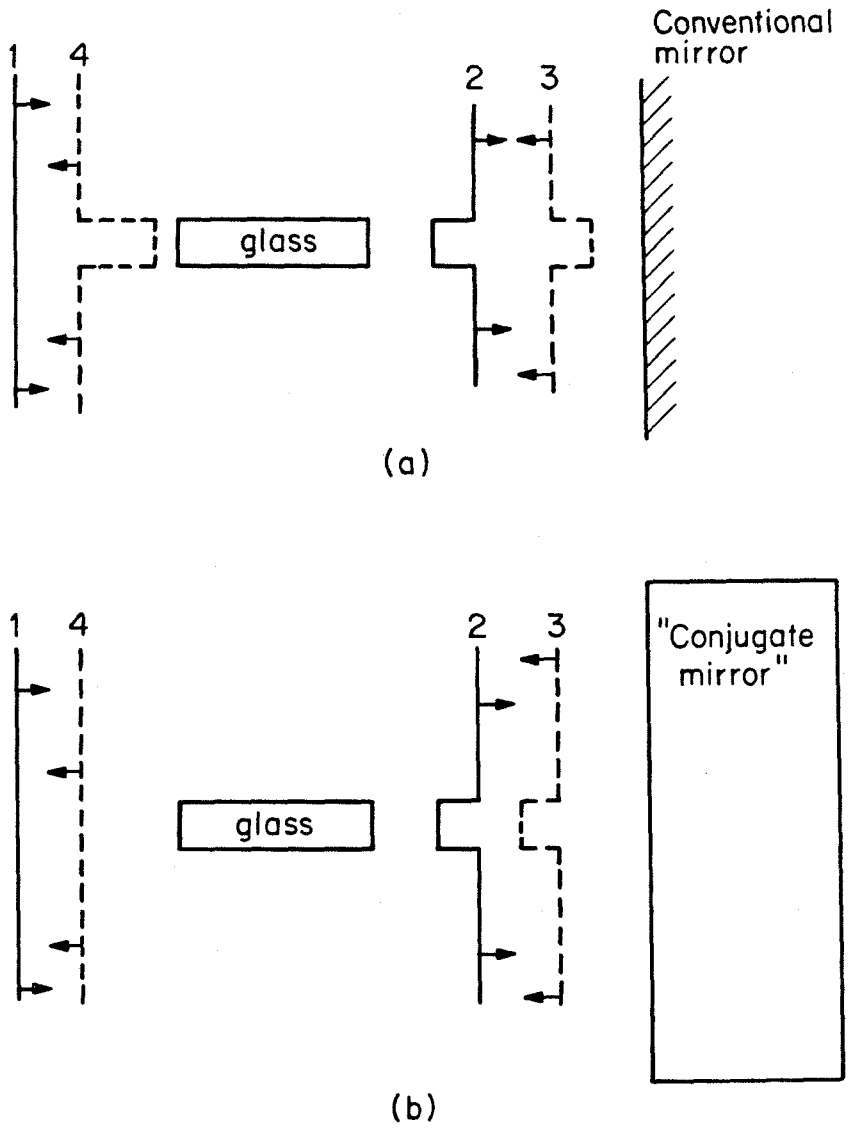

Fig. 2.2 Comparison of a conventional mirror (a) with a conjugate mir-
mirror (b) in terms of its effect upon a phase aberrator. (a) A monochromatic plane wave (1) is incident upon a distorting element (a glass cylinder) emerging with a bulge (2). The wave reflected from a conventional mirror (3) traverses the cylinder in reverse, resulting in a doubling of the bulge depth. (b) A conjugate mirror yields a reflected wavefront (3) which is identical to the incident wave (2). The result is a perfect smoothing of the bulge in (4), so that (4) and (1) have identical equiphase surfaces.

overall phase distortion accumulated is equivalent to propagation through a similar glass slab of length 2L. Figure 2.2b depicts the same geometry but having the real mirror replaced by a "phase conjugate mirror." The profound difference between these two mirrors is that the latter now reverses the phase (in addition to the direction of propagation). The phase bulge is therefore effectively "advanced" with respect to the remainder of the phase front. Thus, upon subsequent traversal through the glass slab, the original planar wavefronts are recovered.

Regarding the causal aspects of the phase conjugator, we note that (in Figure 2.2) the bulge-induced changes in the incident plane wave are a mapping of equiphase fronts, and are not to be considered as temporally delaying the energy flux of the field. If the latter were the case, the conjugate mirror would have to have a priori information concerning the temporal sequence of the (arbitrary) incident field, thus violating the causal aspects of the interaction. This apparent paradox is resolved once we recognize that we are dealing with monochromatic fields; thus the waves are defined to be present for all times. Any sequencing of temporal information would be in violation of this initial condition, since additional frequency components would be introduced into the input field. We note for future reference that the conjugator gives rise to "time-reversed" replicas only at a single frequency. If the input frequency differs from the "operational frequency" of the conjugator, a perfect, time-reversed wavefront is not generated. The associated transient effects (or equivalently, the effects of phase conjugation upon a polychromatic or broadband input frequency spectrum)

will be discussed in Chapter VI.

To conclude this section, we remark that the ability of the phase conjugate mirror to time-reverse an arbitrary monochromatic wavefront is due to the fact that the conjugator is a linear device (in a spatial mode sense). That is, the input and (conjugated) output waves are related to each other linearly. Thus, an arbitrary input field can be decomposed into a superposition of plane wave components, with the conjugate mirror time-reversing each component. This one-to-one mapping of input and output plane waves therefore makes possible the utility of the conjugator to operate on general wavefronts. Most of the spatial domain applications of phase conjugators follow directly from this fact. We leave the formal proof of these assertions to the next chapter. We also remark that thus far we have considered only scalar fields (i.e., $\psi(\vec{r})$ is a tensor of rank zero). In the next section we extend the analysis of phase conjugate operations to vector representations of $\psi(\vec{r})$.

2.3 Effects of Phase Conjugation upon Arbitrary Rotating $\vec{E}$-Fields

In this section we consider a special, yet important case of phase aberrations: that of polarization aberrations. This type of aberration is relevant in that general aberrations can not only affect the shape of the wavefront, but also the polarization state of the field. Examples of such phase distortions can be stress-induced birefringence of optical components, misaligned anisotropic optical elements, or

polarization scrambling effects of optical fibers. These undesirable effects can occur both within a laser resonator itself and upon propagation outside the laser. We will show below that the effect of the phase conjugator is to time-reverse this polarization state (or rotating $\vec{E}$-field) and thus "unravel" or "unwind" this field as it retraces its original trajectory. That the conjugator can give rise to a time-reversed rotating vector field will follow from the previously-mentioned linearity of the interaction with respect to an arbitrary superposition of input modes. This statement will be rigorously proved in the next chapter. Whereas we have previously considered scalar (spatial) modes, we now consider these modes to be the various components of a more general vector field.

Consider a monochromatic optical field at radian frequency ω, possessing an arbitrary polarization state, and propagating primarily in the +z direction, as defined in the [I]-coordinate system (see Figure 2.3). The most general polarization state is that of an elliptically polarized wave [2], which we represent by

$$\vec{E}_1^{[I]}(\vec{r},t) = \mathrm{Re}\{\sum_{\ell}[E_{+\ell}\,\hat{\varepsilon}_{+\ell}^{[I]} + E_{-\ell}\,\hat{\varepsilon}_{-\ell}^{[I]}]\,\exp[i(\omega t-\vec{k}\cdot\vec{r})]\}$$

$$= \mathrm{Re}\{\vec{\psi}(\vec{r})^{[I]}\,\exp[i(\omega t-kz)]\} \qquad (2.3\text{-}1)$$

where $E_{\pm\ell}$ are the complex amplitudes, and $\hat{\varepsilon}_{+}^{[I]}(\hat{\varepsilon}_{-}^{[I]})$ are the unit vectors for the left(right) handed circular polarizations (LHCP and RHCP, respectively) for the ℓ^{th} plane wave "mode." We have approximated a transverse Fourier integral representation as a summation over discrete modes for simplicity. Since each ℓ^{th} mode is conjugated in a

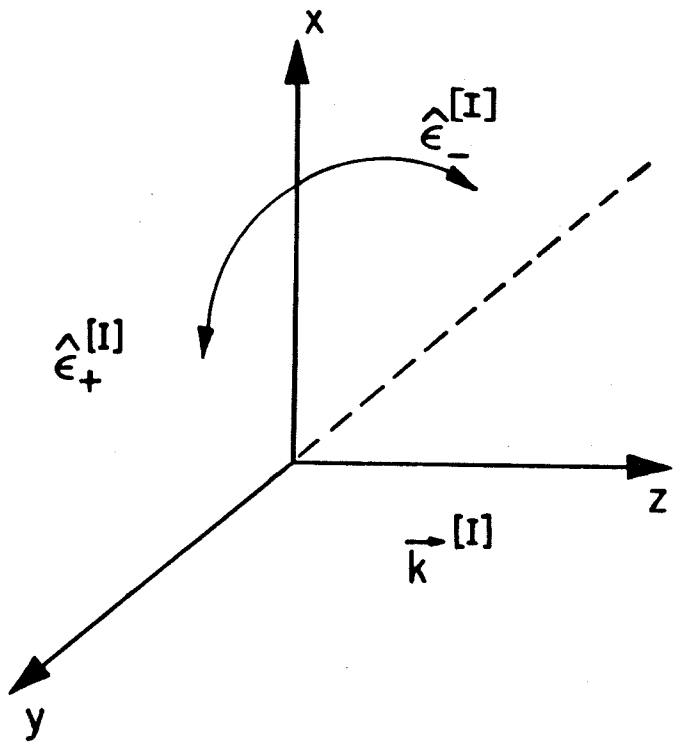

[I] - SYSTEM

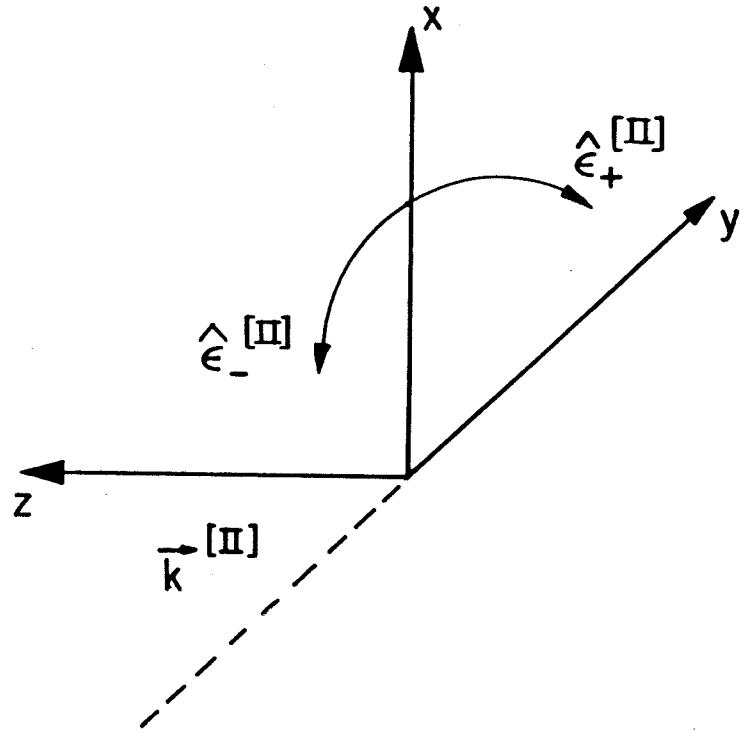

[II] - SYSTEM

Fig. 2.3 Coordinate system conventions used in relating fields of general polarizations upon reflection from real and conjugate mirrors.

linear fashion, we will restrict our discussion to one such plane wave component (which propages in the +z direction). We shall thus drop the ℓ subscript with the understanding that for a general field one must sum (or, more accurately, integrate) over all such spatial modes. Without loss of generality, we assume the $E_{\pm}$ to be real; any nonzero phase can be interpreted as corresponding to a rotation of the elliptically polarized state (by an angle equal to half the phase difference between E_+ and E_-)[2].

The unit vectors for the two circular polarization states in (2.3-1) can be rewritten as

$$\hat{\varepsilon}_{\pm}^{[I]} = \frac{1}{\sqrt{2}} (\hat{\varepsilon}_x \pm i\hat{\varepsilon}_y) \qquad (2.3\text{-}2)$$

where $\hat{\varepsilon}_x$ and $\hat{\varepsilon}_y$ are the unit vectors along the x and y directions, respectively. $\vec{\psi}(\vec{r})$ is thus a vector generalization of the previous analogous scalar quantity [c.f., equation (2.2-1)].

The vector field $(\vec{E}_1)$ is incident on a phase conjugator located at $z = 0$. Following the definition of its operation [equation (2.2-2)], the conjugate field, $\vec{E}_2$, is given as

$$\vec{E}_2^{[I]}(\vec{r},t) = \mathrm{Re}\{(E_+\hat{\varepsilon}_+^{*[I]} + E_-\hat{\varepsilon}_-^{*[I]}) \exp[i(\omega t+kz)]\} \qquad (2.3\text{-}3)$$

From the definition of $\hat{\varepsilon}_{\pm}^{[I]}$, it follows that

$$\hat{\varepsilon}_{\pm}^{*[I]} = \hat{\varepsilon}_{\mp}^{[I]} \qquad (2.3\text{-}4)$$

and we can therefore rewrite equation (2.3-3) as

$$\vec{E}_2^{[I]}(\vec{r},t) = \mathrm{Re}\{(E_+\hat{\varepsilon}_-^{[I]} + E_-\hat{\varepsilon}_+^{[I]}) \exp[i(\omega t+kz)]\} \qquad (2.3\text{-}5)$$

In order to fully appreciate the significance of $\vec{E}_2$, we now define

two (right-handed) coordinate systems, described by a superscript [I] and [II]. The former system has its z-axis pointing along the direction of propagation of $\vec{E}_1$, while the latter system has its z-axis oriented to point along the direction of the conjugate field, $\vec{E}_2$. Figure 2.3 shows these two coordinate systems, along with the polarization and propagation vectors. From the figure, we see that

$$\hat{\varepsilon}_{\pm}^{[I]} = \hat{\varepsilon}_{\mp}^{[II]} \quad ; \qquad \vec{k}^{[I]} = -\vec{k}^{[II]} \tag{2.3-6}$$

All the above descriptions relating $\vec{E}_1$ and $\vec{E}_2$ have been made in the [I]-system. Since $\vec{E}_2$ propagates opposite to $\vec{E}_1$, it is best described in the [II]-system. Using the definitions above [equations (2.3-6)], we can describe $\vec{E}_2$ as

$$\vec{E}_2^{[II]}(\vec{r},t) = \mathrm{Re}\{(E_+\hat{\varepsilon}_+^{[II]} + E_-\hat{\varepsilon}_-^{[II]})\exp[i(\omega t - kz)]\} \tag{2.3-7}$$

Therefore, from equation (2.3-1) we immediately find that

$$\vec{E}_1^{[I]} = \vec{E}_2^{[II]} \tag{2.3-8}$$

Hence, the conjugate wave ($\vec{E}_2$) which has the same polarization and eccentricity as $\vec{E}_1$ propagates exactly in the reversed direction relative to $\vec{E}_1$. As mentioned earlier, this feature follows from the conjugator's linear relationship of the incident field to the conjugate field. The generalization to input fields having arbitrary spatial and polarization modes easily follows from the results of the preceding section.

We now compare the effects of the conjugate mirror with those of a conventional mirror for the special case of an incident unity ampli-

tude left-handed, circularly polarized plane wave. The wave is given by

$$\vec{E}_1^{[I]}(\vec{r},t) = \mathrm{Re}\{\hat{\varepsilon}_+^{[I]} \exp[i(\omega t - kz)]\} \tag{2.3-9}$$

The effect of a (perfect) real mirror is to maintain the sense of rotation of the $\vec{E}$-field by virtue of the boundary conditions (regarding the tangential components of the fields). Therefore

$$\hat{\varepsilon}_\pm^{[I]} \xrightarrow{\text{real mirror}} \hat{\varepsilon}_\pm^{[I]} = \hat{\varepsilon}_\mp^{[II]} \tag{2.3-10}$$

where we have used equation (2.3-6) to again relate the two coordinate systems. The reflected field from the real mirror, which we define to be $\vec{E}_3$, is given in the [II]-system as

$$\vec{E}_3^{[II]}(\vec{r},t) = \mathrm{Re}\{\hat{\varepsilon}_-^{[II]} \exp[i(\omega t - kz)]\} \tag{2.3-11}$$

Thus, the real mirror transforms a LHCP wave to a RHCP wave, and vice versa.

The operation of the conjugate mirror yields, using the same incident field given by (2.3-9), an output field (in the [II]-system) as

$$\vec{E}_2^{[II]}(\vec{r},t) = \mathrm{Re}\{\hat{\varepsilon}_+^{[II]} \exp[i(\omega t - kz)]\} \tag{2.3-12}$$

Therefore, as opposed to the operation of the real mirror, the conjugate mirror transforms a LHCP wave to a LHCP wave and vice versa. To an observer traveling with the field, the conjugate field exactly retraces the spatial locus of points of the "tip" of the rotating $\vec{E}$-vector corresponding to the incident field. In the next section we will investigate the phase conjugate interaction from a microscopic

point of view.

2.4 A Photon Angular Momentum and Helicity Description of the Phase Conjugate Interaction

In this section we will briefly examine a photon picture describing the conjugate mirror interaction. Specifically, we will consider the photon angular momentum and helicity aspects as a result of the interaction of a photon with a phase conjugator.

In order to explore these properties on a quantum level, we recall that a LHCP(RHCP) photon, described earlier by the field unit vector $\hat{\varepsilon}_+(\hat{\varepsilon}_-)$, possesses a $+\hbar(-\hbar)$ component of angular momentum along its direction of propagation [2,5]. Using this definition we see that the angular momentum eigenstates of $\vec{E}_1$, $\vec{E}_2$, and $\vec{E}_3$ (from the last section) are given by $L_z = +\hbar, -\hbar$, and $+\hbar$, respectively (in the [I]-system). Therefore, the angular momentum change (along the z-axis), or equivalently, the photon spin change, upon reflection is given by $[\Delta(L_z) \equiv (L_z)_{2,3} - (L_z)_1]$

$$\Delta(L_z) = \begin{cases} 0 & \text{real mirror} \\ -2\hbar & \text{phase conjugate mirror} \end{cases} \qquad (2.4\text{-}1)$$

From (2.4-1) we therefore see that for the case of a conjugate mirror there is a photon spin-flip upon conjugation with no such spin change for a conventional mirror.

We next wish to examine the effect of these two types of mirrors upon the helicity state of the photon. The helicity operator, H, is defined by [5]

$$H = \frac{\vec{L} \cdot \vec{p}}{|\vec{L}||\vec{p}|} \qquad (2.4\text{-}2)$$

where $\vec{p} = \hbar\vec{k}$ and $|L,L_z> = \hbar|1,\pm 1>$ for photons.

Using the above definitions, the helicity states of $\vec{E}_1$, $\vec{E}_2$, and $\vec{E}_3$ are given by +1, +1, and -1, respectively. We can now calculate the helicity changes. From (2.4-2), and realizing that the "reflected" photon has its $\vec{k}$-vector or linear momentum directed along a direction opposite to the incident vector (for both types of mirrors), the resultant helicity change upon reflection is given by $[\Delta(H) \equiv H_{2,3} - H_1]$

$$\Delta(H) = \begin{cases} -2 & \text{real mirror} \\ 0 & \text{phase conjugate mirror} \end{cases} \qquad (2.4\text{-}3)$$

We note that for a RHCP input field, the magnitude of the results in (2.4-1 and -3) are unchanged, except for a sign change.

From the above arguments we see that a conjugate mirror essentially "unwinds" the helix that describes the input photon trajectory, or equivalently, gives rise to a photon spin-flip. Thus, the sense of both the angular and linear momentum vectors of the photon are reversed. In contrast, the real mirror yields no such spin-flip, leaving the reflected photon angular momentum unchanged, while reversing only its linear momentum. These ideas are summarized in Figure 2.4, where both the wave and photon pictures are given for both a real mirror (Figure 2.4a) and a phase conjugate mirror (Fig. 2.4b).

Hence, as expected, both the photon and field descriptions regarding the action of the phase conjugate mirror (and the corresponding comparison with a real mirror) agree with each other. As mentioned

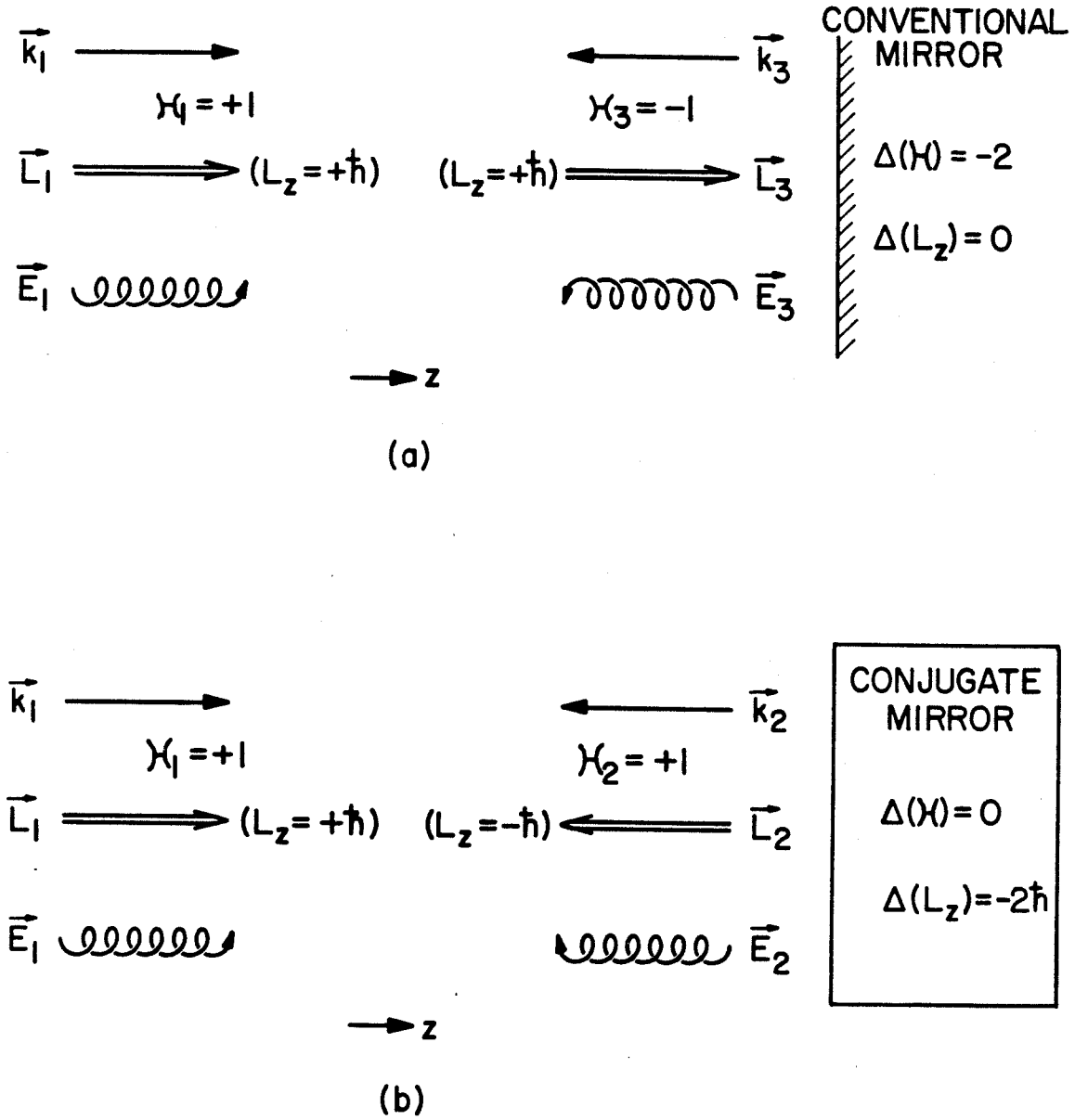

Fig. 2.4 Comparison of a real mirror (a) with a phase conjugate mirror (b) in terms of its effect upon the incident and reflected photon's linear and angular momentum. Also shown is the helicity change upon reflection for each case.

earlier, superpositions of photons (or fields) can now be formed in order to evaluate the properties of a general (monochromatic) complex, conjugate wave. In the next chapter, we will investigate the specific details of the conjugator itself from both a classical (field) and a quantum viewpoint, with emphasis upon phase conjugation via four-wave mixing.

Before proceeding, we emphasize the fact that the kinematic properties of the phase conjugator as discussed in the last several sections assumed the existence of an "ideal" conjugator. In reality, however, these "time-reversal" properties may not all strictly hold. For example, for certain classes of conjugators, not all incident (arbitrary) wave fronts may realize the same "reflection" coefficient. This could be due to angle-dependent effects such as phase mismatching of the input and conjugate waves (to be discussed in the next chapter), or thermal motion effects within the conjugator itself (see Refs. 35 and 63 of Chapter I). Further, the "reflectivity" may not be uniform, due to either the geometrical configuration of the conjugator or saturation effects (to be discussed in the next chapter).

There may also be additional dynamic constraints due to the conjugator which may affect the angular momentum (or helicity) properties that relate the input probe and the (conjugated) output field. For example, the thermal effects as mentioned above may lead to an angle-dependent polarization rotation of the input and output fields. This may not be desirable in terms of correcting for stress-induced birefringence of optical components (or other polarization scrambling effects). Further, the angular momentum selection rules that relate to the

specific quantum levels of the atomic (or molecular) species which constitute the nonlinear medium, or equivalently, the tensorial elements of the nonlinear susceptibility [3,4] could affect the ability of the phase conjugate mirror to "time reverse" arbitrary rotating input $\vec{E}$-fields that are incident along arbitrary directions.

We conclude on a positive note by mentioning that the time-reversal properties of the PCM as discussed thus far in this chapter have all been verified experimentally. One must be judicious in selecting the given class of the PCM (e.g., type of nonlinear interaction), the geometry (e.g., specific shape of the medium; orientation, wavelength, and polarization state of any additional input fields), as well as the specific nonlinear medium comprising the PCM in order to satisfy one's needs (e.g., operating wavelength efficiency, desired reflection coefficient, angular acceptance range, input signal intensity range, input polarization state, etc.).

2.5 Compensation for Nonlinear Optical Phase Distortions via Optical Phase Conjugation

The ability of nonlinear optical phase conjugate mirrors (PCM) to correct for linear phase (refractive index) inhomogeneities has been demonstrated both theoretically and experimentally [1]. In cases involving propagation of high intensity optical beams, there can occur higher order, field-dependent, nonlinear contributions [6,7] to the index of refraction such as thermal blooming or self-focusing that one would wish to compensate. These distortions are often manifested in

high intensity atmospheric propagation of laser beams, thermally-induced lensing within intracavity laser gain media, or in high intensity transmission through optical fibers. In this section, we extend the analysis of Section 2.2 to consider the effect of conjugate-wave propagation through media characterized by a more general complex permittivity containing linear and nonlinear field-dependent contributions [10].

A typical geometry is sketched in Figure 2.5. We consider a monochromatic electromagnetic field at radian frequency ω, which propagates essentially in the +z direction, and is given by

$$E_1(\vec{r},t) = \psi(\vec{r}) \exp[i(\omega t - kz)] + c.c. \qquad (2.5\text{-}1)$$

This field encounters a region of space characterized by a complex intensity- and spatial-dependent permittivity, ε. After passage through this medium, the resultant field is incident upon a PCM which gives rise to a (conjugate) field given by

$$E_2(\vec{r},t) = f(\vec{r}) \exp[i(\omega t + kz)] + c.c. \qquad (2.5\text{-}2)$$

This field (E_2) propagates along the -z direction and therefore back through the nonlinear medium.

We now investigate under what conditions the complex conjugate of the wave equation satisfied by E_1 and the wave equation of E_2 are identical. When that happens, then $f(\vec{r}) = \psi^*(\vec{r})$ everywhere (prior to the PCM), and the "time-reversed" propagation occurs, as discussed in Section 2.2.

We consider the general case when both fields coexist in time (the compensation scheme will also work for the case of temporally separated fields). Hence, the total field in space is given by

$$E(\vec{r},t) = [\psi(\vec{r}) \exp(-ikz) + f(\vec{r}) \exp(ikz)] \exp(i\omega t) + c.c. \qquad (2.5\text{-}3)$$

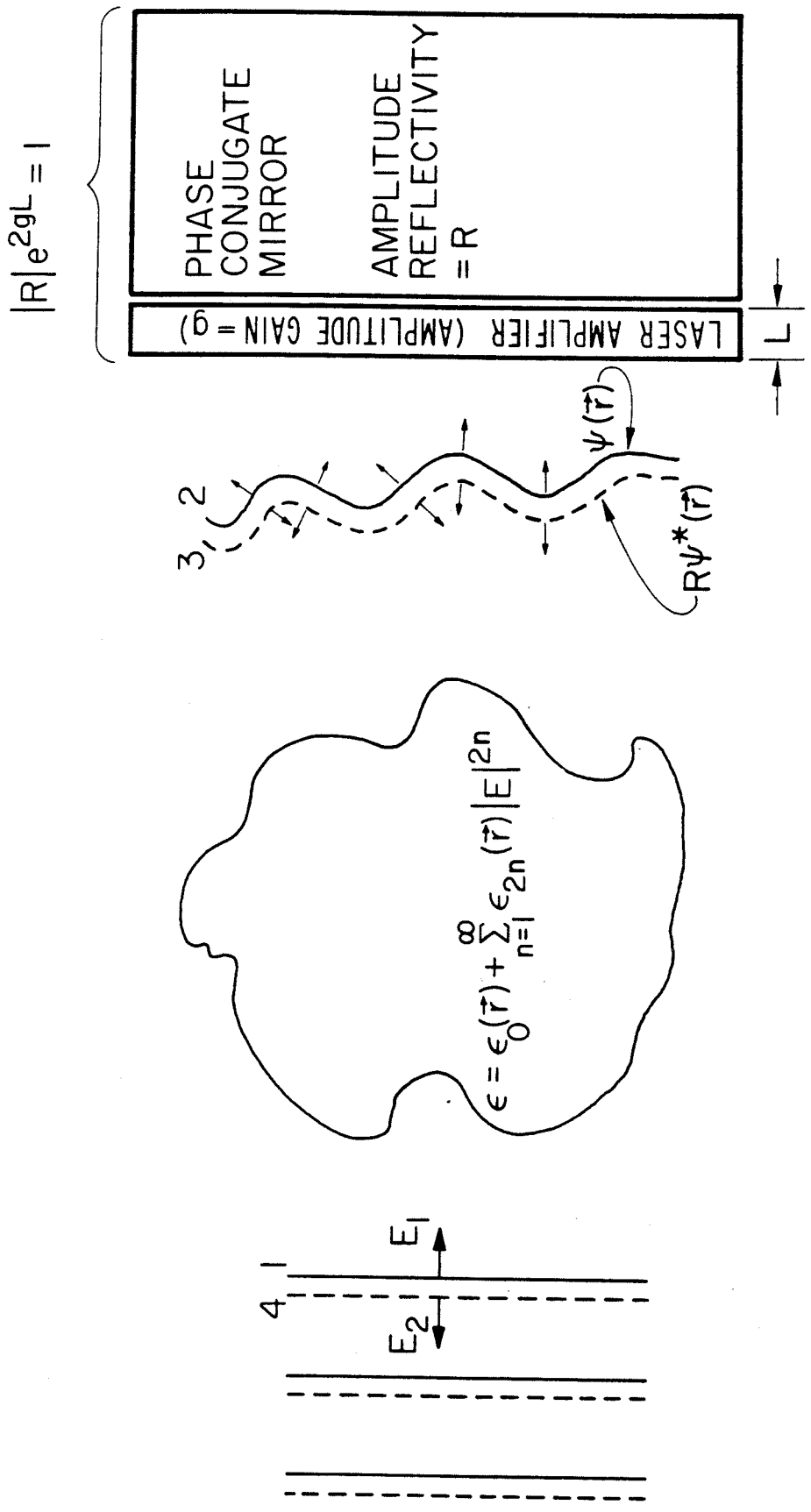

Fig. 2.5 Typical geometry for a PCM in order to compensate for nonlinear phase distortions, ϵ. Solid (dashed) curves correspond to the incident (conjugate, or time-reversed) equiphase surfaces. Arrows indicate local propagation vectors. If $|R| < 1$, then the use of a conventional laser amplifier satisfying $|R|\exp[2gL] = 1$ is required to insure proper nonlinear phase compensation.

We assume that the isotropic nonlinear medium can be described by the following permittivity

$$\varepsilon = \varepsilon_0(\vec{r}) + \sum_{n=1}^{\infty} \varepsilon_{2n}(\vec{r}) \, |E|^{2n} + i\varepsilon_I(\vec{r}) \qquad (2.5\text{-}4)$$

where the first term describes the linear, spatially-dependent refractive index inhomogeneities, and the summation depicts the nonlinear (intensity-dependent), spatially-dependent refractive index contributions. The term proportional to $|E|^2$ (n=1), for example, is called the intensity-dependent refractive index (or the optical Kerr coefficient), and is responsible for the nonlinear effects discussed earlier. Finally, the last (imaginary) term describes the loss (or gain) properties characterizing the medium.

In the analysis that follows, we retain only the first order nonlinear index term in the above power series. It can be easily shown that the analysis will yield similar results for all successive intensity-dependent terms of ε.

Assuming "slow" variations of ε, i.e., $\frac{1}{\varepsilon}|d\varepsilon/dx|\lambda << 1$, the wave equation is given by

$$\nabla^2 E - \frac{\mu}{c^2}\left[\varepsilon_0(\vec{r}) + \varepsilon_2(\vec{r}) \, |E|^2\right] \frac{\partial^2 E}{\partial t^2} = 0 \qquad \text{(in cgs)} \qquad (2.5\text{-}5)$$

Substitution of the field (2.5-3) into (2.5-5) yields

$$\{\nabla^2\psi(\vec{r}) + [\frac{\omega^2\mu}{c^2}\,\varepsilon_0(\vec{r}) + i\varepsilon_I(\vec{r}) - k^2]\,\psi(\vec{r}) + \frac{\omega^2\mu}{c^2}\,\varepsilon_2(\vec{r})|E|^2\psi(\vec{r}) - 2ik\,\frac{\partial\psi(\vec{r})}{\partial z}\}$$

$$\times \exp(-ikz) + \{\nabla^2 f(\vec{r}) + [\frac{\omega^2\mu}{c^2}\,\varepsilon_0(\vec{r}) + i\varepsilon_I(\vec{r}) - k^2]f(\vec{r})$$

$$+ \frac{\omega^2\mu}{c^2}\,\varepsilon_2(\vec{r})|E|^2\,f(\vec{r}) + 2ik\,\frac{\partial f(\vec{r})}{\partial z}\}\,\exp(+ikz) = 0 \qquad (2.5\text{-}6)$$

Using (2.5-3) we express $|E|^2$ as

$$|E|^2 = |\psi(\vec{r})|^2 + |f(\vec{r})|^2 + \psi^*(\vec{r})f(\vec{r})\,\exp(2ikz) + \psi(\vec{r})f^*(\vec{r})\,\exp(-2ikz) \qquad (2.5\text{-}7)$$

which, when substituted in (2.5-6), gives

$$\nabla^2\psi(\vec{r}) + [\frac{\omega^2\mu\varepsilon_0(\vec{r})}{c^2} + i\varepsilon_I(\vec{r}) - k^2]\psi(\vec{r}) + \frac{\omega^2\mu}{c^2}\,\varepsilon_2(\vec{r})[|\psi(\vec{r})|^2 + 2|f(\vec{r})|^2]$$

$$\times\ \psi(\vec{r}) - 2ik\,\frac{\partial\psi(\vec{r})}{\partial z} = 0 \qquad (2.5\text{-}8)$$

and

$$\nabla^2 f(\vec{r}) + [\frac{\omega^2\mu\varepsilon_0(\vec{r})}{c^2} + i\varepsilon_I(\vec{r}) - k^2]f(\vec{r}) + \frac{\omega^2\mu}{c^2}\,\varepsilon_2(\vec{r})[2|\psi(\vec{r})|^2 + |f(\vec{r})|^2]f(\vec{r})$$

$$+ 2ik\,\frac{\partial f(\vec{r})}{\partial z} = 0 \qquad (2.5\text{-}9)$$

In arriving at (2.5-8,9) we set all terms having the exponential dependences, exp(-ikz) and exp(+ikz) equal to zero separately, and neglected any nonsynchronous terms (in this case having exp(±3ikz) dependence).

Note that as a result of the existence of the nonlinear index term (i.e., $\varepsilon_2 \neq 0$), and the coexistence of the counterpropagating fields

[i.e., [2.5-3)], we see from (2.5-7) and (2.5-6) that an additional synchronous term in exp(+ikz) results, which involves the term from the product $\psi^*(\vec{r})f(\vec{r})\psi(\vec{r})$. This term accounts for the additional factor of $|\psi(r)|^2$ in the differential equation in f(r); a similar symmetric coupling yields the added $|f(\vec{r})|^2$ term in the differential equation in $\psi(\vec{r})$.

Taking the complex conjugate (2.5-8) results in

$$\nabla^2\psi^*(\vec{r}) + [\frac{\omega^2\mu\varepsilon_o(\vec{r})}{c^2} - i\varepsilon_I(\vec{r}) - k^2]\psi^*(\vec{r}) + \frac{\omega^2\mu\varepsilon_2(\vec{r})}{c^2}[|\psi(\vec{r})|^2 + 2|f(\vec{r})|^2] \times \psi^*(\vec{r}) + 2ik\frac{\partial\psi^*(\vec{r})}{\partial z} = 0 \qquad (2.5\text{-}10)$$

Upon inspection of (2.5-9,10), we see that the following two conditions need be obeyed in order that $\psi^*(\vec{r})$ and $f(\vec{r})$ satisfy the same wave equation

$$\text{(i)} \quad |\psi(\vec{r})| = |f(\vec{r})|$$

and $\qquad (2.5\text{-}11)$

$$\text{(ii)} \quad \varepsilon_I(\vec{r}) = 0$$

The first condition dictates that the phase conjugate mirror must be adjusted to yield a unity magnitude (nonlinear) reflectivity (i.e., $|R| = 1$, where R is the complex reflection coefficient characterizing the PCM). The second condition is satisfied when the nonlinear medium possesses no loss (or gain).

Under these two conditions, $\psi^*(\vec{r}) = f(\vec{r})$, and thus the form of E_2 as defined in (2.5-2) is

$$E_2(\vec{r},t) = \psi^*(\vec{r}) \exp[i(\omega t + kz)] + c.c. \qquad (2.5\text{-}12)$$

The field E_2 is thus found to be the "conjugate wave" of E_1, as discussed in Section 2.2. We conclude that under the conditions given in (2.5-11), the use of a PCM is capable of yielding a time-reversed replica of an incident monochromatic field which has been initially aberrated as a result of propagation through a general, nonlinear (intensity-dependent), inhomogeneous phase distorting medium, provided the amplitude of the reflected conjugate wave is adjusted to be equal to the incident wave before it enters the nonlinear medium. This last condition was not necessary in phase compensation in linear media.

Perhaps a more subtle point regarding the coexistent forward and backward-going fields case is that, in addition to the discussion above, inherent in the wave equations (2.5-9,10) is a nonlinear coupling of fields $\psi(\vec{r})$ and $f(\vec{r})$ via the intensity-dependent medium itself. In the language of nonlinear optics [6,8], various third order phase-matched nonlinear polarizations are formed within the medium (as a result of a nonzero $\varepsilon_2(\vec{r})$, providing a coupling of fields $\psi(\vec{r})$ and $f(\vec{r})$ into themselves as well as into each other. Under the condition that $\psi^*(\vec{r}) = f(\vec{r})$, these couplings are all symmetric, resulting in identical propagation evolutions as discussed earlier.

In practice it may not always be possible to realize a PCM of unity (magnitude) reflectivity. The "effective" reflectivity can then be set to unity by using a laser amplifier (assumed to be in the unsaturated regime) in front of the PCM such that the product of the double-pass gain of the amplifier and the PCM reflectivity is equal to unity. This geometry is sketched in Figure 2.5. An added bonus of this scheme is that any (non-intensity dependent) phase and/or polarization distortion of the amplifier is corrected by the PCM.

Prior to concluding this section, we discuss a remark made by Bridges and Pearson [10]. The authors mention that for phase aberrations distributed along the propagation path from the near-field region to the far-field (focal plane) region, their COAT [as well as our PCO] system could not yield perfect compensation. This is due to the phase distortions in the far-field transforming to amplitude distortions at the transmitter plane, which was shown earlier in this section to be incapable of perfect compensation.

Alternatively, this result follows physically from the fact that due to the finite size of the target, diffractive effects result in amplitude distortions at the phase conjugator's input plane. In the Fraunhofer limit [11], the field distribution at the conjugator input plane is essentially the spatial Fourier transform of the product of the aperture function of the target with the spatial phase distortion element. These amplitude distortions are due to the interference of the various, complex plane wave (monochromatic) components which are radiated from the target. Now, due to the finite size of the conjugator, only a

finite number of these plane wave components are time reversed. This fact, coupled with the diffractive effects of the conjugator's finite aperture itself, results in a "conjugate" output wave that cannot exactly retrace the path of the input field. Of course, a phase conjugate mirror of essentially infinite spatial extent (or equivalently, possessing a system f-number approaching zero)

<u>can</u> compensate for finite sized targets, since all plane wave components that are diffracted from the target are received by the PCM and are thus perfectly time reversed, regardless of the location of the phase aberrator.

In conclusion, we have shown that any nonlinear (intensity-dependent), spatially-dependent phase aberration can be compensated by the use of a PCM. Thus, undesirable distortions such as atmospheric thermal blooming and even intracavity (circulating laser intensity) induced lensing effects can be corrected through the use of a PCM outside the resonator, or as its use in replacing one (or both) of the mirrors comprising a laser cavity [9], respectively. We note that <u>catastrophic</u> self-focusing, which can lead to other nonlinear effects such as stimulated Brillouin or Raman scattering, optical damage, or beam breakup, obviously <u>cannot</u> be corrected by the scheme discussed herein.

Appendix 2A

Conjugate Wave Propagation in Linear Lossy (or Gain) Media

In this appendix we discuss the conditions under which a PCM can compensate for phase aberrations when the distorting medium is also lossy. For simplicity, we assume that the medium is of length L, and is characterized by an (intensity) absorption coefficient, α .

We take the forward- and backward-going fields as

$$E_1(\vec{r},t) = \psi(\vec{r}) \exp[i(\omega t) - (ik + \alpha/2)z] + c.c. \qquad (2.A\text{-}1)$$

and

$$E_2(\vec{r},t) = f'(\vec{r}) \exp[i(\omega t) + (ik + \alpha/2)z - \frac{\alpha}{2} L] + c.c.$$

$$= f(\vec{r}) \exp[i(\omega t) + (ik + \alpha/2)z] + c.c. \qquad (2.A\text{-}2)$$

respectively. We assume that the PCM is located at the plane z = 0.

The wave equation is given by

$$\nabla^2 E - \frac{\mu(\varepsilon_R - i\varepsilon_I)}{c^2} \frac{\partial^2 E}{\partial t^2} = 0 \qquad (2.A\text{-}3)$$

Now, taking $\varepsilon_R = n^2(1 - \alpha^2/4k^2)$, $\varepsilon_I = n^2\alpha/k$ [6], and $\omega = kc/n$; substituting $E = E_1 + E_2$ in (2.A-3) we get, collecting and setting the synchronous terms $\exp(\pm ikz)$ separately equal to zero, the two following equations:

$$\exp[-\alpha z/2] \{\nabla^2 \psi^*(\vec{r}) + 2(ik - \alpha/2) \frac{\partial \psi^*(\vec{r})}{\partial z} \} = 0 \qquad (2.A\text{-}4)$$

and

$$\exp[+\alpha z/2] \{\nabla^2 f(\vec{r}) + 2(ik + \alpha/2) \frac{\partial f(\vec{r})}{\partial z} \} = 0 \qquad (2.A\text{-}5)$$

where the complex conjugate of the differential equation $\psi(\vec{r})$ has been taken.

We therefore see that if

$$k >> \alpha/2 \tag{2.A-6}$$

then at a given z-plane, the above two differential equations are identical if

$$f(\vec{r}) = \exp(-\alpha z)\ \psi^*(\vec{r}) \tag{2.A-7}$$

The condition (2.A-6) implies that each wave has its amplitude change negligibly over an optical wavelength. We therefore see, in general, that as long as

$$f(\vec{r}) = a(z)\ \psi^*(\vec{r}) \tag{2.A-8}$$

where a(z) is a z-dependent, complex quantity characterizing the <u>linear</u> distorting medium, then the action of a PCM will result in a backward-going field that unravels the phase distortion. Hence, aside from a constant amplitude or phase factor due to a(z), the <u>shape</u> of the equiphase surfaces, even in the case of lossy (but spatially homogeneous) media, is the same for both E_1 and E_2 at a given transverse spatial plane, thus resulting in a time-reversed wavefront.

Chapter II - References

1. See, for example, A. Yariv, "Phase conjugate optics and real-time holography," IEEE J. Quant Electron. QE-14, 650 (1978).

2. J. D. Jackson, Classical Electrodynamics, 2nd ed. (Wiley, New York, 1975), Ch. 7.

3. R. W. Hellwarth, "Method for generating the time-reversed replica of a monochromatic wave having an arbitrary, spatially varying, vector amplitude," Hughes Research Laboratories Interdepartmental Correspondence, Sept. 25, 1978.

4. B. Ya. Zel'dovich and V. V. Shkunov, "Spatial-polarization wavefront reversal in four-photon interaction," Kvant. Elektron. (Moscow) 6, 629 (1979) [Sov. J. Quant. Electron. 9, 379 (1979)].

5. See, for example, W.S.C. Williams, An Introduction to Elementary Particles, 2nd ed. (Academic Press, New York, 1971), Ch. 13. (Note that this reference defines RHCP and LHCP waves opposite to that of Ref. 2 above).

6. A. Yariv, Quantum Electronics, 2nd ed. (Wiley, New York, 1975).

7. R. W. Hellwarth, "Third order optical susceptibilities of liquids and solids," Prog. Quant. Electron. 5, 1 (1977).

8. P. D. Maker and R. W. Terhune, "Study of optical effects due to an induced polarization third order in the electric field strength," Phys. Rev. 137, A801 (1965).

9. J. AuYeung, D. Fekete, D. M. Pepper, and A. Yariv, "A theoretical and experimental investigation of the modes of optical resonators with phase conjugate mirrors," IEEE J. Quant. Electron. QE-15, 1180 (1979).

10. W. B. Bridges and J. E. Pearson, "Thermal blooming compensation using coherent optical adaptive techniques (COAT)," Appl. Phys. Lett. 26, 539 (1975). We note that the COAT technique used in the authors' experiment involved electrooptic aperture phase control of a single, forward propagating beam. The criterion for the phase distribution

of the launched wave was the maximization of the irradiance incident on a target glint following the distorting medium. This differs from our scheme which depends on phase conjugation and reverse propagation for the correction.

11. J. W. Goodman, Introduction to Fourier Optics (McGraw-Hill, New York, 1968), Ch. 4.

Chapter III

PHASE CONJUGATION VIA OPTICAL PARAMETRIC INTERACTIONS

3.1 Introduction

In the last chapter, we discussed the basic properties of phase conjugators and how they affect an incident wave as seen from both a microscopic (i.e., photon) and a macroscopic (i.e., field) description. We are now in a position to investigate the mechanisms of the phase conjugator itself. The class of phase conjugator devices we will consider here consists of those involving optical parametric interactions; or from a photon point of view, those involving elastic photon-atomic scattering processes. We will consider two special cases: that of three-wave and four-wave mixing, and in the process we will compare and contrast these two approaches. In the appendix we tabulate several additional mixing processes that can yield phase conjugate replicas.

Using the formalisms of nonlinear optics we will analyze the specific case of phase conjugation via degenerate four-wave mixing in some detail using a plane wave, coupled-mode treatment. It is to this process that the major portion of this work will be dedicated. We will then extend the analysis to consider conjugation of arbitrary incident wavefronts (i.e., multiplanar spatial mode fields). We will then discuss briefly the effects of certain competing linear and nonlinear loss mechanisms upon the conjugation process.

We will also present a cursory description of the third order nonlinear optical susceptibility which couples the various interacting fields (and which was treated as a phenomenological parameter in the

previous treatment) from a quantum mechanical viewpoint. We will utilize both the time evolution operator formalism (along with the associated Feynman diagrams) and a density matrix perturbation approach, in treating this problem. As specific examples, we will analyze both one- and two-photon transitions (using two- and three-level quantum systems, respectively) in arriving at an expression for the desired, steady state, third order nonlinear coupling function.

The chapter will conclude with a brief discussion of the operational analogs (and also the various differences) of four-wave nonlinear optical mixing with real-time holography. This will provide the motivation for several of the "spatial-domain" applications to be discussed in Chapter V.

The results of this chapter will be relevant to the analysis of several experiments we performed (to be discussed in the next chapter), as well as to providing a formalism upon which a myriad of application areas using four-wave phase conjugators can be examined, several of which will be considered in the last three chapters of this work.

3.2 Phase Conjugation via Three-Wave Mixing

We now consider a specific case of phase conjugate wavefront generation by nonlinear optical mixing: that of phase conjugation via three-wave mixing, first proposed by Yariv [1] and experimentally verified by Avizonis, et al. [2,3]. The scheme involves the nonlinear mixing of two input waves: a "probe" wave, E_1, at a frequency ω with wavevector $\vec{k}_1(\omega)$ and an intense "pump" wave, E_2, at a frequency 2ω with wavevector $\vec{k}_2(2\omega)$. These two fields are incident simultaneously upon a medium, which

couples the fields to yield a third wave, E_3, which is proportional to $E_1^* E_2$ and of frequency $\omega_3 = \omega = 2\omega - \omega$. The medium is assumed to possess a nonzero second order nonlinear optical susceptibility, $\chi_{NL}^{(2)}$.

We consider these fields to be of the form

$$E_i(\vec{r},t) = \frac{1}{2} A_i(r_i) \exp\{i(\omega_i t - \vec{k}_i \cdot \vec{r})\} + \text{c.c.}$$

$$i = 1,2,3 \qquad (3.2\text{-}1)$$

where A_i are the complex amplitudes of the fields, and $A_3 \propto A_1^* A_2$ is sought. A nonlinear polarization [4,5] is formed in the medium as a result of the mixing of the two input fields:

$$P_{NL}^{(\omega_3=\omega=\omega_2-\omega_1)} = \frac{1}{2} \chi_{NL}^{(2)} A_1^* A_2 \exp\{i[(2\omega-\omega)t - (\vec{k}_2(2\omega) - \vec{k}_1(\omega)) \cdot \vec{r}]\}$$

$$+ \text{c.c.} \qquad (3.2\text{-}2)$$

If the pump wave, E_2, is a plane wave, then the nonlinear polarization gives rise to a conjugate replica of E_1 which, in this case propagates in the forward direction. Since the nonlinear polarization has a wavevector $\vec{k}_2(2\omega) - \vec{k}_1(\omega)$, and the field E_3 propagates with a wavevector $\vec{k}_3(\omega)$, constructive interference of the nonlinear dipoles within the medium occurs if

$$|\Delta\vec{k}|L = |\vec{k}_2(2\omega) - \vec{k}_1(\omega) - \vec{k}_3(\omega)|L \lesssim 2\pi \qquad (3.2\text{-}3)$$

where L is the interaction length. This condition, known as the phase matching constraint, ensures that the wavefronts of E_3 add up in phase throughout the medium so as to yield a maximum output amplitude.

Although this process radiates a wave (E_3) that is the conjugate replica of the probe field (E_1), it has several drawbacks. First, for

typical nonlinear media [5] $2\pi/|\vec{\Delta k}|$ is on the order of 100 μm, therefore limiting the maximum interaction length for efficient nonlinear coupling. A second drawback is that the phase matching constraint is angle dependent. This limits the angular acceptance range of the probe wave that will satisfy (3.2-3) for a given interaction length. Also, since the probe and conjugate waves copropagate, the system requires an additional optical element [1] to realize a backward-going (time-reversed) conjugate replica: a conventional "real" plane reflecting mirror, effectively changing $\vec{k}_3 \rightarrow -\vec{k}_1$ for each plane wave component of E_3. Finally, these three-wave mixing processes are restricted to media lacking inversion symmetry [4,5]; otherwise, $\chi_{NL}^{(2)}$ is identically equal to zero.

All the above drawbacks and limitations can be obviated by utilizing a degenerate four-wave nonlinear mixing process.

3.3 Phase Conjugation via Degenerate Four-Wave Mixing

In this section, we present a coupled mode analysis of phase conjugation via backward-wave degenerate four-wave mixing. The geometry is shown in Figure 3.1. We assume two intense counterpropagating cw pump waves, denoted by E_1 and E_2, to be incident on a medium of length L possessing a third-order nonlinear optical susceptibility $\chi_{NL}^{(3)}$. We assume that $\chi_{NL}^{(3)}$ is a constant characterizing the medium; its physical origin will be examined later in the chapter. Also incident simultaneously on the medium is a third (probe) wave, E_4, propagating along an arbitrary direction relative to the pump fields whose phase conjugate replica is sought. The desired output wave is defined to be E_3.

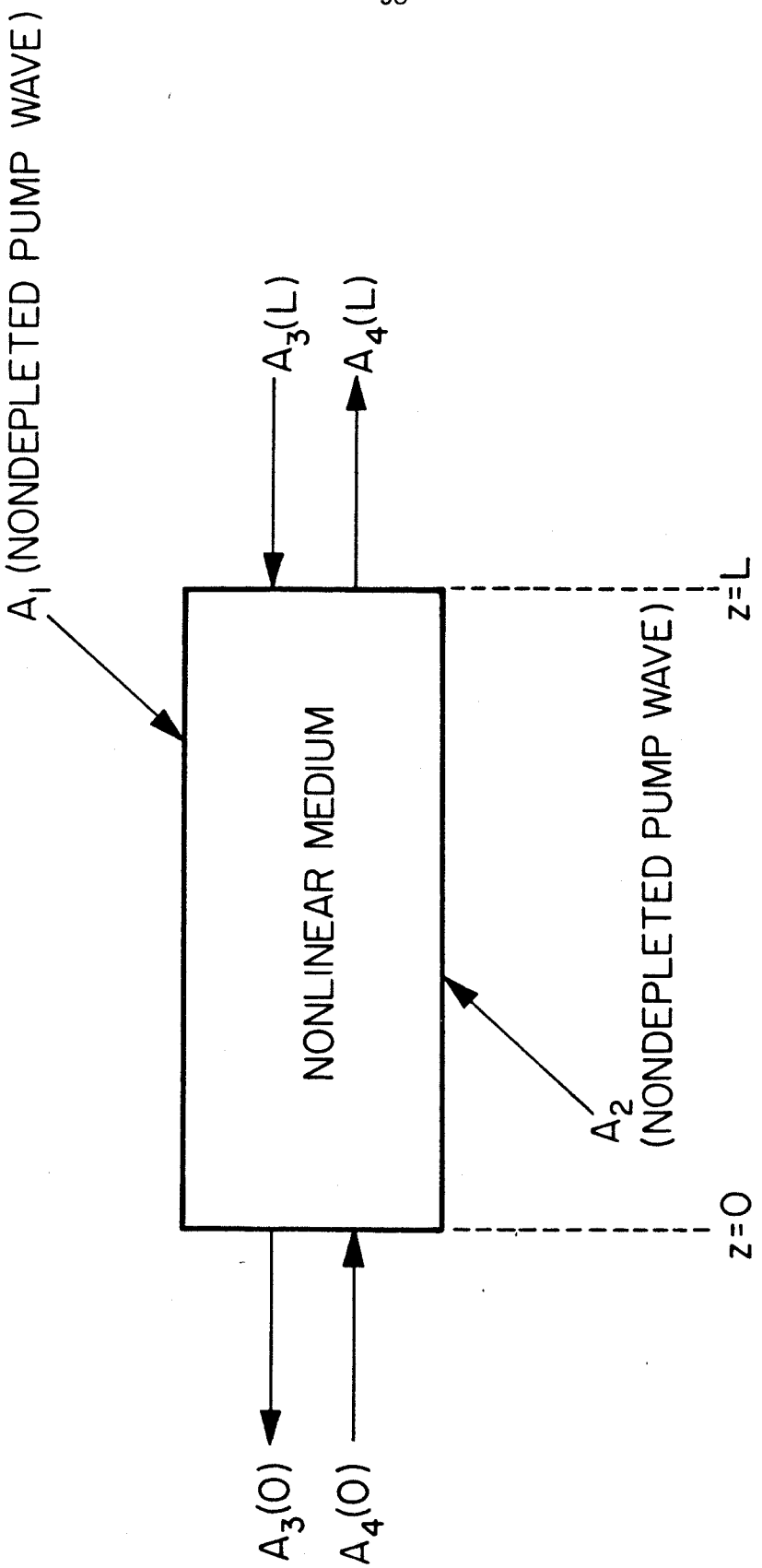

Fig. 3.1 Four-wave mixing geometry. The pump wave amplitudes, A_1 and A_2, are assumed to be nondepleted.

All four fields are taken to be plane waves of the form

$$E_i(\vec{r},t) = \frac{1}{2} A_i(r_i) \exp[i(\omega_i t - \vec{k}_i \cdot \vec{r})] + \text{c.c.} \qquad (3.3\text{-}1)$$

where A_i is a complex amplitude and c.c. denotes the complex conjugate, and all fields are taken to be of the same frequency, ω (i.e., degenerate).

The two pump fields couple with the probe wave via the third order nonlinear optical susceptibility within the medium to yield a nonlinear polarization of the form

$$P_{NL}^{(\omega_3=\omega=\omega+\omega-\omega)} = \frac{1}{2} \chi_{NL}^{(3)} A_1 A_2 A_4^* \exp\{i[(\omega+\omega-\omega)t - (\vec{k}_1+\vec{k}_2-\vec{k}_4)\cdot\vec{r}]\} + \text{c.c.} \qquad (3.3\text{-}2)$$

which radiates to give rise to the field, E_3. This field in turn couples with the pump waves to form a resultant nonlinear polarization given by

$$P_{NL}^{(\omega_4=\omega=\omega+\omega-\omega)} = \frac{1}{2} \chi_{NL}^{(3)} A_1 A_2 A_3^* \exp\{i[(\omega+\omega-\omega)t - (\vec{k}_1+\vec{k}_2-\vec{k}_3)\cdot\vec{r}] + \text{c.c.} \qquad (3.3\text{-}3)$$

Since the pump waves propagate in opposition to each other, the sum of their $\vec{k}$ vectors is equal to zero

$$\vec{k}_1(\omega) + \vec{k}_2(\omega) = 0 \qquad (3.3\text{-}4)$$

and, based upon the phase matching constraint, we also have

$$\vec{k}_3(\omega) + \vec{k}_4(\omega) = 0 \qquad (3.3\text{-}5)$$

This implies that the conjugate wave (E_3) will propagate in opposition to the probe wave (i.e., $\vec{k}_3 = -\vec{k}_4$), thus yielding a time-reversed replica of the probe field. We note that this condition is independent of the direction of the probe field, thus enabling the conjugation process to have the same nonlinear gain (or efficiency) for any arbitrary probe wave input angle. Also, since the phase mismatch is identically equal to zero, constructive interference of the nonlinear (conjugate generating) dipoles occurs for any interaction length.

Without loss of generality, we take the fields E_3 at E_4 to lie along the z-axis. We wish to solve for the spatial evolution of the field amplitudes $A_3(z)$ and $A_4(z)$ within the nonlinear medium (occupying the space $0 \leq z \leq L$). This is accomplished by solving the wave equation for the probe and conjugate fields with the proper nonlinear polarization acting as the driving term:

$$\nabla^2 E_i - \frac{\varepsilon}{c^2} \frac{\partial^2}{\partial t^2} E_i = \frac{4\pi}{c^2} \frac{\partial^2}{\partial t^2} P_{NL} , \quad i = 3,4 \tag{3.3-6}$$

where we assume $\mu = 1$, with ε denoting the linear permittivity of the medium.

Neglecting depletion of the pump waves, i.e., putting

$$\frac{dA_i}{dz} = 0 , \qquad i = 1,2 \tag{3.3-7}$$

and invoking the adiabatic approximation

$$\left|\frac{d^2A_i}{dz^2}\right| << \left|\frac{k_i dA_i}{dz}\right|, \left|k_i^2 A_i\right| \quad , \quad i = 3,4 \tag{3.3-8}$$

we obtain the following coupled mode equations

$$\frac{dA_3}{dz} = i\kappa^* A_4^*$$

and (3.3-9)

$$\frac{dA_4^*}{dz} = i\kappa A_3$$

The complex coupling constant, κ, is given by

$$\kappa^* = \frac{2\pi\omega}{nc} \chi_{NL}^{(3)} A_1 A_2 \quad , \tag{3.3-10}$$

where n is the linear index of refraction of the nonlinear medium.

Since the coupled mode equations require two boundary conditions, we can choose to specify the signal and conjugate wave amplitudes at their respective input planes as $A_3(z=L)$ and $A_4(z=0)$. The solutions, subject to these boundary conditions are

$$A_3(z) = \frac{\cos|\kappa|z}{\cos|\kappa|L} A_3(L) + \frac{i\kappa^*}{|\kappa|} \frac{\sin|\kappa|(z-L)}{\cos|\kappa|L} A_4^*(0)$$

and (3.3-11)

$$A_4^*(z) = \frac{i|\kappa|\sin|\kappa|z}{\kappa^*\cos|\kappa|L} A_3(L) + \frac{\cos|\kappa|(z-L)}{\cos|\kappa|L} A_4^*(0)$$

A case of particular interest is one where there exists only a single input probe field, $A_4(0)$, with $A_3(L) = 0$. Under these conditions the reflected wave at the input plane is, from equation (3.3-11),

$$A_3(0) = -i\left(\frac{\kappa^*}{|\kappa|} \tan|\kappa|L\right) A_4^*(0) \tag{3.3-12}$$

while the forward-going probe amplitude at the output plane is

$$A_4(L) = \frac{A_4(0)}{\cos|\kappa|L} \tag{3.3-13}$$

From equations (3.3-12) and (3.3-13) we note some of the major features of this interaction. First, from (3.3-12) we see that $A_3(0) \propto A_4^*(0)$, thus rendering the interacting medium equivalent to a "time-reversal" mirror, with the output wave propagating in a direction opposite to and thus retracing the path of the input field. Second, from (3.3-13), the forward-going field at the output plane is always an <u>amplified</u> version of its initial amplitude. Next, the nonlinear power reflection coefficient, defined to be

$$R \equiv \left|\frac{A_3(0)}{A_4(0)}\right|^2 = \tan^2|\kappa|L \tag{3.3-14}$$

can exceed unity when $|\kappa|L > \pi/4$, thus yielding an <u>amplified</u>, time-reversed output. This can be accomplished in practice by either increasing the interaction length (i.e., L) or by increasing the pump field intensity (since $\kappa^* \propto A_1A_2$). Finally, in the limit $|\kappa|L \to \pi/2$, the reflectivity becomes infinite, resulting in a mirrorless self-oscillation mode. That is,

$$\frac{A_3(0)}{A_4(0)}, \frac{A_4(L)}{A_4(0)} \to \infty \tag{3.3-15}$$

even with no input probe present. This system is a special case of an optical parametric oscillator [6]. Figures 3.2 and 3.3 depict cases of

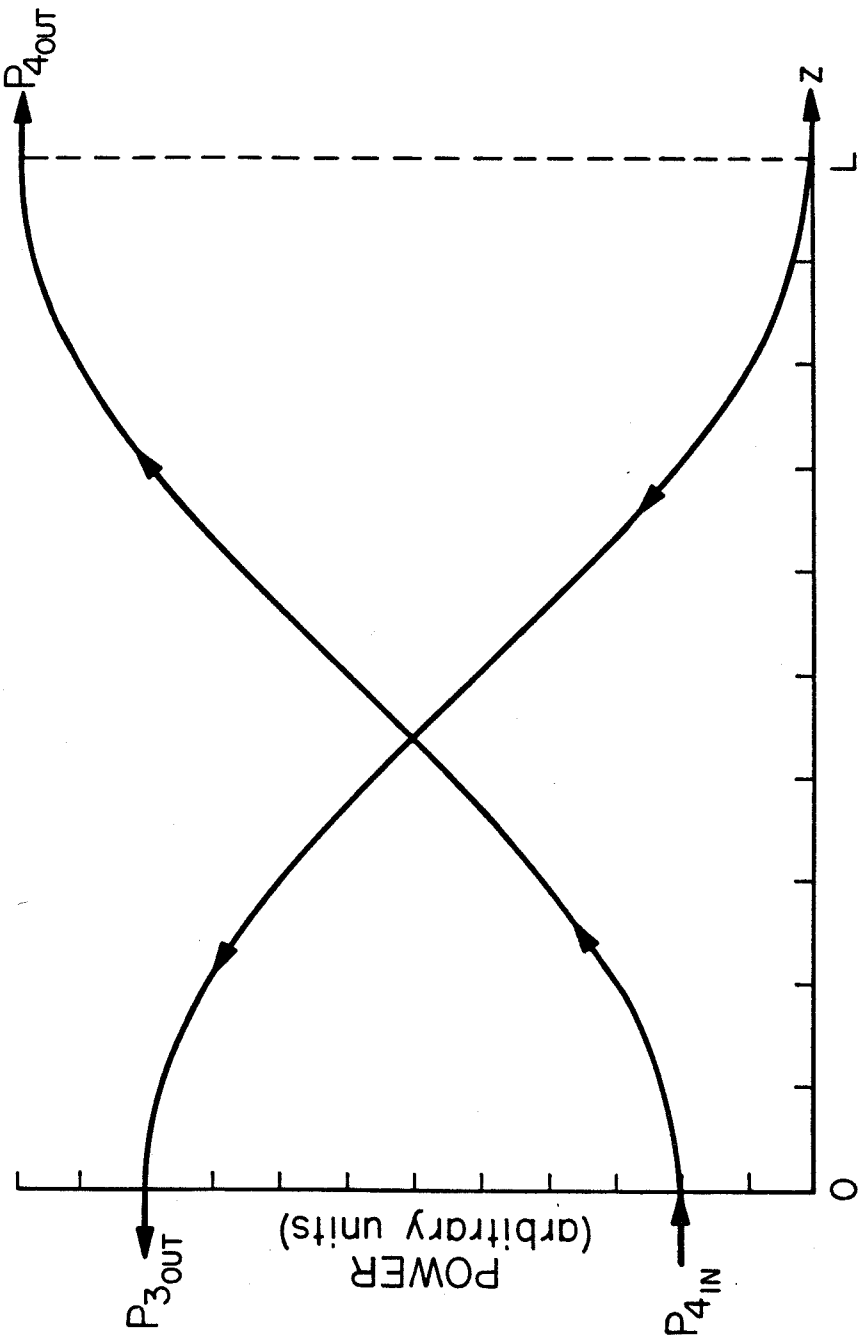

Fig. 3.2 Amplification by four-wave mixing. The power transmission and reflection coefficient for this calculation yields a value of T = 5 and R = 4, respectively.

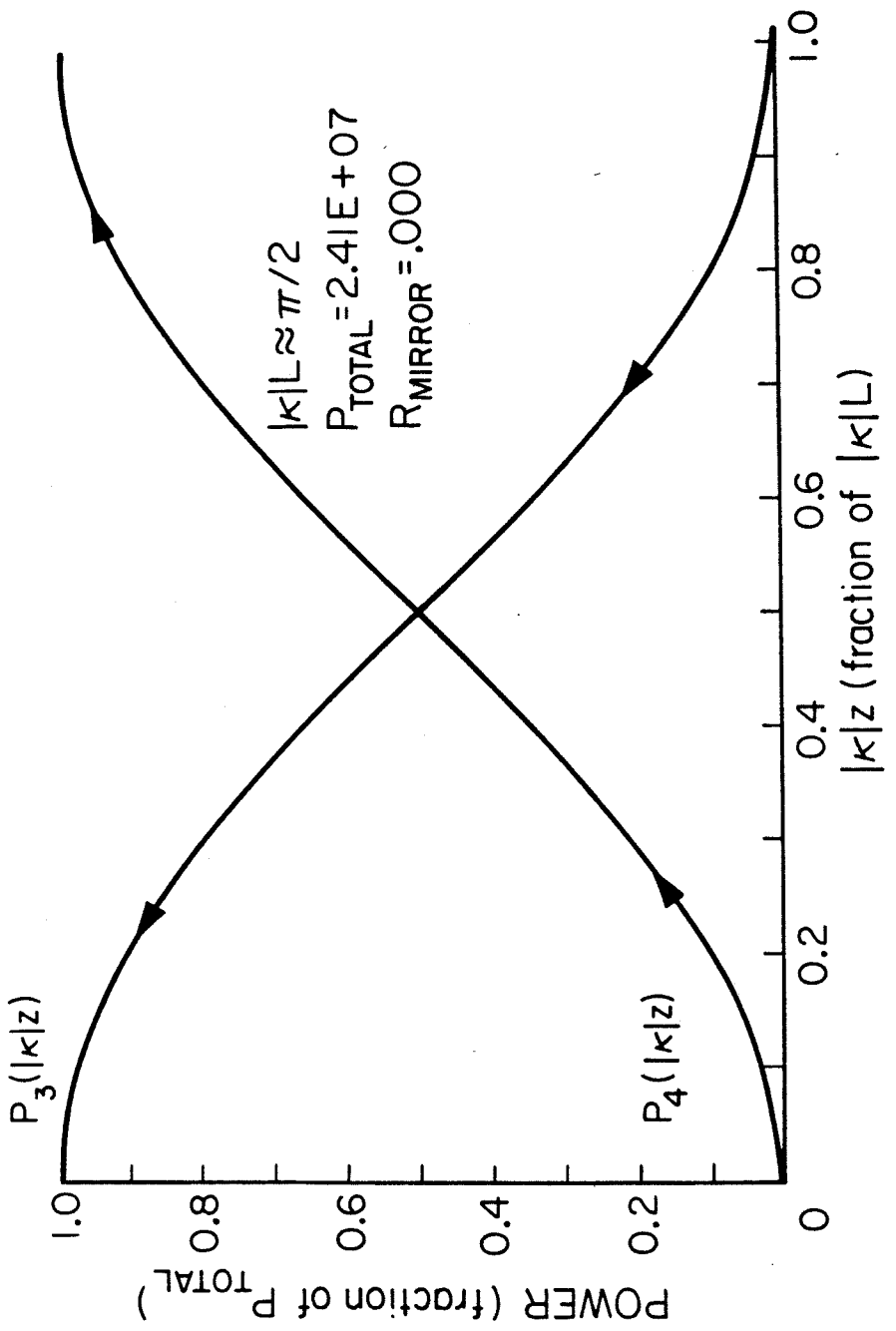

Fig. 3.3 The intensity distributions of the input power (P_4) and the conjugate field power (P_3) within the nonlinear medium as a function of $|\kappa|z$ near the oscillation condition, ($|\kappa|L = \pi/2$).

amplified reflection and oscillation, respectively, where the spatial evolution of the probe and conjugate wave (power) is plotted as a function of the normalized interaction length, $|\kappa|z$. We note that in our model, the oscillation mode is possible only if $\vec{k}_1 + \vec{k}_2 = 0$ (i.e., exactly counterpropagating pump waves) for the degenerate case. We will show in Section 6.2 that for any nonzero phase mismatch (thus violating the above constraint), oscillation ceases.

The above features of amplification and oscillation follow physically from the fact that both E_3 and E_4 continuously couple to each other throughout the nonlinear medium at the expense of the pump photons. In Figure 3.4 we sketch diagrammatically the nonlinear process from a photon point of view. At each interaction "site" two pump photons are annihilated, with the simultaneous stimulation of one photon along the direction of the probe photon (having identical quantum numbers of the probe photon) and a second photon (having opposite quantum numbers) along a direction counterpropagating with respect to the probe photon. We thus see that the probe photon imparts no net linear momentum, and hence no radiation pressure to the "conjugate mirror," for the degenerate, lossless case. This is in contrast to a perfect real mirror, where a net photon momentum transfer of $2\hbar\vec{k}$ is imparted.

Alternatively, one can view the "interaction" as an elastic scattering of pump photons off of the interaction site into the appropriate directions, consistent with conservation of total photon number and momentum. Thus, the forward-going photon flux always exceeds that of its input; the conjugate photon flux can exceed that of the corresponding

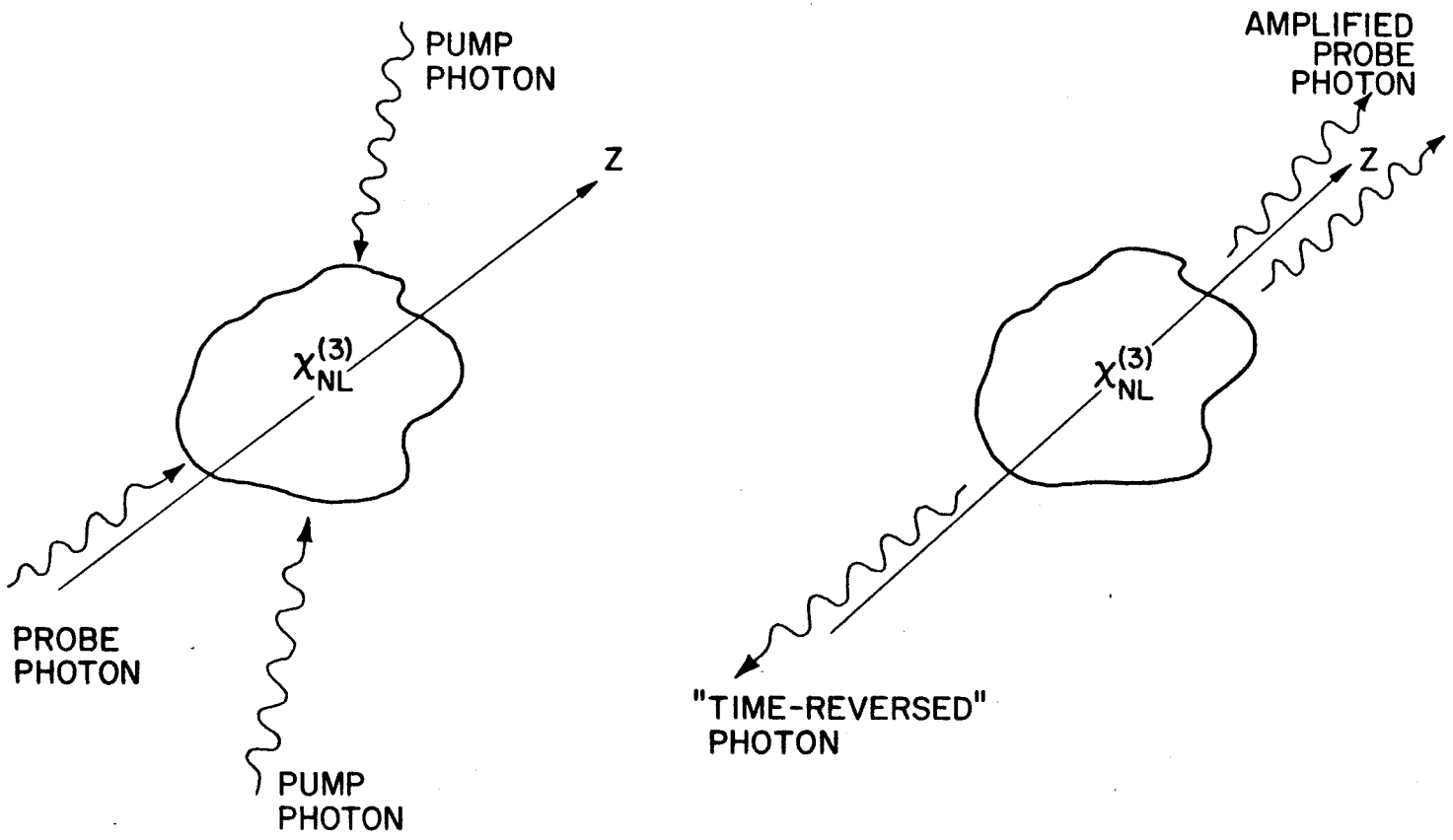

Fig. 3.4 A diagrammatic photon view of a degenerate four-photon interaction. (a) Two counterpropagating pump photons and a probe photon (along the z direction) are incident upon an interaction "site" ($\chi^{(3)}_{NL}$). (b) After the interaction, two new photons emerge along the $\pm z$ directions, resulting in an amplification of the probe photon flux and the creation of a backward-going (conjugate) photon; the pump photons are annihilated.

input flux if there exists a sufficient number of interaction sites within the medium, or alternatively, if the nonlinear gain $|\kappa|L$ exceeds $\pi/4$. This fact can be seen by the following simple argument. Recall that from (3.3-14), the power nonlinear reflection coefficient is given by $R = \tan^2|\kappa|L$. Now, from (3.3-13), we define the power transmission coefficient of the probe field as

$$T \equiv \left| \frac{A_4(L)}{A_4(0)} \right|^2 = \sec^2 |\kappa| L \qquad (3.3\text{-}16)$$

One can now define the effective gain (in excess of unity) experienced by the forward-going wave as

$$G \equiv T - 1 \qquad (3.3\text{-}17)$$

since, in the limit of $|\kappa|L \to 0$ (i.e., no nonlinear interaction) we expect no amplification of A_4. From (3.3-14,16, and 17) we see that $G = R$, implying that any photons gained by the forward-going beam are equal to the number of photons generated for the conjugate wave.

We also note that for small nonlinear gains, the nonlinear power reflection and transmission coefficients become

$$R \xrightarrow{|\kappa| L << \pi} (|\kappa|L)^2 \quad ; \quad T \to 1 + \mathcal{O}[(|\kappa|L)^2] \qquad (3.3\text{-}18)$$

respectively, where the small angle approximation for $\tan(\theta) \sim \theta$ was used. The small signal limit for R was first derived by Hellwarth [7]. Due to the small gain approximation, the possibility for amplified reflection, transmission, or oscillation was not revealed. This result

for R can be obtained from the coupled mode equations directly by assuming no depletion of the probe wave (in addition to the pump fields). Hence, $dA_4/dz = 0$, and the differential equation for $A_3(z)$ [the first of equations (3.3-9)] can be integrated directly, yielding (3.3-18).

The photon picture as described in Figure 3.4 can be made explicit by the following discussion. Assume that the participating electromagnetic fields can be quantized. We further assume that each field (E_ℓ) has n_ℓ photons initially. Thus, the initial photon state of the system has the form [5]

$$|i\rangle = |n_1, n_2, n_3, n_4\rangle \tag{3.3-19}$$

The perturbation Hamiltonian [5] of the system is given by

$$H' = -\vec{\mu}_{NL}\cdot\vec{E} = -\left(\frac{1}{N}\right)\vec{P}_{NL}\cdot\vec{E} \tag{3.3-20}$$

where $\vec{P}_{NL}$ is the nonlinear polarization as given by (3.3-2). Hence, we can write (3.3-20) as

$$H' \propto \chi^{(3)} E_1 E_2 E_3^* E_4^* \tag{3.3-21}$$

or, in terms of the creation ($a_i^\dagger$) and annihilation (a_i) operators [5],

$$H' \propto a_1 a_2 a_3^\dagger a_4^\dagger \tag{3.3-22}$$

consistent with the previous arguments.

We thus have the following nonzero matrix element:

$$H'_{fi} \equiv \langle f|H'|i\rangle \quad \propto$$

$$\langle n_1-1, n_2-1, n_3+1, n_4+1|a_1 a_2 a_3^\dagger a_4^\dagger|n_1 n_2 n_3 n_4\rangle \tag{3.3-23}$$

Using the definition of these operators (i.e., $a^\dagger|n\rangle = \sqrt{n+1}|n+1\rangle$, and $a|n\rangle = \sqrt{n}\,|n-1\rangle$) leads to the following transition rate

$$\Gamma \propto |H'_{fi}|^2 \propto n_1 n_2 (n_3+1)(n_4+1) \tag{3.3-24}$$

We see from (3.3-23) by inspecting the final state $|f\rangle$, and the definition of the operators, that the result of the perturbation Hamiltonian is to annihilate one photon from each pump beam ($E_{1,2}$), and to stimulate (or create) a photon in both the probe (E_4) and conjugate (E_3) states. This result is, of course, in agreement with the previous field description leading to (3.3-16,17) and also with the schematic representation shown in Figure 3.4. We further see from (3.3-24) the possibility of mirrorless oscillation, since there exists a nonzero transition rate even in the absence of probe or conjugate photons (i.e., if $n_3 = n_4 = 0$, $\Gamma \neq 0$), which is in agreement with the arguments leading to (3.3-15). Finally, energy is conserved in the above description, since the total photon energy in the initial state is $E(|i\rangle) = \hbar\omega(n_1+n_2+n_3+n_4)$, whereas the total energy in the final state is $E(|f\rangle) = \hbar\omega[(n_1-1)+(n_2-1)+(n_3+1)+(n_4+1)] = E(|i\rangle)$. This result will be seen to be consistent with a quantum mechanical description of the interaction (see Sections 3.8 and 3.9), where we will show that the atomic (or molecular) species responsible for the nonlinear coupling

remains in the same energy state before and after the interaction; thus the photons, or, equivalently, the interacting fields, possess the same total energy prior to and following the nonlinear mixing. (This is merely a restatement of the elastic photon-atom scattering description alluded to earlier.)

3.4 Conjugation of Arbitrary Wavefronts via Degenerate Four-Wave Mixing

Thus far we have considered only plane waves for the probe and conjugate fields. However, since the coupled mode equations are linear in terms of A_3 and A_4, with the resultant solutions being independent of their propagation directions, the principle of superposition can be applied. That is, for an arbitrary probe wave, one can formally decompose linearly this field into its plane wave components, each component having a well defined complex amplitude with its associated wave vector. Now, each of these components will give rise to its own conjugate replica by virtue of equation (3.3-12), all having the same nonlinear reflection coefficient (this assumes of course a "spherical" nonlinear medium, such that all components encounter the same nonlinear gain, $|\kappa|L$). This set of conjugated components can now be superposed in order to yield the resultant conjugate replica of the input field.

The above statements can be proved formally as follows: We use the same notation as in Section 3.3 and take the four fields as

$$E_i(\vec{r},t) = \frac{1}{2} A_i(x,y,z)\, e^{i(\omega_i t - k_i z)} + \text{c.c.} \qquad (3.4\text{-}1)$$

The waves propagate predominantly in the z-direction, but in contrast to Section 3.3 we allow the input wave A_4 and the reflected wave A_3 to be arbitrary complex functions of the transverse coordinates rather than plane waves. The pump waves A_1, A_2 are again taken as nondepleted plane waves.

$$A_1(x,y,z) = A_2(x,y,z) = \text{const.} \tag{3.4-2}$$

$$\vec{k}_1 + \vec{k}_2 = 0$$

$$\omega_1 + \omega_2 = \omega_3 + \omega_4 \tag{3.4-3}$$

The four waves are coupled through the nonlinear polarization as in (3.3-2,3)

$$P_{NL}(\omega_4=\omega_1+\omega_2-\omega_3) = \frac{1}{2}\chi^{(3)}_{NL} A_1 A_2 A_3^* \, e^{i\omega_4 t} \, e^{-i(\vec{k}_1+\vec{k}_2-\vec{k}_3)\cdot\vec{r}}$$

$$P_{NL}(\omega_3=\omega_1+\omega_2-\omega_4) = \frac{1}{2}\chi^{(3)}_{NL} A_1 A_2 A_4^* \, e^{i\omega_3 t} \, e^{-i(\vec{k}_1+\vec{k}_2-\vec{k}_4)\cdot\vec{r}} \tag{3.4-4}$$

Assume $\chi^{(3)}_{NL}(\omega_4=\omega_1+\omega_2-\omega_3) = \chi^{(3)}_{NL}(\omega_3=\omega_1+\omega_2-\omega_4)$. The wave propagation equation with the nonlinear polarization as the source term is given by

$$\vec{\nabla} \times (\vec{\nabla} \times \vec{E}) + \frac{\mu\varepsilon}{c^2}\frac{\partial^2}{\partial t^2}\vec{E} = -\frac{4\pi\mu}{c^2}\frac{\partial^2}{\partial t^2}\vec{P}_{NL} \tag{3.4-5}$$

Equating terms of the same dependence on both sides, we get, assuming $\vec{k}_3 + \vec{k}_4 = 0$, $\mu = 1$, scalar amplitudes , and

$$\left|\frac{d^2A_i}{dz^2}\right| << \left|k_i \frac{dA_i}{dz}\right|, \text{ and } \left|k_i^2 A_i\right| , \quad \text{for } i = 3,4 ,$$

the following two relationships

$$-2ik_3 \frac{\partial}{\partial z} A_3(x,y,z) + \nabla_t^2 A_3(x,y,z) = - \frac{4\pi}{c^2} \omega_3^2 \chi A_1 A_2 A_4^* \qquad (3.4\text{-}6)$$

$$-2ik_4 \frac{\partial}{\partial z} A_4(x,y,z) + \nabla_t^2 A_4(x,y,z) = - \frac{4\pi}{c^2} \omega_4^2 \chi A_1 A_2 A_3^* \qquad (3.4\text{-}7)$$

We expand $A_4(x,y,z)$ and $A_3(x,y,z)$ in terms of Fourier transforms involving the transverse coordinates x and y

$$A_3(x,y,z) = \int A_3(\vec{k}_\perp,z)\, e^{i\vec{k}_\perp \cdot \vec{r}_\perp} d^2\vec{k}_\perp \qquad (3.4\text{-}8)$$

$$A_4(x,y,z) = \int A_4(\vec{k}_\perp,z)\, e^{i\vec{k}_\perp \cdot \vec{r}_\perp} d^2\vec{k}_\perp$$

$$= \int A_4(-\vec{k}_\perp,z)\, e^{-i\vec{k}_\perp \cdot \vec{r}_\perp} d^2\vec{k}_\perp \qquad (3.4\text{-}9)$$

where we assumed $k_\perp^2 << k^2$, so that $E_3(x,y,z)$ and $E_4(x,y,z)$ satisfy (3.4-5). Substituting (3.4-8,9) into (3.4-6,7) and equating the terms with the same x,y dependence, we get

$$2ik_3 \frac{\partial}{\partial z} A_3(\vec{k}_\perp,z) + k_\perp^2 A_3(\vec{k}_\perp,z) = \frac{4\pi\chi\omega_3^2}{c^2} A_1 A_2 A_4^*(-\vec{k}_\perp,z) \qquad (3.4\text{-}10)$$

$$2ik_4 \frac{\partial}{\partial z} A_4(\vec{k}_\perp,z) + k_\perp^2 A_4(\vec{k}_\perp,z) = \frac{4\pi\chi\omega_4^2}{c^2} A_1A_2A_3^*(-\vec{k}_\perp,z) \qquad (3.4\text{-}11)$$

Next, we rearrange (3.4-10,11), take the complex conjugate of (3.4-11), and use

$$\vec{k}_4 = \frac{\omega}{c} n\hat{k}_4 \quad , \qquad \vec{k}_3 = -\frac{\omega}{c} n\hat{k}_4 \qquad (3.4\text{-}12)$$

The result is

$$\frac{\partial}{\partial z} A_3(\vec{k}_\perp,z) = i \frac{-k_\perp^2}{2\frac{\omega}{c} n} A_3(\vec{k}_\perp,z) + i\kappa^* A_4^*(-\vec{k}_\perp,z) \qquad (3.4\text{-}13)$$

$$\frac{\partial}{\partial z} A_4^*(\vec{k}_\perp,z) = i \frac{-k_\perp^2}{2\frac{\omega}{c} n} A_4^*(\vec{k}_\perp,z) + i\kappa A_3(-\vec{k}_\perp,z) \qquad (3.4\text{-}14)$$

where

$$\kappa^* \equiv \frac{4\pi\chi\omega^2}{c^2 2(\frac{\omega}{c} n)} A_1A_2 \ .$$

Replacing $\vec{k}_\perp$ by $-\vec{k}_\perp$ in equation (3.4-14) we get

$$\frac{\partial}{\partial z} A_3(\vec{k}_\perp,z) = -i \frac{\lambda k_\perp^2}{4\pi} A_3(\vec{k}_\perp,z) + i\kappa^* A_4^*(-\vec{k}_\perp,z) \qquad (3.4\text{-}15)$$

$$\frac{\partial}{\partial z} A_4^*(-\vec{k}_\perp,z) = -i \frac{\lambda k_\perp^2}{4\pi} A_4^*(-\vec{k}_\perp,z) + i\kappa A_3(\vec{k}_\perp,z) \qquad (3.4\text{-}16)$$

where $\lambda \equiv \frac{2\pi}{k} = \frac{2\pi}{(\frac{\omega}{c} n)}$. Integrating (3.4-15) and (3.4-16), we get

$$A_3(\vec{k}_\perp,z) = e^{-i \frac{\lambda k_\perp^2}{4\pi} z} \{C_1 \cos|\kappa|z + C_2 \sin|\kappa|z\} \qquad (3.4\text{-}17)$$

$$A_4^*(-\vec{k}_\perp,z) = \frac{1}{i\kappa^*}\left\{\frac{\partial}{\partial z} A_3(\vec{k}_\perp,z) + i\frac{\lambda k_\perp^2}{4\pi} A_3(\vec{k}_\perp,z)\right\}$$

$$= e^{-i\frac{\lambda k_\perp^2}{4\pi}}\{iC_1\sin|\kappa|z - iC_2\cos|\kappa|z\}\frac{|\kappa|}{\kappa^*} \qquad (3.4\text{-}18)$$

As in Section 3.3, we take the field $A_4(x,y,0)$ as given and $A_3(x,y,L) = 0$. In the Fourier domain this amounts to specifying $A_4(\vec{k}_\perp,0)$ and taking $A_3(\vec{k}_\perp,L) = 0$

$$A_4^*(-\vec{k}_\perp,0) \Longrightarrow \frac{|\kappa|}{\kappa^*} C_2 = iA_4^*(-\vec{k}_\perp,0)$$

$$A_3(\vec{k}_\perp,L) = 0 \Longrightarrow C_1\cos|\kappa|L + C_2\sin|\kappa|L = 0$$

These conditions are used to determine C_2 and C_1, giving

$$C_2 = i\frac{\kappa^*}{|\kappa|} A_4^*(-\vec{k}_\perp,0)$$

$$C_1 = -C_2\tan|\kappa|L$$

so that (3.4-17) and (3.4-18) yield

$$A_3(\vec{k}_\perp,z) = i\, e^{-i\frac{\lambda k_\perp^2}{4\pi} z}\frac{\kappa^*}{|\kappa|}\frac{A_4^*(-\vec{k}_\perp,0)}{\cos|\kappa|L}\sin|\kappa|(z-L) \qquad (3.4\text{-}19)$$

$$A_4^*(-\vec{k}_\perp,z) = e^{-i\frac{\lambda k_\perp^2}{4\pi} z} A_4^*(-\vec{k}_\perp,0)\frac{\cos|\kappa|(z-L)}{\cos|\kappa|L} \qquad (3.4\text{-}20)$$

The Fourier transform of the reflected wave at $z = 0$ is

$$A_3(\vec{k}_\perp,0) = -\frac{\kappa^*}{|\kappa|} i(\tan|\kappa|L)\, A_4^*(-\vec{k}_\perp,0) \qquad (3.4\text{-}21)$$

where κ is independent of $\vec{k}_\perp$. The reflected wave at $z = 0$ is uniquely

determined by the parabolic equation

$$-2i(-\frac{\omega}{c}n)\frac{\partial}{\partial z}A_3(x,y,z) + \nabla_t^2 A_3(x,y,z) = 0 \qquad (3.4\text{-}22)$$

and the boundary condition at $z = 0$

$$A_3(x,y,0) = \int A_3(\vec{k}_\perp,0)\, e^{i\vec{k}_\perp\cdot\vec{r}_\perp}\, d^2\vec{k}_\perp$$

$$= -i(\frac{\kappa^*}{|\kappa|}\tan|\kappa|L)\int A_4^*(-\vec{k}_\perp,0)\, e^{i\vec{k}_\perp\cdot\vec{r}_\perp}\, d^2\vec{k}_\perp \qquad (3.4\text{-}23)$$

The incident wave obeys the differential equation

$$-2i(\frac{\omega}{c}n)\frac{\partial}{\partial z}A_4(x,y,z) + \nabla_t^2 A_4(x,y,z) = 0 \qquad (3.4\text{-}24)$$

and the boundary condition

$$A_4(x,y,0) = \int A_4(\vec{k}_\perp,0)\, e^{i\vec{k}_\perp\cdot\vec{r}_\perp}\, d^2\vec{k}_\perp \qquad (3.4\text{-}25)$$

Taking the complex conjugate of (3.4-25) and also replacing $\vec{k}_\perp$ by $-\vec{k}_\perp$ results in

$$(2i\frac{\omega}{c}n)\frac{\partial}{\partial z}A_4^*(x,y,z) + \nabla_t^2 A_4^*(x,y,z) = 0 \qquad (3.4\text{-}26)$$

$$A_4^*(x,y,0) = \int A_4^*(-\vec{k}_\perp,0)\, e^{i\vec{k}_\perp\cdot\vec{r}_\perp}\, d^2\vec{k}_\perp \qquad (3.4\text{-}27)$$

We thus find that at $z < 0$, $A_3(x,y,z)$ and $A_4^*(x,y,z)$ obey the same differential equation (3.4-22 or 26) and, within a multiplicative constant (equal to $(-i\kappa^*/|\kappa|)\tan|\kappa|L$), the same boundary condition (3.4-23 or 27). It thus follows from the uniqueness property of the solutions of (3.4-22) that

$$A_3(x,y,z<0) = -i\left(\frac{\kappa^*}{|\kappa|}\tan|\kappa|L\right)A_4^*(x,y,z) \qquad (3.4\text{-}28)$$

which is the desired result; this result reduces to that of the plane wave case as derived in Section 3.3 (in the limit of no transverse dependence of the fields A_4 and A_3).

3.5 One-Mirror Assisted Parametric Oscillation

In the above discussion we derived a condition for mirrorless oscillation, $|\kappa|L \to \pi/2$. This mode of oscillation, which would occur most probably along the direction of the pump waves, may be undesirable due to the degeneracy of both the frequency and direction of the oscillating fields with respect to the pump fields. In certain nonlinear media, polarization discrimination can be used to distinguish between the pump and oscillating waves (the experiment discussed in the next chapter utilizes this scheme). To solve the problem, we may add a single reflector along an arbitrary direction as shown in Figure 3.5. The presence of this mirror, assumed to be at z = L, now imposes a new boundary condition given by

$$A_3(L) = rA_4(L) \qquad (3.5\text{-}1)$$

where r is the amplitude reflectivity of the mirror. Using this boundary condition in equation (3.3-11), the oscillation condition now becomes

$$|\kappa|L = \tan^{-1}\left(\frac{1}{|r|}\right) \qquad (3.5\text{-}2)$$

We see that in the limit of zero reflectivity ($|r| \to 0$) the (now mirrorless) oscillation condition $|\kappa|L = \pi/2$ is obtained, consistent

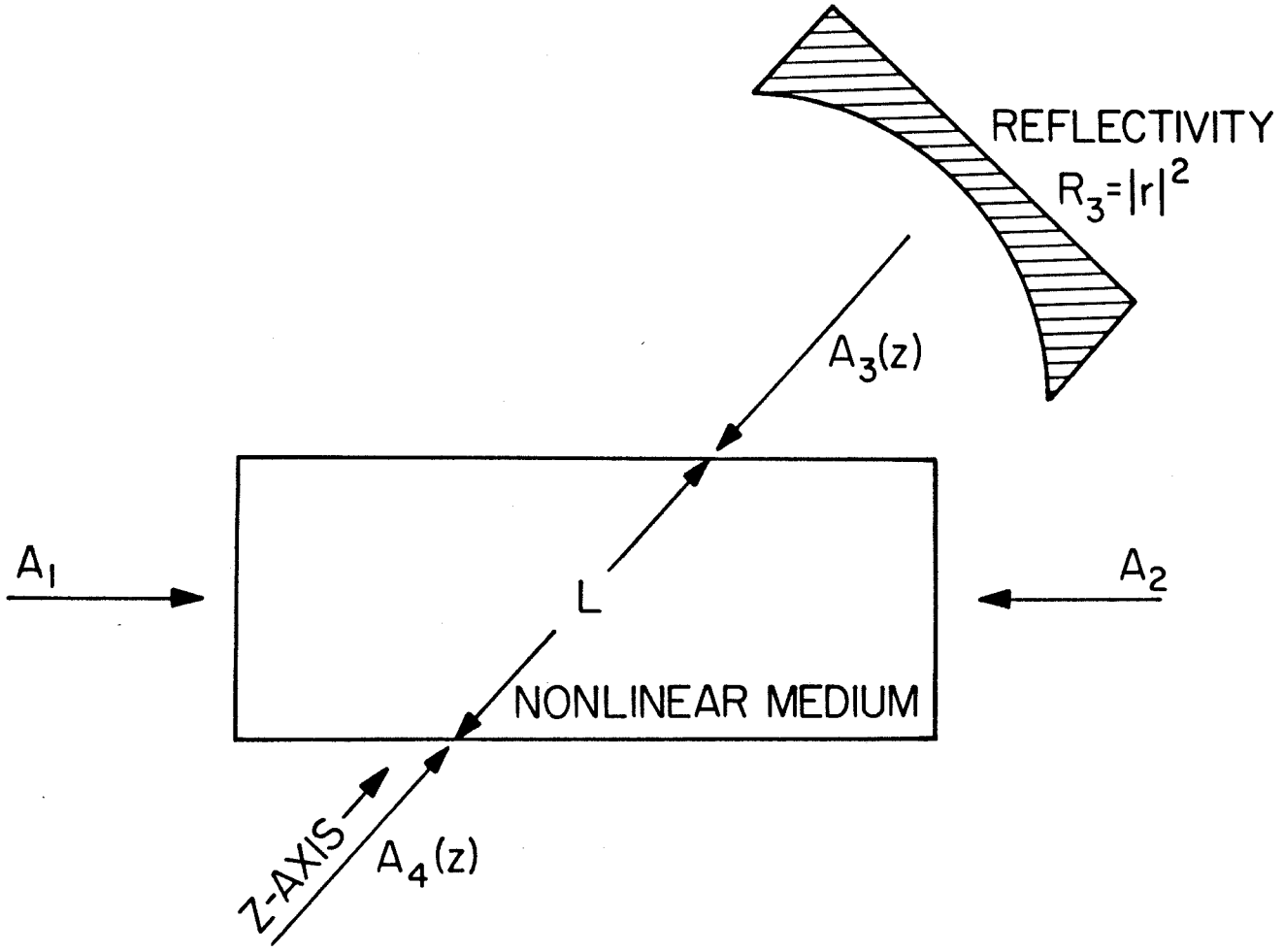

Fig. 3.5 Four-wave mixing utilizing an external mirror of (power) reflectivity R_3, which provides a preferred direction for oscillation.

with equation (3.3-14). However, when the reflection coefficient (defined to be $R_3 = |r|^2$) approaches unity, the oscillation condition becomes

$$|\kappa|L = \pi/4 \tag{3.5-3}$$

thus yielding a condition which is a factor of two less than that of the no-mirror case. This result has been experimentally verified recently by Bloom, et al. [8] using sodium vapor as the nonlinear medium. In the next chapter, we discuss an experiment we performed using a transparent nonlinear medium (CS_2), which also yielded one-mirror assisted parametric oscillation.

The above result for the oscillation condition makes physical sense in that a value of $|\kappa|L = \pi/4$ yields a nonlinear reflection coefficient, R, of unity for the conjugate mirror. We note that a passive resonator comprised of two unity-reflectivity lossless mirrors ($R, R_3 = 1$) satisfies the amplitude oscillation condition constraint when analyzed in the conventional, self-consistent formalism [5].

The above scheme may be of practical use if the conjugator is placed within an existing laser oscillator. Assuming that the laser (with this intracavity conjugator) is still above its oscillation threshold, the laser intracavity fields would constitute the two counterpropagating pump waves (A_1 and A_2 in Figure 3.5). One can then couple out the laser photons by merely placing an "output coupling" mirror of the desired curvature in the vicinity (e.g., at the $z = L$ plane) of the conjugator. This system could be important for use in high power lasers, which may require water cooled optics. Hence, the two laser mirrors as well as the

"output coupling" mirror may be highly reflecting and water cooled; the laser output would then emerge from the $z = 0$ surface of the phase conjugator.

In conclusion, we note that this scheme has been applied to a plane wave analysis describing the phase conjugator. Care must be taken when treating the more general case of Gaussian modes within this one-mirror oscillator. This situation will be considered in Chapter VII. However, despite this fact, the above results are qualitatively accurate.

3.6 Effects of Linear Losses upon Degenerate Four-Wave Mixing

Thus far in this chapter we have assumed that the nonlinear optical processes which gave rise to phase conjugated fields occurred in lossless media. In this and the next section, we will consider the effects of various loss mechanisms, as well as competing nonlinear optical processes upon the interaction of interest. We start by considering linear losses; the effects of nonlinear losses such as pump depletion, self-focusing, other third order (i.e., elastic photon scattering) processes, as well as stimulated Brillouin and Raman scattering, will be discussed in the next section.

We now consider the effects of linear losses denoted by an intensity absorption coefficient, α, upon the phase conjugate interaction. We assume this loss factor to be a constant, independent of the intensity of the interacting fields; that is, an unsaturable loss mechanism. Physically, this can be due to Rayleigh scattering, where the optical frequencies are far from any material resonances. Many materials, nominally transparent, have small absorption coefficients in the visible

region of the spectrum due to U.V. and I.R. transitions. The linear losses will be shown below to eventually dominate the interaction when the interaction lengths exceed $1/\alpha$. These lengths, which can be on the order of 100 m, can be realized in optical fibers (to be considered in the next chapter).

We thus characterize the medium by two parameters: the loss factor α, and the third order nonlinear optical susceptibility $\chi_{NL}^{(3)}$. We note that rigorously, α and $\chi_{NL}^{(3)}$ are intimately related to each other due to the fact that quantum mechanically they both arise from the interaction of the input photons with the various quantized levels characterizing the medium. For simple resonant systems such as two-level systems [9], or rotation-vibration structures [10], the connections between α and $\chi_{NL}^{(3)}$ can be shown explicitly. In the former case, atomic motion effects can also be treated [11]. However, in more complex systems, such as transparent liquids and solids or glasses, there is no simple tractable relationship between these two parameters, due to the photons' interaction with a large number of nonresonant energy levels. Hellwarth [12] discusses and tabulates these parameters from a phenomenological viewpoint for many common materials.

Since the loss factors merely attenuate all the participating fields, we expect that the various features described in the last sections which characterize the phase conjugate interaction to still hold. However, we now anticipate that the overall efficiency of the interaction will decrease, and that the onset of oscillation will be more difficult to realize. We further expect that a system with linear losses to faithfully yield a phase conjugate replica by recalling the

discussion of Appendix 2A. There we considered the ability of a (lossless) phase conjugator to compensate for phase aberrations incurred as a result of propagation through a lossy medium possessing linear refractive index inhomogeneities. Although the amplitude of the time-reversed field did not match that of the incident wave, phase compensation was predicted, since the necessary condition for compensation is that the equiphase surfaces of the forward and conjugate waves match at each point in space (and not necessarily the amplitude). In the present case, the losses are concentrated within the conjugator itself, as opposed to being present in the aberrating medium.

We consider a geometry where the counterpropagating pump fields propagate along some arbitrary (x) axis, over a distance L_p within the nonlinear medium; the probe and conjugate fields propagate along the z axis over a distance L, not necessarily orthogonal to the pump field axis; the geometry shown earlier in Figure 3.1 applies. We write

$$E_1 = \frac{1}{2} A_1 e^{i(\omega t - kx)} e^{-\frac{1}{2}\alpha x} + c.c.$$

and

$$E_2 = \frac{1}{2} A_2 e^{i(\omega t + kx)} e^{\frac{1}{2}\alpha(x - L_p)} + c.c. \qquad (3.6\text{-}1)$$

for the pump beams, while

$$E_4 = \frac{1}{2} A_4 e^{i(\omega t - kz)} e^{-\frac{1}{2}\alpha z} + c.c.$$

and

$$E_3 = \frac{1}{2} A_3 e^{i(\omega t + kz)} e^{\frac{1}{2}\alpha(z - L)} + c.c. \qquad (3.6\text{-}2)$$

describe the probe and conjugate fields, respectively. All fields are assumed to be of the same frequency (i.e., degenerate) and are taken to be plane waves for simplicity; α is the linear (intensity) absorption coefficient.

We form the nonlinear polarization pair at $\omega_3 = \omega$ and $\omega_4 = \omega$, and insert these functions into the wave equation (with $\mu = 1$)

$$\nabla^2 E_j - \frac{(\varepsilon_R - i\varepsilon_I)}{c^2} \frac{\partial^2 E}{\partial t^2} = \frac{4\pi}{c^2} \frac{\partial^2 P_{NL}}{\partial t^2}, \quad j = 3,4 \tag{3.6-3}$$

which now is seen to contain a complex permittivity to describe the linear losses. We obtain straightforwardly the following coupled mode equations

$$(ik - \tfrac{\alpha}{2}) \frac{dA_4^*}{dz} = i\kappa A_3 \, e^{-\frac{1}{2}\alpha(L_p+L)} \, e^{\alpha z} \, (ik)$$

and (3.6-4)

$$(ik + \tfrac{\alpha}{2}) \frac{dA_3}{dz} = i\kappa^* A_4^* \, e^{-\frac{1}{2}\alpha(L_p-L)} \, e^{-\alpha z} (ik)$$

where κ^* is defined by equation (3.3-10). In the wave equation, $\varepsilon_R = n^2(1 - \alpha^2/4k^2)$ and $\varepsilon_I = n^2\alpha/k$, which follows after assuming $E \sim e^{i(\omega t - kz)} \, e^{-\alpha z/2}$ in the unperturbed case ($P_{NL} = 0$); $k = \omega n/c$.

In deriving equation (3.6-4), we followed the same procedure and approximations as in the lossless case (c.f., Section 3.3). We now assume that

$$ik \pm \frac{\alpha}{2} \sim ik \tag{3.6-5}$$

since $k(= 2\pi/\lambda \sim 10^4 cm^{-1})$ is much greater than α for most transparent materials ($\alpha \sim 10^{-4} cm^{-1}$ for CS_2 at $\lambda \sim 1$ μm). This assumption is also consistent with the adiabatic (or WKB) approximation, which physically means that the interacting fields do not change appreciably over a wavelength.

Solving equation (3.6-4) subject to the boundary condition for a single (probe) input, $A_4(z=0) \equiv A_4(0)$ and $A_3(z=L) = 0$, yields the following result for the amplitude reflectivity,

$$r \equiv \frac{E_3(z=0)}{E_4(z=0)} = \left. \frac{A_3(z)\, e^{-\frac{1}{2}\alpha(z-L)}}{A_4^*(z)\, e^{-\frac{1}{2}\alpha z}} \right|_{z=0}$$

$$= \frac{-2i\kappa^* e^{-\frac{1}{2}\alpha L_p} \tan(\kappa_{eff} L)}{\alpha \tan(\kappa_{eff} L) + 2\kappa_{eff}} \qquad (3.6\text{-}6)$$

where

$$\kappa_{eff} = \sqrt{|\kappa|^2 e^{-\alpha L_p} - (\tfrac{\alpha}{2})^2} \qquad (3.6\text{-}7)$$

The oscillation condition results when the reflectivity approaches infinity, or equivalently, when the denominator of (3.6-6) vanishes. We thus obtain the following transcendental equation for the oscillation condition:

$$\tan(\kappa_{eff} L) = -\frac{2\kappa_{eff}}{\alpha} \qquad (3.6\text{-}8)$$

We note that both the reflectivity and the oscillation condition reduce correctly to their respective lossless expressions [(3.3-12) and $|\kappa|L = \pi/2$, respectively], in the limit of $\alpha \to 0$. In this limit, $\kappa_{eff} \to |\kappa|$. To examine the effects of α upon the interaction explicitly we plot in Figure 3.6 the nonlinear power reflection coefficient, $R \equiv |r|^2$, as a function of interaction length for two different values

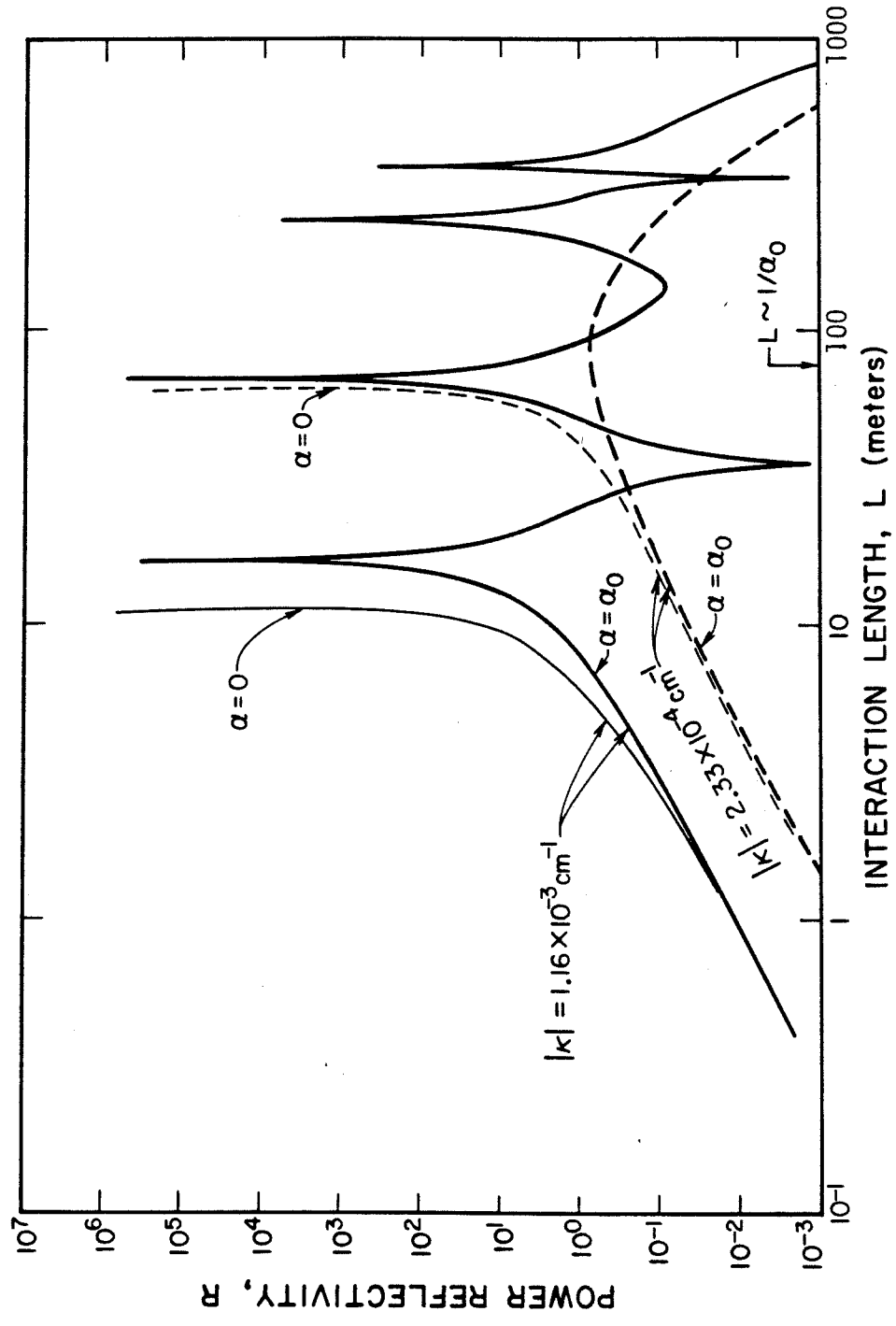

Fig. 3.6 The nonlinear (power) reflection coefficient (R) as a function of interaction length (L) for two different values of $|\kappa|$ ($1.16 \times 10^{-3} cm^{-1}$: solid curve; $2.33 \times 10^{-4} cm^{-1}$: dashed curve), with and without linear intensity losses, α ($\alpha_0 = 1.37 \times 10^{-4} cm^{-1}$ for CS_2).

of $|\kappa|$. These two values of $|\kappa|$ correspond to the case where the nonlinear medium is CS_2 ($\chi^{(3)}_{NL} \sim 1.2 \times 10^{-12}$esu; $\alpha = 1.37 \times 10^{-4}$cm^{-1} or 59 db/km), and is irradiated with pump beams (at 1.06 μm wavelength) of 796 kw/cm^2 and 159 kw/cm^2, respectively. This corresponds to $|\kappa| = 1.16 \times 10^{-3}$ cm^{-1} and 2.33×10^{-4} cm^{-1}, respectively, where $|\kappa|[\text{cm}^{-1}] = (32 \times 10^7\ \pi^3/c)(\chi^{(3)}_{NL}[\text{esu}]/\lambda[\text{cm}]n^2)(\sqrt{I_1 I_2[\text{w/cm}^2]}\ )$. The long interaction lengths shown in the figure can be realized using optical fibers (see next chapter); in fact, for a CS_2 filled optical fiber of 20 μm I.D., the two above values for $|\kappa|$ can be realized using a cw laser of 2.5 and 0.5 watts (within the fiber), respectively.

Also plotted for each value of $|\kappa|$ is a second curve assuming no linear losses (α=0). We have neglected competing effects such as stimulated Brillouin or Raman scattering, and have assumed that the laser coherence length is greater than the interaction length (the laser coherence length places a fundamental limit upon the maximum interaction length due to destructive interference effects of the nonlinearly induced dipoles); we further assume that the pump and signal interaction lengths are equal ($L_p = L$). From the figure, we see that due to the presence of linear losses, the nonlinear reflection coefficient is lower than that obtained without loss. In addition, to achieve oscillation requires longer interaction lengths, or equivalently, greater nonlinear gains. Further, for "insufficient" pumping ($|\kappa| = 2.33 \times 10^{-4}$cm^{-1}), the linear losses dominate over the non-

linear coupling coefficient, resulting in the lack of oscillation. In this case, κ_{eff} becomes pure imaginary, with the tangent functions being replaced by hyperbolic tangent functions in the expressions for r. Hence, the maximum reflection coefficient occurs at an interaction length on the order of $L_{opt} \sim 1/\alpha$, as shown in the figure. This value for the optimal interaction length is not unlike those obtained for other third order nonlinear optical processes such as SRS in long fibers [13] under similar (linear) lossy conditions. We finally note that the region between oscillation peaks in the figure is not physical, due to nonlinear pump depletion or saturation (i.e., photon number conservation), which were neglected. In actuality, once oscillation begins, a small increase in the interaction length would result in an increased oscillation output power [14-16] and not a decrease in the reflectivity as the figure indicates. This assumes that another oscillation peak follows the one considered; after the last oscillation peak, the linear losses finally begin to dominate the other processes, ultimately resulting in a cessation of oscillation.

It is seen from the expression for the nonlinear reflectivity (3.6-6) that the pump beam interaction length enters through the exponent that multiplies κ^*, thus rendering an effective decreased pump beam intensity ($I_{pump} \rightarrow I_{pump} e^{-\alpha L_p}$) as well as appearing in κ_{eff}. This suggests that by choosing interaction geometries that minimize the pump beam interaction length relative to the signal/conjugate length, one can realize more efficient conjugators. To illustrate this effect, we

show in Figure 3.7 the family of locus of points satisfying the oscillation condition [equation (3.6-8)], where $|\kappa|L$, the nonlinear gain, is plotted as a function of αL, the signal extinction coefficient, for several values of the pump-to-signal interaction length ratio, L_p/L. We see that for a fixed value of $|\kappa|L$ and αL, one can optimize the phase conjugate efficiency (at least in terms of the oscillation condition) by minimizing [maximizing] the ratio L_p/L for the lossy ($\alpha > 0$) [gain($\alpha < 0$)] case.

In the limit of large αL, the oscillation requirements (i.e., the necessary magnitude of $|\kappa|L$) impose such great demands upon the pump intensity that competing effects (such as SRS, SBS, self-focusing, etc.) thus far neglected, become appreciable. For αL small, the oscillation condition is seen to approach $|\kappa|L = \pi/2$, consistent with the lossless case analysis.

Also sketched in Figure 3.7 are the two values of $|\kappa|L$ vs. αL (the straight lines) that were considered in plotting Figure 3.6. It is seen that for the larger value of $|\kappa|$, oscillation is possible (at the intersection of the straight line and the $L_p/L = 1$ curve, point "A"). On the other hand, for the smaller value of $|\kappa|$, one cannot realize oscillation (for $L_p/L = 1$), which is consistent with the results presented in Figure 3.6. However, it is seen in Figure 3.7 that if we choose $L_p/L = 0.1$, then (at "B") there exists a point where the oscillation condition is satisfied (at $|\kappa|L = 1.45 \times \pi/2$) for the smaller value of $|\kappa|$.

Finally, in Figure 3.7, we plot the locus of points for the oscillation condition of the case of $\alpha < 0$, that is, four-wave mixing

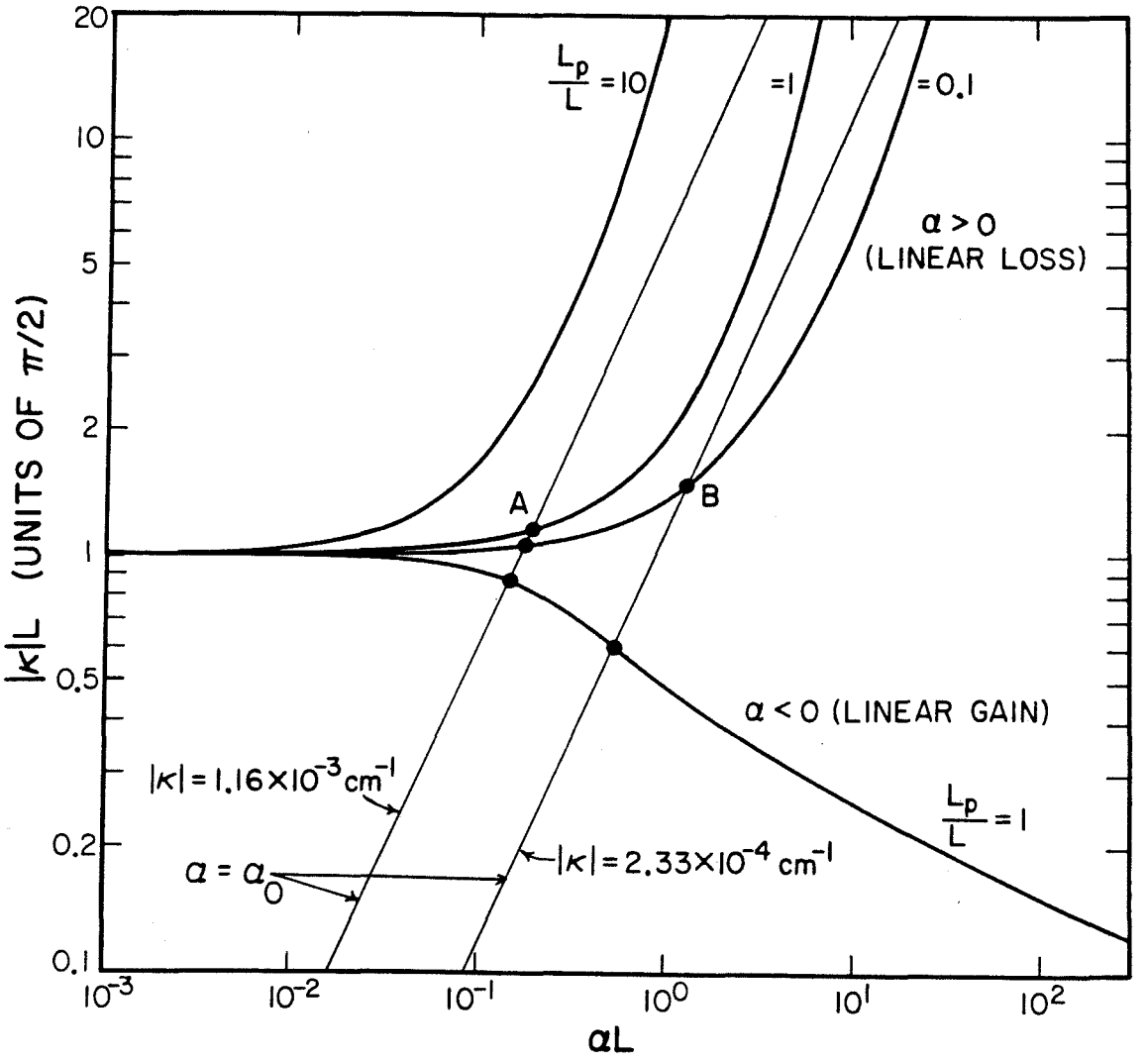

Fig. 3.7

Plot of the locus of points that satisfy the oscillation condition [equation (3.6-8)] as a function of $|\kappa|L$ and αL, for different values of the pump-to-signal interaction length, L_p/L. Also shown are plots of $|\kappa|L$ vs. αL (straight lines) for $|\kappa| = 1.16 \times 10^{-3}cm^{-1}$ and $|\kappa| = 2.33 \times 10^{-4}cm^{-1}$ for CS_2; dots indicate possible oscillation points.

in the presence of a linear, unsaturable gain. For this plot we set $L_p/L = 1$. It is seen that the resultant oscillation condition requires values of $|\kappa|L < \pi/2$ as expected.

3.7 Effects of Nonlinear Interactions upon Degenerate Four-Wave Mixing

In this section we will discuss briefly the effect of nonlinear processes upon degenerate four-wave phase conjugators. We will consider first how pump depletion affects the efficiency of the interaction. Next, other third-order processes such as self-focusing will be discussed. Finally, stimulated, inelastic interactions (SRS, SBS, etc.) will be considered.

A. Pump Depletion

Thus far in our analysis of four-wave mixing we have assumed that the pump fields were not affected by the presence of the probe field within the nonlinear medium, hence not strictly conserving the total photon number. The only loss mechanism we considered was that involving linear losses. The nondepleted pump approximation (i.e., neglecting nonlinear losses) can be justified as long as the probe field amplitudes are small ($|A_{3,4}| << |A_{1,2}|$) and also when the nonlinear gain is small enough to be far from the oscillation condition ($|\kappa|L < \pi/2$). The use of the nondepleted pump approximation results in the simple, coupled mode analysis discussed in Section 3.3. However, when the above conditions are no longer met, a more detailed analysis is required, which must conserve the total photon number, in order to more precisely evaluate parameters such as the nonlinear power reflectivity and, more important,

the fidelity of the "time-reversed" wave so generated. Qualitatively, one expects that the nonlinear reflectivity is reduced from that of the nondepleted approximation, and further, that the conjugate wave "degrades," that is, it begins to deviate from a perfect time-reversed replica of the input probe field. This latter effect is expected to occur at large nonlinear gains since, among other things, the spatial regions within the nonlinear medium, corresponding to large probe amplitudes, will result in smaller local nonlinear reflectivities. This implies that the conjugator will have a nonuniform (spatially dependent) reflectivity. Hence, the conjugate wave will acquire this effect in the form of a transverse spatial modulation of its amplitude, thus yielding a degraded time-reversed replica.

In the analysis that follows, we assume that all four plane wave, interacting fields propagate colinearly within the nonlinear medium. As mentioned previously, polarization discrimination can be used to distinguish between the pump field pair and the probe/conjugate wave pair. Further, we assume that the medium also possesses a linear loss, characterized by an (intensity) absorption coefficient α which is assumed real.

Following the same procedure leading to the coupled mode equations (3.3-9), we form two new nonlinear polarizations at ω_1 and ω_2 by writing equations (3.3-2) and (3.3-3), replacing A_1 and A_2 with A_4 and A_3 (along with the corresponding frequencies and wave vectors), respectively. Using

the adiabatic approximations for A_1 and A_2 via (3.3-8), we arrive at the following set of coupled mode equations

$$\begin{aligned}
\frac{dA_1^*}{dz} &= i\beta A_3^* A_4^* A_2 - \frac{\alpha}{2} A_1^* \\
\frac{dA_2}{dz} &= i\beta A_3 A_4 A_1^* - \frac{\alpha}{2} A_2 \\
\frac{dA_3}{dz} &= i\beta A_1 A_2 A_4^* - \frac{\alpha}{2} A_3 \\
\frac{dA_4^*}{dz} &= i\beta A_1^* A_2^* A_3 - \frac{\alpha}{2} A_4^*
\end{aligned} \tag{3.7-1}$$

where $\beta = \frac{2\pi\omega}{nc} \chi_{NL}^{(3)}$; β is assumed to be real for simplicity, and α is the intensity (nonsaturating) absorption coefficient. In this form we see that the pair A_1 and A_4 propagate along the same direction. The same is true for the pair A_2 and A_3. The two pairs propagate in opposite directions with respect to each other.

We wish to solve these four <u>complex</u>, coupled differential equations (actually a set of eight equations) for the spatial evolution of their complex amplitudes, given the values of each complex amplitude at its respective input plane: $A_1(0)$, $A_2(L)$, $A_3(L)$, and $A_4(0)$. Given values for α and β, equations (3.7-1) were solved numerically using the following self-consistent iteration procedure. The complex amplitudes $A_1(z)$ and $A_4(z)$ were first assumed fixed and constant over the entire interaction length, L; that is, $A_1(z) = A_1(0)$ and $A_4(z) = A_4(0)$ for $0 \leq z \leq L$. Using these values, $A_2(z)$ and $A_3(z)$ were solved by numerically integrat-

ing their respective differential equations from z = L to z = 0, given the boundary conditions $A_2(L)$ and $A_3(L)$. The differential equations for $A_1(z)$ and $A_4(z)$ were then numerically integrated from z = 0 to z = L, using the values for $A_2(z)$ and $A_3(z)$ from the previous integrations, as well as the initial values for $A_1(0)$ and $A_4(0)$. The procedure would then repeat until a self-consistent set of solutions was obtained. We assumed the solutions to be self-consistent when the set of complex amplitudes of the four fields at their respective output planes agreed within a preset fraction with that from the previous iteration. We note, however, that the above numerical technique did not converge as the oscillation condition was approached, due to the large exchange of photon flux from the pump to the probe/conjugate fields.

Results of two different cases are shown in Figures 3.8 and 3.9 where the spatial evolution of the pump fields along with the conjugate and probe fields (i.e., $|A_i|^2$ $i = 1,2,3,4$, respectively) within the nonlinear medium is plotted as a function of the normalized interaction length (L). For both plots, we have assumed that the input fields (at their respective input planes) are given by $A_1(z=0) = 1/\sqrt{2}$, $A_2(z=L) = 1/\sqrt{2}$, $A_3(z=L) = 0$, and $A_4(z=0) = \sqrt{3}/2$; with $\beta = \pi/2$ and L = 1. These values were chosen so as to yield a unity nonlinear reflection coefficient (i.e. $|\kappa|L = \pi/4$), if the effects of pump depletion and linear losses are neglected. The difference between Figures 3.8 and 3.9 is that in the former case we assumed no linear losses (i.e., $\alpha = 0$), while for the latter case we assumed large linear losses (i.e., $\alpha = 2$,

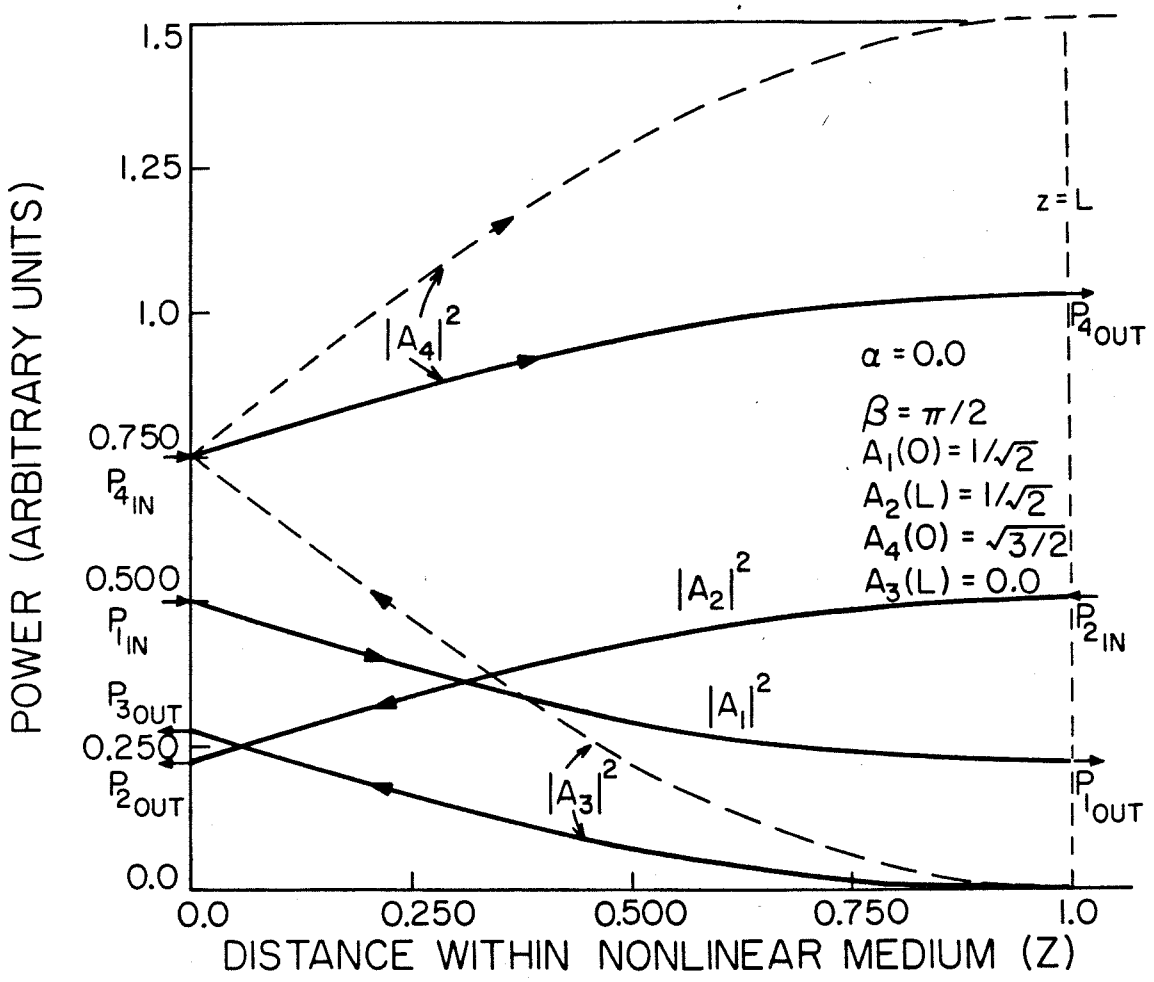

Fig. 3.8 Intensity distributions (solid curves) $|A_i|^2$ (i=1,2,3,4) inside the interaction region. Boundary conditions: $A_1(0) = A_2(L) = 1/\sqrt{2}$, $A_3(L) = 0$, $A_4(0) = \sqrt{3}/2$; $\beta = \pi/2$, $\alpha = 0$ (no linear losses). Dashed curves show $|A_3|^2$ and $|A_4|^2$ assuming no pump depletion. The parameters yield $|\kappa|L=\pi/4$ ($\Longrightarrow$ R = 1) in this limit.

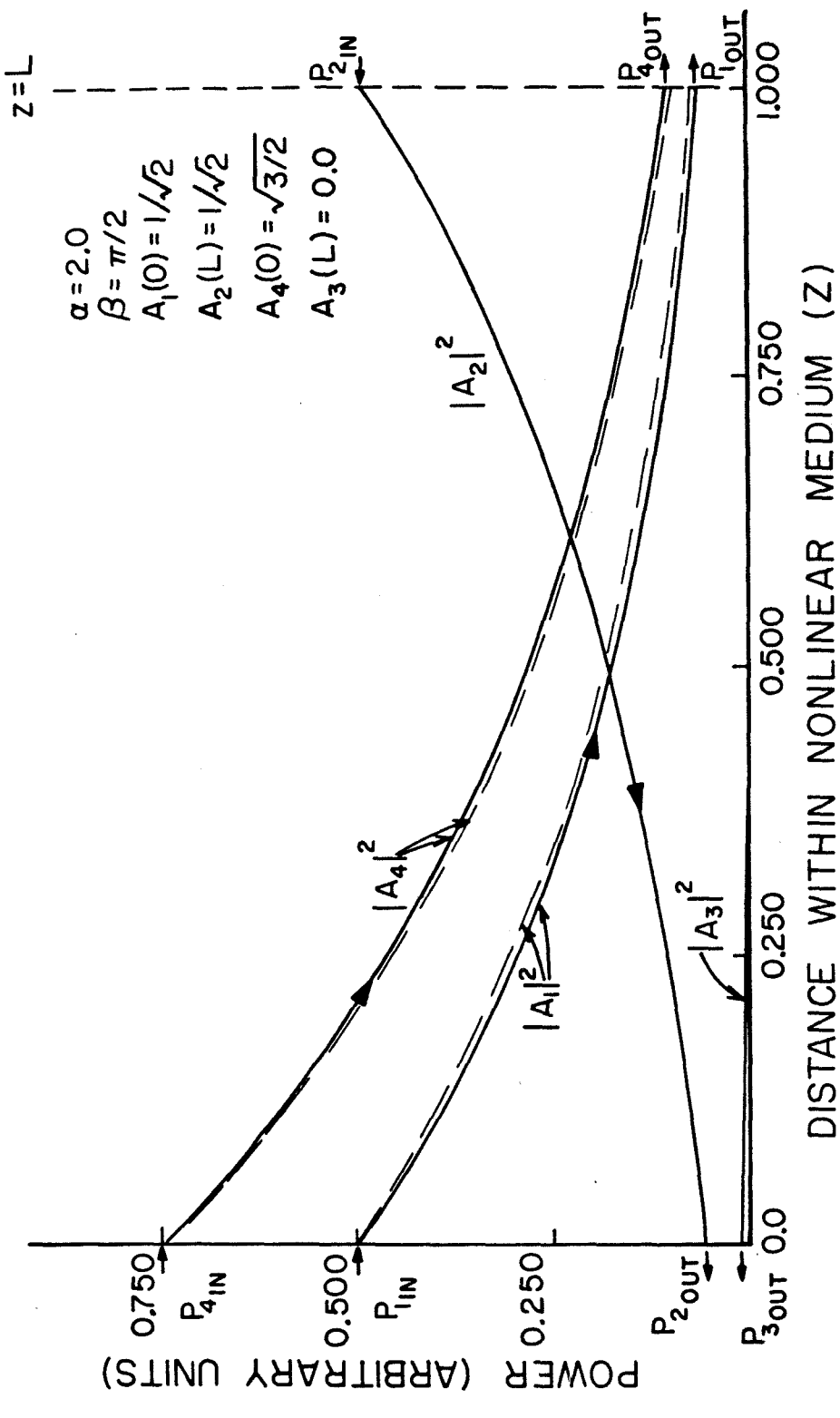

Fig. 3.9 Intensity distributions (solid curves) of $|A_i|^2$ ($i = 1,2,3,4$). Same parameters as Fig. 3.8, except $\alpha = 2$. Dashed curves show $|A_1|^2$ and $|A_4|^2$, assuming $|A_{1,4}(z)|^2 = |A_{1,4}(0)|^2 \exp(-\alpha z)$.

which implies that $\alpha L/2 > |\kappa|L)$. We note that the large value of A_4 relative to $A_{1,2}$ was chosen to "stress" the system relative to the small-signal case.

Referring to Figure 3.8, we see that as a result of pump depletion the nonlinear (power) reflection coefficient ($R \equiv |A_3(0)/A_4(0)|^2$) is 37% as compared to the small-signal value [from (3.3-14)] of 100% for the parameters chosen. In addition, the (power) transmission coefficient ($T \equiv |A_4(L)/A_4(0)|^2$) is $\sim$ 137%, as compared to the small signal value of 200%. We thus see clearly the effects of pump depletion upon the interaction efficiency. For comparative purposes, we also plot the spatial evolution of $|A_4|^2$ and $|A_3|^2$ assuming no pump depletion (dashed curves), as obtained from (3.3-11).

There are several additional interesting features to be recognized from Figure 3.8. First, since we have assumed no linear losses, we see from (3.7-1) that

$$\frac{d(|A_1|^2 + |A_2|^2)}{dz} = 0$$

and

$$\frac{d(|A_3|^2 + |A_4|^2)}{dz} = 0$$

$$\Longrightarrow \quad \frac{d}{dz}\left(\sum_{i=1}^{4} |A_i|^2\right) = 0 \tag{3.7-2}$$

Hence, the sum of the pump wave intensities, as well as the sum of the probe and conjugate pair intensities remain constant throughout the nonlinear medium. The last result in (3.7-2) is merely a confirmation of the conservation of photons; that is, without losses, the elastic scat-

tering of photons does not modify the total photon number within the system. The above features can easily be seen from the figure. We further note that the pump wave photon flux does not vary symmetrically (in a spatial sense) in terms of the depletion (i.e., the point within the medium at which the value of $|A_1|^2 = |A_2|^2$ occurs at $z \simeq 0.31$, not at 0.5). The asymmetry is, of course, introduced as a result of the fact that $A_4(0) \neq A_3(L)$. However, from (3.7-2) and the boundary conditions chosen $[A_1(0) = A_2(L)]$, despite this asymmetry, the pump wave amplitudes at their respective output planes are equal. We also remark that from (3.7-2) and the boundary conditions chosen, the increase in photon flux in terms of the conjugate wave at its output plane is equal to the corresponding increase in the probe wave flux (recall that we proved this for the small signal case in Section 3.3). We finally mention that even though we displayed results here assuming purely real input amplitudes, similar results were obtained upon specifying complex amplitudes for the various input waves. The numerical results also (correctly) bear out the conjugate nature of the field A_3 when we set $A_3(L) = 0$, and choose a complex probe wave input amplitude.

We now direct our attention to Figure 3.9 , which is basically identical to the previous figure, except now we assume a (large) linear intensity loss factor of $\alpha = 2$. We see that the nonlinear power reflection coefficient is drastically reduced relative to the lossless case discussed above (i.e., $R \simeq 1.33\%$, as compared to $\sim$37% previously). Again, $|\kappa|L = \pi/4$, which yields R = 100% in the lossless, small signal approxi-

mation. For the parameters chosen in generating Figure 3.9, we see that in terms of loss mechanisms, the linear loss factor (α) totally dominates the nonlinear loss effects. To show this explicitly, we also plot in the figure (dashes) the spatial evolution of one of the pump waves (A_1), along with that of the input probe wave (A_4), assuming only a simple linear loss effect; that is, $|A_{1,4}(z)|^2 = |A_{1,4}(0)|^2 \exp(-\alpha z)$. We see that the effect of the nonlinear process is to slightly amplify the probe wave, while barely modifying the pump wave's spatial evolution within the interaction region. To verify this fact further, we see that now both pump waves vary spatially in a nearly symmetric fashion, with their respective amplitudes intersecting (i.e., being equal) rather close to the midpoint of the nonlinear medium. As a final check, we calculated the nonlinear power reflection assuming only a linear loss mechanism present, using (3.6-6). Assuming the same input pump wave amplitudes as above, we obtain a value of $R = 1.59\%$ compared to $\sim 1.33\%$ from the figure. The slight overestimation is due, of course, to the neglect of nonlinear pump depletion. Therefore, for large linear losses (i.e., $\alpha >> |\kappa|$) and nearly equal input field amplitudes, we can safely neglect nonlinear pump depletions in terms of estimating conjugate reflection coefficients.

Recent analytical analyses by Marburger and Lam [14,16] and by Hsu [15] consider pump depletion as well as other nonlinear contributions (and their associated effects) in describing the conjugate wave nonlinear reflection coefficient under all pump-to-probe ratios and nonlinear gains. They, however, neglect linear losses, as considered here.

B. Additional Nonlinear Optical Processes

In this section we mention briefly other various mechanisms which are generated as a result of $\chi^{(3)}_{NL}$, as well as other nonlinear processes and their effect upon the conjugation process. We will discuss elastic four-photon scattering processes such as self-focusing, nonlinear phase distortions, and other phase matched, degenerate, third-order processes. These mechanisms must be considered, since they all depend on the same nonlinear susceptibility that is responsible for the generation of the phase conjugate fields. Also, inelastic interactions will be discussed.

We first consider self-focusing. If a wave $E(\vec{r})$ having a transverse amplitude dependence propagates through a medium possessing a nonlinear index, the local index is modified according to

$$n(\vec{r}) = n_o + n_2|E(\vec{r})|^2 \qquad (3.7\text{-}3)$$

where n_o is the linear index of refraction, n_2 is called the nonlinear index and is related to the nonlinear susceptibility as

$$n_2 = \frac{2\pi\chi^{(3)}_{NL}}{n_o} \qquad (3.7\text{-}4)$$

Since the pump wave amplitudes are typically much greater than the probe or conjugate amplitude, we limit our discussion to the former quantities. We see that if the pump waves possess any transverse amplitude dependence (e.g., Gaussian in shape), they will give rise to a distributed positive or negative lensing effect within the medium, depending upon the sign of n_2. This state of affairs leads to essentially an increase in the number of effective plane wave "modes" contained within each pump field, the result being a "cross-coupling" of pump plane wave components

(not necessarily counterpropagating) with the probe wave. This would lead to a degradation of the fidelity of the conjugate wave. Qualitatively, if we assume that each pump wave (A_i) has N such plane wave modes (given by A_{i_p} $(i = 1,2)$, then the nonlinear polarization yields N^2 possible nonlinear mixing terms given by

$$P_{NL}^{(\omega_3)} \sim \chi_{NL}^{(3)}\left[\sum_{p=1}^{N} A_{1_p} \exp(-i\vec{k}_{1_p}\cdot\vec{r})\right]\left[\sum_{q=1}^{N} A_{2_q} \exp(-i\vec{k}_{2_q}\cdot\vec{r})\right]A_4^* e^{i\omega_3 t} \qquad (3.7\text{-}5)$$

We see that only N of the product fields will be phase matched (i.e., $\vec{k}_{1_p} + \vec{k}_{2_q} = 0$ for $p = q$). The remaining N(N-1) product fields will result in a distortion of the time-reversed wave (even though their efficiency is decreased somewhat due to phase mismatching). Here we have assumed E_4 to be a plane wave for simplicity; in the general case there will be additional distortions, since a given "mode" of the probe field may be coupled into an undesirable conjugate wave mode, leading to further degradation. Note that as the self-focusing becomes more pronounced, an increase in the number of pump wave modes results, which gives rise to even more severely distorted conjugate wave replicas.

In the limit of large optical powers, a catastrophic self-focusing effect will take place which would ultimately render the phase conjugate mirror useless. This occurs when the input laser power exceeds a critical value [5,17] of

$$P_c \sim \frac{n_o c^3}{24\pi\omega^2 \chi_{NL}^{(3)}} \qquad (3.7\text{-}6)$$

The value predicted by (3.7-6) places an upper limit upon the nonlinear gain coefficient ($|\kappa|$), given the beam's cross section. We note that the deleterious effects of self-focusing can be controlled somewhat by

the proper choice of the pump beams' transverse spatial profile.

The use of optical fibers or waveguides as providing for the nonlinear medium is one possible scheme for avoiding self-focusing problems, since one can realize rather large intensities (and hence large values of $|\kappa|$) over long interaction lengths with only modest input powers (which may be orders of magnitude less than P_c).

Even in the absence of self-focusing (i.e., if we assume no transverse dependence of the pump waves), there are still other undesirable effects that can be present, which involve the same, third-order, nonlinear susceptibility that provides for the phase conjugate interaction. That is, there may be additional sets of product fields by which phase-matched, third-order nonlinear polarizations can be realized. One such example would be the presence of terms as

$$P_{NL}^{(\omega_3,\omega_4)} = \chi_{NL}^{(3)}(A_1A_1^* + A_2A_2^*)A_{3,4}\ \exp[i(\omega_{3,4}t - \vec{k}_{3,4}\cdot\vec{r})] \qquad (3.7\text{-}7)$$

This nonlinear polarization merely modifies the local index of refraction [c.f. (3.7-3)]. However, if the two pump waves are unequal in amplitude, undesirable nonlinear phase shifts result which basically affect the frequency dependence and the fidelity of the conjugation interaction. Marburger and Lam [14,16], as well as Jensen [18], discuss these effects in more detail.

As a final example of undesirable (and in this case, unavoidable) third-order effects, consider the special case of a colinear pump and probe geometry. Assuming that the proper tensorial components of $\chi_{ijk\ell}^{(3)}$ are nonzero, one can separate out the pump from the probe/conjugate fields by polarization discrimination. (This is precisely the geometry

employed in an experiment we performed, to be discussed in the next chapter.) However, in the colinear case, there can exist undesirable backward-propagating fields that result from the following nonlinear polarization

$$P_{NL}^{(\omega_3)} = \chi_{NL}^{(3)} A_1^* A_2 A_4 \exp[i(\omega_2+\omega_4-\omega_1) - (\vec{k}_2+\vec{k}_4-\vec{k}_1)\cdot\vec{r}] \qquad (3.7\text{-}8)$$

Physically, this process is equivalent to replacing one of the pump fields (A_1) with the probe wave and vice versa. Thus, the overall backward-going, phase-matched, output wave is seen to be, from (3.3-12) and (3.7-8), in the limit of negligible pump depletion (and neglecting any nonlinearly-induced phase distortions)

$$A_3(0) = [-i \frac{\kappa^*}{|\kappa|} \tan(|\kappa|L)]A_4^*(0) + [- \frac{i\kappa}{|\kappa|} \tanh(|\kappa|L)]A_4(0) \qquad (3.7\text{-}9)$$

Recall that only if A_4 and A_1 copropagate, in the degenerate case, does this undesirable wave (the second term) result. The undesirable output wave is essentially equivalent to replacing the nonlinear medium with a real mirror. Two comments regarding this undesirable wave are in order. First, the phase matching constraints of the nonlinear interaction limit the "acceptance angle," or equivalently, the number of modes of the wave A_4 capable of yielding an apparent "real" reflection. Second, this "real" reflectivity [19] can never exceed unity by virtue of the effective forward-going "pump field" being A_4 itself. Of course, the desirable (conjugate) wave does not suffer from the above two constraints; all modes of the probe wave A_4 are capable of the same efficiency (or reflectivity), and reflectivities exceeding unity are possible. Marburger and Lam [16] discuss this case further with regard to nonlinear phase shifts and the oscillation condition.

We conclude this section with a brief discussion regarding inelastic nonlinear optical interactions, and their effects upon the desired phase conjugation interaction. Specifically, we will consider stimulated Brillouin scattering (SBS) and stimulated Raman scattering (SRS) processes. These interactions [5] are inherently inelastic in nature, since they involve the scattering of an input photon within a given medium into an output photon of lower energy with the concomitant creation of an acoustical phonon (in the case of SBS) or an optical phonon (in the case of SRS). Since the output photon is frequency shifted downward (by $\sim$1 cm^{-1} for SBS and $\sim$1000 cm^{-1} for SRS), these photons are to be considered as being no longer active in terms of participating in a degenerate four-wave, phase conjugate generation process. Hence, SBS and SRS can be viewed as being a (nonlinear) source of pump wave depletion. Again, we limit our discussion to the pump waves, since they will ultimately experience the nonlinear effects described here due to the fact that $|A_{1,2}|^2 >> |A_4|^2$ (typically). Since both SBS and SRS are "threshold" interactions [5], one must first exceed a critical input optical <u>intensity</u> prior to the onset of "oscillation" (recall that the onset of self-focusing requires a critical input <u>power</u>). The effective threshold intensities may be increased somewhat by the use of broadband optical excitation (this technique is practical in the case of SBS, where the gain bandwidth is $\sim 5 \times 10^{-3} cm^{-1}$; the corresponding bandwidth of SRS, being typically $\sim$ 5 cm^{-1}, is far too broad in frequency with respect to coherence lengths, etc.) for the pump fields.

Therefore, the threshold intensities for SBS and SRS, as well as the self-focusing critical power (for a fixed beam cross section) will place upper limits on the value of $|\kappa|$ and therefore limit the maximum nonlinear conjugate reflection coefficient for a given interaction geometry.

3.8 On the Origin of $\chi_{NL}^{(3)}$ in a Two-Level System, Assuming Single Photon Transitions

In this and the next section we present a description using a quantum mechanical viewpoint regarding the origin of the third order nonlinear optical susceptibility $\chi_{NL}^{(3)}$. Recall that previously we have described $\chi_{NL}^{(3)}$ as a phenomenological parameter which characterizes a given medium. We now consider the nature of $\chi_{NL}^{(3)}$ for two different atomic (or molecular) systems: a two-level system, and a three-level system, assuming allowed dipole transitions. The former case will be discussed below; the latter system will be analyzed in the next section. For both cases, we will use a time evolution operator formalism [20] with the associated Feynman diagram description to evaluate $\chi_{NL}^{(3)}$. In addition, in the three-level systems (next section) we will use a density matrix approach [5] to calculate $\chi_{NL}^{(3)}$, and compare the results with those of the former approach. In both approaches, we will rely on a perturbation expansion to simplify the analysis. This enables us to exploit simple diagrammatic rules to obtain the expression for $\chi_{NL}^{(3)}$ almost by inspection. Due to this perturbation technique, however, higher order effects such as saturation would require the addition of higher order perturbation terms, which we will not consider here. We

note that in certain cases, the density matrix equations can be solved exactly, thus yielding saturation effects [9]. However, the Feynman diagrammatic approach is a very powerful technique as well as being quite physical in nature, and is thus easy to grasp and utilize.

We note that in the analysis to be discussed in this and the next section, we will consider the steady state value of $\chi_{NL}^{(3)}$. We thus assume that all the participating optical fields are monochromatic and are on for all times. The transient effects of a three-level system irradiated by pulsed optical fields will be considered in Chapter VI, with respect to two-photon coherent states.

In order to evaluate $\chi_{NL}^{(3)}$, we must solve for the third order dielectric polarizability, defined classically to be

$$\langle \mu^{(3)} \rangle = \frac{\chi_{NL}^{(3)}}{N} E_1 E_2 E_4^* \tag{3.8-1}$$

where N is the atomic (or molecular) density. Quantum mechanically, the expectation value is defined by

$$\langle \mu \rangle = \langle \psi(t) | \mu | \psi(t) \rangle \tag{3.8-2}$$

where $|\psi(t)\rangle$ is the wave function of the system. By employing a perturbation evaluation of (3.8-2) which is third order in the optical fields, $\chi_{NL}^{(3)}$ can be found by using (3.8-2) in (3.8-1). We will use the time evolution operator perturbation technique in order to express $|\psi(t)\rangle$ to the various desired orders in the perturbing fields.

Prior to considering specific cases, we first review the time evolution operator formalism as presented by Yariv [21] in terms of its

application to nonlinear optics problems in general. We consider a semi-classical treatment: that is, the atomic system is described by Schrödinger's equation, whereas the optical perturbation is approximated in terms of macroscopic harmonic electromagnetic fields (i.e., not quantized). This approximation is valid, since we are considering fields with large photon densities.

The problem of evaluating the eigenfunction $|\psi(t)\rangle$ of an atom subjected to an external electromagnetic field can be solved by using Schrödinger's equation

$$H|\psi\rangle = i\hbar \frac{\partial}{\partial t} |\psi\rangle \tag{3.8-3}$$

An equivalent approach is to introduce the time evolution operator, $U(t_b,t_a)$ which operates on a wave function $|\psi(t_a)\rangle$ to yield a new wave function at a different time, t_b

$$|\psi(t_b)\rangle = U(t_b,t_a)\,|\psi(t_a)\rangle \tag{3.8-4}$$

where $U(t_b,t_a)$ satisfies

$$HU(t_b,t_a) = i\hbar \frac{\partial U(t_b,t_a)}{\partial t_b} \tag{3.8-5}$$

If H is time independent, $H \equiv H_o$, where $\partial H_o/\partial t = 0$. Thus we get from (3.8-5)

$$U(t_b,t_a) = \exp[-i \frac{H_o}{\hbar} (t_b-t_a)]$$

$$= \sum_m |m\rangle \langle m| \exp[-i\omega_m(t_b-t_a)] \tag{3.8-6}$$

where $\omega_m = E_m/\hbar$, and $|m\rangle$ is an eigenfunction with eigenvalue E_m. That is,

$$H_o|m> = \hbar\omega_m|m> \qquad (3.8\text{-}7)$$

These eigenfunctions form a complete orthonormal set. Hence,

$$\sum_m |m><m| = I \; ; \qquad <m|n> = \delta_{mn} \qquad (3.8\text{-}8)$$

For our case we take the Hamiltonian to be

$$H(t) = H_o + V(t) \qquad (3.8\text{-}9)$$

where H_o is the unperturbed Hamiltonian, and V(t) represents the time-dependent perturbation of the atomic system as a result of the interacting optical fields.

Formally, (3.8-5) can be expressed in its integral form

$$U(t_b,t_a) = -\frac{i}{\hbar}\int_{t_a}^{t_b} H(\tau)\, U(\tau,t_a)\,d\tau + I \qquad (3.8\text{-}10)$$

Following standard techniques[20,21] we assume that $U(t_b,t_a)$ can be expanded in a power series in powers of V(t) as

$$U(t_b,t_a) = U^{(0)}(t_b,t_a) + U^{(1)}(t_b,t_a) + U^{(2)}(t_b,t_a) + \cdots$$

$$\cdots + U^{(n)}(t_b,t_a) \qquad (3.8\text{-}11)$$

where , as an example, the first three terms are given by

$$U^{(0)}(t_b,t_a) = \exp[-\frac{iH_o}{\hbar}(t_b-t_a)]$$

$$U^{(1)}(t_b,t_a) = (\frac{-i}{\hbar})\int_{t_a}^{t_b} U^{(0)}(t_b,t)\, V(t)\, U^{(0)}(t,t_a)\, dt$$

$$U^{(2)}(t_b,t_a) = \left(\frac{-i}{\hbar}\right)^2 \int_{t_a}^{t_b > t_1} \int_{t_a}^{t_1} dt_1 dt_2 U^{(0)}(t_b,t_1)\, V(t_1)\, U^{(0)}(t_1,t_2)$$

$$\times\, V(t_2) U^{(0)}(t_2,t_a) \qquad (3.8\text{-}12)$$

where $t_b > t_1 > t_2 > \cdots > t_a$. We see that in general, from (3.8-4) and (3.8-11), $|\psi(t_b)\rangle$ can be related to $|\psi(t_a)\rangle$ by

$$|\psi(t_b)\rangle = U(t_b,t_a)|\psi(t_b)\rangle = \sum_{\ell=0}^{\infty} |\psi^{(\ell)}(t_b)\rangle = \{\sum_{\ell=0}^{\infty} U^{(\ell)}(t_b,t_a)\}|\psi(t_a)\rangle \qquad (3.8\text{-}13)$$

We now follow the procedure given by Yariv [21] to solve for the induced dipole moment to ℓ^{th} order in the perturbation $\langle\mu_i^{(\ell)}\rangle$ along the i^{th} axis (where $\ell = p+q$)

$$\langle\mu_i^{(p+q)}\rangle = \langle\psi^{(p)}|\mu_i|\psi^{(q)}\rangle = \langle n|U^{\dagger(p)}(t,0)\mu_i U^{(q)}(t,0)|n\rangle \qquad (3.8\text{-}14)$$

where $A^{\dagger}$ denotes the Hermitian conjugate of the operator A. We have used the fact that $|\psi^{(p)}\rangle$ and $|\psi^{(q)}\rangle$ can be expressed by (3.8-13) as

$$|\psi^{(\ell)}(t)\rangle = U^{(\ell)}(t,0)|\psi(0)\rangle \equiv U^{(\ell)}(t,0)|n\rangle \qquad (3.8\text{-}15)$$

Note that $|\psi^{(\ell)}\rangle$ involves the perturbation (contained in $U^{(\ell)}$) to the ℓ^{th} power and we have assumed that at t = 0 the atom is initially in the ground state $|n\rangle$.

Since we are concerned with evaluating perturbations that are <u>third order</u> in V(t), we have from (3.8-12) and (3.8-14), the constraint

$$p + q = 3 \qquad (3.8\text{-}16)$$

In what follows, we will be concerned only with $|\psi^{(\ell)}(t)\rangle$ having $\ell = 0,1,2,$ and 3 in (3.8-15). Once we have calculated (3.8-12), we will use (3.8-15) in (3.8-14) to form the nonlinear polarization

$$P_{NL}^{(3)} = N\langle\mu_i^{(3)}\rangle \tag{3.8-17}$$

This polarization will, in view of (3.8-16), contain the electric field to third power so that we can write

$$P_{NL}^{(3)} = \chi_{NL}^{(3)} E_1 E_2 E_4^* \tag{3.8-18}$$

where the fields have been chosen to be consistent with the phase conjugation interaction of interest. We thus obtain $\chi_{NL}^{(3)}$ from (3.8-17) and (3.8-18) as

$$\chi_{NL}^{(3)} = \frac{N\langle\mu_i^{(3)}\rangle}{E_1 E_2 E_4^*} \tag{3.8-19}$$

Using (3.8-6) in (3.8-12) and (3.8-15) results in the following perturbed wave function to the desired orders as discussed above

$$|\psi^{(0)}(t)\rangle = U^{(0)}(t,t_o)|n\rangle = \exp[-i\omega_n(t-t_o)]|n\rangle, \tag{3.8-20}$$

$$|\psi^{(1)}(t)\rangle = U^{(1)}(t,t_o)|n\rangle = -\frac{i}{\hbar}\sum_m \int_{t_o\to-\infty}^{t} |m\rangle\langle m|\exp[-i\omega_m(t-t_1)]V(t_1) \times \exp[-i\omega_n(t_1-t_o)]|n\rangle\, dt_1 \tag{3.8-21}$$

$$|\psi^{(2)}(t)\rangle = U^{(2)}(t,t_o)|n\rangle = \left(\frac{-i}{\hbar}\right)^2 \sum_{m,s} \int_{t_o}^{t} \int_{t_o \to -\infty}^{t_1 > t_2}$$

$$\times \exp[-\omega_s(t-t_1)]|s\rangle \langle s| V(t_1)$$

$$\times \exp[-i\omega_m(t_1-t_2)]|m\rangle \times \langle m|V(t_2)$$

$$\times \exp[-i\omega_n(t_2-t_0)]|n\rangle \, dt_2 dt_1 \qquad (3.8\text{-}22)$$

and

$$|\psi^{(3)}(t)\rangle = U^{(3)}(t,t_o)|n\rangle$$

$$= \left(\frac{-i}{\hbar}\right)^3 \sum_{m,\ell,s} \int_{t_o}^{t} \int_{t_o}^{t_1 > t_2} \int_{t_o \to -\infty}^{t_2 > t_3}$$

$$\times \exp[-i\omega_s(t-t_1)]|s\rangle \langle s|V(t_1)$$

$$\times \exp[-i\omega_\ell(t_1-t_2)]|\ell\rangle \langle \ell|V(t_2)$$

$$\times \exp[-i\omega_m(t_2-t_3)]|m\rangle \langle m|V(t_3)$$

$$\times \exp[-i\omega_n(t_3-t_0)]|n\rangle \, dt_3 dt_2 dt_1 \qquad (3.8\text{-}23)$$

Since we are concerned with the steady state values for the perturbed wave functions (and hence for the evaluation of the nonlinear susceptibility), we take the lower limit of the above integrals to be $t = -\infty$. We thus consider the perturbing optical fields to be turned on adiabatically from $t = -\infty$.

By virtue of the three perturbing optical fields that we are considering, the perturbing Hamiltonian (assuming only dipole allowed transitions) becomes

$$V(t) = \frac{-\vec{\mu}}{2} \cdot \{ \sum_{\ell=1,2,\text{and } 4} \vec{E}_\ell \exp[i(\omega_\ell t - \vec{k}_\ell \cdot \vec{r})] + \text{c.c.} \} \qquad (3.8\text{-}24)$$

In what follows we drop the wave vector terms; we will insert them in the final results below. We note that the form of the above perturbation Hamiltonian is a result of the dipole approximation, which applies here, since the optical wavelengths are much greater than the atomic dimensions (by 3 to 4 orders of magnitude).*

Using (3.8-24) in (3.8-21) and performing the prescribed integration, we obtain terms of the form (where $\omega_{mn} \equiv \omega_m - \omega_n$)

$$|\psi^{(1)}_{\pm\omega_i}(t)\rangle = \frac{1}{2\hbar} \sum_m (\mu_i)_{mn} E_i^{(\pm)} \frac{\exp[i(\pm\omega_i - \omega_n)t]}{\omega_{mn} \pm \omega_i - i\gamma} |m\rangle \qquad (3.8\text{-}25)$$

where $E_i^{(+)} \equiv E_i$, $E_i^{(-)} \equiv E_i^*$, and μ_i is the projection of $\vec{\mu}$ along $\vec{E}_i$. In order to arrive at the above expression, we introduced a convergence factor, γ, such that the perturbing fields at $t < 0$ become

$$\vec{E}(t) \rightarrow \lim_{\gamma \rightarrow 0^+} e^{\gamma t} \vec{E}(t) \qquad (3.8\text{-}26)$$

This procedure removes the divergence at $t = -\infty$. This is physically equivalent to neglecting any transient responses of the atomic system to the perturbing fields, which is exactly what we want, since we wish to investigate the steady state polarizability of the system. The procedure is equivalent to solving for the steady state response of a

*Based on this approximation, $\vec{k}$ and $\vec{r}$ in (3.8-24) are to be considered as being "c-numbers" (a la Dirac) and not quantum mechanical operators.

damped harmonic oscillator driven by an external harmonic force. We remark that the transient response of an optical system driven by the same set of fields given above has been analyzed using a time evolution operator approach (with regard to phase conjugation processes) by Yariv and AuYeung [22]. We further remark that Yariv [21] has identified the convergence factors (γ) in (3.8-25) with the finite linewidth, or equivalently, with the lifetime of a given transition. In the analysis that follows, we set all such convergence factors to be γ. The precise description of the γ's in terms of the various relaxation times of the atomic system will be given later, where a density matrix approach will be employed to calculate the same $\chi^{(3)}_{NL}$.

Returning to the above result, (3.8-25), we note that $|\psi^{(1)}_{+\omega_i}(t)\rangle$ [$|\psi^{(1)}_{-\omega_i}(t)\rangle$] involves an emission [absorption] of a photon of radian frequency ω_i. The result of this perturbation thus scatters the atomic system from the ground state ($|n\rangle$) to a final state ($|m\rangle$), with the summation of (3.8-25) taken over all such possible states. We have dropped the phase factor $\exp(i\omega_n t_o)$ from (3.8-25), since it cancels out in the calculation of physical observables (e.g., $\langle\mu\rangle$).

We next calculate the second-order perturbed wave function by using (3.8-24) in (3.8-22). The result is seen to be

$$|\psi^{(2)}_{\pm\omega_i,\pm\omega_j}(t)\rangle = \sum_{m,s} \left(\frac{1}{2\hbar}\right)^2 E_i^{(\pm)} E_j^{(\pm)} \times \frac{(\mu_i)_{mn} (\mu_j)_{sm} \exp[i(-\omega_n \pm \omega_i \pm \omega_j)t]}{(\omega_{mn} \pm \omega_i - i\gamma)(\omega_{sn} \pm \omega_i \pm \omega_j - i\gamma)} |s\rangle \tag{3.8-27}$$

We see that (3.8-27) contains 16 possible combinations of $\pm\omega_i$ and $\pm\omega_j$ in the final wave function. Symbolically, this wave function implies an emission (absorption) of a photon at ω_i, followed by a subsequent emission (absorption) of a photon at ω_j, as indicated by the (+) [(-)] sign. Physically, ω_i causes a scattering of the initial state $|n\rangle$ to a state $|m\rangle$ at time t_2, followed by an interaction with the second photon ω_j, which scatters the atom to the final state, $|s\rangle$ at time t_1 (where $t > t_1 > t_2$). Again, the summation is taken over all possible quantum levels in the atomic system.

In an analogous manner, the third-order wave function can be written as

$$\left|\psi^{(3)}_{\pm\omega_i,\pm\omega_j,\pm\omega_k}(t)\right\rangle = \sum_{m,\ell,s} \left(\frac{1}{2\hbar}\right)^3 E_i^{(\pm)} E_j^{(\pm)} E_k^{(\pm)}$$

$$\times \frac{(\mu_i)_{mn}\,(\mu_j)_{\ell m}(\mu_k)_{s\ell}\,\exp[i(-\omega_n \pm\omega_i \pm\omega_j \pm\omega_k)t]}{(\omega_{mn}\pm\omega_i - i\gamma)(\omega_{\ell n}\pm\omega_i\pm\omega_j - i\gamma)(\omega_{sn}\pm\omega_i\pm\omega_j\pm\omega_k - i\gamma)}\ |s\rangle \qquad (3.8\text{-}28)$$

In (3.8-28) there are $6^3 = 216$ possible combinations, involving summations over two sets of intermediate states ($|m\rangle$ and $|\ell\rangle$), with the atoms finally being scattered into state $|s\rangle$, as a result of the perturbations introduced by the three photons.

We now consider the possible interaction processes that yield nonlinear dipoles of the form (3.8-14) subject to the condition (3.8-16) for the case of single (dipole-allowed) photon transitions involving a two-level system. The other constraint is that the product of the three fields have the form as in (3.8-18). The energy level diagram, along with the interacting photons is shown in Figure 3.10a.

From equations (3.8-25), (3.8-27), and (3.8-28) we see that the possible sets of perturbed wave functions yielding the desired nonlinear dipoles are given symbolically as

$$\langle \mu_i^{(3)} \rangle = \langle \psi^{(1)}_{-\omega_1}(t) | \mu_i | \psi^{(2)}_{-\omega_4,\omega_2}(t) \rangle + \langle \psi^{(3)}_{-\omega_1,\omega_4,-\omega_2}(t) \; | \mu_i | \psi^{(0)}(t) \rangle + \; (1 \leftrightarrows 2 \text{ terms}) \tag{3.8-29}$$

The first term involves a first-order perturbed wave function which originates in the ground state and is scattered to the excited state $|b\rangle$ via absorption of a photon at ω_1. This wave function is coupled via μ_i to a second-order wave function which scatters from the ground state $|a\rangle$ to the excited state $|b\rangle$ via absorption of a photon at ω_4, and subsequently scatters back to the ground state $|a\rangle$ via emission of a photon at ω_2.

The second term in (3.8-29) involves a third-order wave function

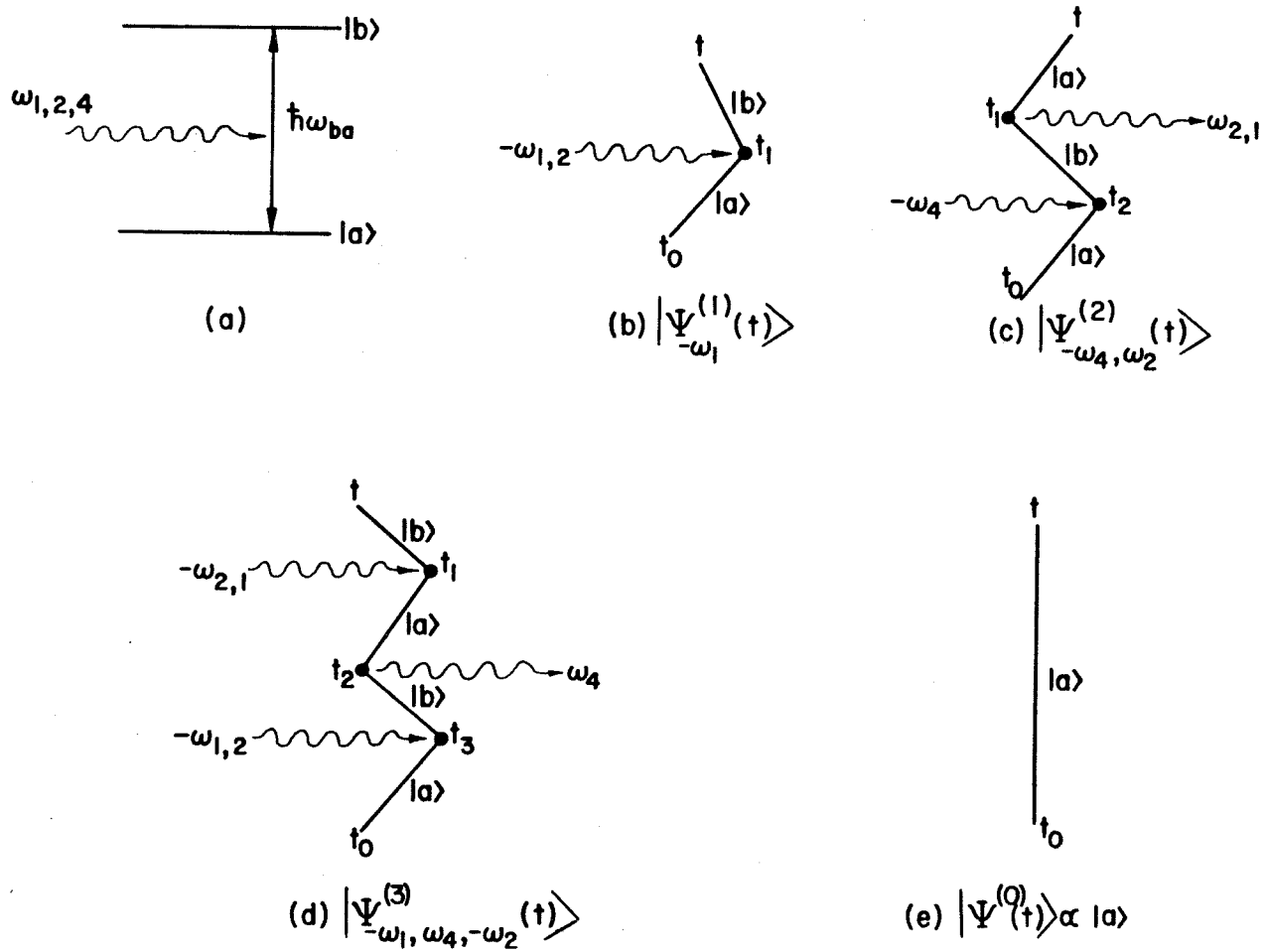

Fig. 3.10 (a) Energy level diagram and input photon frequencies for a two-level system. (b)-(e) Feynman diagrams used for $|\psi^{(1)}_{-\omega_1}(t)\rangle$, $|\psi^{(2)}_{-\omega_4,\omega_2}(t)\rangle$, $|\psi^{(3)}_{-\omega_1,\omega_4-\omega_2}(t)\rangle$, and $|\psi^{(0)}(t)\rangle$, respectively.

which is excited to $|b\rangle$ via ω_1, scatters to $|a\rangle$ via emission of ω_4 and finally is excited again to $|b\rangle$ via ω_2. This wave function is coupled via μ_i to a zeroth-order wave function which is unperturbed, and hence remains in the ground state, $|a\rangle$.

We see that the above processes can be depicted schematically in terms of Feynman diagrams, as shown in Figure 3.10b-e. Each photon changes the state of the system (solid line). A photon pointing toward (away) from a vertex implies an absorption (emission) of a quantum at ω_i in effecting the change of the eigenstate.

For brevity we evaluate here only the first term in (3.8-29). It can be shown that the second term, together with the associated permutations of ω_1 and ω_2, yields identical results.

The first term yields, using (3.8-25) and (3.8-27)

$$\langle \psi^{(1)}_{-\omega_1}(t)|\mu_i|\psi^{(2)}_{-\omega_4,\omega_2}(t)\rangle = \left(\frac{1}{2\hbar}\right)^3$$

$$\times \Big\langle \{E_1^* \mu_{1_{ba}} \frac{\exp[i(-\omega_1-\omega_b)t]}{(\omega_{ba}-\omega_1-i\gamma)} |b\rangle\}^\dagger |\mu_i|$$

$$\times \{E_4^* E_2 \mu_{4_{ba}} \mu_{2_{ab}} \frac{\exp[i(-\omega_4+\omega_2-\omega_a)t]}{(\omega_{ba}-\omega_4-i\gamma)(-\omega_4+\omega_2-i\gamma)} |a\rangle\}\Big\rangle \qquad (3.8\text{-}30)$$

Setting $\omega_1 = \omega_2 = \omega_4 = \omega$ (the degenerate case), assuming line-center operation ($\omega \simeq \omega_{ba}$), defining $|\mu_{ab}| = |\mu_{ba}| \equiv |\mu|$ and including the other contributing terms in (3.8-29), we get

$$\langle \mu^{(3)} \rangle = \frac{iE_1E_2E_4^* |\mu|^4 \exp(i\omega t)}{2\hbar^3\gamma^3} \qquad (3.8\text{-}31)$$

Using the definition for the nonlinear polarization given by (3.8-18), we have

$$P_{NL}^{(3)} = \underset{\text{1-photon}}{\chi_{NL}^{(3)}} E_1 E_2 E_4^* \exp\{i[\omega t - (\vec{k}_1+\vec{k}_2-\vec{k}_4)\cdot\vec{r}]\} \qquad (3.8\text{-}32)$$

where we have included the wave vector part of the macroscopic fields from (3.8-24). The third order nonlinear optical susceptibility is thus seen to be from (3.8-19), assuming parallel field polarizations

$$\underset{\text{1-photon}}{\chi_{NL}^{(3)}} = \frac{iN|\mu|^4}{2\hbar^3\gamma^3} \qquad (3.8\text{-}33)$$

We therefore see from (3.8-32) that if $\vec{k}_1+\vec{k}_2 = 0$ (i.e., counter-propagating pump fields), the nonlinear polarization will give rise to a field that radiates at frequency ω in the $-\vec{k}_4$ direction, with an amplitude proportional to E_4^*. This field is recognized as the conjugate replica of E_4, as discussed in Section 3.3.

3.9 On The Origin of $\chi_{NL}^{(3)}$ for Two-Photon Transitions

In this section we will derive the third order nonlinear optical susceptibility assuming that the three incident optical fields given in (3.8-24) interact with a three-level system. The energy levels considered are shown in Figure 3.11a. We assume that there exist dipole moments connecting the ground and intermediate states, and the intermediate and upper levels; further, no dipole-allowed transition connects the ground and upper levels. We will first use the time evolution approach as described in the last section. The section will conclude with a brief derivation of the susceptibility

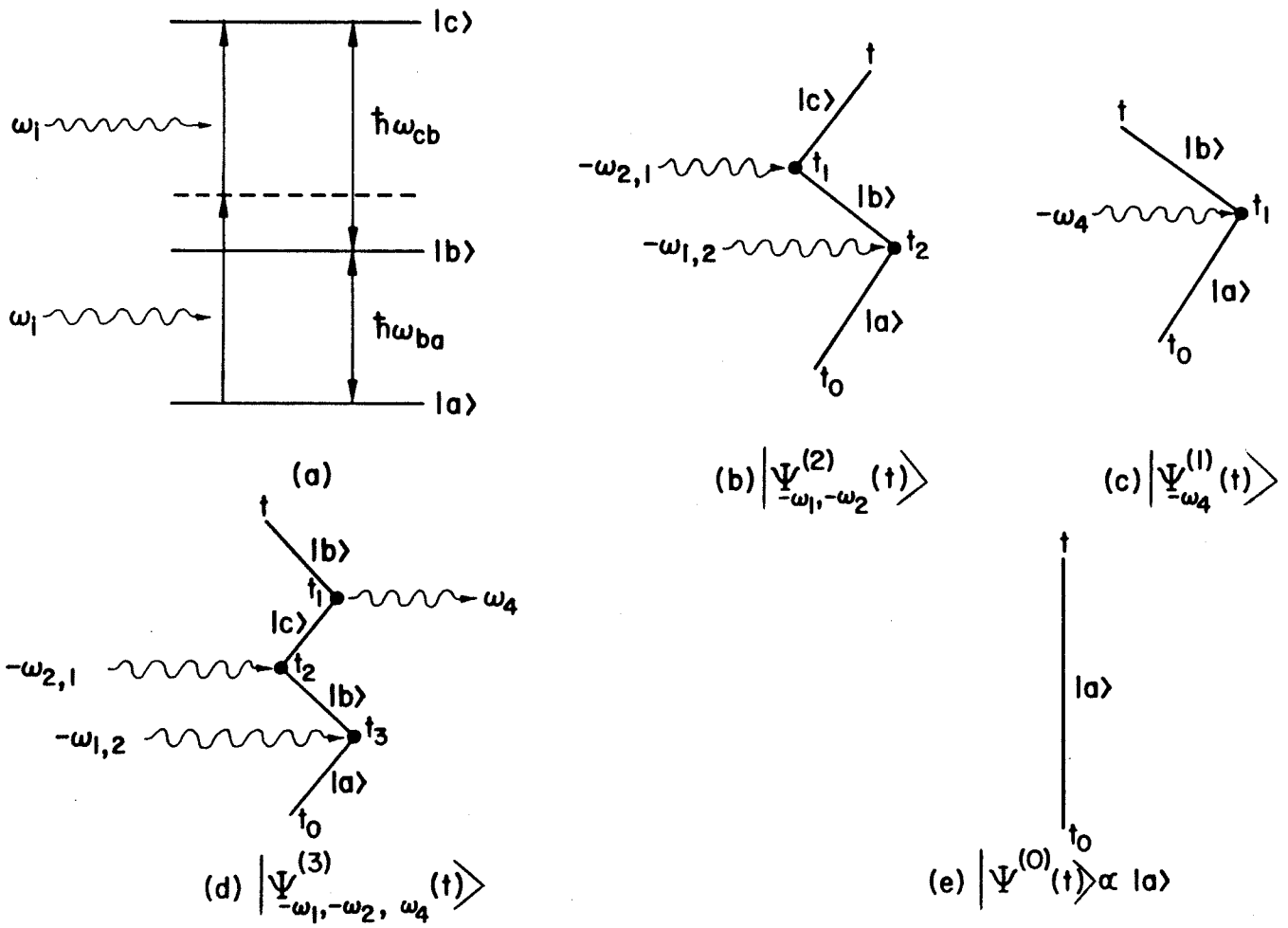

Fig. 3.11(a) Energy level diagram and input photon frequencies for a three-level system.
(b)-(e) Feynman diagrams used for $|\psi^{(2)}_{-\omega_1,-\omega_2}(t)\rangle$, $|\psi^{(1)}_{-\omega_4}(t)\rangle$, $|\psi^{(3)}_{-\omega_1,-\omega_2,\omega_4}(t)\rangle$, and $|\psi^{(0)}(t)\rangle$, respectively.

using a density matrix approach.

A. Time Evolution Operator Evaluation of $\chi^{(3)}_{NL_{2\text{-photon}}}$

Using the notation of the last section, the nonlinearly induced dipole moment is given by

$$\langle \mu_i^{(3)} \rangle = \langle \psi^{(2)}_{-\omega_1,-\omega_2}(t) | \mu_i | \psi^{(1)}_{-\omega_4}(t) \rangle + \langle \psi^{(3)}_{-\omega_1,-\omega_2,\omega_4}(t) | \mu_i | \psi^{(0)}(t) \rangle + (1 \leftrightarrows 2 \text{ terms}) \quad (3.9\text{-}1)$$

The associated Feynman diagrams are sketched in Figures 3.11b to 3.11e. As discussed in the last section, the results are not modified upon exchange of ω_1 and ω_2; thus each term need only be evaluated once, with the result multiplied by a factor of 2.

We will outline only the derivation of the first term. From the Feynman diagrams, we see that $|\psi^{(2)}(t)\rangle$ corresponds to the absorption of two (pump) photons which leads to a transition to the upper level $|c\rangle$. This now couples with $|\psi^{(1)}(t)\rangle$, which absorbs a photon at ω_4, thus inducing a transition to the intermediate level $|b\rangle$, with the resultant dipole moment in (3.9-1) coupling states $|c\rangle$ and $|b\rangle$.

Using (3.8-27) for $|\psi^{(2)}(t)\rangle$ we get

$$|\psi^{(2)}_{-\omega_1,-\omega_2}(t)\rangle = \left(\frac{1}{4\hbar^2}\right) \frac{E_1^* E_2^* \mu_{1_{ba}} \mu_{2_{cb}} \exp[i(-\omega_a-\omega_1-\omega_2)t]}{(\omega_{ba}-\omega_1-i\gamma_{ba})(\omega_{ca}-\omega_1-\omega_2-i\gamma_{ca})} |c\rangle \quad (3.9\text{-}2)$$

and from (3.8-25) we get for $|\psi^{(1)}(t)\rangle$

$$\left|\psi^{(1)}_{-\omega_4}(t)\right\rangle = \left(\frac{1}{2\hbar}\right) \frac{E_4^* \mu_{4_{ba}} \exp[i(-\omega_a-\omega_4)t]}{(\omega_{ba} - \omega_4 - i\gamma_{ba})} |b\rangle \qquad (3.9\text{-}3)$$

Forming $\langle\mu^{(3)}\rangle$ assuming that $\omega_1 = \omega_2 = \omega_4 \equiv \omega$ as before, assuming parallel field polarizations, and setting $\Delta_2 \equiv \omega_{ca} - (\omega_1+\omega_2)$ corresponding to the two-photon resonance offset, we get

$$\langle\mu^{(3)}\rangle = \frac{E_1 E_2 E_4^* |\mu_{ba}|^2 |\mu_{cb}|^2 (\Delta_2 - i\gamma_{ca})}{4\hbar^3 (\Delta_1^2 + \gamma_{ba}^2)(\Delta_2^2 + \gamma_{ca}^2)} \exp(i\omega t) \qquad (3.9\text{-}4)$$

where $\Delta_1 \equiv \omega_{ba}-\omega$ is the energy offset from exact resonance with the intermediate state. An extra factor of two has been inserted to account for the exchange of ω_1 and ω_2. Using (3.8-18), we get the contribution for the nonlinear polarization for the first term (I) of (3.9-1) to be

$$P^{(3)}_{NL} = \chi^{(3)}_{\substack{NL \\ 2\text{-photon}_{(I)}}} E_1 E_2 E_4^* \exp\{i[\omega t - (\vec{k}_1 + \vec{k}_2 - \vec{k}_4)\cdot\vec{r}]\} \qquad (3.9\text{-}5)$$

where we have inserted the wave vector factor in the perturbing fields. It thus follows from (3.8-17,19) and (3.9-4,5) that

$$\chi^{(3)}_{\substack{NL \\ 2\text{-photon}_{(I)}}} = \frac{N|\mu_{ba}|^2 |\mu_{cb}|^2 (\Delta_2 - i\gamma_{ca})}{4\hbar^3 (\Delta_1^2+\gamma_{ba}^2)(\Delta_2^2 + \gamma_{ca}^2)} \qquad (3.9\text{-}6)$$

We therefore see that from (3.9-5), the nonlinear polarization radiates the desired conjugate field along the backward ($-\vec{k}_4$) direction of the probe field if the pump fields are counterpropagating (i.e., $\vec{k}_1 + \vec{k}_2 = 0$).

Applying the same procedure for the evaluation of the second term in (3.9 -1) leads to the following result

$$\chi^{(3)}_{\substack{NL \\ 2\text{-photon} \\ (II)}} = \frac{N}{4\hbar^3} \frac{|\mu_{ba}|^2 |\mu_{bc}|^2 (\Delta_1 - i\gamma_{ba})^2 (\Delta_2 - i\gamma_{ca})}{(\Delta_1^2 + \gamma_{ba}^2)^2 (\Delta_2^2 + \gamma_{ca}^2)} \qquad (3.9\text{-}7)$$

Forming the resultant sum from (3.9-6) and (3.9-7) yields the final value for the two-photon nonlinear susceptibility

$$\chi^{(3)}_{\substack{NL \\ 2\text{-photon}_{(total)}}} = \frac{N}{2\hbar^3} \frac{|\mu_{ba}|^2 |\mu_{cb}|^2 \Delta_1 (\Delta_1 - i\gamma_{ba})(\Delta_2 - i\gamma_{ca})}{(\Delta_1^2 + \gamma_{ba}^2)^2 (\Delta_2^2 + \gamma_{ca}^2)} \qquad (3.9\text{-}8)$$

Equation (3.9-8) has the interesting property that if the interacting photons are resonant with the intermediate state (i.e., $\Delta_1 = 0$), then $\chi^{(3)} \to 0$. This result needs to be qualified. First, we have restricted the evaluation of $\chi^{(3)}$ to a limited set of Feynman diagrams. For the field polarizations chosen, a complete description of the problem requires additional contributions from single photon transitions (recall last section). In addition, the physical nature of the convergence factors (γ's) needs further consideration. The density matrix approach (see next subsection) is a technique which considers these points in more detail.

B. Density Matrix Evaluation of $\chi^{(3)}_{NL_{2\text{-photon}}}$

Before concluding this section, we wish to discuss briefly a second, and more complete, approach useful in evaluating nonlinear optical processes: that of the time-dependent, density matrix perturba-

tion technique. Recall that a major advantage of the time evolution/ Feynman diagram treatment as discussed above lies in its ease of evaluating resonantly enhanced optical processes, virtually by inspection. The "cost" of resorting to this method, however, is that several other processes of interest may be overlooked and, perhaps, a more fundamental drawback is that the linewidths obtained (i.e., the γ's) resulted from the ad hoc insertion of a convergence factor necessary in performing the various temporal integrations. In the density matrix approach, the linewidths enter the formalism from the onset, and are thus treated in a more physical fashion. This formalism yields results that will be shown to differ subtly from the evolution operator approach, and at the same time are to be considered as being more accurate and complete.

We note further that in general when we consider an ensemble of atoms, the system is not necessarily in a pure state at the onset (as was assumed in the time evolution formalism). Typically, one knows only the equilibrium population distribution, which is usually given by the Boltzmann distribution function [23]

$$\rho_{nn} = \rho_{gg} \exp[-(E_n-E_g)/kT] \qquad (3.9\text{-}9)$$

where ρ_{nn} denotes the population density of the n^{th} state with energy E_n; ρ_{gg} is the ground state density. Also, the lineshape of each energy level is not precisely known in general, due to collisions, spontaneous emission, etc. [24].

The density matrix equation of motion is given by [5,25]

$$\frac{d}{dt}\rho_{mn} = -\frac{i}{\hbar}[H,\rho]_{mn} - \frac{1}{T_{mn}}(\rho_{mn} - \bar{\rho}_{mn}) \qquad (3.9\text{-}10)$$

where the subscripts (m and n) denote the energy level indices, and [A,B] is the commutator of the operators A and B. In (3.9-10), ρ_{mn} is a matrix element of the density operator, ρ, and is defined to be $\rho_{mn} = \overline{\langle\psi|n\rangle\langle m|\psi\rangle}$ where the bar denotes a statistical average over the ensemble; the $|n\rangle$'s form a complete orthonormal set describing the atomic system. $\bar{\rho}_{mn}$ is the equilibrium density matrix element, which is diagonal in the energy representation. We assume that the only level populated under the thermal equilibrium condition is the ground state (since $\hbar\omega_{mn} >> kT$ for the energy levels considered).

We note that for $m = n$, T_{mn} equals T_1 (known as the longitudinal relaxation time). T_{nn}^{-1} describes the relaxation rate of the n^{th} state and is given roughly by [5]

$$T_{nn}^{-1} \sim \frac{1}{t_{spont}} + \frac{1}{T_{inelastic}} \qquad (3.9\text{-}11)$$

where t_{spont} is the spontaneous (radiative) lifetime of the n^{th} state, and $T_{inelastic}$ is the inelastic collision time.

For $m \neq n$, T_{mn} equals T_2 (known as the transverse relaxation time). T_{mn}^{-1} thus accounts for the decay of the off-diagonal density matrix elements, due to dephasing collisions. T_{mn}^{-1} is given roughly by [26,27]

$$T_{mn}^{-1} \sim \frac{1}{2}(T_{mm}^{-1} + T_{nn}^{-1}) + \gamma'_{mn} \qquad (3.9\text{-}12)$$

where other factors which can make ρ_{mn} decay, such as phase-

interrupting collisions [28], velocity changing collisions [29], etc. are lumped into γ'_{mn} (where we assume that $\gamma'_{mn} = \gamma'_{nm}$). For the analysis that follows, we assume that T_1 and T_2 are numerical constants that characterize the atomic system.

In terms of the density matrix, the expectation value of the dipole moment operator is given by [5]

$$\langle \mu_i \rangle = \text{Trace}(\rho \mu_i) \tag{3.9-13}$$

We now wish to solve equation (3.9-10) for ρ, and subsequently to evaluate $\langle \mu_i \rangle$ in order to obtain an expression for $\chi^{(3)}_{NL}$. We proceed by using a perturbation expansion in V of ρ_{mn} [5]

$$\rho_{mn} = \rho^{(0)}_{mn} + \rho^{(1)}_{mn} + \rho^{(2)}_{mn} + \rho^{(3)}_{mn} + \ldots \tag{3.9-14}$$

where $\rho^{(\ell)}$ depends on the perturbation to the ℓ^{th} power or, in our case, $(V = -\vec{\mu}\cdot\vec{E})^{\ell}$. Recall from (3.8-9) that $H = H_o + V(t)$.

Upon substitution of (3.9-14) into (3.9-10), we obtain the well known result [5]

$$\frac{d\rho^{(\ell)}_{mn}}{dt} - i\omega_{nm}\,\rho^{(\ell)}_{mn} + \frac{\rho^{(\ell)}_{mn}}{T_{mn}} = \frac{-i}{\hbar}\,[V(t),\rho^{(\ell-1)}]_{mn} \tag{3.9-15}$$

where $\omega_{nm} = (E_n - E_m)/\hbar$.

We see that, if we know the commutator involving the perturbation to order k with respect to the density matrix, we can evaluate the time dependence of ρ_{mn} to order k+1. We desire to obtain

$\langle \mu_i^{(3)} \rangle$, which therefore requires knowledge of $\rho_{mn}^{(3)}$. The specific product of the perturbing fields we wish to consider is again of the form $E_1 E_2 E_4^*$. In the analysis that follows, we assume that $\rho_{11}^{(0)} = 1$ and $\rho_{mn}^{(0)} = 0$ for all other values of m and n.

We assume that the interaction takes place in a three-level system, as shown in Figure 3.11a, which implies that the density matrix is a 3 x 3 array.

Now, assuming that the only nonzero dipole operators are $\vec{\mu}_{ab}$ (thus $\vec{\mu}_{ba}$) and $\vec{\mu}_{bc}$ (thus $\vec{\mu}_{cb}$) and that there are three interacting harmonic electromagnetic fields present, the perturbation Hamiltonian becomes

$$V(t) = -\tilde{\vec{\mu}} \cdot \vec{E} = -\frac{1}{2} \begin{pmatrix} 0 & \vec{\mu}_{ab} & 0 \\ \vec{\mu}_{ba} & 0 & \vec{\mu}_{bc} \\ 0 & \vec{\mu}_{cb} & 0 \end{pmatrix} \cdot \{ \vec{E}_1 \exp[i(\omega_1 t - \vec{k}_1 \cdot \vec{r})]$$

$$+ \vec{E}_2 \exp[i(\omega_2 t - \vec{k}_2 \cdot \vec{r})] \qquad (3.9\text{-}16)$$

$$+ \vec{E}_4 \exp[i(\omega_4 t - \vec{k}_4 \cdot \vec{r})] + \text{c.c.} \}$$

Upon inspection of (3.9-13) and (3.9-16), we see that the only nonzero elements in $\langle \mu_i^{(3)} \rangle$ that contain terms that are third order in the applied fields are

$$\langle \mu_i^{(3)} \rangle = \rho_{12}^{(3)} (\mu_{21})_i + \rho_{23}^{(3)} (\mu_{32})_i + \text{c. c.} \qquad (3.9\text{-}17)$$

We obtain $\rho_{12}^{(3)}$ and $\rho_{23}^{(3)}$ as follows. The solution of (3.9-15) is given by [5]

$$\rho_{mn}^{(\ell)}(t) = \frac{-i}{\hbar}\int_{t_o}^{t} e^{i(\omega_{mn} - i\gamma_{mn})(t'-t)} [V(t'),\rho^{(\ell-1)}(t')]_{mn}\, dt' \qquad (3.9\text{-}18)$$

where $\omega_{mn} \equiv \omega_m - \omega_n$, and we have set the linewidths $\gamma_{mn} = T_{mn}^{-1}$.

In the analysis that follows, we set $t_o \to -\infty$, since we assume that the perturbing fields are on indefinitely. Thus, we neglect any transient effects (consistent with the evolution operator analysis of the preceding subsection).

The nonzero elements of the commutator in (3.9-18) are seen to be, using (3.9-16),

$$[V,\rho] = \begin{pmatrix} (V_{12}\rho_{21} - \rho_{12}V_{21}) & (V_{12}\rho_{22} - \rho_{11}V_{12} - \rho_{13}V_{32}) & (V_{12}\rho_{23} - \rho_{12}V_{23}) \\ (V_{21}\rho_{11} + V_{23}\rho_{31} - \rho_{22}V_{21}) & (V_{21}\rho_{12} + V_{23}\rho_{32} - \rho_{21}V_{12} - \rho_{23}V_{32}) & (V_{21}\rho_{13} + V_{23}\rho_{33} - \rho_{22}V_{23}) \\ (V_{32}\rho_{21} - \rho_{32}V_{21}) & (V_{32}\rho_{22} - \rho_{31}V_{12} - \rho_{33}V_{32}) & (V_{32}\rho_{23} - \rho_{32}V_{23}) \end{pmatrix} \qquad (3.9\text{-}19)$$

From the form of (3.9-19) we see that there are five density matrix perturbation "pathways" (or "sequences") that give rise to the desired third order terms in (3. 9-17). We have assumed that the only nonzero zeroth-order density matrix element is given by $\rho_{11}^{(0)} = 1$. Figure 3.12 shows these five sequences.

We note that from the above density matrix sequences, $\rho_{11}^{(2)}$ and $\rho_{22}^{(2)}$ give rise to population shifts of levels 1 and 2, respec-

$$\rho_{mn}^{(\ell)} \propto \left[V, \rho^{(\ell-1)} \right]_{mn}$$

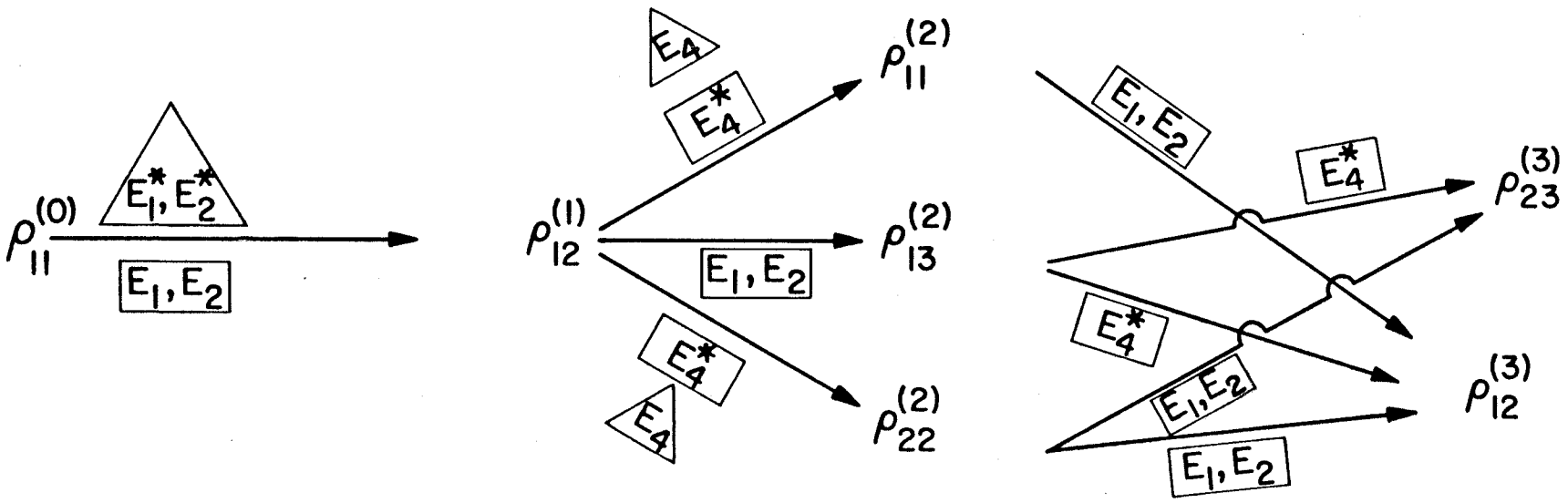

Fig. 3.12 The 5 nonzero density matrix perturbation sequences (which follow from the commutator as shown) that yield the desired nonlinear polarization ($P_{NL} \propto E_i E_j E_k^*$) for a three-level system. The E_i contained in the boxes or triangles depict the desired, near-resonant perturbation fields necessary to yield the next order, perturbed density matrix element.

tively, thus modulating the atomic densities spatially. It can be shown that these two terms arise from a product of fields proportional to $E_i E_j^*$. In the next section we discuss the holographic analogs of certain four-wave processes; we point out here that $\rho_{11}^{(2)}$ and $\rho_{22}^{(2)}$ being of the form above, imply the formation of a hologram through the spatial modulation of population densities. On the other hand, the term $\rho_{13}^{(2)}$, being proportional to a product of fields $E_i E_j$ (in our case the pump fields), oscillates at 2ω and therefore has no direct holographic analog (the next section as well as Section 6.4 discusses this further). The term $\rho_{13}^{(2)}$ is called the "two-photon coherent state" [30] contribution to $\chi_{NL}^{(3)}$ [31].

Applying the above formalism [via (3.9-18) and (3.9-19)] to third order in the fields, assuming that only $\rho_{11}^{(0)} \neq 0$ ($N\rho_{11}^{(0)} \equiv N$), seeking the desired form of the field product, retaining only terms that are nearly resonant ("the rotating wave approximation"), and using (3.9-17) with the definition of the nonlinear polarization $P_{NL}^{(3)} = N\langle \mu_i^{(3)} \rangle$, results in the following expression of $P_{NL}^{(3)}$ after tedious, yet straightforward algebra :

$$P_{NL}^{(3)} = \frac{N}{(2\pi)^3} E_1^* E_2 E_4 (\mu_{ba})_1 \quad (\mu_{ab})_2 \quad \frac{e^{i(-\omega_1+\omega_2+\omega_4)t} \; e^{-i(-\vec{k}_1+\vec{k}_2+\vec{k}_4)\cdot\vec{r}}}{(\omega_1-\omega_{ba}-i\gamma_{ab})}$$

$$\times \left\{ \left[\frac{(\mu_{ba})_3 \; (\mu_{ab})_4}{(-\omega_1+\omega_2+\omega_4-\omega_{ba}-i\gamma_{ab})} \left(\frac{1}{(\omega_2-\omega_1-i\gamma_{bb})} + \frac{1}{(\omega_2-\omega_1-i\gamma_{aa})} \right) \right] \right.$$

$$\left. - \left[\frac{(\mu_{cb})_3 \; (\mu_{bc})_4}{(-\omega_1+\omega_2+\omega_4-\omega_{ab}-i\gamma_{bc})} \left(\frac{1}{(\omega_2-\omega_1-i\gamma_{bb})} \right) \right] \right\}$$

$$+ \frac{N}{(2\pi)^3} E_1 E_2 E_4^* (\mu_{ab})_1 \quad \frac{e^{i(\omega_1+\omega_2-\omega_4)t} \; e^{-i(\vec{k}_1+\vec{k}_2-\vec{k}_4)\cdot\vec{r}}}{(\omega_1-\omega_{ba}-i\gamma_{ab})}$$

$$\times \left\{ \left[\frac{-(\mu_{ab})_2 (\mu_{ba})_3 (\mu_{ba})_4}{(\omega_1+\omega_2-\omega_4-\omega_{ba}-i\gamma_{ab})} \left(\frac{1}{(\omega_1-\omega_4-i\gamma_{bb})} + \frac{1}{(\omega_1-\omega_4-i\gamma_{aa})} \right) \right] \right.$$

$$+ \left[\frac{(\mu_{bc})_2 (\mu_{cb})_3 (\mu_{ba})_4}{(\omega_1+\omega_2-\omega_4-\omega_{cb}-i\gamma_{bc})} \left(\frac{1}{(\omega_1-\omega_4-i\gamma_{bb})} \right) \right]$$

$$\left. + \left[\frac{(\mu_{bc})_2}{(\omega_1+\omega_2-\omega_{ca}-i\gamma_{ac})} \left(\frac{(\mu_{cb})_3 (\mu_{ba})_4}{(\omega_1+\omega_2-\omega_4-\omega_{cb}-i\gamma_{bc})} - \frac{(\mu_{ba})_3 (\mu_{cb})_4}{(\omega_1+\omega_2-\omega_4-\omega_{ba}-i\gamma_{ab})} \right) \right] \right\}$$

(3.9-20)

In (3.9-20) we have added the wave vector factors to account for the spatial evolution of the fields. We thus see that the first term in the equation gives rise to a backward-going conjugate wave ($\propto E_1^*$) if we set $\vec{k}_2 + \vec{k}_4 = 0$, and assume degenerate fields, while the second term yields a conjugate wave ($\propto E_4^*$) if $\vec{k}_1 + \vec{k}_2 = 0$. The various contributions can be realized through the proper selection of the interacting fields' polarization orientations. Recall that $(\mu_{ij})_k$ defines the projection of the k^{th} vector field $\vec{E}_k$ along the dipole moment $\vec{\mu}_{ij}$.

To be complete, we must also add terms that are permuted in the various fields to (3.9-20). Several interesting features are to be noted from this equation. The first product of terms contained within each square bracket from each curly bracket involves interactions only among states |a> and |b>; these are recognized to be the terms responsible for phase conjugation from a two-level system, as discussed in the last section; here, however, the form of the resonant denominators is to be considered as being more physical in nature as

compared to (3.8-32) and (3.8-33). The very last square-bracketed term is due to the interaction of the pump fields with the two-photon transition directly. It is here that we wish to point out the subtle differences between the density matrix approach and that presented earlier using the time-evolution operator method. If we make the same assumptions regarding this term as were invoked in arriving at (3.9-8), we get:

$$P^{(3)}_{NL_{2\text{-photon}}} \rightarrow \frac{N}{4\hbar^3} E_1 E_2 E_4^* |\mu_{ba}|^2 |\mu_{cb}|^2 \frac{e^{i(\omega t+\vec{k}_4\cdot\vec{r})}(\Delta_2 - i\gamma_{ca})}{(\Delta_2^2 + \gamma_{ca}^2)}$$

$$\times \frac{[2\Delta_1 + i(\gamma_{ab}-\gamma_{bc})][\Delta_1 - i\gamma_{bc}]}{[\Delta_1^2 + \gamma_{ab}\gamma_{bc} + i\Delta_1(\gamma_{ab}-\gamma_{bc})]^2} \qquad (3.9\text{-}21)$$

Thus, only if $\gamma_{ab} = \gamma_{bc}$ does this result reduce to that derived using the time evolution approach (3.9-8).

We conclude this section by noting that any polarization rotation effects of the phase conjugate interaction are contained in the product of the $(\mu_{ij})_k$ terms in (3.9-20). That is, there exists in general an angular dependence of the probe to conjugate polarization states for a given set of pump wave polarizations, subject to the selection rules of the interacting atom. As an example of this effect, we consider the two-photon contribution to $P^{(3)}_{NL}$, and assume for simplicity that all the interacting fields are colinear. We compare the polarization effects for a $\Delta L_z = 0$ and $\Delta L_z = 2$ two-photon allowed transition. In the former case, the pump waves must both add up to zero angular momentum*; therefore, so must the signal (E_4) and conjugate (E_3) fields.

*For this discussion we consider only the z-component of the angular momentum.

Hence, in this case, from a helicity point-of-view (as discussed in Section 2.3) the conjugate wave is truly time-reversed from both a spatial phase and an angular momentum viewpoint (e.g., RHCP → RHCP). However, in the $\Delta L_z = 2$ case, the pump waves' angular momenta must add to $2\hbar$; thus the conjugate wave's angular momentum must be in the same direction as that of the input signal wave. This interaction proceeds if L_z of the signal and pump waves have the same sign. (Recall that the nonlinear optical process also stimulates a photon in the direction of the signal wave.) Hence, in this case, the conjugate return wave will be spatially time-reversed, but will <u>not</u> possess a time-reversed rotating $\vec{E}$-vector (e.g., RHCP → LHCP); the conjugator will therefore resemble a real perfectly reflecting mirror from this latter viewpoint. For a complete description of the polarization properties of the interaction, one must permute the interacting fields in the preceding argument as well as include additional nonzero terms in (3.9-20).

We therefore see that, although the density matrix approach is not as easy to manipulate as the time evolution technique, it does yield all possible contributions to $P_{NL}^{(3)}$ which are allowed to occur, including angular-dependent polarization effects, given the selection rules of the atomic species, and the quantum numbers of the pump waves.

3.10 Degenerate Four-Wave Mixing as Real-Time Holography

It has been pointed out [19] that some degenerate four-wave mixing is analogous to real-time or dynamic holography [32,33]. In this section we will point out briefly these formal analogies, and also discuss some of the differences. We note a special case, that of phase conjugation via a two-photon coherent state [31] has no direct analogy with holography(as discussed in the last section).

The identification of this class of nonlinear optical interactions as being equivalent to holography immediately establishes potential application areas that were previously relegated to conventional holographic techniques. Examples of such applications will be the topic of Chapters V and VII.

Consider the procedure of hologram recording and reconstruction as shown in Figure 3.13. The first step (Fig. 3.13a) shows the recording of a thin hologram using an interference between a "reference" beam A_1 and a "signal" beam A_4. The resulting transmission function is

$$T \propto (A_4 + A_1)(A_4^* + A_1^*)$$

$$= |A_4|^2 + |A_1|^2 + A_4 A_1^* + A_1 A_4^* \qquad (3.10\text{-}1)$$

$A_1(x)$ and $A_4(x)$ denote the complex amplitudes of the reference and object fields, respectively, in the hologram plane $z = 0$.

In the reconstruction step, the hologram is illuminated by a single reference wave A_2 impinging from the right in a direction opposite to that of A_1 as shown in Figure 3.13b. We thus have $A_2 = A_1^*$ so that the

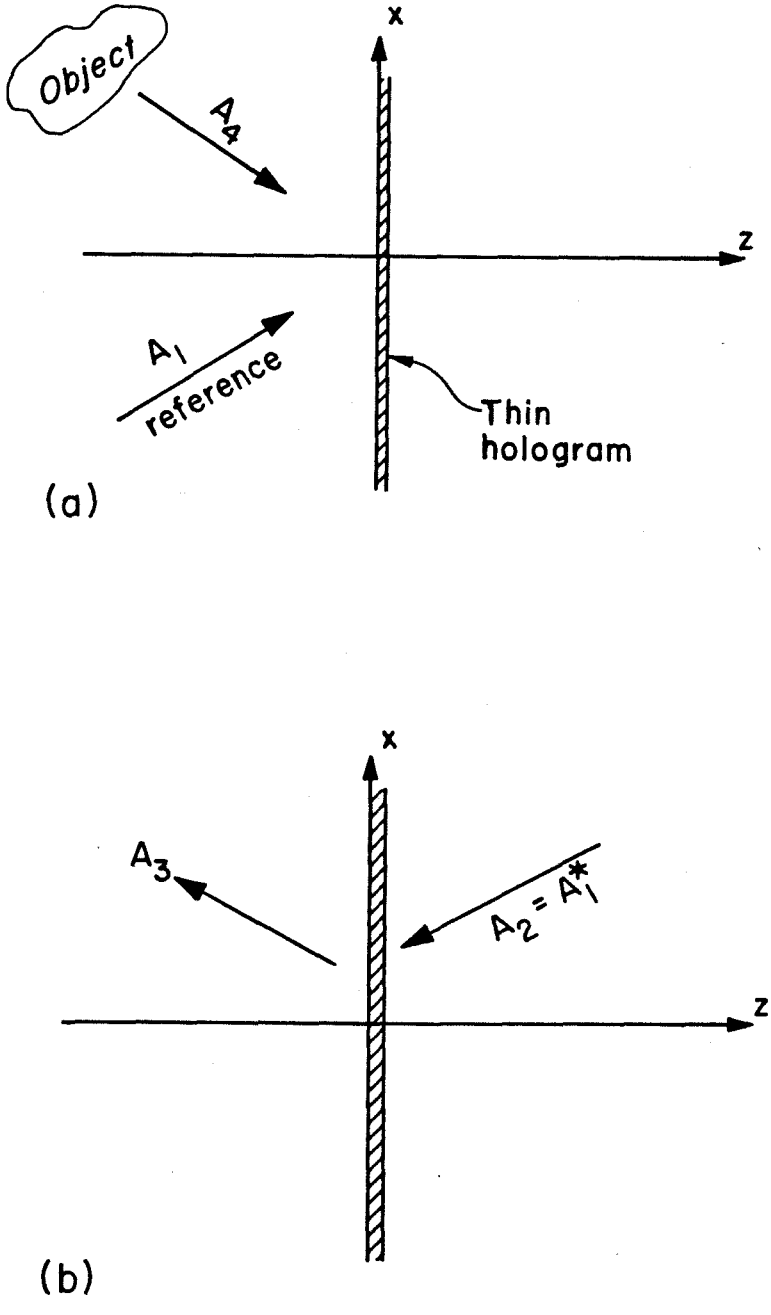

Fig. 3.13 Conventional holography. (a) Recording of a hologram; (b) Reconstruction of a hologram so as to yield the "pseudoscopic image."

diffracted field to the left of the hologram is

$$A_3 = TA_2 \propto (|A_4|^2 + |A_1|^2 + A_4A_1^* + A_4^*A_1)A_1^*$$

$$= (|A_4|^2 + |A_1|^2)A_1^* + (A_1^*)^2 A_4 + |A_1|^2 A_4^* \qquad (3.10\text{-}2)$$

The first term on the right side of (3.10-2) is proportional to the incident field $A_2(= A_1^*)$ and is of no interest in the present discussion. The term $(A_1^*)^2A_4$ will, in a thick hologram, have a phase factor $\exp[-i(2\vec{k}_1 - \vec{k}_4)\cdot\vec{r}\,]$ and is thus phase mismatched, i.e., will not radiate [5]. The term of interest is

$$A_3 \propto |A_1|^2 A_4^* = A_1A_2 A_4^* \qquad (3.10\text{-}3)$$

which at $z < 0$ corresponds to a "time-reversed" phase conjugate replica of the original object field A_4. It has been shown formally in Chapter II that such a field compensates in its reverse propagation for the distortion undergone by A_4, provided the propagation medium remains stationary during this time.

Let us next recall the four-wave mixing geometry of Figure 3.1, and the analysis given in Section 3.3. Comparing (3.3-12) to (3.10-3), it is clear that formally the nonlinear mixing of Figures 3.13 and 3.1 is equivalent. The analogy can be appreciated more fully if we write (3.3-12) in the limit of $|\kappa|L \ll 1$. In this case

$$A_3(z<0) \propto |A_1A_2|A_4^* \ (z < 0) \qquad (3.10\text{-}4)$$

which form is identical to (3.10-3). As a matter of fact, if we overlay

Figure 3.13b on 3.13a, the resulting figure is equivalent to Figure 3.1. This establishes the formal analogy between the two operations, and hence the real-time holographic nature of four-wave mixing.

It should be emphasized that the two processes represent different physical phenomena, and that the analogy is only operational.

Four-wave mixing can thus be viewed as constructing and reconstructing a hologram "essentially" simultaneously, or more precisely, within the relaxation times of the atoms (see below). Of course, since we assumed that both pump beams are present at the same time, there are actually two "holograms" of interest formed in the nonlinear medium (each due to the interference of the probe wave with one pump field), which are both read out by the other pump beam, with the same overall efficiency, assuming a stationary nonlinear medium (nonstationary media are discussed by Wandzura [11]).

Quantum mechanically, one can view each pump beam and the probe field as spatially modulating the susceptibility of the medium [9]. If the medium is nearly resonant with the photon fields, then this modulated complex susceptibility (χ) can be viewed as forming both a phase-type (via the real part of χ) and an amplitude-type (via the imaginary part of χ) "hologram." For transparent media the "hologram" formed is primarily phase-type in nature, being spatially modulated via the nonlinear refractive index (where $n = n_0 + n_2|E|^2$, n_2 being the nonlinear index) characterizing the medium [5,12].

One difference between conventional holography and four-wave mixing lies in the fact that the third order susceptibility is actually a fourth rank tensor. Thus, a nonzero, nonlinear polarization can result

even if the pump and probe waves have orthogonal polarizations. This property, in fact, will be discussed in relation to experiments we performed (see Chapter IV). This is not the case in conventional holography, where the recording medium (e.g., film emulsion) has essentially a square law response with the transmission function being proportional to $\vec{E}_1 \cdot \vec{E}_4^*$ (or $\vec{E}_2 \cdot \vec{E}_4^*$). Therefore, if the polarization of $\vec{E}_1$ (or $\vec{E}_2$) is orthogonal to $\vec{E}_4$, no hologram is formed.

Yariv and AuYeung [22], using a time evolution operator formalism and a density matrix approach, treat the case of "transient" four-wave mixing, where an atomic (or molecular) medium is exposed to a sequence of three optical pulses. They conclude that, using the geometry of Figure 3.1, a conjugate wave can be realized only if the probe pulse is either the first or second pulse incident upon the medium (both single- and two-photon transitions were considered); the other two pulses are those of each of the pump fields. Thus, the first two pulses essentially "write" the hologram by spatially modulating the population difference of the levels considered, and the third pulse diffracts off this spatially modulated "grating." The first two pulses must be temporally spaced by less than the dephasing time of the medium (T_2, or the transverse relaxation time), while the third pulse must occur within the spontaneous decay time of the medium (T_1, or the longitudinal relaxation time) after the second pulse in order for the process to be most efficient. This scheme therefore reinforces the concept of constructing and reading out a hologram in real time. Additionally, the first two pulses must have parallel polarizations in

order for the grating to be formed (also in operational agreement with the square law nature of conventional holographic recording media).

The nonlinear polarization for this process can be written vectorially as

$$\vec{P}_{NL}^{(3)} \propto A(\vec{E}_1 \cdot \vec{E}_4^*)\vec{E}_2 + B(\vec{E}_2 \cdot \vec{E}_4^*)\vec{E}_1 \qquad (3.10\text{-}5)$$

where a "hologram" is written by one pump wave plus the probe, and the second pump wave is diffracted off the hologram. Alternatively, the term in the parentheses can be considered to yield a spatial modulation of atomic densities at zero optical frequency (i.e., temporally stationary) and hence a spatial modulation of the susceptibility, from which the other pump wave scatters, yielding the conjugate wave.

On the other hand, note that from the last term of (3.9-20), a nonlinear polarization can also exist in the form

$$\vec{P}_{NL}^{(3)} \propto (\vec{E}_1 \cdot \vec{E}_2)\vec{E}_4^* \qquad (3.10\text{-}6)$$

where the interaction takes place in a three-level system, for example. This has no direct holographic analog, in that $\vec{E}_1 \cdot \vec{E}_4^*$ can be chosen to be zero. Yet, as long as $\vec{E}_1 \cdot \vec{E}_2 \neq 0$, a conjugate wave will result. The term within the parentheses gives rise to the so-called two-photon coherent state, which oscillates at an optical frequency of 2ω, with the probe field scattering off this "dynamic" temporally (not spatially) modulated nonlinear index, yielding the conjugate wave[31]. This subtle departure from the holographic analog is very useful in certain four-wave interactions [34,35,36] and will be discussed further in Section 6.4. This process also gives rise to an experimental geometry where the pump

and probe fields can be made orthogonal, thus increasing the signal-to-noise figure of the conjugate wave (to be discussed in the next chapter).

Appendix 3A

Phase Conjugation via N-Wave Mixing

In this appendix we show how one can generalize the generation of phase conjugated wavefronts to nonlinear optical mixing involving different geometries as well as higher order parametric interactions.

We assume a set of N monochromatic plane waves given by (3.2-1), where the first N-1 of these fields are the input waves [D.C. fields ($\omega = 0$) can also be present]. We define the field E_1 as being the input (probe) wave whose phase conjugate replica is sought. The next N-2 fields ($E_2, E_3, \cdots, E_{N-1}$) are intense input plane waves which are defined to be the pump waves. The N-1 input waves are incident upon a medium that possesses a nonzero $(N-1)^{th}$ order nonlinear optical susceptibility, $\chi_{NL}^{(N-1)}$. The directions, frequencies, and field polarizations of these N-1 input waves are chosen so that an output wave $E_N \propto E_1^*$ is generated as a result of the interaction (other possible products of the N-1 fields are assumed to be phase mismatched and do not radiate constructively). Specifically, the following nonlinear polarization at frequency ω_N is formed in the medium:

$$P_{NL}^{(\omega_N)} = \chi_{NL}^{(N-1)} A_1^* \exp[i(-\omega_1 t + \vec{k}_1 \cdot \vec{r})] \times \prod_{\ell=2}^{N-1} \{A_\ell \exp[i(\omega_\ell t - \vec{k}_\ell \cdot \vec{r})]\}^{[*]_\ell} \qquad (3.A\text{-}1)$$

A difference frequency contribution of the ℓ^{th} pump wave to $P_{NL}^{(\omega_N)}$ is denoted by the superscript [*] , which implies a conjugation operation upon A_ℓ as well as a reversal of the sign of both ω_ℓ and $\vec{k}_\ell$.

From the form of (3.A-1), a phase matched, conjugate wave is gen-

erated if the product of the pump waves yields the following resulting frequency and wavevectors*

$$\omega_{pump} = \sum_{\ell=2}^{N-1} [\pm]_\ell \omega_\ell$$
$$= 2\omega_1$$

and

$$\vec{k}_{pump} = \sum_{\ell=2}^{N-1} [\pm]_\ell \vec{k}_\ell(\omega_\ell) \qquad (3.A\text{-}2)$$

$$\simeq \begin{cases} 0 & \text{backward-wave conjugation} \\ 2\vec{k}_1(\omega_1) & \text{forward-going conjugation} \end{cases} \qquad (3.A\text{-}3)$$

where $|\vec{k}_\ell| = \frac{\omega_\ell n(\omega_\ell)}{c}$ and $n(\omega_\ell)$ is the linear index of refraction (in the nonlinear medium) at frequency ω_ℓ. Each ω_ℓ (and corresponding $\vec{k}_\ell$) is either positive or negative, depending upon whether a sum $[+]_\ell$ or difference $[-]_\ell$ frequency is employed.

The phase matching constraint [5] is given by

$$|\Delta\vec{k}|L = |\vec{k}_{pump} - \vec{k}_1(\omega_1) - \vec{k}_N(\omega_N=\omega_1)|L \lesssim 2\pi \qquad (3.A\text{-}4)$$

---

*Note that $\vec{k}_{pump}$ is merely a vector sum of the pump field wavevectors, and is not to be considered as corresponding to a physical wavevector in itself.

where L is the interaction length. For both the wavevector constraints given in (3.A-3) the input amplitude (A_1) is conjugated (i.e., $A_N \propto A_1^*$), resulting in time-reversed wave fronts at frequency ω_1; only in the former case ($\vec{k}_{pump} = 0$) does the output field (E_N) propagate in a direction opposite to E_1 at each point in space; the latter case requires an additional reflection [1] off a "real" (plane) mirror in order to yield the desired replica of E_1. The mirror in effect changes $\vec{k}_N \rightarrow -\vec{k}_N$, thus yielding a backward-going conjugate replica.

We note that for $\vec{k}_{pump} = 0$, the phase matching condition is satisfied exactly for all $\vec{k}_1$ (since $\vec{k}_1 = -\vec{k}_N$) and hence for all L; thus, there is no restriction upon the input angular range of the wave to be conjugated. On the other hand, for the latter case [$\vec{k}_{pump} \simeq 2\vec{k}_1(\omega_1)$], the phase matching constraint can be rigorously satisfied for only <u>one</u> input probe wave direction. This limits both the efficiencies and the angular input acceptance range [1-3] for forward-going conjugation processes.

Using the above formalism, several cases of three- and four-wave mixing (N = 3,4, respectively) leading to phase conjugate waves (i.e., $E_{3,4} \propto A_1^*$) are shown in Figure 3A.1. In 3A.1a,b forward-going, three- and four-wave [37] conjugate geometries are shown; in 3A.1c, a degenerate, backward-going four-wave mixing geometry is shown. We note that the N-wave mixing processes where N is an odd integer are limited to nonlinear media lacking inversion symmetry, while the even-N processes can, in principle, take place in any (even isotropic) medium.

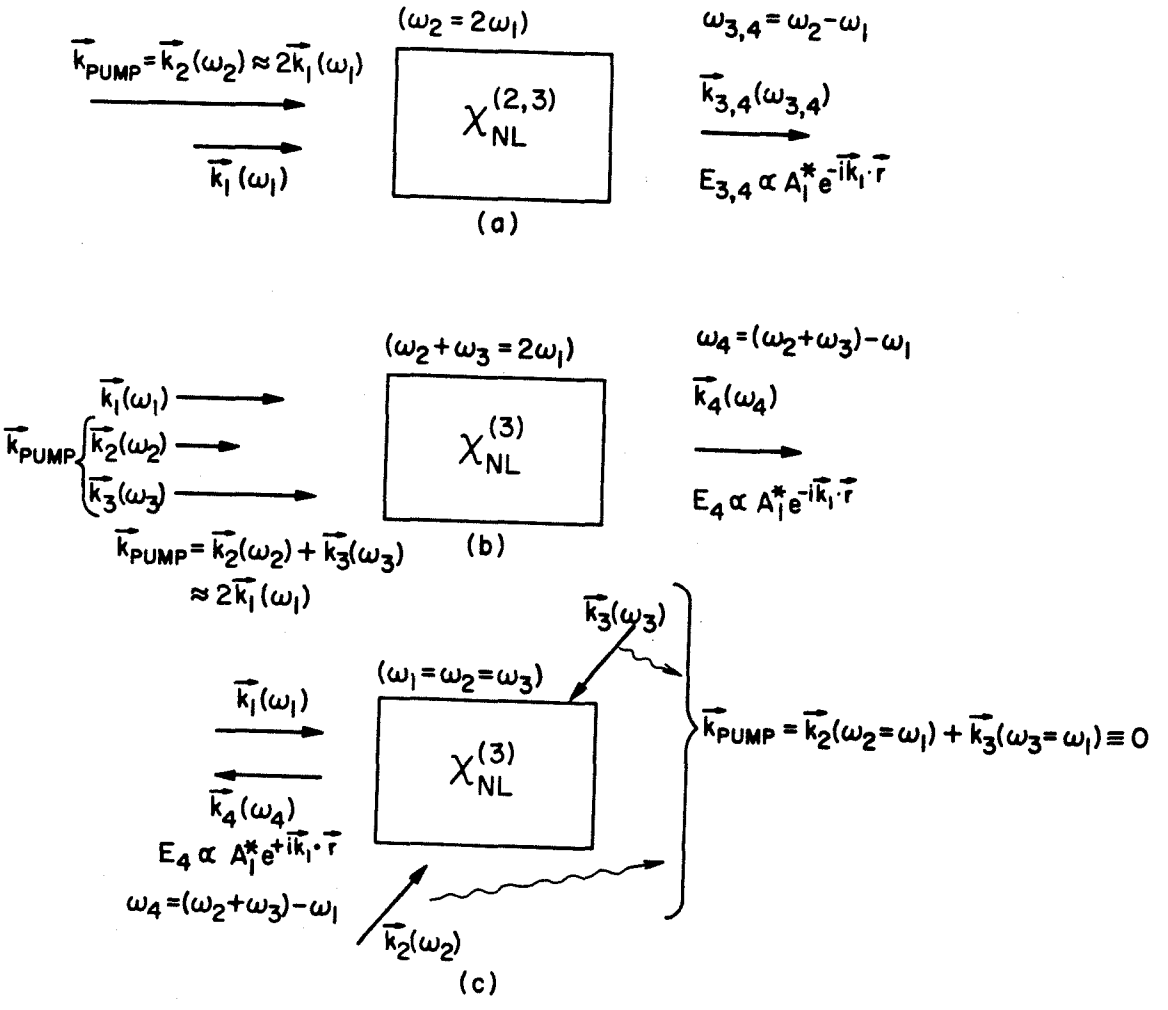

Fig. 3A.1 Geometries for 3- and 4-wave phase conjugate interactions. (a) 3-wave and D.C. induced 3-wave geometry (utilizing $\chi^{(2)}$ and $\chi^{(3)}$, respectively); (b),(c) 4-wave geometry. Note that (a) and (b) yield forward-going conjugate fields and thus have angular acceptance limitations, while (c) yields a backward-going conjugate replica and is capable of ~4π angular acceptance.

The above general approach enables one to evaluate rapidly a system as a potential phase conjugator, given the available optical sources, geometry, and nonlinear media (e.g., resonances, tensorial aspects of χ_{NL}, etc.). A recently published letter [38] deals (independently) with these topics.

Chapter III - References

1. A. Yariv, "Compensation of atmospheric degradation of optical beam transmission by nonlinear optical mixing," Opt. Commun. 21, 49 (1976).

2. P. V. Avizonis, F. A. Hopf, W. D. Bamberger, S. F. Jacobs, A. Tomita, and K. H. Womack, "Optical phase conjugation in a lithium formate crystal," Appl. Phys. Lett. 31, 435 (1977).

3. F. A. Hopf, A. Tomita, K. H. Womack, and J. L. Jewell, "Optical distortion in nonlinear phase conjugation by three-wave mixing," J. Opt. Soc. Am. 69, 968 (1979).

4. R. W. Minch, R. W. Terhune, and C. C. Wang, "Nonlinear optics," Appl. Opt. 5, 1595 (1966).

5. A. Yariv, Quantum Electronics, 2nd ed. (Wiley, New York, 1975).

6. S. E. Harris, "Proposed backward wave oscillation in the infrared," Appl. Phys. Lett. 9, 114 (1966).

7. R. W. Hellwarth, "Generation of time-reversed wavefronts by nonlinear refraction," J. Opt. Soc. Am. 67, 1 (1977).

8. D. M. Bloom, P. F. Liao, and N. P. Economou, "Observation of amplified reflection by degenerate four-wave mixing in atomic sodium vapor," Opt. Lett. 2, 58 (1978).

9. R. L. Abrams and R. C. Lind, "Degenerate four-wave mixing in absorbing media," Opt. Lett. 2, 94 (1978), and ibid. 3, 205 (1978).

10. A. Elci and D. Rogovin, "Phase conjugation in nonlinear molecular gases," Chem. Phys. Lett. 61, 407 (1979).

11. S. M. Wandzura, "Effects of atomic motion on wavefront conjugation by resonantly enhanced degenerate four-wave mixing," Opt. Lett. 4 208 (1979).

12. R. W. Hellwarth, "Third order optical susceptibilities of liquids and solids," Prog. Quant. Electron. 5, 1 (1977).

13. J. AuYeung and A. Yariv, "Stimulated Raman scattering in long, low-loss fibers," IEEE J. Quant. Electron. QE-14, 347 (1978).

14. J. H. Marburger and J. F. Lam, "Nonlinear theory of degenerate four-wave mixing," Appl. Phys. Lett. 34, 389 (1979).

15. H. Hsu, "Large signal theory of phase-conjugate backscatterings," Appl. Phys. Lett. 34, 855 (1979).

16. J. H. Marburger and J. F. Lam, "Effects of nonlinear index changes on degenerate four-wave mising," Appl. Phys. Lett. 35, 249 (1979).

17. J. H. Marburger, "Self-focusing: Theory," Prog. Quant. Electron. 4, 35 (1975).

18. S. M. Jensen, Ph.D. Thesis, University of Southern California, 1979.

19. A. Yariv, "Four-wave nonlinear optical mixing as real time holography," Opt. Commun. 25, 23 (1978).

20. A. Messiah, Quantum Mechanics (Wiley, New York, 1958), Ch. 8 & 17.

21. A. Yariv, "The application of time evolution operators and Feynman diagrams to nonlinear optics, " IEEE J. Quant. Electron. QE-13 , 943 (1977).

22. A. Yariv and J. AuYeung, "Transient four-wave mixing and real-time holography in atomic systems," IEEE J. Quant. Electron. QE-15, 224 (1979).

23. K. Huang, Statistical Mechanics (Wiley, New York, 1963).

24. V. B. Berestetskii, E. M. Lifshitz, and L. P. Pitaevskii, Relativistic Quantum Theory (Pergamon Press, New York, 1973).

25. See, for example, N. Bloembergen, Nonlinear Optics (W. A. Benjamin, New York, 1965); or M. Sargent III, M. O. Scully, and W. E. Lamb, Jr., Laser Physics (Addison-Wesley, Mass., 1974).

26. P. R. Berman, "Quantum-mechanical transport equation for atomic systems," Phys. Rev. A5, 927 (1972).

27. M. Sargent III, P. E. Toschek, and H. G. Danielmeyer, "Unidirectional saturation spectroscopy, I. Theory and short dipole lifetime limit," Appl. Phys. 11, 55 (1976).

28. P. R. Berman and W. E. Lamb, Jr., "Theory of collision effects on line shapes using a quantum-mechanical description of the atomic center-of-mass motion. Application to lasers. I," Phys. Rev. A2, 2435 (1970).

29. P. R. Berman and W. E. Lamb, Jr., "Theory of collision effects on line shapes using a quantum-mechanical description of the atomic center-of-mass motion. Application to lasers. II, The pseudoclassical collision model and steady-state laser intensities," Phys. Rev. A4, 319 (1971).

30. See, for example, R. G. Brewer and E. L. Hahn, "Coherent two-photon processes: Transient and steady-state cases," Phys. Rev. A11, 164 (1975), and references therein.

31. The concept of phase conjugation via two-photon coherent states was proposed by Juan F. Lam. He has since analyzed the problem considering atomic motion effects and saturation effects (which were neglected here for simplicity), for both the steady-state and the transient cases; to be published in Phys. Rev. A.

32. B. I. Stepanov, E. V. Ivakin, and A. S. Rubanov, "Recording two-dimensional and three-dimensional dynamic holograms in transparent substances," Doklady Akademii Nauk SSR 196, 567 (1971) [Sov. Phys. Doklady 16, 46 (1971)].

33. J. P. Woerdman, "Formation of a transient free carrier hologram in Si," Opt. Commun. 2, 212 (1970).

34. P. F. Liao, N. P. Economou, and R. R. Freeman, "Two-photon coherent transient measurements of Doppler-free linewidths with broadband excitation," Phys. Rev. Lett. 39, 1473 (1977).

35. D. G. Steel, R. C. Lind, J. F. Lam, and C. R. Giuliano, "Polarization, rotation, and thermal motion studies via resonant four-wave mixing," Appl. Phys. Lett. 35, 376 (1979).

36. D. G. Steel and J. F. Lam, "Two-photon coherent transient measurement of the nonradiative collisionless dephasing rate in SF_6 via Doppler-free degenerate four-wave mixing," Phys. Rev. Lett. 43, 1588 (1979).

37. C. V. Heer and N. C. Griffen, "Generation of a phase conjugate wave in the forward direction with thin Na-vapor cells," Opt. Lett. 4, 239 (1979).

38. I. M. Bel'dyugin, V. N. Seminogov and E. M. Zemskov, "Possible wavefront reversal of fields using nonlinear-optics methods," Kvant. Elektron. (Moscow) 6, 638 (1979); [Sov. J. Quant. Electron. 9, 385 (1979)].

Chapter IV

OBSERVATION OF PHASE CONJUGATED WAVES VIA A DEGENERATE FOUR-WAVE NONLINEAR OPTICAL INTERACTION IN AN ISOTROPIC, TRANSPARENT MEDIUM

4.1 Introduction

In this chapter we will discuss two experiments that were performed using a degenerate four-wave nonlinear optical interaction to yield phase conjugate fields. Both experiments utilized carbon disulfide, a transparent liquid, as the nonlinear medium. The basic description of these experiments will be given in the first part of this chapter. Each experiment confirmed various aspects of the effects of a phase conjugate interaction upon an incident optical field. The first experiment was performed in a bulk nonlinear medium using a pulsed ruby laser as the source; the second experiment was performed with the nonlinear medium in an optical fiber using a cw argon ion laser as the source. In the course of this chapter, various diagnostic tests will be discussed that confirmed the conjugate nature of the interaction. Finally, a brief theoretical description of the basic four-wave nonlinear coupling in an optical waveguide will be given.

4.2 Degenerate Four-Wave Mixing in Bulk CS_2

In this section we will describe an experiment that demonstrated the ability of a degenerate four-wave mixing interaction in a bulk nonlinear medium to yield phase conjugate (time-reversed) fields. In addition, we observed an amplified phase conjugate replica of a given input signal, as well as a one-mirror assisted optical parametric oscillation mode. These results will be shown to be consistent with the theoretical

descriptions of the last chapter and those presented below. We will discuss several diagnostic tests performed that verified both the time-reversal character and the degenerate frequency nature of the observed output waves. The experiment utilized a pulsed (Q-switched) ruby laser as the source and carbon disulfide, an isotropic, transparent liquid substance, as the nonlinear medium. A colinear mixing geometry was used (i.e., all fields propagated along a common axis) to realize long interaction lengths (hence greater nonlinear coupling) with polarization discrimination employed to separate the pump and signal fields.

The experimental arrangement is shown in Figure 4.1. Stripped of details, which will be discussed below, it consists of a CS_2 cell which is pumped simultaneously by laser beams A_1 and A_2 of the same frequency, ω, polarized in the plane of the figure (parallel, π-polarization) and which travel in opposition to each other. Simultaneously, an orthogonally polarized (s-polarization) probe beam A_4 at ω is introduced from the left and propagates in a direction antiparallel to that of A_1.

The experiment consists of (1) measuring the intensity of the nonlinearly "reflected" beam A_3 with polarization parallel to that of A_4 (i.e., orthogonal, s-polarization) as a function of the pumping intensity ($\sim A_1A_2$); (2) demonstrating one-mirror assisted parametric oscillation, i.e., finite outputs at A_3 and A_4 with no corresponding inputs; and (3) to establish that A_3 is the phase conjugate of A_4.

Due to the material properties of CS_2, it is necessary to provide additional background governing its nonlinear susceptibility.

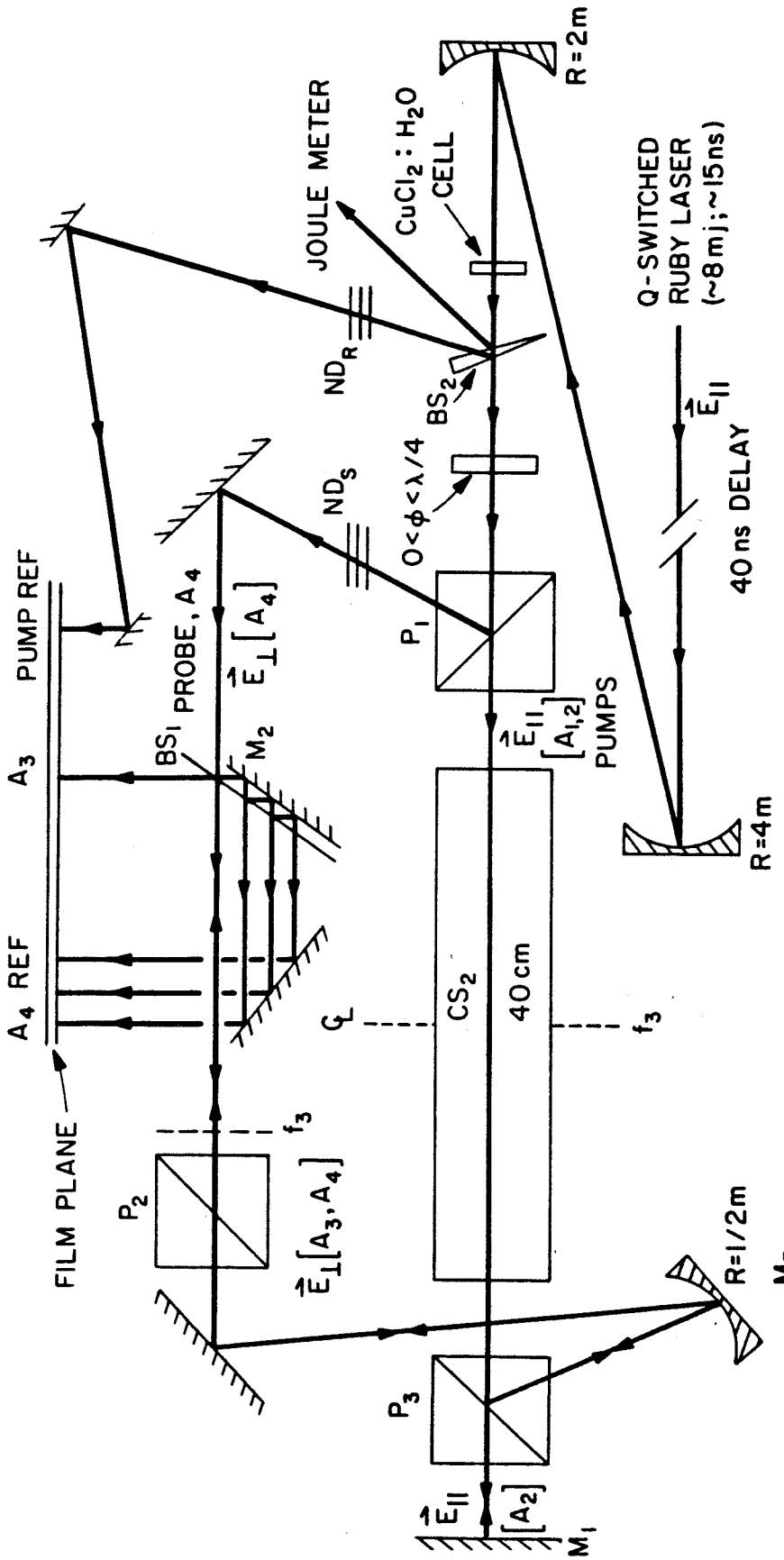

Fig. 4.1 Experimental apparatus for the measurement of the nonlinear reflection coefficient (all mirrors are totally reflecting).

The polarization of a material is, in general, a function of the applied optical fields and is conveniently expressed as a power series of these applied fields as [1]

$$P = \chi \cdot E + \chi^{(2)} : EE + \chi^{(3)} : EEE + \cdots \qquad (4.2\text{-}1)$$

The first term contains the linear susceptibility of the material, χ, which characterizes the linear index of refraction, dispersion, and absorption of the medium. The next term contains the second order nonlinear optical susceptibility, $\chi^{(2)}$, which describes effects such as second harmonic generation, and sum or difference frequency wave generation of two fields. This term is absent in isotropic media, due to the presence of an inversion symmetry [2]. The third term (which is therefore the lowest order nonlinear polarization in isotropic media) contains the third order nonlinear optical susceptibility, $\chi^{(3)}$, which describes effects such as four-wave mixing, self-focusing, two-photon absorption, and Raman scattering processes.

The i^{th} component of the third order nonlinear optical polarization in an isotropic medium can be written as [1,3]

$$\begin{aligned} P_i(\omega) = \sum_j 6[&\chi^{(3)}_{iijj} E_i(\omega) E_j(\omega) E_j^*(\omega) \\ &+ \chi^{(3)}_{ijij} E_j(\omega) E_i(\omega) E_j^*(\omega) \\ &+ \chi^{(3)}_{ijji} E_j(\omega) E_j(\omega) E_i^*(\omega)] \end{aligned} \qquad (4.2\text{-}2)$$

where j is summed over the field polarizations present.

In terms of the holographic analogs (and notations) presented in the last chapter, we note that the first two terms yield nonlinear

polarizations of the form $(\vec{A}_1 \cdot \vec{A}_4^*)\vec{A}_2$. Thus, the probe and one of the pump beams interfere and form a grating in the nonlinear medium via the nonlinear index ($\propto \chi_{iijj}$ and χ_{ijij}); the second pump beam then diffracts off this nonlinearly generated grating, yielding the desired conjugate wave. The last term, however, gives rise to nonlinear polarization of the type $(\vec{A}_1 \cdot \vec{A}_2)\vec{A}_4^*$, and is hence reminiscent of phase conjugation via a two-photon coherent state; the probe polarization need not necessarily be parallel to either of the pump beams, thus not forming an analogous holographic-type diffractive process. As we describe below, it is precisely this latter term that is exploited in our experiment, since we wish the probe beam to have its polarization vector orthogonal to that of the pump beams.

Since the quantum mechanical description of $\chi^{(3)}_{ijk\ell}$ is not easily tractable due to the multitude of electronic and rotation-vibration levels needed for consideration in a transparent molecular medium such as CS_2, the tensor elements of (4.2-2) are treated as consisting of two phenomenological components. The analysis involves the use of the Born-Oppenheimer approximation [3] in treating the electronic and molecular degrees of freedom for molecular media. The result for $\chi^{(3)}_{ijji}$, for example, can be written as [3]

$$\chi^{(3)}_{ijji} = \frac{1}{24}(\sigma + 2\beta) \qquad (4.2\text{-}3)$$

where σ is the "electronic contribution" which is due to the optically-induced deformation of the electronic clouds surrounding the nuclei; β is the "nuclear contribution" which is due to the nuclei's response to the applied fields. The response (and relaxation) time of σ is typi-

cally on the order of an optical period (or subpicosecond) for transparent media. The corresponding times of β are strongly material dependent and can vary from picoseconds (e.g., 2.3 psec for CS_2[4,5]) to tens of nanoseconds (e.g., 40 nsec for MBBA near its transition temperature [6]). Since the Q-switched laser output pulses are typically 15 nsec long, we can safely assume that both components that comprise the third order susceptibility for CS_2 respond instantaneously on these time scales. Thus, the nonlinear polarization generated in our experiments would have a temporal dependence involving only that of the applied fields.

Further, we also expect that the nonlinear polarization reflects the spatial and phase dependence of the pump beams. Thus in the small nonlinear gain limit, where $\tan(|\kappa|L) \sim |\kappa|L$, and assuming that the pump waves are nearly planar, the output field amplitude would be of the form from eq. (3.3-12)

$$A_3 \propto (A_4 e^{f_4(r,t)})^* (A_1 e^{f_1(r,t)}) (A_2 e^{f_2(r,t)}) \chi^{(3)}_{NL} L \qquad (4.2\text{-}4)$$

where f_i is a complex function describing both the temporal and spatial dependence of the i^{th} wave. If all input fields have the same Gaussian temporal and spatial dependence, for example, then the conjugate wave amplitude would be temporally shortened (by a factor of $\sqrt{3}$) as would the spot size.

Returning to the tensorial nature of $\chi^{(3)}_{NL}$, we see from equation (4.2-2) that the nonlinear coupling between the various waves for our experimental conditions is given by [1,3]

$$P_y^{(\omega_3=\omega=\omega_1+\omega_2-\omega_4)} \propto \chi^{(3)}_{yxxy} A_{1x}^{(\omega_1=\omega)} A_{2x}^{(\omega_2=\omega)} A_{4y}^{*(-\omega_4=-\omega)} \qquad (4.2\text{-}5)$$

where the two pump waves are π-polarized, and the probe wave is s-polarized. Thus, the conjugate wave is polarized parallel to the probe field. As discussed earlier, this choice of polarizations is reminiscent of forming a two-photon coherent state via the pump beams. The probe field interacts subsequently with this state, yielding the desired conjugate output wave.

The employment of a colinear geometry for both the signal (A_3,A_4) and pump (A_1,A_2) waves enabled us to use very long interaction paths ($\geq$ 40 cm) and thus realize high gains and even oscillation. This colinear geometry entails the use of $\chi^{(3)}_{yxxy}$ in the nonlinear coupling. Since for CS_2 [3], $\chi^{(3)}_{yxxy} / \chi^{(3)}_{xxxx} \simeq 0.706$, the small loss in coupling is easily tolerable.

The nonlinear reflection coefficient was measured using the experimental arrangement illustrated in Figure 4.1. The pump source was a passively Q-switched ruby laser, operating in both a single longitudinal and transverse mode [7]. The laser output was monitored for each shot to ensure single mode and single pulse operation. A typical output pulse energy was 7 to 13 mJ with a duration of 15 ns. The typical

intensity spot size was determined to be 2.2 mm diameter, using a variation of the technique described in Ref. [8]; Appendix 4A discusses our approach.

The output beam was reflected by a 2:1 spherical mirror collimator and folded to yield an optical path delay of 40 ns before entering the interaction region. Thus, return signals were prevented from reaching the laser throughout the duration of the pulse. A 1 cm thick cell containing varying concentrations of $CuCl_2$ in H_2O was used to attenuate the laser beam for various input energies [7]. The beam passed next through a calcite Glan laser prism (P_1), and then into the CS_2 medium, which was contained in a 40 cm long, 2 cm diameter glass cell. Mirror M_1 retroreflected the pump beam, giving rise to a counter-propagating component A_2. The cell was tilted off-axis to prevent Fresnel reflections from interfering with measured fields. Prism P_1 served a dual function: it passed the pump beam (A_1), "π" polarized into the interaction medium, and in addition, coupled an "s" polarized probe A_4 pulse of order 10^{-3} times that of the pump energy (energy determined by the orientation of wave plate, ϕ). This probe was then beam-split, and passed through a calibrated beam splitter-mirror system (BS_1,M_2) providing a sequence of reflected beams, each being reduced in intensity by a factor of two, which were incident upon the film plane. For comparison, a Fresnel reflected (via BS_2) pump beam was also recorded. Both of these beams were attenuated through neutral density stacks (ND_S and ND_R) prior to impinging on the film plane, which employed type 47, 3000 ASA high speed oscilloscope film. We note that the laser spot size was determined

photographically, using the same sequence of reflected spots (following the procedure of Ref. [8]); thus, both the nonlinear reflection coefficient and the spot size could be determined for the same given run. The laser energy was monitored by a calibrated Fresnel reflection (off BS_2) using a Gen-Tec model #ED-100 pyroelectric detector and model #PRJ-D digital readout.

The forward-going probe beam, A_4, propagated through prism P_2, oriented to pass s-polarized fields (thus serving to eliminate any scattered or Fresnel reflected π-polarized fields from interfering with the measurement), and was then coupled into the CS_2 cell through a spherical mirror M_3 and another Glan laser prism, P_3 (oriented similar to that of P_1) between the cell and M_1. Thus, prisms P_1 and P_3 constrained the probe beam to interact only in the CS_2 cell. The purpose of M_3 was to focus and confine the probe to propagate within the pump beam volume.

The phase conjugate nature of the reflected wave, i.e., $A_3(0) \propto A_4^*(0)$, was established through the use of the mirror M_3 (see Fig. 4.1). This mirror focuses the collimated input probe beam A_4 on the mid-plane f_3. A phase conjugate reflection A_3, being a "time-reversed" replica of the input wave A_4, should emerge from the CS_2 cell with virtual emanation from the focal spot at f_3 and thus be collimated. That this was the case was established using the beam spot photographs (taken by reflecting A_3 off BS_1) in the film plane.

The nonlinear nature of the reflected wave was also established through its temporal (pulse shortening), spatial (well-defined spot size) and frequency (via Fabry-Perot spectra) characteristics. Figure

4.2 shows several Fabry-Perot spectra, taken to indeed verify that the conjugate wave was degenerate in frequency (within the resolution of the instrument) and also that other competing (inelastic) nonlinear processes such as stimulating Raman scattering and stimulated Brillouin scattering were not present. The Burleigh Inc. Fabry-Perot interferometer utilized $\lambda/200$ flatness, high energy density mirrors of $\sim$97% reflectivity and a spacing of 1.91 cm. Thus, the free spectral range is $\sim$ 8 GHz with $\sim$ 150 MHz resolution (i.e., a finesse of $\sim$50). Figure 4.2a shows the conjugate wave as well as a reference pump wave. Within the resolution of the Fabry-Perot, these fields are seen to be degenerate in frequency. Figure 4.2b shows the system except with the counter-propagating pump beam (A_2) blocked. Note the absence of the conjugate wave, as expected. As a check of the ability of the Fabry-Perot to detect SBS shifts, Figure 4.3 shows a Fabry-Perot spectrum with the probe wave intensity chosen to be above the threshold for SBS; note the secondary ring, which is displaced fractionally away from the reference wave, in accordance with the expected SBS Stokes shift of 5.8 GHz in CS_2 [2].

As a second check for the absence of other third order nonlinear processes in our experiment, the laser energy was measured before and after the CS_2 cell to insure that the pump intensity was below that for the onset of stimulated Brillouin scattering. Also, the laser spot size was measured on either side of the cell to verify that self-focusing was not taking place.

As an additional check to verify the absence of competing nonlinear processes, the temporal evolution of the pump wave A_1 was measured

CONJUGATE OUTPUT DIAGNOSTICS

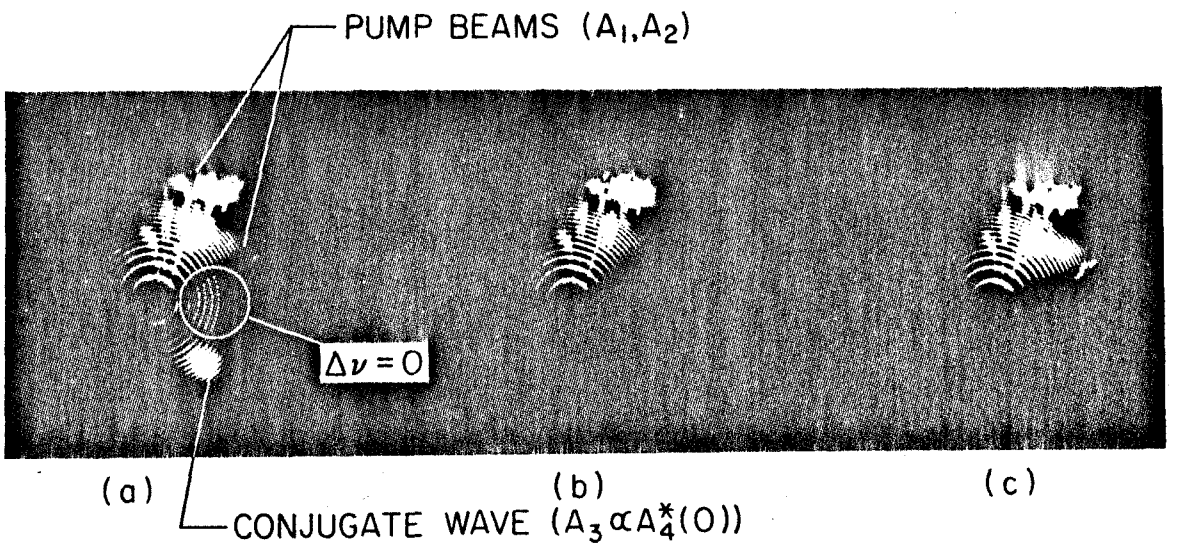

(a) ALL BEAMS PRESENT
(b) REAR MIRROR BLOCKED (NO A_2 PUMP)
(c) PROBE BLOCKED (NO A_4 INPUT)

Fig. 4.2 Fabry-Perot spectrum of the conjugate wave (A_3), as compared with that of the pump waves ($A_{1,2}$).

SBS DIAGNOSTICS

[PROBE BEAM INTENSITY > SBS THRESHOLD]

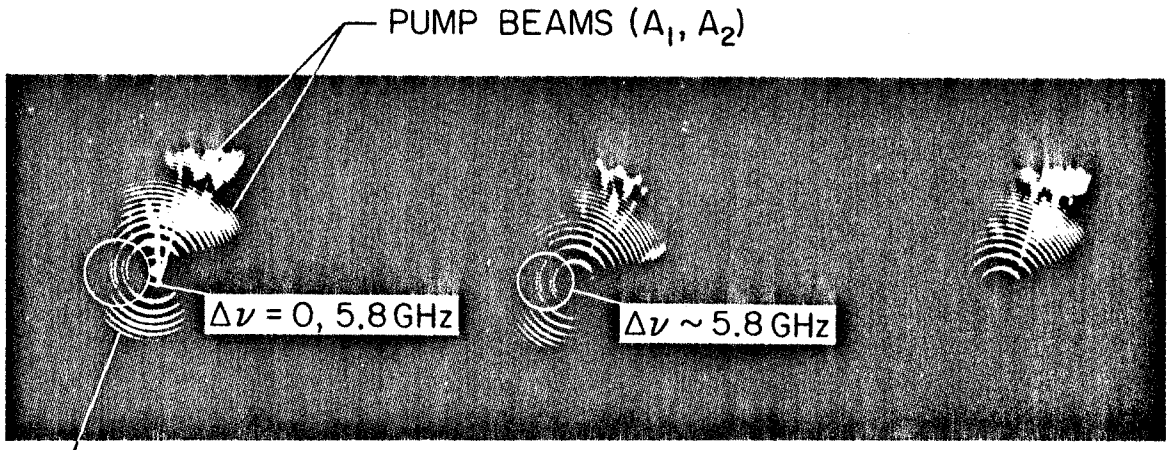

(a) ALL BEAMS PRESENT ($\Rightarrow$ SBS + 4-WAVE MIXING)

(b) REAR MIRROR BLOCKED (NO A_2 PUMP $\Rightarrow$ ONLY SBS)

(c) PROBE BLOCKED (NO A_4 INPUT)

Fig. 4.3 Fabry-Perot spectrum of a highly focused probe wave (A_4) to check the resolution of the device in detecting the frequency shift due to stimulated Brillouin scattering.

after passage through the CS_2 cell. Since the retro-mirror (M_1) that gave rise to the counterpropagating pump wave (A_2) was not exactly 100% reflecting, there was adequate residual transmitted optical intensity to be detected. Figure 4.4 shows the temporal evolution of the pump wave A_1 prior to the CS_2 cell and also after passage through the mirror M_1. The amplitudes have been attenuated for visual purposes. These measurements were made under experimental conditions (i.e., all interacting beams were present). We see that the temporal profile of the pump beam is essentially unaffected by the nonlinear interaction. The slight flattening of the residual pump pulse may be due to pump depletion effects. Hence, in conjunction with the previously mentioned diagnostics, the absence of competing nonlinear effects* can be safely assumed. We note that the over-all detector oscilloscope response time is approximately 0.5 to 1 nsec for our system.

The presence of a spherical mirror M_3 insures that only reflected phase conjugated radiation is collimated in the film plane. The presence of unwanted s-polarized radiation due to residual birefringence in the optical components, imperfect extinction in the polarizers, and ellipse rotation in CS_2 [9] gave rise to a divergent output and did not affect the measurement of the reflection coefficient materially. In addition, any output fields that were proportional to $A_4(0)$ (as discussed in Section 3.7B for the case of a colinear geometry) would also result in a

*Self-focusing, for example, could give rise to a "pulse-steepening" effect which was not seen. See J. Marburger and W. G. Wagner, "Self-focusing as a pulse sharpening mechanism," IEEE J. Quant. Electron. QE-3, 415 (1967).

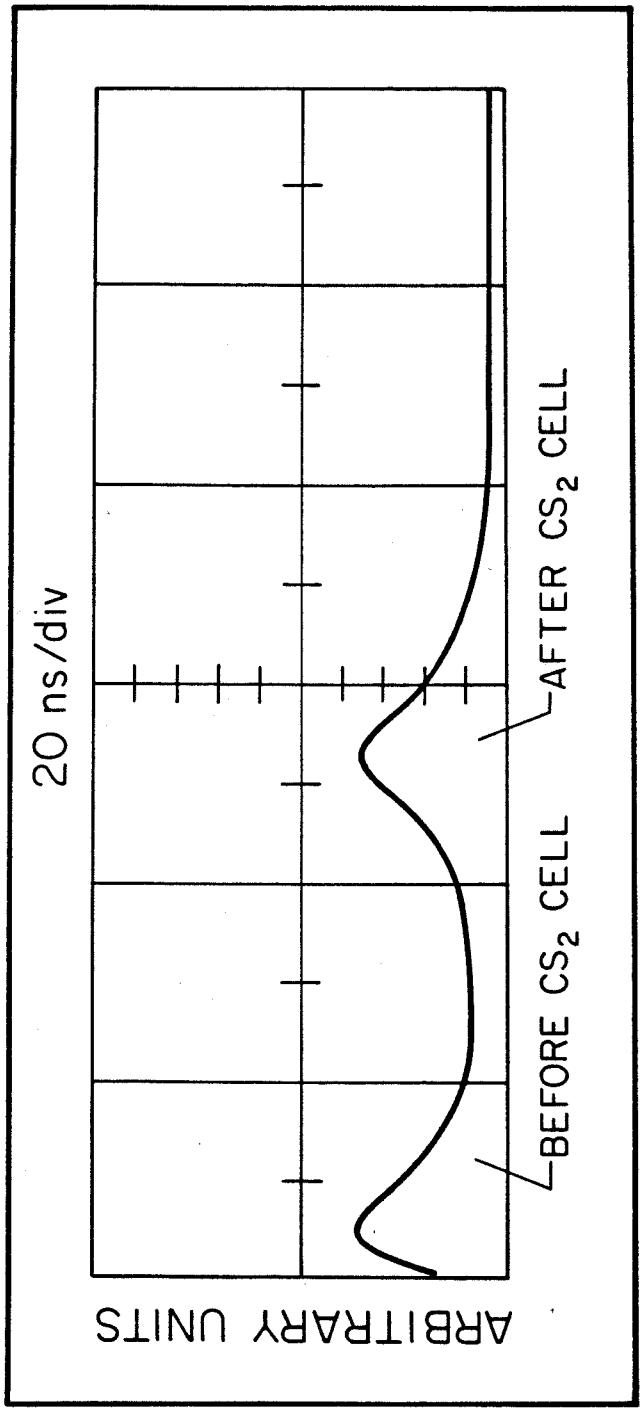

Fig. 4.4 Temporal evolution of the pump wave (A_1) prior to the CS_2 cell and after passage through the experimental apparatus.

divergent output.

Figure 4.5 shows the measured reflection coefficient as a function of the pumping pulse energy, ε_p. We note that for energies exceeding 11 mJ the reflection coefficient exceeds unity. Also plotted in Fig.4.5 is a least square fit of the function

$$R = \tan^2(\alpha\, \varepsilon_p) \qquad (4.2\text{-}6)$$

which is in the form predicted by (3.3-12). The value of α thus determined is employed, using (3.3-12), to calculate the value of $\chi^{(3)}_{yxxy}$ of CS_2. The result is

$$\chi^{(3)}_{yxxy} = (1.64\ {}^{+0.14}_{-0.20}) \times 10^{-12}\ \text{esu} \qquad (4.2\text{-}7)$$

compared with a generally accepted value [3] of $\chi^{(3)} \sim 1.8 \times 10^{-12}$ esu. This check serves to reassure us that the observed reflection is due to the four-wave mixing process described by (3.3-12).

We note that in arriving at (4.2-7) the measured Fresnel losses of both the CS_2 cell optics and glan prisms were considered, as was the linear loss due to the CS_2. The expression given in equation (3.6-6) was then used with $L_p = L$ (i.e., equal pump and probe interaction lengths) to extract $\chi^{(3)}_{NL}$.

Not shown in Figure 4.5 are the error bars for the data points which were estimated to be +25% and -12.5% for each measured value of the nonlinear reflection coefficient (these values are asymmetric owing to the factor-of-two difference between measured energy values of the sequence of photographic spots mentioned earlier); the horizontal error bar is $\pm$5% for each energy measurement (specifications of the Gen-Tec

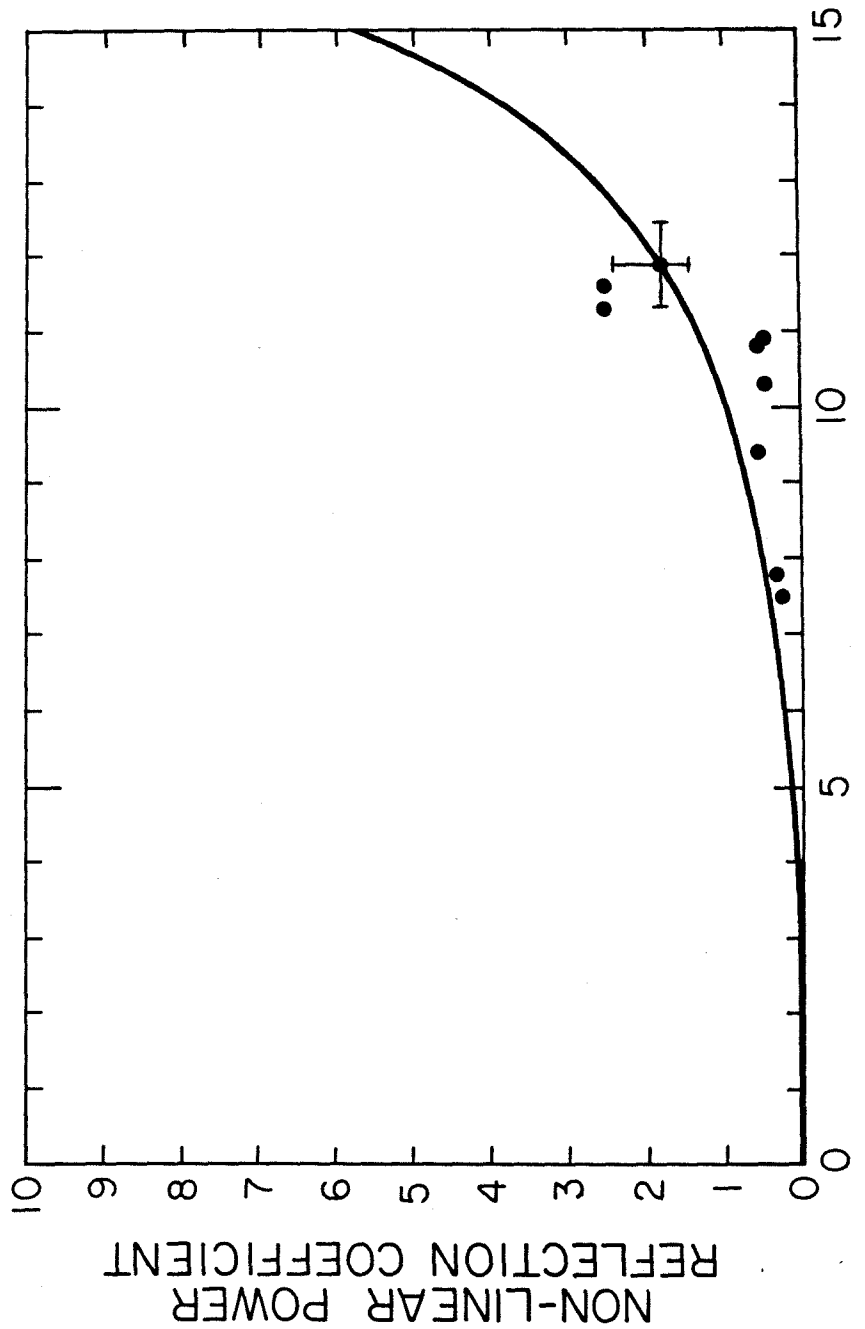

Fig. 4.5 Plot of the nonlinear power reflection coefficient versus pump energy ε_p (in mJ). Data [•]; least-square fit to $R = \tan^2(\alpha\varepsilon_p)$ [solid curve].

energy meter). Finally, the theoretical fit for the nonlinear reflection coefficient was corrected for the temporal conjugate pulse shortening effect described by (4.2-4) and also measured, thus forming the nonlinear power reflection coefficient as being the ordinate of the plot.

In conclusion, we note that the observation of nonlinear reflection coefficients in excess of unity is in conflict (i.e., greater) with the upper limit implied by (3.7-6) for CS_2, given our geometry. The peak power of our pump laser was measured to be more than an order of magnitude greater than the critical self-focusing power for CS_2 (recall, however, that catastrophic self-focusing effects were not seen). The apparent explanation for this discrepancy is that the pump beam quality of our Q-switched ruby laser was such that its output was presumably comprised of a large number of filaments ($\sim$ 20-50), with each one having an output power less than that required for self-focusing. In fact, later in our experimental efforts, we had the end faces of the ruby rod from our pump laser repolished and AR coated. After this processing, self-focusing effects were clearly seen upon passage of the pump beam through the 40 cm long CS_2 cell. In fact, the maximum attainable nonlinear reflection power reflection coefficient (for our geometry) after processing was not greater than 25%, which is now in rough agreement with that predicted by (3.7-6).

We note that the typical linewidth of a Q-switched ruby laser (operating in a single longitudinal and transverse mode) is found to be roughly $\Delta\nu_L \sim 100$ MHz [10]. This value is greater than $\Delta\nu_{SBS}$ by about a factor of 2 [2], thus (theoretically) obviating the problem of stimulated Brillouin scattering (SBS) from interfering with the phase

conjugation parametric interaction (for our experimental parameters). This fact is also in agreement with our experimental results, where SBS was not seen (see Figure 4.2).

We conclude this section with a comment regarding the pump laser coherence length. The coherence length (L_c) of ruby lasers is typically 1.5 meters [10], which includes frequency chirping effects [10]. (This value is obviously less than that assuming transform limited output lineshapes, when $L_c \sim c/\Delta\nu_L \sim 3$ meters.) This value, being greater than the length of our nonlinear medium, and also greater than any path length differences of the interacting fields assures us that the third-order nonlinear dipoles generated throughout our nonlinear medium constructively interfere, giving rise to the results as predicted in Section 3.3 (where monochromatic fields possessing infinite coherence lengths are assumed).

4.3 One-Mirror Assisted Optical Parametric Oscillation

In this section, we describe an experiment that revealed an optical parametric oscillation mode in a degenerate four-wave mixing geometry. From the coupled mode analysis described in Section 3.5, we concluded that the oscillation condition for the geometry considered is given by

$$|\kappa|L = \tan^{-1}(1/|r|) \qquad (4.3\text{-}1)$$

where r is the amplitude reflectivity of the added mirror (see Figure 3.5). We thus see that (4.3-1) implies that the oscillation condition is reduced by a factor of 2 (compared to the case without an external mirror), to a value of $|\kappa|L = \pi/4$ when the external mirror is totally reflecting

($|r|$ = 100%). We therefore expect the onset of oscillation to occur when the conjugate mirror reflection coefficient is also "totally reflecting" (or $|A_3/A_4|$ = 100%). Physically, this geometry therefore forms a passive "resonator" bounded by a conventional mirror on one end and a conjugate mirror on the other. The modes of such optical cavities, and further experimental results will be the topic of Chapter VI.

Self-oscillation was observed using the apparatus shown in Figure 4.6. The difference between this and the previous experimental geometry (Figure 4.1) is two-fold: first, prism P_1 is used to couple out any oscillation ("s" polarized) signal, while passing the pump beams. Second, the absence of prism P_3 now allows the totally reflecting flat mirror, M_1, to serve a dual function: (1) it retroreflects the pump beam (A_1), thus providing for its counterpropagating component (A_2); and (2) M_1 serves as a reflector for the orthogonally polarized oscillation field. As discussed above, this reduced the oscillation threshold by a factor of 2.

At pumping intensities exceeding 8.8 MW/cm^2 and with no input field ($A_4(0) = 0$) an intense oscillation pulse with orthogonal (s) polarization resulted. The oscillation pulse energy was approximately 1% of the pump energy. We note that the spot size of the oscillation beam was smaller than that of the input pump beam. This is due to the fact that the coupling constant κ is proportional to the product of two beams, A_1 and A_2, each with a Gaussian intensity profile [c.f. (4.2-4)] . We note that the value of the pump intensity at the oscillation threshold corresponds to a power reflection coefficient of $\sim$60%, thus being less than the theoretical value of 100% expected for oscillation to occur. This is to be expected, since in our system the oscillation grew not out of black-

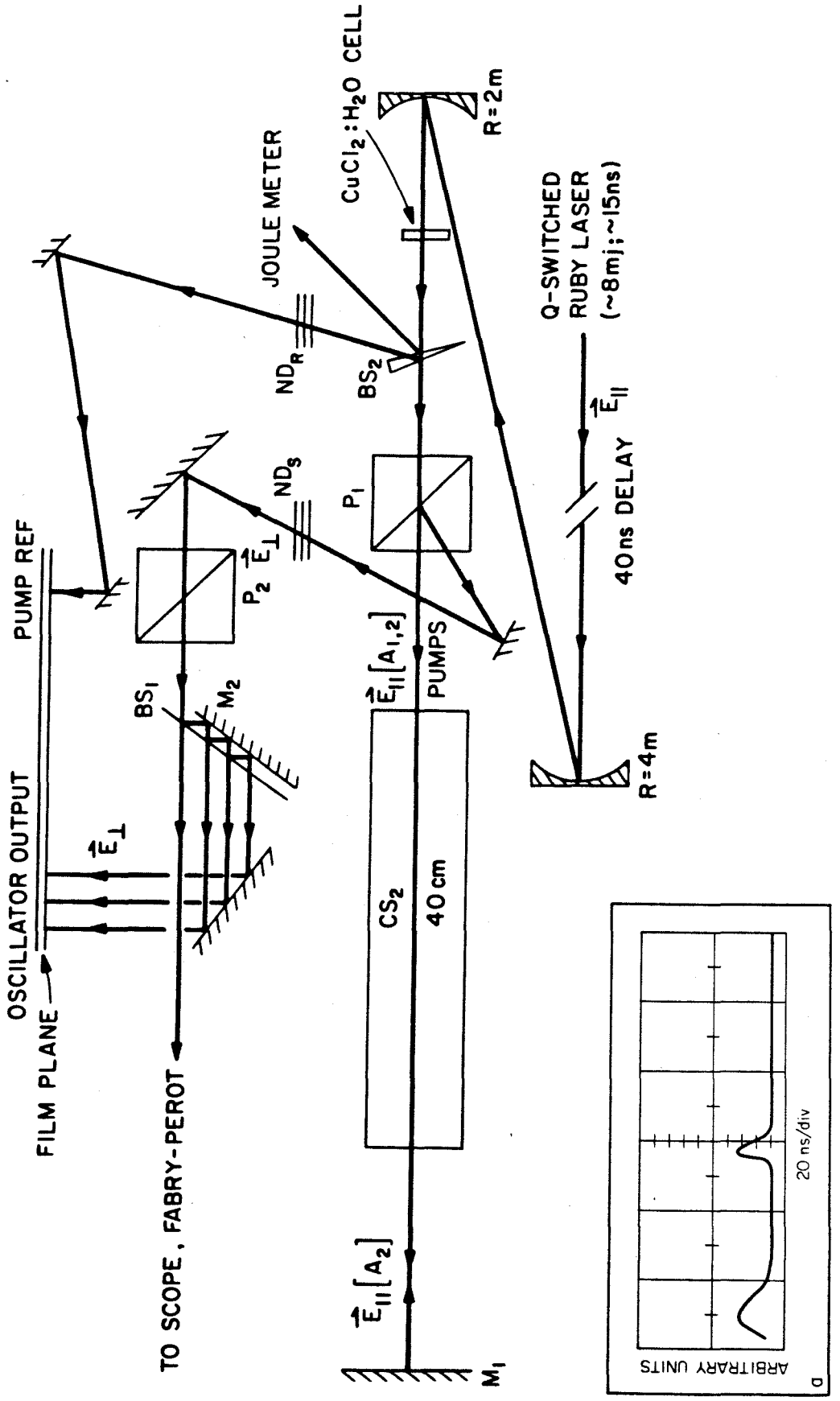

Fig. 4.6 Experimental apparatus for viewing one-mirror assisted parametric oscillation. Inset (a): Time evolution of the pump wave (left) and the oscillator output (right).

body photon noise modes, but from (depolarized) Rayleigh scattered pump photons within the CS_2 and associated optics. Finally, due to shot-to-shot laser output power fluctuations, coupled with the strong nonlinear dependence of the conjugate mirror reflectivity near the oscillation threshold ($R \propto \tan^2 \kappa L$), one would not expect very precise agreement of experimental values with theoretical predictions. Similar results have been observed for one-mirror assisted oscillation in sodium vapor [11].

A typical set of temporal pulse shapes is shown in Figure 4.6a. The first pulse is the laser output, while the second pulse (properly delayed and of arbitrary amplitude) is the output due to the oscillation. The nonlinearity of the interaction is also evident from this datum. Since the nonlinear gain requires the temporal overlap of the pump beams, the evolution of the gain in the time domain is essentially the temporal convolution of the two Gaussian pulses. This results in a nonlinear gain with a sharper and shorter Gaussian temporal characteristic. Fabry-Perot spectra of these signals verified the degenerate frequency nature of the oscillator output. Figure 4.7 shows a typical set of such spectra. In 4.7a the parametric oscillator output is seen to be degenerate in frequency with respect to the reference pump fields (again within the 150 MHz resolution of the instrument), while in Figure 4.7b no oscillator output is seen with the rear mirror (M_1) blocked. The parameters of the Fabry-Perot are identical with those used in the former experiment. Thus no additional frequency components, and hence no competing nonlinear optical processes were observed. Finally, the threshold nature of the oscillator output was verified by the nonlinear increase of its output as a function of input pump energy.

ONE MIRROR OSCILLATOR

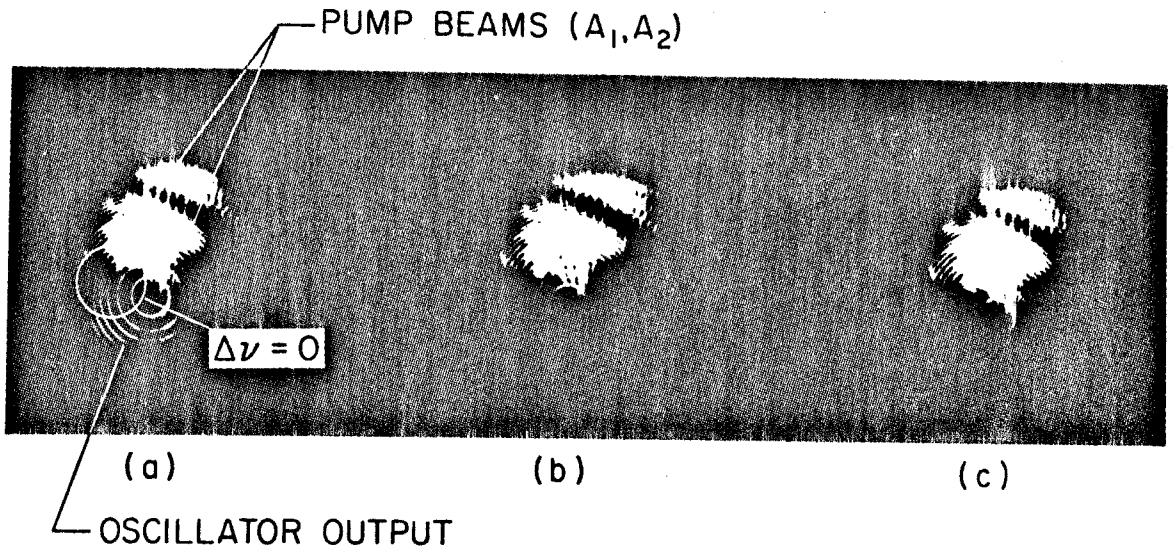

(a) ALL BEAMS PRESENT
(b) REAR MIRROR BLOCKED
(c) OSCILLATOR OUTPUT BLOCKED

Fig. 4.7 Fabry-Perot spectrum of the one-mirror assisted degenerate parametric oscillator output, as compared with that of the pump waves ($A_{1,2}$).

In conclusion, we have demonstrated that, in addition to phase conjugation, the process of four-wave mixing can result in amplification and oscillation, in accordance with theoretical predictions. Polarization discrimination was used to separate pump and signal beams. The temporal, spatial, and frequency characteristics of the observed signals were shown to be consistent with those expected from such a nonlinear interaction.

The use of a colinear geometry affords the possibility of performing real-time holographic operations and (time-reversed) image compensation at efficiencies large enough to be of more practical interest than previously observed.

4.4 Phase Conjugation via Four-Wave Mixing in Optical Waveguides: Theory

In this and the following section we will consider phase conjugation via degenerate four-wave mixing in optical waveguides. We will first present qualitative arguments and discuss several features pertaining to the use of optical fibers or waveguides as suitable geometrical media for optical phase conjugators. Next, we will present a derivation to prove the feasibility of generating phase conjugate fields by accomplishing the nonlinear interaction within a multimode optical waveguide. In the next section, we will outline an experiment we performed which used a liquid filled (in our case CS_2) optical fiber as the nonlinear medium and a cw argon ion laser as the source. Experimental results will be compared with the theoretical discussion presented below.

Thus far in this work we have considered nonlinear optical interactions in bulk media. By virtue of the magnitude $\chi_{NL}^{(3)}$ in the media discussed, one requires large optical intensities to realize sufficient nonlinear gains; hence, in bulk media, this constraint necessitated the

use of high peak power, Q-switched laser sources, as well as focusing optics to increase the intensity. For the third order interactions in bulk media considered thus far, the nonlinear efficiency ε_{bulk} scales as $\varepsilon_{bulk} \sim \chi_{NL}^{(3)} IL$, where the pump beam intensity and the interaction length are given by I and L, respectively. As an example, if we consider Gaussian beams, and allow the interaction to take place in the region of the focal plane of an optical system and over an interaction length on the order of the confocal parameter [2] ($L = \pi\omega_o^2/\lambda$, where ω_o is the radius of the spot size), the efficiency scales as $\varepsilon_{bulk} \sim \chi_{NL}^{(3)}(P/\pi\omega_o^2)\ (\pi\omega_o^2/\lambda) = \chi_{NL}^{(3)} P/\lambda$, for a given laser power $P_{bulk} \equiv P$.

If, on the other hand, we assume the interaction to occur in an optical waveguide (or optical fiber) possessing the same nonlinear susceptibility ($\chi_{NL}^{(3)}$), then one can exploit the fact that the optical waveguide is capable of maintaining a fixed beam profile, or eigenmode, over its entire length [12]. This fact has made possible many interesting device applications as well as the investigation of numerous nonlinear optical phenomena in fibers and other optical waveguides [13]. Thus, for third order interactions in waveguide geometries, the nonlinear efficiency ε_{guide} scales as $\varepsilon_{guide} \sim \chi_{NL}^{(3)}(P_{guide}/\pi r_o^2)L$, where r_o is the core radius of the fiber of length L, and the laser power is P_{guide}. Hence, the ratio of these efficiencies goes as

$$\frac{\varepsilon_{guide}}{\varepsilon_{bulk}} \sim \left(\frac{\lambda L}{r_o^2}\right) \frac{P_{guide}}{P_{bulk}} \qquad (4.4\text{-}1)$$

For typical optical fibers $r_o \sim 1\text{-}100\lambda$ and $L \sim 1\text{-}100$m.
Thus the first factor of (4.4-1) can be on the order of 10^6.
Therefore, as opposed to using pulsed, high

power lasers ($P \sim MW$) in the bulk, one can in principle realize similar nonlinear efficiencies using cw lasers having only several watts of optical power in optical fibers. There are, however, several limitations that provide constraints upon both the efficiency of the interaction and the information processing capability of such fiber systems. First, there exist length constraints. The degenerate four-wave interaction, being dependent upon the complex field amplitudes of the various beams present, requires that all the interacting waves maintain a definite phase relationship throughout the nonlinear medium. Therefore, the coherence length [10] of the laser must exceed the interaction length in order for constructive interference of the nonlinear dipoles (which radiate the conjugate wave) to take place. Second, the interaction length should not exceed the linear loss e-folding length. That is, $L \leq 1/\alpha$, where α is the linear loss coefficient (recall Section 3.6). Another set of constraints involves the consideration of competing nonlinear effects such as stimulated Raman or Brillouin scattering. These effects have been considered in detail in arriving at maximum power handling capabilities for given fibers [14,15]. We note that since these Raman-type gains depend upon the local laser <u>intensity</u> (as opposed to the laser amplitude), these effects do not involve the additional laser coherence length constraint. Another constraint involves the spatial information handling capacity of the fibers. Since a given fiber can confine or support a finite number of eigenmodes (analogous to the number of eigenstates possible for a given quantum mechanical particle in a box), this number of modes places an upper limit upon the number

of diffraction limited resolution elements which can be phase conjugated. Thus, for a given laser power and fiber parameters there is a trade-off between the number of resolution elements capable of conjugation and the nonlinear gain attainable. This therefore forms an equivalent nonlinear gain-spatial bandwidth product that would characterize a given fiber.

Having motivated the use of optical waveguides as potential guiding media for the realization of efficient nonlinear optical phenomena, we next present an analysis of phase conjugation by four-wave mixing in multimode optical fibers. It will be found that complex image fields can be phase-conjugated and amplified without loss of spatial information, i.e., without mode mixing. A calculation shows that this can be done on a cw basis with moderate ($\sim$ 1 watt) pump powers in a few meters of fiber. This suggests that four-wave mixing in fibers is a serious candidate for real-time holographic applications including image transmission and compensation for distorting media.

The basic geometry involved in the experiment is illustrated in Figure 4.8. An input field E_i is incident on a fiber whose core medium possesses an appreciable third-order nonlinear coefficient $\chi^{(3)}$. The input field E_i may correspond to an image field transmitted by another fiber or to some other field whose phase conjugate is sought. The fiber is multimode with a number of propagating modes essentially equal to the number of resolution elements contained in the incident field E_i. The number of confined modes N for a given waveguide geometry and input wavelength (λ) is approximately [16]

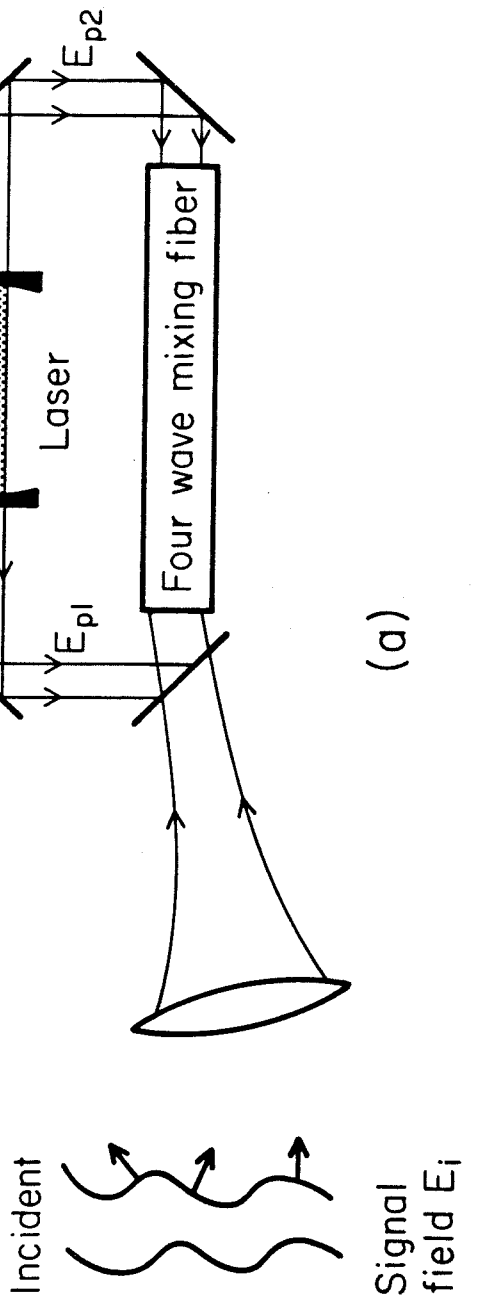

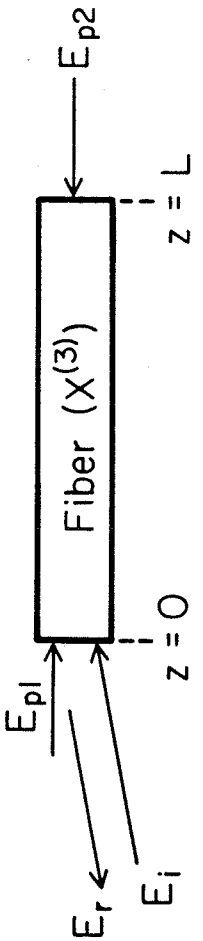

Fig. 4.8 The geometry for four-wave mixing in an optical fiber.

$$N \simeq \left(\frac{2\pi a}{\lambda}\right)^2 (N.A.)^2 \qquad (4.4\text{-}2)$$

where a is the effective radius of the guiding layer (or fiber core) and N.A. is the "numerical aperture" of the waveguide. For a step index configuration, the N.A. is given by [16]

$$N.A. = (n_2 - n_1)^{1/2} \simeq (2n\Delta n)^{1/2} \qquad (4.4\text{-}3)$$

where n_2 and n_1 are the index of refraction of the core and cladding layer, respectively ($\Delta n = n_2 - n_1$; in the second equality we assume that $n_2 \sim n_1 \equiv n$).

The fiber is pumped simultaneously by two strong, oppositely traveling fields, E_{p1} and E_{p2}, whose frequency is the same as that of E_i. A reflected field E_r, generated by the four-wave mixing interaction, will be shown to be a complex conjugate of the input field. For sufficiently intense pump waves, E_r will be an amplified phase conjugate version of the input field E_i. The set of propagating eigenmodes of the fiber is denoted by $\{\mathcal{E}_\ell(x,y)\}$. The pump waves are taken as

$$\begin{aligned} E_{p1} &= \tfrac{1}{2}\mathcal{E}_{p1}(x,y)\, e^{i(\omega t - \beta_1 z)} + \text{c.c.} \\ E_{p2} &= \tfrac{1}{2}\mathcal{E}_{p2}(x,y)\, e^{i(\omega t + \beta_1 z)} + \text{c.c.} \end{aligned} \qquad (4.4\text{-}4)$$

where $\mathcal{E}_{p1}(x, y)$ and $\mathcal{E}_{p2}(x,y)$ are the respective transverse modal distributions. The pump fields will be coupled ideally into the lowest order propagating mode of the fiber so that their confinement over the full interaction length is assured. We thus have $\mathcal{E}_{p1}(x,y) = \mathcal{E}_{p2}(x,y) \equiv \mathcal{E}_1$.

Hellwarth [18] treats the case where the pump waves are multimode. We will see that the single mode pump wave approach is the more efficient scheme. The input signal wave E_i and the reflected output wave E_r are expanded in terms of the propagating eigenmodes $\mathcal{E}_\ell(x,y)$ of the fiber as

$$\begin{aligned} E_i &= \frac{1}{2} \sum_m B_m(z)\, \mathcal{E}_m(x,y)\, e^{i(\omega t - \beta_m z)} + \text{c.c.} \\ E_r &= \frac{1}{2} \sum_\ell A_\ell(z)\, \mathcal{E}_\ell(x,y)\, e^{i(\omega t + \beta_\ell z)} + \text{c.c.} \end{aligned} \tag{4.4-5}$$

The complex amplitudes $B_m(0)$ are determined by the input conditions. We are seeking a solution for $B_m(z)$ and $A_m(z)$. The wave equation is

$$\nabla^2 E - \mu\varepsilon(\vec{r})\, \frac{\partial^2 E}{\partial t^2} = \mu\, \frac{\partial^2}{\partial t^2} P_{NL}(\vec{r},t) \tag{4.4-6}$$

The functions $\mathcal{E}_\ell(x,y)$ satisfy (4.4-6) with $P_{NL} = 0$

$$\left(\frac{\partial^2}{\partial x^2} + \frac{\partial^2}{\partial y^2} - \beta_\ell^2\right) \mathcal{E}_\ell(x,y) + \omega^2 \mu\varepsilon(\vec{r})\, \mathcal{E}_\ell(x,y) = 0 \tag{4.4-7}$$

and are orthonormal such that

$$\iint_{-\infty}^{\infty} dx\,dy\, \mathcal{E}_\ell(x,y)\, \mathcal{E}_m(x,y) = \delta_{\ell m} \tag{4.4-8}$$

Substituting equation (4.4-5) into equation (4.4-6)

$$\sum_{\ell} \left[\left(\frac{\partial^2}{\partial x^2}+\frac{\partial^2}{\partial y^2}-\beta_\ell^2+\omega^2\mu\varepsilon(\vec{r})\right)\frac{A_\ell}{2}+i\beta_\ell\frac{dA_\ell}{dz}+\frac{1}{2}\frac{d^2A_\ell}{dz^2}\right]\mathcal{E}_\ell \exp[i(\omega t+\beta_\ell z)]+c.c. = \frac{\mu\partial^2}{\partial t^2}P_{NL}(\vec{r},t) \tag{4.4-9}$$

Using (4.4-7) to eliminate the first factor inside the square bracket, and assuming that $|d^2A_\ell/dz^2| << |\beta_\ell^2 A_\ell|$ leads to

$$\sum_{\ell} i\beta_\ell\frac{dA_\ell}{dz}\mathcal{E}_\ell \exp[i(\omega t+\beta_\ell z)]+c.c. = \frac{\mu\partial^2}{\partial t^2}P_{NL}(\vec{r},t) \tag{4.4-10}$$

In a similar fashion we obtain for the input field

$$\sum_{m} -i\beta_m\frac{dB_m}{dz}\mathcal{E}_m\exp[i(\omega t-\beta_m z)]+c.c. = \frac{\mu\partial^2}{\partial t^2}P_{NL}(\vec{r},t) \tag{4.4-11}$$

The induced nonlinear polarization is third order in the field amplitudes and is taken as

$$P_{NL}^{\omega=\omega+\omega-\omega} = \chi^{(3)}E_{p1}E_{p2}E_i^* \tag{4.4-12}$$

Substituting (4.4-12) into (4.4-10), we obtain

$$\sum_{\ell}\beta_\ell\frac{dA_\ell}{dz}\mathcal{E}_\ell(x,y)e^{i\beta_\ell z} = \frac{i\omega^2\mu\chi^{(3)}}{2}\mathcal{E}_{p1}\mathcal{E}_{p2}\sum_{m}B_m^*(z)\mathcal{E}_m(x,y)\,e^{i\beta_m z} \tag{4.4-13}$$

In a similar fashion from (4.4-11)

$$\sum_{m}\beta_m\frac{dB_m}{dz}\mathcal{E}_m(x,y)\,e^{-i\beta_m z} = -\frac{i\omega^2\mu\chi^{(3)}}{2}\mathcal{E}_{p1}\mathcal{E}_{p2}\sum_{\ell}A_\ell^*(z)\,\mathcal{E}_\ell(x,y)\,e^{-i\beta_\ell z} \tag{4.4-14}$$

or by conjugation (and taking $\mathcal{E}_{p1}$, $\mathcal{E}_{p2}$, and $\chi^{(3)}$ as real)

$$\sum_m \beta_m \frac{dB_m^*}{dz} \mathcal{E}_m(x,y)\, e^{i\beta_m z} = \frac{i\omega^2\mu\chi^{(3)}}{2} \mathcal{E}_{p1}\mathcal{E}_{p2} \sum_\ell A_\ell(z)\, \mathcal{E}_\ell(x,y)\, e^{i\beta_\ell z} \tag{4.4-15}$$

Multiply (4.4-13) by $\mathcal{E}_s$ and integrate over the cross section using (4.4-8)

$$\frac{dA_s}{dz} = \frac{i\omega^2\mu\chi^{(3)}}{2\beta_s} \sum_m B_m^*(z)\, e^{i(\beta_m-\beta_s)z} \iint_{c.s.} \mathcal{E}_{p1}\mathcal{E}_{p2}\mathcal{E}_m\mathcal{E}_s \, dx\, dy \tag{4.4-16a}$$

and from (4.4-15)

$$\frac{dB_s^*}{dz} = \frac{i\omega^2\mu\chi^{(3)}}{2\beta_s} \sum_m A_m(z)\, e^{i(\beta_m-\beta_s)z} \iint_{c.s.} \mathcal{E}_{p1}\mathcal{E}_{p2}\mathcal{E}_m\mathcal{E}_s \, dx\, dy \tag{4.4-16b}$$

Equations (4.4-16) are the basic coupling equations. We note that a given mode A_s of the reflected field is coupled to all modes B_m of the incident field. This is undesirable, since it causes a loss of spatial information. Two physical facts combine to remedy this mode scrambling: (a) We note that for a length of fiber $L >> 2\pi(\beta_m-\beta_s)^{-1}$, modes A_s and B_m are grossly mismatched so that no cumulative power exchange between them can take place unless $\beta_m = \beta_s$. (b) In addition, if the pump fields $\mathcal{E}_{p1}(x,y)$ and $\mathcal{E}_{p2}(x,y)$ are more or less uniform over the cross section, then the overlap integrals appearing in (4.4-16) are zero unless $m = s$. The combined effect of (a) and (b) is that a given reflected mode A_s of the reflected field couples almost exclusively to the incident field mode of the same index, i.e., to B_s. We thus have:

$$\frac{dA_s}{dz} = \frac{i\omega^2\mu\chi^{(3)}}{2\beta_s} \mathcal{E}_{p1}\mathcal{E}_{p2}B_s^* \tag{4.4-17a}$$

$$\frac{dB_s^*}{dz} = \frac{i\omega^2\mu\chi^{(3)}}{2\beta_s}\mathcal{E}_{p1}\mathcal{E}_{p2}A_s \qquad (4.4\text{-}17b)$$

Since the input field E_i is specified, the mode amplitudes B_s $(z = 0)$ are given. Another boundary condition is that the reflected field E_r is zero at the output end $z = L$ of the fiber, so that $A_s(L) = 0$. With these boundary conditions we can solve (4.4-17), obtaining

$$A_s(z) = iB_s^*(0)(\sin \kappa_s z - \tan \kappa_s L \cos \kappa_s z)$$

$$B_s(z) = B_s(0)(\tan \kappa_s L \sin \kappa_s z + \cos \kappa_s z) \qquad (4.4\text{-}18)$$

where $\kappa_s = \dfrac{\omega^2\mu\chi^{(3)}\mathcal{E}_{p1}\mathcal{E}_{p2}}{2\beta_s}$. Equations (4.4-18) display the same amplification and oscillation features as the plane wave case outlined in Chapter III. We are particularly interested in what happens to the image information. We find that at $z = 0$,

$$A_s(0) = -iB_s^*(0) \tan \kappa_s L \qquad (4.4\text{-}19)$$

The total reflected image field can be reconstructed, using equation (4.4-5) as

$$E_r(x,y,z=0) = -i \tan \kappa L \sum_{\ell} \frac{1}{2} B_\ell^*(0)\, \mathcal{E}_\ell(x,y) \exp(i\omega t) + \text{c.c.} \qquad (4.4\text{-}20)$$

where, neglecting the weak dependence of κ_s on s, we took $\kappa_s \equiv \kappa$. The

original input field is, according to (4.4-5)

$$E_i(x,y,z=0) = \sum_{\ell} \frac{B_\ell(0)}{2} \mathcal{E}_\ell(x,y)\, e^{i\omega t} + \text{c.c.} \tag{4.4-21}$$

so that as far as the total complex field amplitudes are concerned, we have

$$E_r(x,y,z=0) = -i \tan(\kappa L)\, E_i^*(x,y,z=0) \tag{4.4-22}$$

The reflected field at the fiber input is thus an amplified (for $\kappa L > \pi/4$) complex conjugate replica of the input field.

The tremendous advantage of performing the phase conjugation inside a fiber is due to the fact that pump waves can be launched as fiber modes so that large pump intensities over the whole interaction path can result from moderate pump powers. If we consider, as an example, a multimode fiber with a core diameter of 20 μm which is filled with CS_2 and take the two pump wave powers as 1 watt, we obtain (using $\chi^{(3)} \simeq 1.2 \times 10^{-12}$ esu)κ $\simeq 5 \times 10^{-4}$ cm^{-1}, so that $\kappa L \simeq 1$ is achieved with a fiber length of L = 20m. It should be noted that if the pump propagates as a low order mode, the overlap integrals of (4.4-16) may be appreciable for near-lying modes, i.e., incident and reflected modes of different indices can interact. This interaction, however, is negligible, since the phase mismatch $(\beta_s - \beta_m)L$ can be shown to be $>> 2\pi$ in the above example.

The theory and example presented above clearly demonstrate the advantage of performing four-wave mixing in long fibers. Under such conditions, it is important to consider the effect of optical absorption. If the intensity absorption coefficient of the four waves involved in

the interaction is taken as α, we obtain instead of equation (4.4-22),

$$E_r(x,y,0) = \frac{-2i\kappa \tan(\kappa_e L) \exp(-\frac{1}{2}\alpha L)}{\alpha \tan(\kappa_e L) + 2\kappa_e} E_i^*(x,y,0) \qquad (4.4-23)$$

where $\kappa_e = [\kappa^2 \exp(-\alpha L) - (\frac{1}{2}\alpha)^2]^{1/2}$. This equation follows from the arguments presented in Section 3.6 if we assume equal pump and probe interaction lengths (i.e., $L = L_p \equiv L$) in equation (3.6-6). It follows from (4.4-23) that for substantial reflections we need fulfill $\alpha L << 1$, $\kappa > \alpha/2$. If $\alpha L >> 1$, then

$$\frac{E_r(x,y,0)}{E_i^*(x,y,0)} = -i \exp(-\frac{1}{2}\alpha L) \frac{\kappa}{\alpha} \qquad (4.4-24)$$

The pump intensity in the above example is below that for the onset of stimulated Brillouin scattering in CS_2 and also is such that amplified spontaneous Stokes radiation is insignificant [14,15].

4.5 Demonstration of Degenerate Four-Wave Mixing in a Liquid-Filled Fiber

In this section, the observation of cw backward-wave generation using degenerate four-wave mixing in a nonresonant medium will be reported. The interaction took place inside a 3m long CS_2-filled 4 μm i.d. optical fiber. Defining the backward-wave conversion efficiency as the ratio of the reflected wave intensity to the input wave intensity, a 0.45% conversion efficiency was measured with a pump power of 6 mW inside the fiber.

In the experiment sketched in Figure 4.9, the pump and the probe waves originated in a cw single transverse and longitudinal mode argon ion laser, operating at a wavelength of 5145Å using an intracavity, temperature stabilized etalon. The laser output had a 10 m long coherence length, which ensured the coherence of the nonlinear interaction over the entire fiber length. The two fiber ends and the objective lenses were carefully aligned to allow maximum coupling of the two linearly polarized pump beams into the lower order fiber modes. Typically, fifty percent of the incident light was coupled into each end. Each fiber end was securely positioned inside a stainless steel CS_2-filled cell (not shown in the figure). The CS_2 inside the cell was under a nitrogen pressure of 80 psi (4100 Torr) which prevented the liquid from boiling when illuminated by the focused pump beams. The probe beam, whose power was roughly equal to that of the pump beams, was introduced nearly parallel to the forward-going pump beam, E_{p2}, and was coupled into the fiber by the same objective lens. Since the probe beam was slightly separated from the on-axis pump beam, the coupling efficiency was typically a factor of five lower than that of E_{p2}. All the beams were chopped (at 57 Hz) to reduce the duty cycle (and consequently to inhibit the degradation of CS_2) of the optical fields as well as to allow the use of temporal discrimination techniques for the detection of the backward signal. The probe beam also passed through an optical isolator consisting of a linear polarizer and quarter-wave plate prior to coupling into the fiber. This isolator served two functions. First, it minimized any spurious Fresnel reflected probe signals from interfering with the backward-going wave. Second, being a polarization

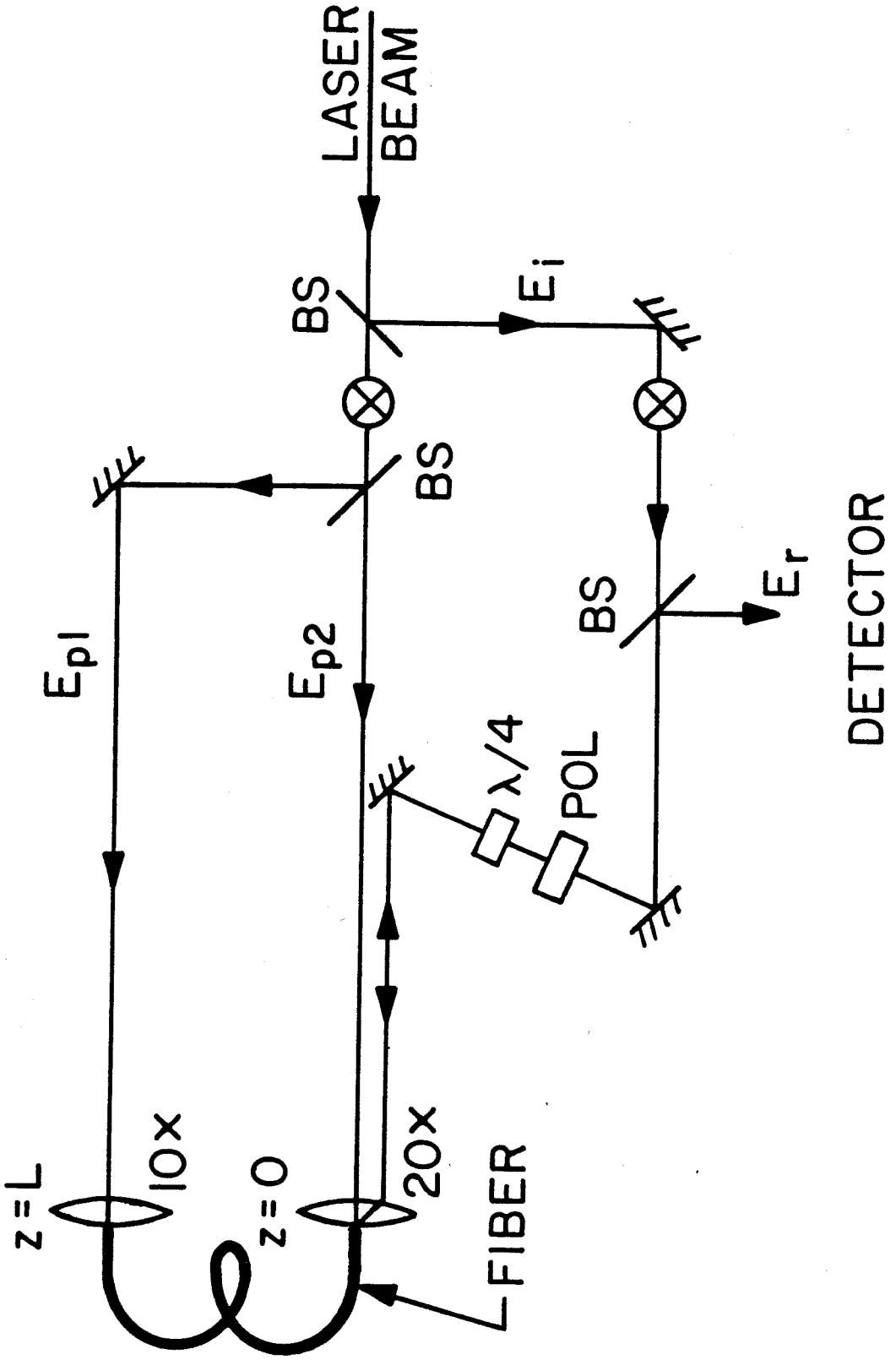

Fig. 4.9 The experimental set-up for four-wave mixing in a liquid-filled fiber.

dependent phase "aberrator," the isolator would pass only the conjugate probe field, which could correct for this phase "distortion." Hence, the conjugate reflection of a RHCP field, which is also a RHCP wave, will be passed by the isolator in contrast to a LHCP wave which is the result of a Fresnel reflection, as discussed in Section 2.3.

Due to the proximity of the probe and pump fields (constrained by the aperture of the objective lens), additional background noise arose from both the forward-going pump, E_{p2} (via Fresnel reflections), and the counterpropagating pump, E_{p1} (due to the residual throughput from the fiber). Attempts to reduce these background noise sources via polarization discrimination were not utilized due to polarization scrambling of the fields within the 3 m long fiber. In order to extract the conjugate signal from the background by temporal discrimination techniques, the pump beams and the probe beam were chopped with different "on" durations as shown in Figure 4.10. The conjugate wave was generated only in the time interval when both the pumps and the probe passed through the chopper. During the interval when the beams did not overlap in time, the light detected was due to the Fresnel reflection of E_{p2} and the residual throughput of E_{p1}, plus residual Fresnel reflections of the probe wave that leaked through the isolator. The conjugate signal was obtained by subtracting the signal detected during the non-overlapping time intervals from that of the overlapping time interval. The conjugate signal disappeared when either pump beam was blocked. For an input power of 6 mW in each pump beam within each fiber end, a conversion efficiency of 0.45% was observed. For $n = 1.628$, $\alpha = 2.5 \times 10^{-3} cm^{-1}$ [13] and $(2\pi\chi^{(3)})/n = 1.1 \times 10^{-11}$ esu [3], equation (4.4-23) predicts a

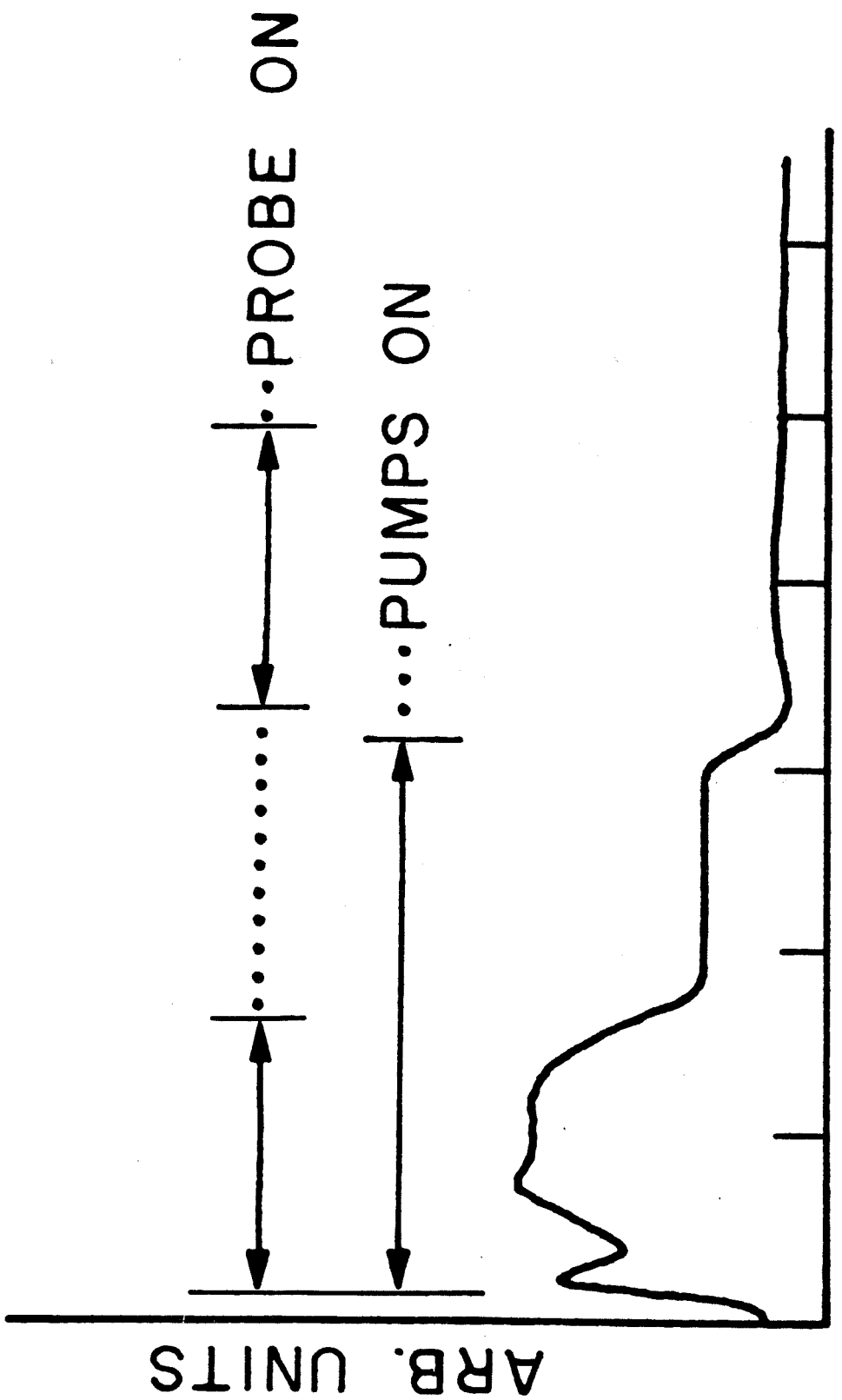

Fig. 4.10 Oscilloscope trace of the detector output.

conversion efficiency of 0.23%. The discrepancy between theory and experiment can be attributed to the rough estimate of the conjugate signal as well as the values of α and $\chi^{(3)}$ used in (4.4-23).

The pump powers employed were well below the threshold for both stimulated Brillouin scattering and Raman scattering [14,15]. The backward wave was observed only when both pump waves and the probe wave overlapped in time, even at a larger pumping power; thus other nonlinear effects such as optically induced birefringence or thermally induced index of refraction changes could not have generated the signal that was observed. Although there is polarization scrambling inside the fiber, a simple consideration of the magnitudes of the various third order susceptibility tensor elements [3] shows that the dominant backward-wave signal is indeed proportional to the complex conjugate of the probe signal.

In a separate experiment, we used only two waves, E_{p1} and E_{p2}, which were chopped with different duty cycles. In this case, a 1.6 m long 7 μm i.d. CS_2-filled fiber was used. Prior to entering the objective lens, E_{p2} passed through a crosshair made of fine wires, so that its diffracted wave had additional structure surrounding the central spot. The purpose of the crosshair was to divert some energy of E_{p2} to higher order fiber modes. The light in the higher order modes essentially served as the probe wave [17], as mentioned in the previous experiment. A backward-going wave was also detected as in the previous case. With E_{p2} blocked, a bright spot was observed that was due to the residual light from E_{p1} emanating from the fiber. When both E_{p1} and E_{p2} illumin-

ated the fiber, we observed additional spatial structure in the form of a peripheral ring, which was not due to the Fresnel reflection of E_{p2}. At higher pump powers, distinct dots were seen that surrounded the central bright spot. This indicated that a backward-going wave with its energy mainly located in the higher order fiber modes was generated.

In conclusion, a cw backward-wave generation by four-wave mixing in optical fibers was demonstrated. In addition, the phase conjugate interaction was shown capable of correcting polarization dependent aberrations and distortions such as optical component birefringence. The lifetime of the CS_2-filled fiber was rather short (on the order of a few hours), especially when subjected to continuous laser beam illumination. Other Kerr media such as benzene or possibly a mixture of CS_2 and benzene may alleviate this problem and thus yield potential practical device applications.

Appendix 4A

Evaluation of the Gaussian Spot Size of an Optical Beam by a Photographic Technique

In this appendix we discuss the photographic technique used to determine the Gaussian spot size in our pulsed laser experiments. Not only does this technique yield the spot size, but in conjunction with a reference beam, it can yield the beam energy. The procedure basically follows the description of reference [8]; the major difference, and hence the advantage of our approach, is that the spot size (as well as the relative energy) can be obtained in one shot (laser pulse). Previous techniques, such as that of reference [8], or "energy in the bucket" methods require several laser shots and thus assume that the laser output parameters remain constant over all the shots recorded in performing the measurement. The measurement of the relative laser energy to that of an optional reference beam provides a further "bonus" of the technique.

The basic geometry is shown in Figure 4A.1. The laser output beam whose spot size (and even relative energy) are sought is directed as shown into a (parallel) mirror-beam splitter system that beam splits and reflects a sequence of beams that are incident upon a recording medium (in our case, type 47 polaroid film emulsion). In our system we employed a 50% beam splitter for the given input optical polarization state. Hence, a sequence of parallel spots, each being reduced by a factor of two from the preceding spot, is recorded on the film. Also (optionally) incident upon the film is a reference beam, whose energy is known--for example through the measurement of a calibrated Fresnel-reflected spot upstream.

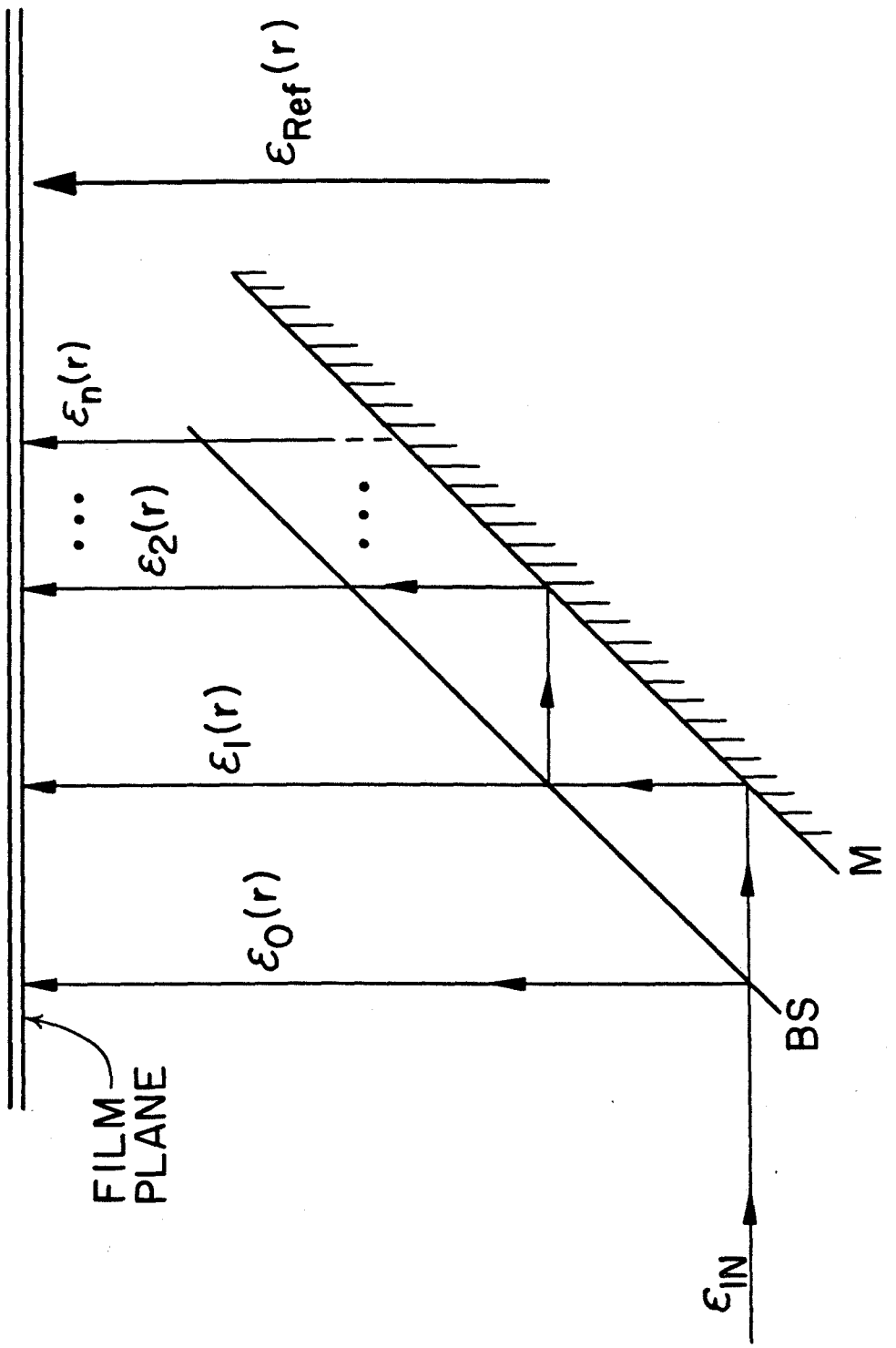

Fig. 4A.1 Apparatus to determine the Gaussian spot size. $\varepsilon_{Ref}(r)$ is an optional reference beam, M is a 100% reflecting mirror; BS is a 50% (intensity) beam splitter.

Both beams pass through neutral density stacks prior to impinging upon the film plane to insure a nonsaturating film exposure. Of course, the energy of the reference spot need not be measured if one desires a relative comparison of this reference with the spot sequence of the other beam. In fact, for our experiment, this technique provided the direct measurement of the nonlinear reflection coefficient, where the "reference spot" was that of the conjugate wave (A_3), while the sequence of spots was generated by the probe field (A_4) (see Section 4.2 and Figure 4.1 for details).

The procedure used to determine the spot size is to measure the "radius" chosen to correspond to the same exposed point of each spot. Since we are examining the same degree of exposure for each spot in the sequence, this technique does not require that the system operate within the linear region of the recording medium (e.g., the linear region of the Hurter-Driffield curve [10] for film emulsion). Of course, if we also wish to measure relative energies (e.g., the measurement of the nonlinear reflection coefficient), then the linear portion of the H-D curve must be used; we verified operation within this region for our experiment by utilizing various calibrated neutral density stacks to compare the spot sequence with various (attenuated) reference spots.

Assume a sequence of N photographed Gaussian spots, with the intensity of each successive spot attenuated by a factor of two. The n^{th} spot in the sequence has an intensity

$$I_n(r) = g|\varepsilon_n(r)|^2 \tag{4.A-1}$$

where g is a numerical constant. The radial dependence of the field goes as

$$\varepsilon_n(r) = \varepsilon_n(0)\ \exp(-r^2/a^2) \tag{4.A-2}$$

We wish to extract the value of "a," the Gaussian spot size. By virtue of the beam-splitter/mirror pair, we have

$$\varepsilon_n(r) = \varepsilon_o(r) / 2^{(n/2)} \tag{4.A-3}$$

where $\varepsilon_o(r)$ corresponds to the first (greatest amplitude) field.

We now assume that we can measure the "radius" of each spot at the same contrast point on the film. Hence, we compile a list of radii, r_n, for the sequence of spots, with the value for $r_n > r_{n+1}$.

Since each measured value of the radius corresponds to the same intensity, we have

$$I_n(r=r_n) = I_o(r=r_o) \equiv C_1 \tag{4.A-4}$$

Using (4.A-2 and -3) with (4.A-4), we obtain

$$g|\varepsilon_n(r_n)|^2 = g\left|\frac{\varepsilon_o(0)}{2^{(n/2)}}\right|^2 \exp(-2r_n^2/a^2) = C_1 \tag{4.A-5}$$

Solving(4.A-5) for n yields

$$n = \frac{-2}{a^2 \ell n\, 2}\, r_n^2 + C_2 \tag{4.A-6}$$

where C_2 is another constant.

We see that (4.A-6) is of the form

$$y = mx + b \tag{4.A-7}$$

where $m = -2/(a^2 \ell n\, 2)$ and $b = C_2$, $x = r_n^2$, and $y = n$.

Therefore, for a given set of measured data $\{n, r_n\}$, a least squares fit to the function (4.A-7) can be obtained, with the intensity spot size given by

$$w_I = \sqrt{\frac{1}{m\, \ell n\, 2}} \tag{4.A-8}$$

where m is the best fit slope to (4.A-7). The "effective" beam area is given by $A_{eff} = 2\pi\, w_I^2$.

Chapter IV - References

1. J. A. Armstrong, N. Bloembergen, J. Ducuing, and P. S. Persham, "Interactions between light waves in a nonlinear dielectric," Phys. Rev. 127, 1918 (1962); P. D. Maker and R. W. Terhune, "Study of optical effects due to an induced polarization third order in the electric field strength," Phys. Rev. 137, A801 (1965).
2. A. Yariv, Quantum Electronics, 2nd ed. (Wiley, New York, 1975).
3. R. W. Hellwarth, "Third order optical susceptibilities of liquids and solids," Prog. Quant. Electron. 5, 1 (1977).
4. S. L. Shapiro and H. P. Broida, "Light scattering from fluctuations in orientations of CS_2 in liquids," Phys. Rev. 154, 129 (1967).
5. J. Reintjes and R. L. Carmen, "Direct observation of the orientational Kerr effect in the self-focusing of picosecond pulses," Phys. Rev. Lett. 28, 1697 (1972).
6. G.K.L. Wong and Y. R. Shen, "Study of pretransitional behavior of laser-field-induced molecular alignment in isotropic nematic substances," Phys. Rev. A10, 1277 (1974).
7. B. E. Newman and L. G. DeShazer, "Direct nondestructive measurement of self-focusing in laser glass," in Damage in Laser Materials (NBS Spectral Publication #356), p. 113 (1971); L. G. DeShazer and J. H. Parks, "Investigation toward understanding the physics of laser damage to thin dielectric films," ibid., p. 124.
8. V. Wang and C. R. Giuliano, "Correction of phase aberrations via stimulated Brillouin scattering," Opt. Lett. 2, 4 (1978).
9. See, for example, R. W. Hellwarth, A. Owyoung, and Nicholas George, "Origin of the nonlinear refractive index of liquid CCl_4," Phys. Rev.

A4, 2342 (1971), and references therein.

10. R. J. Collier, C. B. Burckhardt, and L. H. Lin, Optical Holography (Academic Press, New York, 1971).

11. D. M. Bloom, P. F. Liao, and N. P. Economou, "Observation of amplified reflection by degenerate four-wave mixing in atomic sodium vapor," Opt. Lett. 2, 58 (1978).

12. See, for example, D. Marcuse, Theory of Dielectric Optical Waveguides (Academic Press, New York, 1974).

13. E. P. Ippen, "Nonlinear effects in optical fibers," in Laser Application to Optics and Spectroscopy, S.F. Jacobs, M.O. Scully, and M. Sargent, eds. (Addison-Wesley, Reading, Mass., 1975), p. 213, and references therein.

14. R. G. Smith, "Optical power handling capacity of low loss optical fibers as determined by stimulated Raman and Brillouin scattering," Appl. Opt. 11, 2489 (1972).

15. J. AuYeung and A. Yariv, "Stimulated Raman scattering in long, low loss fibers," IEEE J. Quant. Electron. QE-14, 347 (1978).

16. D. Gloge, "Weakly guiding fibers," Appl. Opt. 10, 2252 (1971).

17. S. M. Jensen and R. W. Hellwarth, "Generation of time-reversed waves by nonlinear refraction in a waveguide," Appl. Phys. Lett. 33, 404 (1978).

18. R. W. Hellwarth, "Theory of phase-conjugation by four-wave mixing in a waveguide," IEEE J. Quant. Electron. QE-15, 101 (1979).

Chapter V

SPATIAL DOMAIN APPLICATIONS OF PHASE CONJUGATE OPTICAL INTERACTIONS

5.1 Introduction

In this and the remaining chapters, we will discuss and analyze several applications of Phase Conjugate Optical interactions (PCO). As discussed in Chapter I, one can categorize potential applications to lie in three different domains: spatial, temporal, and spatial-temporal regimes. This chapter will focus upon the first category; that is, applications that exploit the spatial-mode features inherent in phase conjugate processes.

We will discuss first the ability of a phase conjugate system to compensate for various undesirable phase and/or polarization distortions in bulk media [1,2]. Next, the concept of image transmission through multimode guided structures, e.g., optical fibers, and the ability of PCO interactions to compensate for modal-dependent phase aberrations will be briefly reviewed [3,4].

Guided by the holographic analogs of degenerate four-wave mixing (DFWM) optical processes as discussed in Chapter III, we will investigate a class of coherent image processing techniques which can be realized in real time using DFWM. These techniques will include spatial convolution and correlation of optical fields (or intensities) with the associated matched filters (or Van der Lugt filters) [5], and pattern recognition schemes[6]. Finally, the application of DFWM as applied to the field of nonlinear optical microscopy will be discussed.

As discussed earlier, one may realize the above-mentioned applications using other classes of conjugators. However, DFWM and other backward-going conjugate schemes (see Sections 3.2 through 3.4) are a "natural" for the spatial domain type applications due to their large "spatial-frequency bandwidth" (i.e., $\sim 4\pi$ angular acceptance range). On the other hand, forward-going conjugators (see Section 3.2 and Appendix 3A) which suffer from phase matching constraints as well as from finite length-induced distortions may find limited use in certain spatial domain applications.

5.2 Correction of Phase Aberrations in the Bulk and in Multimode Waveguides

A major class of potential applications for phase conjugators lies in the area of phase aberration correction (or compensation). As was discussed and proved in Chapter II, the "time-reversed" fields generated by a phase conjugate mirror satisfy Maxwell's equations for waves propagating in a backward direction through various media. Hence, unwanted or undesirable phase distortions encountered by an electromagnetic wave as a result of propagation through an aberrating medium may be corrected or removed if the distorted wave is conjugated and retraverses the same (or similar) stationary medium. We recall from Chapter II that this technique can compensate for both spatial and polarization type aberrations, for a polarization type distortion is merely a special case of the more general tensor-dependent permittivity $\varepsilon(\vec{r})$. Applications of this scheme in bulk media include laser communication scenarios [1,2],

autotracking devices, as well as potential laser fusion schemes. The general characteristics of these applications are illustrated in Figure 5.1. Here target 2 is illuminated by the output of a low power laser oscillator 1 (e.g., pulsed). The reflected light 3 is collimated by lens 4 and traverses the amplifier 5 in reverse (away from the target). The distorted wave front 6 is incident on the conjugator 7, and is reflected as a conjugate wave 8. The wave retraverses the amplifier 5, emerging as a plane wave 9, which is focused on the target as a diffraction limited spot. If the conjugator possesses a nonlinear gain large enough so as to reproduce the same amplitude at the target (for example) upon each round trip, then the system can be capable of yielding a mode of laser oscillation. The conjugator and the target thus form a unique "resonator," bounding the aberrating (and/or amplifying) medium. In this mode of operation, no additional optical source is necessary to illuminate the target, as the system itself, via the oscillation modes, provides diffraction limited target illumination.

The nature of the "target" depends upon the specific application. For a laser communication system, the target could be a laser transmitter, with the phase conjugator regarded as being a laser transceiver. The conjugator thus forms a narrowband receiver/amplifier (recall from Section 3.3 that the forward-going wave is amplified), as well as being capable of encoding amplitude and/or phase (via the pump waves) modulated conjugate waves that propagate back to the transmitter. The high power amplifier (#5 in the Figure) could symbolically depict a turbulent atmosphere, and/or a laser amplifier. The conjugator would compensate

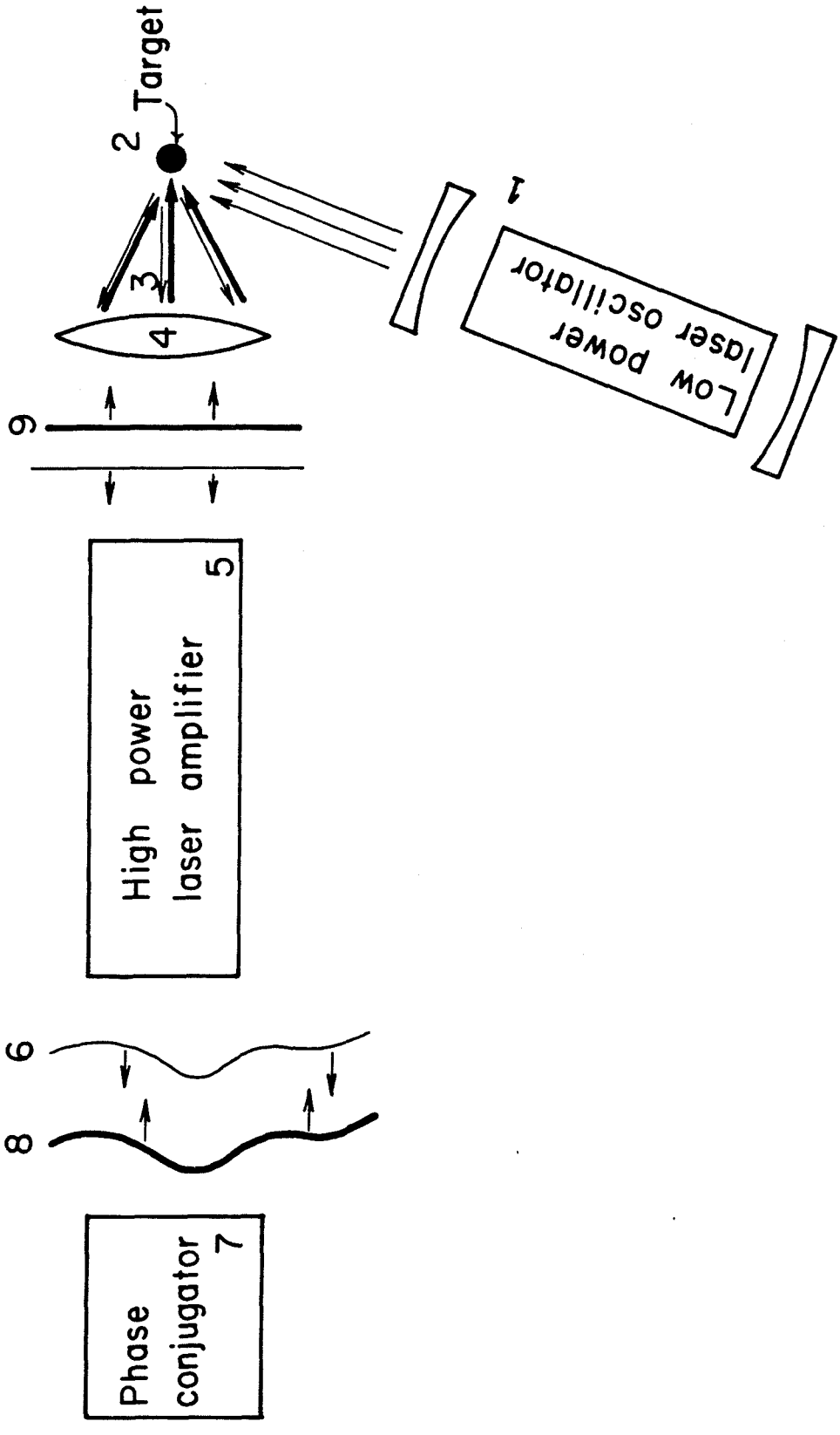

Fig. 5.1 A configuration designed to focus the output of a high power (e.g. pulsed) laser on a target.

for any phase distortions encountered during each round trip.

For the "autotracker" application, the target may be a moving object possessing a "glint." If the target's motion during a round trip time (i.e., twice the photon transit time between the target and the conjugator) spans a transverse distance (perpendicular to the optical axis) small compared to the spot size, then the system could "track" this moving target via constant illumination upon the glint. This illumination would be in the form of a diffraction limited laser beam focused onto the glint.

The scheme shown in Figure 5.1 may also be of use in potential laser fusion systems, with the target being a pellet (e.g., Deuterium). The distorting medium could be a series of laser amplifiers, with the conjugator obviating any phase aberrations. In this mode of operation, the system would be capable of optimally extracting the stored energy within the amplifiers in the form of a diffraction limited output beam incident upon the target.

We conclude the discussion of bulk media phase conjugator applications by recalling the discussion of Section 3.5, where a one-mirror assisted optical parametric oscillation mode was discussed. We postulated that by placing a four-wave mixer within an existing laser resonator, the intracavity laser fields could provide the required counter-propagating pump beams. Further, by placing an additional mirror in the vicinity of the conjugator (as in Figure 3.5) a preferred direction of a parametric oscillation would result along this axis if $|\kappa|L \geq \pi/4$. The laser output can thus be coupled out from the front surface of the conjugator, with a radius of curvature determined by the external mirror and its location.

A second class of spatial domain applications using phase conjugators involves the retrieval of pictorial information upon transmission through multimode fibers [3,4]. Consider a situation where one desires to transmit a two- or three-dimensional spatial image along a given length of a multimode optical fiber. Due to the fact that each confined waveguide mode propagates with a different phase velocity β (where $n_2 k \leq \beta \leq n_1 k$, n_1 and n_2 being the refractive index of the core and cladding, respectively; k is the wave number), there results an undesirable modification (i.e., distortion) of the resultant field [3,11]. However, since this phase aberration is well-defined in the sense that a similar fiber of equal length yields the same distortion, then the use of a phase conjugator at the midpoint of a given fiber channel, for example, with the conjugate signal directed to propagate along the second half of the fiber, would result in an effective cancellation of the phase distortion at the output end of the fiber. The generalization of this scheme to polarization scrambling and/or nonlinear (intensity-dependent) phase distortions follows directly from the discussion presented in Chapter II.

We note that all the above spatial domain applications are a direct consequence of the linearity of the phase conjugate interaction with respect to multiplanar spatial modes of the input (probe) field. The phase conjugator can thus be viewed as a device that compensates for spatial-mode dispersion encountered as a result of monochromatic field propagation through various media. In the next chapter, we will

show the ability of a phase conjugator to compensate for group-velocity dispersion encountered as a result of broadband (pulsed) field propagation through dispersive channels.

5.3 Real-Time Spatial Information Processing via Degenerate Four-Wave Mixing

It has been shown in Chapter III that degenerate four-wave mixing can be operationally associated with real-time holography. Guided by these analogies, one can easily envision a myriad of potential application areas using this nonlinear optical interaction. Specifically, one can replace most conventional coherent holographic image processors [6] with four-wave mixing elements. Thus, the many procedures required to realize conventional holographic devices--namely, the exposure, development, alignment, and reconstruction steps--can now be performed in real time, essentially instantaneously. Further, the finite grain size of most holographic recording materials (film emulsions, etc.) which can place constraints upon the resolving power in certain applications is essentially eliminated by the use of nonlinear optical devices. This follows, since the effective "grain size" of most nonlinear optical devices is the spacing between optical interaction sites, which is on the order of lattice constants for solids, and is $\rho^{-1/3}$ (ρ is the density) for liquids and vapors. Typical numbers are 10-100$\mathring{A}$ for solids and liquids, and 10$\mathring{A}$ to 1 μm for vapors (corresponding roughly to 1 Torr down to 10^{-2} μm of pressure, respectively.)

In this section we will show how a degenerate four-wave nonlinear optical interaction can be used to perform, essentially instantaneously, the operations of spatial convolution and correlation of spatially encoded optical fields. We note that various schemes which use other nonlinear optical interactions (viz., three-wave mixing) to realize these operations have been recently discussed [7]; these three-wave interactions suffer from the phase matching constraints discussed earlier and also from wavelength-dependent scaling factors.

Consider the nature of the resultant field produced as a result of the simultaneous mixing of three optical fields, all of radian frequency ω, incident upon a thin medium possessing a third-order nonlinear optical susceptibility, $\chi_{NL}^{(3)}$, centered at the common focal plane of two identical lenses (or mirrors) of focal length f. The geometry is illustrated in Figure 5.2. Each field is specified spatially at the front focal plane of its respective lens with the following amplitudes:

$$\begin{aligned} E_1 &= \tfrac{1}{2} A_1(x,y,z)\, e^{i(kz-\omega t)} + \text{c.c.} \\ E_2 &= \tfrac{1}{2} A_2(x,y,z)\, e^{-i(kz+\omega t)} + \text{c.c.} \\ E_4 &= \tfrac{1}{2} A_4(x,y,z)\, e^{i(kz-\omega t)} + \text{c.c.} \end{aligned} \qquad (5.3\text{-}1)$$

where $A_{1,4}(x,y,0) \equiv u_{1,4}(x,y)$, and $A_2(x,y,4f) \equiv u_2(x,y)$. Fields E_1 and E_2 are essentially counterpropagating, with E_4 being parallel to

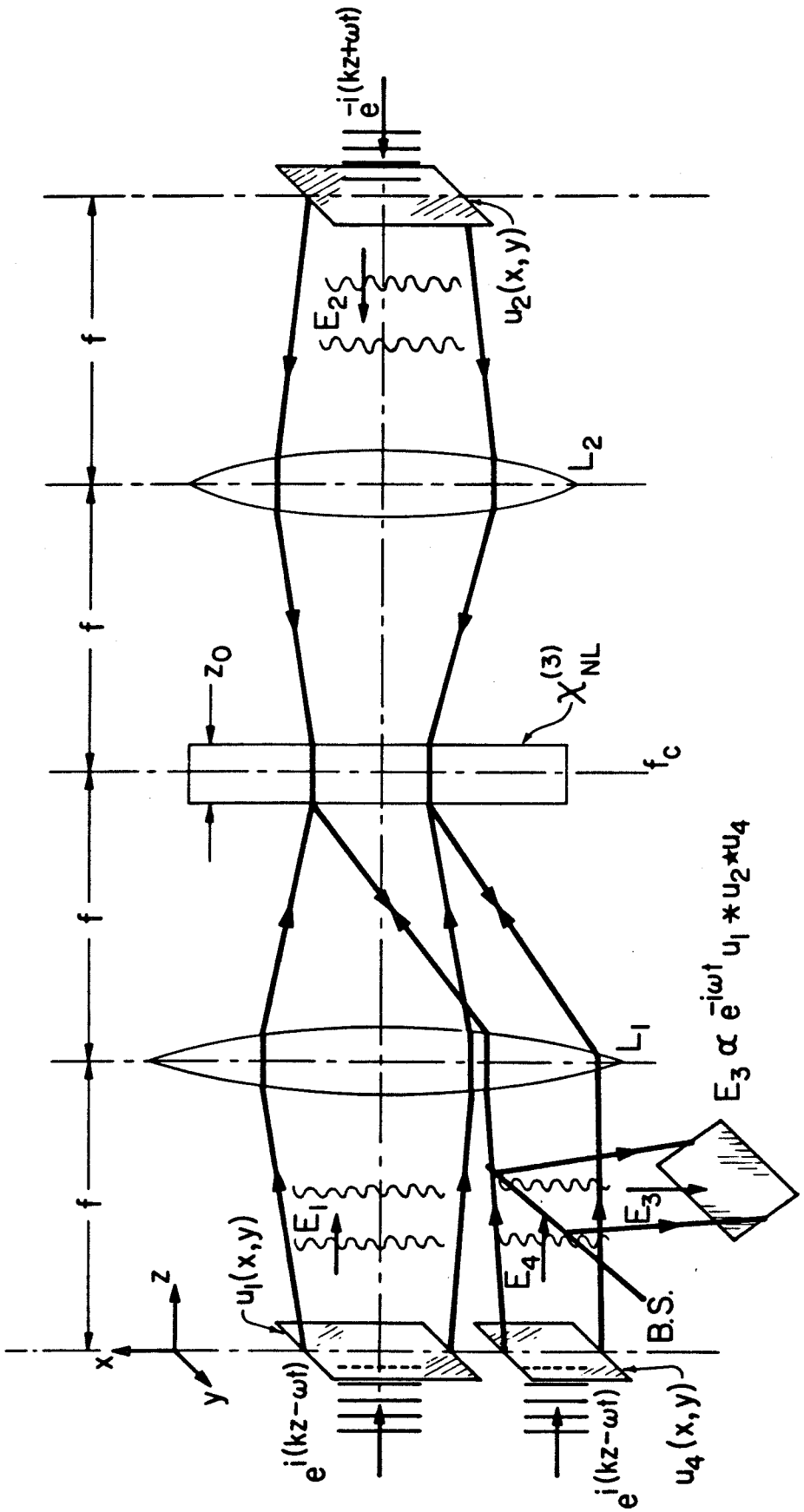

Fig. 5.2 Convolution/correlation geometry. All input optical fields are at radian frequency, ω. BS is a beam splitter necessary to view the desired output, E_3, which is evaluated at a plane located a distance f from the lens L_1.

these fields and separated either spatially [e.g., shifted by (x_s,y_s)] or via orthogonal polarizations. The u_i contain the input information to be convolved or correlated, which can, for example, be in the form of phase and/or amplitude transparencies. The u_i are assumed to be illuminated by unity amplitude plane waves, all of the same frequency ω.

We wish to evaluate the spatial amplitudes of A_1, A_2 and A_4^* in the region of the common focal plane, f_c as shown in the figure. We first make use of a familiar result of scalar diffraction theory, which relates the spatial amplitude of a given electromagnetic field $u(x,y,z)$ at a plane $z > 0$, given the initial distribution at the plane $z = 0$ $u(x,y)$. This result is [6]

$$u(x,y,z) = \frac{1}{i\lambda z} \exp(ikz) \exp\left[\frac{ik}{2z}(x^2+y^2)\right] \times \int_{-\infty}^{\infty}\int dx'dy'\, u(x',y') \exp\left[\frac{ik}{2z}(x'^2+y'^2)\right] \times \exp\left[\frac{-ik}{z}(xx'+yy')\right] \tag{5.3-2}$$

where the Fresnel approximation [6]

$$z^3 >> \frac{\pi}{4\lambda}\left[(x-x')^2 + (y-y')^2\right]^2_{max} \tag{5.3-3}$$

has been imposed and $k = 2\pi/\lambda$. We will see that this condition will place constraints upon the information-handling capacity of the system.

We next make use of the transmission function of a thin lens (in the paraxial approximation) which relates the field distribution after the lens to the input distribution, and is given by [6]

$$h = e^{ikn\Delta}\, e^{-\frac{ik}{2f}(x^2+y^2)} \tag{5.3-4}$$

where the linear index of refraction, maximum thickness, and focal length of the lens are denoted by n, Δ, and f, respectively.

After propagating through lens L_1, A_1 has the following form (in the Fresnel approximation) in the region of the focal plane (f_c):

$$A_1(x,y;\, f \le z \le 3f) = \frac{e^{ikn\Delta}\, e^{ikz}}{i\lambda f} \times \mathcal{F}\left[u_1(x',y')e^{\frac{ik}{2f}(2-\frac{z}{f})(x'^2+y'^2)}\right]_{f_x = \frac{x}{\lambda f};\ f_y = \frac{y}{\lambda f}} \tag{5.3-5}$$

In (5.3-5), $\mathcal{F}[a] \equiv \tilde{a}$ is the spatial Fourier transform of a, given by

$$\mathcal{F}[a] = \int_{-\infty}^{\infty}\int dx'dy'\; a(x',y')\, \exp\left[-2\pi i(f_x x' + f_y y')\right] \tag{5.3-6}$$

where f_x and f_y, the transform variables, are the spatial frequencies along the x and y axes, respectively.

Similarly, the complex amplitude of E_2 has the form (after propagating through lens L_2)

$$A_2(x,y;\, f \le z \le 3f) = \frac{e^{ikn\Delta}\, e^{ik(4f-z)}}{i\lambda f}$$

$$\times\ \mathcal{F}\left[u_2(x',y')e^{-\frac{ik}{2f}(2-\frac{z}{f})(x'^2+y'^2)}\right]_{f_x = \frac{x}{\lambda f};\ f_y = \frac{y}{\lambda f}} \qquad (5.3\text{-}7)$$

Anticipating the mixing process of interest, we express the complex conjugate amplitude of E_4 (after propagating through lens L_1) as

$$A_4^*(x,y;\, f \le z \le 3f) = \frac{e^{-ikn\Delta}\, e^{-ikz}}{-i\lambda f}$$

$$\times \left\{\mathcal{F}\left[u_4(x',y')e^{\frac{ik}{2f}(2-\frac{z}{f})(x'^2+y'^2)}\right]_{f_x = \frac{x}{\lambda f};\ f_y = \frac{y}{\lambda f}}\right\}^* \qquad (5.3\text{-}8)$$

The fields A_i in (5.3-5), (5.3-7), and (5.3-8) become directly proportional to the Fourier transforms of their respective u_i if the terms inside the square brackets in the exponents can be neglected. This happens when

$$|z-2f| \ll \frac{2f^2\lambda}{r_{max}^2} \qquad (5.3\text{-}9)$$

where r_{max} is the maximum spatial extent of the set $\{u_i\}$.

We now place a medium centered at the focal plane f_c of thickness z_o [satisfying the constraint (5.3-9)] which possesses a third order nonlinear optical susceptibility, $\chi_{NL}^{(3)}$. Without loss of generality, we assume a transparent, lossless medium, and neglect linear refractive effects.

The complex amplitude of the nonlinear polarization at $\omega = \omega+\omega-\omega$ generated by the mixing of the three waves is, according to equation (3.3-2)

$$P_{NL_i} = \chi^{(3)}_{ijk\ell}\, A_{1_j} A_{2_k} A^*_{4_\ell} \tag{5.3-10}$$

where repeated indices are summed over the field polarizations. The resultant field, E_3, which satisfies both photon energy and momentum, is given by [6,8]

$$A_3(\vec{x}) = -\frac{4\pi\omega^2}{c^2}\int P_{NL}(\vec{x}')\, G(\vec{x},\vec{x}')\, d^3\vec{x}' \tag{5.3-11}$$

where

$$G(\vec{x},\vec{x}') = -\frac{1}{4\pi}\frac{e^{ikr}}{r} \tag{5.3-12}$$

is the Green's function that satisfies the wave equation. Using (5.3-5), (5.3-7), and (5.3-8) in (5.3-10) and (5.3-11), as well as condition (5.3-9), integrating over the volume of the nonlinear medium, and "propagating" back to $z = 0$ through lens L_1, we get

$$A_3(x_o,y_o,0) = -i\,\frac{2\pi\omega}{c}\,\frac{z_o}{\lambda^2 f^2}\,\exp[2ik(n\Delta+2f)]$$
$$\mathcal{F}\left[\tilde{u}_1(f_x,f_y)\,\tilde{u}_2(f_x,f_y)\,\tilde{u}^*_4(f_x,f_y)\chi^{(3)}_{NL}(x,y)\right]_{f_x=\frac{x_o}{\lambda f};\ f_y=\frac{y_o}{\lambda f}} \tag{5.3-13}$$

where $\chi^{(3)}_{NL}(x,y)$ is the proper tensor element in (5.3-10) connecting fields 1, 2, 3, and 4.

If $\chi^{(3)}_{NL}$ is spatially homogeneous, the output field can be written in the form

$$A_3(x_o,y_o,0) = \psi u_1(-x,-y) * u_2(-x,-y) \bigstar u_4(-x,-y) \qquad (5.3\text{-}14)$$

where

$$\psi = -i \frac{2\pi\omega}{c} \frac{z_o \chi^{(3)}_{NL}}{\lambda^2 f^2} \exp[2ik(n\Delta + 2f)]$$

In (5.3-14) the symbols * and $\bigstar$ denote the standard operations of convolution and correlation, respectively [6]. The convolution (*) and correlation ($\bigstar$) operations are defined by

$$a * b \equiv \int_{-\infty}^{\infty}\int a(\xi,\eta)\ b(x-\xi,y-\eta)d\xi d\eta \qquad (5.3\text{-}15a)$$

and

$$a \bigstar b \equiv \int_{-\infty}^{\infty}\int a(\xi,\eta)\ b^*(\xi-x,\eta-y)\ d\xi\ d\eta \qquad (5.3\text{-}15b)$$

respectively.

Equation (5.3-14) is our primary result. We obtain the spatial convolution of u_1 and u_2 by taking u_4 as a point source. This leads to

$$A_3(x_o,y_o,0) \simeq \psi\ u_1 * u_2 \qquad (5.3\text{-}16)$$

Similarly, the correlation operation is performed by placing information on fields u_1 and u_4, with a point source for u_2 yielding

$$A_3(x_o,y_o,0) \simeq \psi\ u_1 \bigstar u_4 \qquad (5.3\text{-}17)$$

where the u_i in (5.3-16) and (5.3-17) are the inverted images of the input fields [c.f., (5.3-14)].

The correlation of u_2 and u_4 is similarly obtained by using a point source for u_1. For Gaussian beams (which will be discussed below), the finite spot size in the focal plane (f_c) of the "point source" input will

ultimately limit the spatial frequency bandwidth of the above operations.

We can now appreciate the advantage of using a degenerate four-wave mixing approach to real-time operations. The third field (which corresponds to the point source input mentioned above) provides an optical carrier frequency upon which the convolution or correlation information is placed. No frequency scaling factors are present (c.f., reference 7), the entire system requires only a single frequency source, and within the Fresnel approximation, the phase matching condition is satisfied. Finally, the "degenerate" operations of autoconvolution and autocorrelation can be performed with a single optical frequency.

The approximations used in the above discussion place upper limits on both the resolution (or spatial frequency bandwidth), and the efficiency (or nonlinear gain) of the interaction. The Fresnel approximation is related to f_{max}, the greatest spatial frequency present, by

$$f_{max} < \left(\frac{4}{\pi\lambda^3 f}\right)^{1/4} \qquad (5.3\text{-}18)$$

This same approximation also places an upper limit on the input field spot size, which is given by

$$d < \left(\frac{4\lambda f^3}{\pi}\right)^{1/4} \qquad (5.3\text{-}19)$$

Hence, the maximum number of resolution elements possible is derivable through (5.3-18) and (5.3-19), yielding

$$N_{max} = \frac{16f}{\pi\lambda} \qquad (5.3\text{-}20)$$

Using values of 10 cm and 0.5μ for f and λ, respectively, leads to a value of $10^3 cm^{-1}$ for f_{max}, which corresponds to a grid of 1000 x 1000

resolution elements. Therefore, since the phase matching condition is satisfied for all the field momentum components in the Fresnel approximation, this technique can be useful for complex spatial information processing.

The second constraint, (5.3-9), yields an upper limit to the nonlinear gain of the interaction. From (5.3-9) we obtain

$$z_o << b_o = \frac{2\pi^2 \omega_o^2}{\lambda} \tag{5.3-21}$$

where ω_o is the spot size in the focal plane. For Gaussian beams, the value of b_o corresponds to 2π times the confocal parameter [9]. The spot size in the focal plane of the Gaussian "point source" (or the field corresponding to the optical carrier frequency) determines the maximum spatial frequency of the convolution or correlation operation. It can be shown that the number of resolution elements is

$$N \simeq (d_1/d_2)^2 \tag{5.3-22}$$

where d_1 is the spatial extent of the input field, and d_2 is the input aperture size of Gaussian "point source," assuming both are satisfying the Fresnel approximation limitation upon the spot size (5.3-19). It follows that for a given input power and choice of lens focal length, the output power with information present in the two input fields is related to that for no information present by

$$P_{out_{info}} \simeq P_{out_{no\ info}} \Big/ N \tag{5.3-23}$$

Thus, we see that there is a tradeoff between the spatial bandwidth product, N, and the output power (or nonlinear gain) of the interaction. For the lens and optical wavelength used above, we find for CS_2 (using a value of $\chi^{(3)}_{NL} \sim 1.8 \times 10^{-12}$ e.s.u.) that $P_{out_{info}} \sim$ 200 watts for $P_{1,2,4} \sim 0.5$ MW, with $d_1 = 1$ cm, and $d_2 = 0.01$ cm. This corresponds to $N \sim 10^4$. Other media such as $Bi_{12}SiO_{20}$, ruby, resonantly enhanced vapors (e.g., Na), etc., should provide adequate nonlinear efficiencies to realize the above spatial operations (and resolution elements) with modest input intensities.

We next give a brief discussion regarding a potential source of nonlinearly-induced spatial distortions. Recall that from Section 3.3, the output (conjugate) amplitude scales as

$$A_3(0) \propto A_4^*(0) \tan(|\kappa|L)$$

$$\propto A_4^*(0) \left[\chi^{(3)}_{NL} A_1 A_2 L + \frac{1}{3}(\chi^{(3)}_{NL} A_1 A_2 L)^3 + \frac{2}{15}(\chi^{(3)}_{NL} A_1 A_2 L)^5 + \cdots\right] \qquad (5.3\text{-}24)$$

However, since the desired convolution or correlation operations necessarily require an output field given by (5.3-13), the small angle approximation to $\tan(|\kappa|L)$ must be valid. Hence, as the nonlinear gain, $|\kappa|L$, becomes larger, and the higher order terms contained in the power series expansion of (5.3-24) become appreciable, distortions in the desired output operations result. We are thus limited to a nonlinear interaction where the amplitude changes for all the input fields are minimal (which is satisfied in the above numerical example).

We note that aside from the constraint given above, the previously mentioned limitations imposed by the Fresnel approximation apply equally to conventional coherent holographic image processors [5,6] having the same geometry as shown in Figure 5.2.

In conclusion, we have shown that a degenerate four-wave mixing interaction in the common focal volume of a two-lens system can lead (for small nonlinear gains) to the operations of spatial convolution and correlation of optically encoded fields. This interaction operationally corresponds to a real-time holographic analog of a Van der Lugt filter system [5]. The extension of these concepts to real-time matched filters, pattern recognition [6], and other forms of image processing follows directly. The implementation of this scheme to integrated optics using geodesic lenses [10] or graded fibers [11] is a viable possibility, considering the increased intensities present in optical waveguides.

5.4 Nonlinear Microscopy via Real-Time Holography

We conclude this chapter with a discussion of the implementation of the geometry discussed in the previous section for use as a nonlinear optical microscope [12] . The technique of nonlinear microscopy basically involves the mapping (or probing) of a material for spatial regions having varying nonlinear optical coefficients. This diagnostic procedure has potential applications in the study of optical damage of materials and defect analyses, for example. Due to the specific nonlinear mechanism of a particular solid, these effects may be more strongly manifested in spatial variations of the nonlinear optical coefficient as compared to similar variations of the linear refractive index.

Thus far, the literature [12] has revealed that such spatial variations of nonlinear coefficients have been investigated only for the case of the second-order susceptibility, $\chi^{(2)}_{ijk}$. In their experiments, Hellwarth and Christensen [12] employed the process of second harmonic generation to investigate crystals of ZnSe, CdTe, CdS, and GaAs. In the discussion that follows, we present a brief analysis to investigate the spatial properties of the nonlinear index of refraction, n_2 (recall that $n_2 = \frac{2\pi}{n_o} \chi^{(3)}_{NL}$). Knowledge of the spatial frequency spectrum of n_2 may be relevant in analyzing optical damage mechanisms. For example, the presence of large n_2 spatial domains may reduce the local threshold for potentially catastrophic optical damage mechanisms, such as self-focusing, etc.

Consider a geometry identical to that shown in Figure 5.2, where the nonlinear medium (located at the common focal plane of the two-lens system) has a spatially dependent $\chi^{(3)}_{NL}$. If we now assume that all three input fields u_i are "point sources," then the output field is, according to (5.3-13),

$$A_3(x_o,y_o,0) \propto \mathcal{F}[\chi^{(3)}_{NL}(x,y)]_{f_x = \frac{x_o}{\lambda f};\ f_y = \frac{y_o}{\lambda f}} \qquad (5.4\text{-}1)$$

where we have further assumed that the system meets all the constraints as discussed in the last section.

We thus have an output field that maps the spatial periodicities of the nonlinear optical components in a material. Hence the nonlinear

structure of a medium (which, for example, may be approximately homogeneous in its linear susceptibility) can be revealed.

In conclusion, the application of real-time image processing can be utilized both as a material probe and as a data processing device. The use of four-wave nonlinear mixing to real-time convolution and correlation has been proposed and analyzed.

Chapter V - References

1. V. Wang and C. R. Giuliano, "Correction of phase aberrations via stimulated Brillouin scattering," 1977 IEEE/OSA Conference on Laser Engineering and Applications, Washington, D.C., June 1977, paper 17.6; also Opt. Lett. 2, 4 (1978).

2. A. Yariv, "Compensation of atmospheric degradation of optical beam transmission by nonlinear optical mixing," Opt. Commun. 21, 49 (1977).

3. A. Yariv, "Three-dimensional pictorial transmission in optical fibers," Appl. Phys. Lett. 28, 88 (1976).

4. A. Yariv, "Phase conjugate optics and real-time holography," IEEE J. Quant. Electron. QE-14, 650 (1978).

5. A. B. Van der Lugt, "Signal detection by complex spatial filtering," IEEE Trans. Inform. Theory IT-10, 2 (1964).

6. J. W. Goodman, Introduction to Fourier Optics (McGraw-Hill, New York, 1968).

7. R. A. Eremeeva, V. A. Kudryashov, I. N. Matrieev, T. G. Usacheva, and A. I. Chekemenev, "Convolution and correlation of optical signals by nonlinear optics techniques," Sov. J. Quant. Electron. 5, 1429 (1976).

8. J. D. Jackson, Classical Electrodynamics, 2nd ed. (Wiley, New York, 1975), Ch. 6.

9. A. Yariv, Quantum Electronics, 2nd ed. (Wiley, New York, 1975).

10. See, for example, B. Chen, E. Marom, and A. Lee, "Geodesic lenses in single-mode $LiNbO_3$ waveguides," Appl. Phys. Lett. 31, 263 (1977), and references therein.

11. A. Yariv, "On transmission and recovery of three-dimensional image information in optical waveguides," J. Opt. Soc. Amer. 66, 301 (1976).

12. R. W. Hellwarth and P. Christensen, "A nonlinear optical microscopic examination of structure in polycrystalline ZnSe," Opt. Commun. 12,

318 (1974); R. W. Hellwarth and P. Christensen, "Nonlinear optical microscope using second harmonic generation," Appl. Opt. 14, 247 (1975).

Chapter VI

TEMPORAL DOMAIN APPLICATIONS OF PHASE CONJUGATE OPTICAL INTERACTIONS

6.1 Introduction

In this chapter we will consider several potential applications of phase conjugate optics (PCO) that involve the "temporal-frequency" (as opposed to the spatial frequency) aspects of the interaction. That is, we wish to investigate the properties of phase conjugators when the probe wave either (i) differs fractionally in optical frequency from the pump waves, or (ii) contains a broad frequency spectrum. In the former case, which we call "nearly degenerate" four-wave mixing, all the participating waves are monochromatic. However, due to the frequency differences of the fields, phase matching constraints now affect the bandwidth of the system. The result of this constraint makes it possible for the "phase conjugate mirror" (PCM) to act as a narrow optical band-pass filter, even if the third order nonlinear optical susceptibility which couples the fields is nondispersive. In the first part of this chapter we will show this fact explicitly. Using the coupled-mode formalism, a frequency-dependent PCM reflectivity will be derived. The resultant "filter" bandwidth will be shown to depend not only upon the phase mismatch, but also upon the nonlinear gain of the system. This filter formalism will be useful in evaluating the PCO application that follows, as well as deriving the modes of optical cavities bounded by a PCM (see next chapter).

Next, we will investigate the broad spectrum case [(ii)] mentioned above; that is, the properties of a PCM, when the input probe beam possesses

a broad frequency spectrum, or equivalently, it is pulsed. We will show that if this pulse has been temporally broadened due to propagation through a dispersive channel (via group velocity dispersion, for example) the PCM is capable of essentially "renarrowing" the pulse as it subsequently propagates (after conjugation) through a second, equivalent channel. The analysis will use the results of the nearly-degenerate filter function described above. The result of the pulse renarrowing is that one may increase the operating bandwidth (or data rate) of such a dispersive channel, limited ultimately by the filter bandpass discussed above. In the process of this discussion, we will also consider certain causal aspects with respect to temporal sequencing of information incident upon the PCM. The ability of other classes of conjugators to yield group velocity dispersion compensation, along with their potential bandwidth constraints, will be discussed in an appendix.

We will conclude this chapter with a rather interesting application of PCO in the field of laser spectroscopy: that of probing the so-called two-photon coherent state of a given atomic (or molecular) species. The concept of a two-photon coherent state was introduced in Chapter III, when we discussed the origin of $\chi_{NL}^{(3)}$ in a two-photon allowed transition. There, we considered monochromatic fields, thus evaluating the steady-state aspects of such a system. In the present chapter, we generalize the analysis to consider a sequence of optical pulses, which "prepare" and subsequently "scatter" off this two-photon coherent state. We will show that it is possible to perform Doppler-free laser spectroscopy to study the various relaxation times of the system (i.e., T_1 and T_2).

Additionally, by examining the so-called optical free-induction decay signal of the two-photon coherent state, one can determine the degree of anharmonicity of a nearly harmonic potential in the time domain, a technique recently referred to as "α-beat spectroscopy." The analysis will utilize a time-dependent, density matrix perturbation approach.

6.2 Narrow Optical Bandpass Filter via Nearly Degenerate Four-Wave Mixing

In Chapter III, we have shown that the process of degenerate four-wave mixing is capable of generating phase conjugate (or time-reversed) and amplified fields. These effects have been verified experimentally as described in Chapter IV. Further, as discussed in Chapter III, this four-wave nonlinear interaction has been shown to be operationally analogous to real-time holography. In these cases, all the interacting fields were taken to be of the same optical frequency. In this section we show that this interaction can be used to obtain narrow optical bandpass filtering.

The "filter" characteristics to be presented here (specifically, the frequency-dependent phase and amplitude dependence of the nonlinear reflection coefficient) are relevant to analyzing problems such as broadband (nondegenerate) signal inputs to phase conjugators. Examples include channel dispersion compensation (see next section), and to deducing the modal features of optical resonators where one (or both) of the cavity mirrors is replaced by a phase conjugate mirror (see next chapter).

The filter effect in the small nonlinear gain limit has been independently proposed [1], and experimental evidence of the filter bandpass (also in the small nonlinear gain regime) has been recently verified [2]. In principle, any nonlinear interaction can be utilized to perform filtering functions due to phase matching constraints. However, in general, these interactions require a specific angle of incidence of the field to be filtered, and yield an output wavelength differing from its input. Using a nearly degenerate four-wave mixing approach provides for a large field of view for the input field and an output field of essentially the same wavelength. In addition, the conjugate nature of the output field can be used to spatially filter out various noise fields, thus increasing the signal-to-noise performance of the filter. The degree of spatial filtering and detection geometry will, however, limit the field-of-view of the filter. Being essentially an active device, the filter will be capable of yielding an amplified output bandpass. As the filter gain increases, its bandpass will be shown to become sharper, with a concomitant decrease in the passband sidelobe structure. Finally, physical analogs with real-time holographic diffraction gratings will be shown to be consistent with the resolving power of the filter.

We assume the interaction to take place in a nondispersive, lossless medium. Consider the frequency dependence of the amplitude of a field E_3 generated as a result of a nonlinear interaction involving the simultaneous incidence of two intense counterpropagating pump fields E_1 and E_2 of frequency ω, upon a medium possessing a third-order nonlinear

optical susceptibility $\chi_{NL}^{(3)}$. Also incident (simultaneously) upon the medium is a third weak field E_4 of frequency $\omega + \delta$, $[(\delta/\omega) << 1]$, propagating along an arbitrary direction. The geometry is shown in Figure 6.1. The fields, which we assume to be monochromatic plane waves, are taken as

$$E_i(\vec{r},t) = \frac{1}{2} A_i(r_i) \exp[i(\omega_i t - \vec{k}_i \cdot \vec{r})] + c.c. \qquad (6.2\text{-}1)$$

where r_i is the distance along $\vec{k}_i$. Without loss of generality, we assume that $\chi_{NL}^{(3)}$ is polarization, frequency, and spatially (i.e., homogeneous and isotropic) invariant. The nonlinear polarization coupling fields A_3 and A_4 is given by

$$P_{NL}^{(\omega_3 = \omega - \delta)} = \frac{1}{2} \chi_{NL}^{(3)} A_1 A_2 A_4^* \, e^{i\{[\omega + \omega - (\omega + \delta)]t - [\vec{k}_1 + \vec{k}_2 - \vec{k}_4] \cdot \vec{r}\}} + c.c. \qquad (6.2\text{-}2)$$

Since $\vec{k}_1 + \vec{k}_2 = 0$, the resultant field that minimizes the phase mismatch will propagate along a direction opposite that of A_4 as shown in Figure 6.1. Forming a similar nonlinear polarization at frequency ω_4 and following the procedure outlined in Section 3.3 results in the following set of coupled mode equations:

$$\begin{aligned} \frac{dA_3}{dz} &= i \kappa_3^* A_4^* e^{i\Delta kz} \\ \frac{dA_4^*}{dz} &= i \kappa_4 A_3 e^{-i\Delta kz} \end{aligned} \qquad (6.2\text{-}3)$$

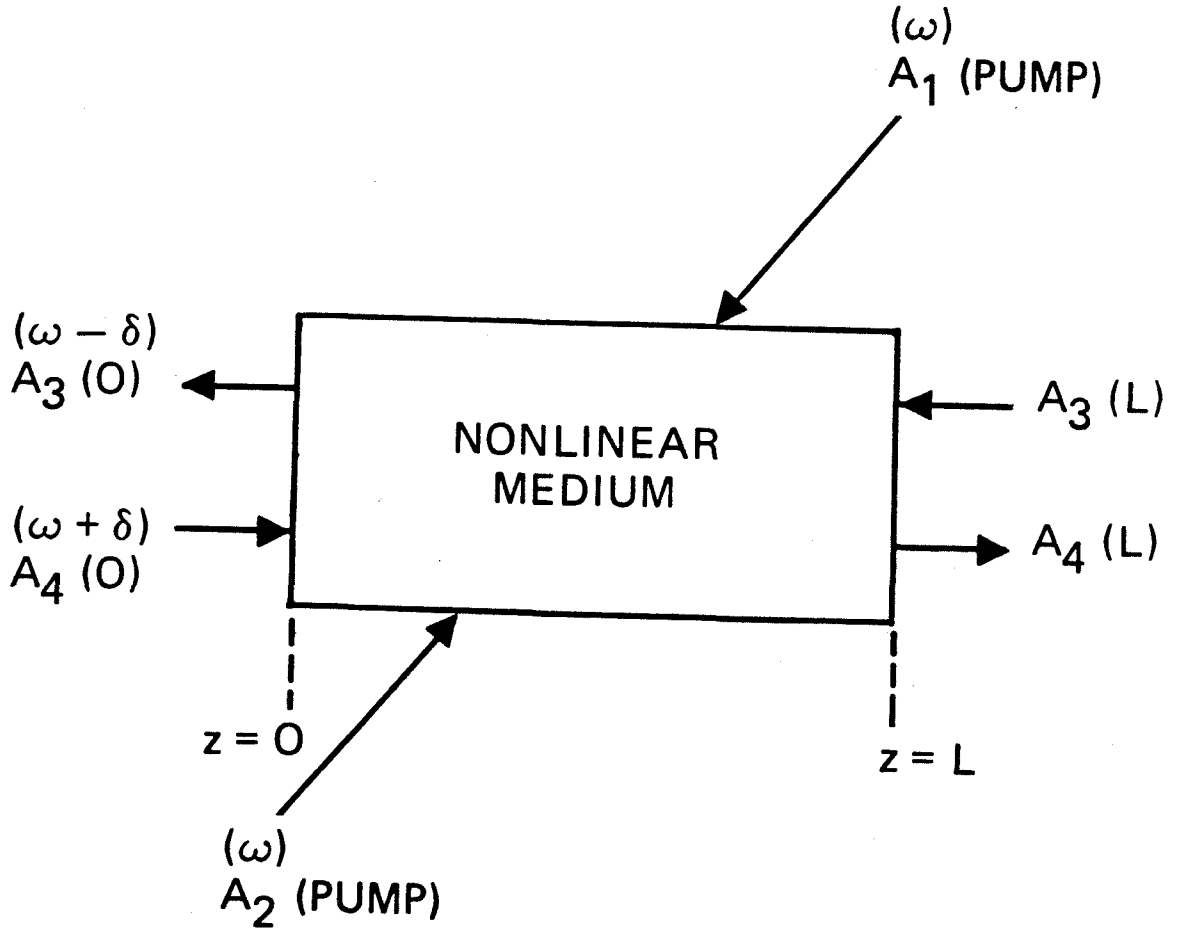

Fig. 6.1 Nearly degenerate four-wave mixing geometry. The pump waves (at frequency ω) are assumed nondepleted. The probe field A_4 is at frequency ω+δ.

where the complex coupling coefficient is given by $\kappa_\ell^* = 2\pi\omega_\ell \chi_{NL}^{(3)} A_1 A_2/nc$ and the phase mismatch is

$$|\Delta k| = 2n\pi(|\Delta\lambda|/\lambda^2) = 2n\delta/c \qquad (6.2\text{-}4)$$

Note that $|\Delta\lambda|$ is the wavelength difference between the fields A_3 and A_4. In arriving at equation (6.2-3) we assumed that the pump fields ($A_{1,2}$) were nondepleted and used the adiabatic approximation, $|d^2A_i/dz^2| \ll |k_i dA_i/dz|$.

The solutions to equation (6.2-3) using the boundary conditions of $A_3(z=L) \equiv A_3(L)$ and $A_4(z=0) \equiv A_4(0)$ are

$$A_3(z) = \frac{e^{i\Delta kz/2}}{D}\left\{e^{-i\Delta kL/2}\left[\beta\cos(\beta z) - \frac{i\Delta k}{2}\sin(\beta z)\right]A_3(L) + i\kappa_3^*\sin(\beta(z-L))\,A_4^*(0)\right\}$$

$$A_4^*(z) = \frac{e^{-i\Delta kz/2}}{D}\left\{i\kappa_4 e^{-i\Delta kL/2}\sin(\beta z)\,A_3(L) + \left[\beta\cos(\beta(z-L)) + \frac{i\Delta k}{2}\sin(\beta(z-L))\right]A_4^*(0)\right\}$$

where $D \equiv \beta\cos(\beta L) - (i\Delta k/2)\sin(\beta L)$, and $\beta \equiv [\kappa_3^*\kappa_4 + (\Delta k/2)^2]^{1/2}$ (6.2-5)

For the filter application, we assume that $A_3(L) = 0$, with only a single input at $z = 0$. In this case, the reflected wave at the input plane ($z = 0$) becomes

$$A_3(0) = \frac{-i\kappa_3^*\tan(\beta L)\,A_4^*(0)}{\beta - \frac{i\Delta k}{2}\tan(\beta L)} \qquad (6.2\text{-}6)$$

We can now appreciate several filter characteristics of the four-wave interaction. First, $A_3(0) \propto A_4^*(0)$, implying the near (since $\Delta k \neq 0$) time-reversed nature of the filter output. Hence, through

spatial filtering, the signal-to-noise ratio of the filter can be improved. For example, passing the input signal (to be filtered) through various optical elements (spatial filters, lens, etc.) will result in a time-reversed, filtered field; in contrast, undesirable noise terms (e.g., Rayleigh-scattered fields) will be minimized on passage through the given optical train. Second, the wave $A_3(0)$ can be greater in amplitude than the input field (i.e., amplification) for the proper range of κ_ℓ and Δk. Also, from equation (6.2-2) we note that the output frequency is downshifted by the same amount as the input frequency is upshifted with respect to the pump wavelength, and vice versa.

There are several useful limits that can be imposed on equation (6.2-5) to verify its physical nature. If, for example, we let $\Delta k \to 0$, the resultant expressions for $A_3(z)$ and $A_4^*(z)$ approach those of Section 3.3, equation (3.3-11), where a degenerate mixing case was considered. Another useful limit is that of weak nonlinear coupling, i.e., $|\kappa_\ell/\Delta k| \to 0$. In this case, the power reflection coefficient, defined as

$$R \equiv \left|\frac{A_3(0)}{A_4(0)}\right|^2 \tag{6.2-7}$$

becomes

$$R \to |\kappa L|^2 \left\{\frac{\sin(\frac{\Delta kL}{2})}{(\frac{\Delta kL}{2})}\right\}^2 \tag{6.2-8}$$

In equation (6.2-8) and what follows, we set $\kappa_3 \simeq \kappa_4 \equiv \kappa$, since $\delta/\omega << 1$. We note that the $\text{sinc}^2(x)$ dependence of equation (6.2-8) is a typical result of coherent, phase-mismatched, nondepleted interactions [3]. This result can be obtained directly by assuming in equation

(6.2-3) that $dA_4^*/dz = 0$ (i.e., weak perturbation of the input fields) and simply integrating the remaining differential equation for $A_3(z)$. We note that the filter character in this limit has recently been verified experimentally [2]. The expression in equation (6.2-8) is also consistent with that expected of a real-time holographic analog of the four-wave interaction [4]. The nonlinear mixing process can be viewed as forming and illuminating a real-time diffraction grating. According to equation (6.2-8), phase matching occurs when $(\Delta kL/2) \lesssim \pi$. Using equation (6.2-4), this constraint implies that the wavelength resolution of the interaction goes as $(\Delta\lambda/\lambda) \lesssim (\lambda/L)$. This result is consistent with that of the resolving power of a grating [5] $(\Delta\lambda/\lambda) \sim (1/mN)$, where m is the order of the grating and N is the number of lines illuminated. Setting $m = 1$, corresponding to the first order and realizing that in the nonlinear medium the maximum path-length difference (MPLD) is 2L, where the resolving power is, in general [6] $\Delta\lambda/\lambda \sim \lambda/\text{MPLD}$, verifies the analogy (recall that the MPLD for a grating is $mN\lambda$). The holographic analog only holds for $m = 1$, since higher orders in the nonlinear case are phase mismatched.

The filter-bandpass characteristic is obtained by using equation (6.2-7), yielding

$$R = \frac{|\kappa L|^2 \tan^2(\beta L)}{|\kappa L|^2 + \left(\frac{\Delta kL}{2}\right)^2 \sec^2(\beta L)} \qquad (6.2\text{-}9)$$

Using (6.2-9) we plot in Figure 6.2 the power-reflection coefficient R versus a normalized wavelength-detuning parameter ψ for several values of the nonlinear gain $|\kappa|L$. By definition, $\psi = [(\Delta\lambda/2)(2nL/\lambda^2)]$,

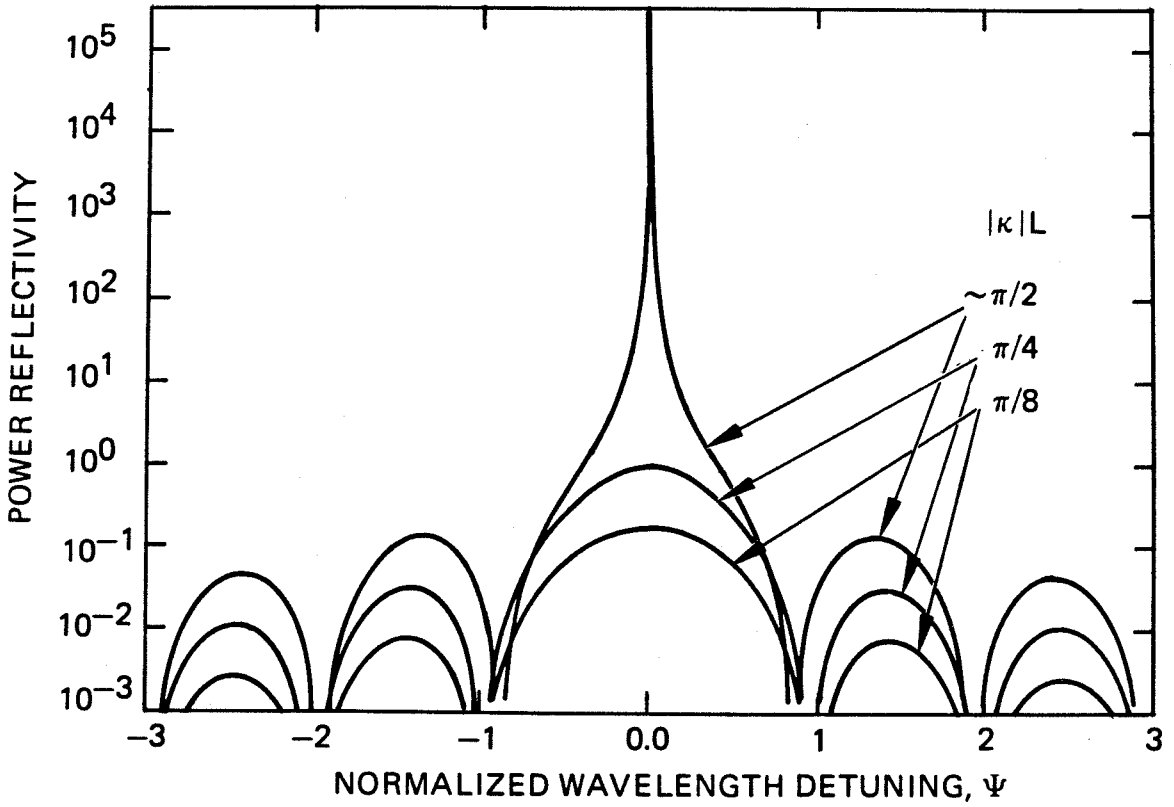

Fig. 6.2 Power reflectivity R versus normalized wavelength detuning ψ for several values of the nonlinear gain $|\kappa|L$. For the example given in the text, unity along the abscissa corresponds to $\Delta\lambda/2 = 0.0772\text{Å}$, or $\Delta\nu = 9.26$ GHz. $\psi = [(\Delta\lambda/2)(2nL/\lambda^2)]$.

which is also equal to the phase mismatch ΔkL divided by 2π. In the wavelength detuning parameter, $\Delta\lambda/2$ corresponds to the difference in wavelength of the probe field (A_4) relative to the pump fields ($A_{1,2}$). For an interaction length L of 1 cm, a wavelength λ of 0.5 μm, and a linear index of refraction n of 1.62 (that of CS_2), a value of unity in Figure 6.2 corresponds to a wavelength detuning $\Delta\lambda/2$ of 0.0772 $\mathring{A}$ or 9.26 GHz. We note that the $\text{sinc}^2(x)$ nature of the response holds only in the limit of weak nonlinear coupling (i.e., $|\kappa/\Delta k| << 1$). As $|\kappa|L$ increases, the bandpass becomes more sharply peaked, with the zeros of the response occurring at decreasing values of the frequency offset. This follows from the fact that the amplitude of the output wave increases with $|\kappa|L$ and because zeros of the tangent in equation (6.2-9) occur at smaller values of $(\Delta kL)/2$ as $|\kappa|L$ increases. The filter is seen to exhibit a power-reflection coefficient exceeding unity as $|\kappa|L > \pi/4$ over regions of the bandpass.

The wavelength response of the filter becomes apparent if we recast the family of curves of the previous figure normalized to unit power reflectivity, as shown in Figure 6.3. Several prominent features are to be noted. First, as $|\kappa|L$ increases, the bandwidth dramatically decreases. Second, the side-lobe structure of the filter also decreases with increasing nonlinear gain, yielding a sharper, better defined, and amplified bandpass. Physically, these features follow if we recognize that the filter is analogous to a real-time distributed Bragg-reflecting resonator with an internal gain medium. Since the finesse of a resonator increases as we add gain to the cavity, a sharper response (or Q) results [7]. We see that, as the oscillation

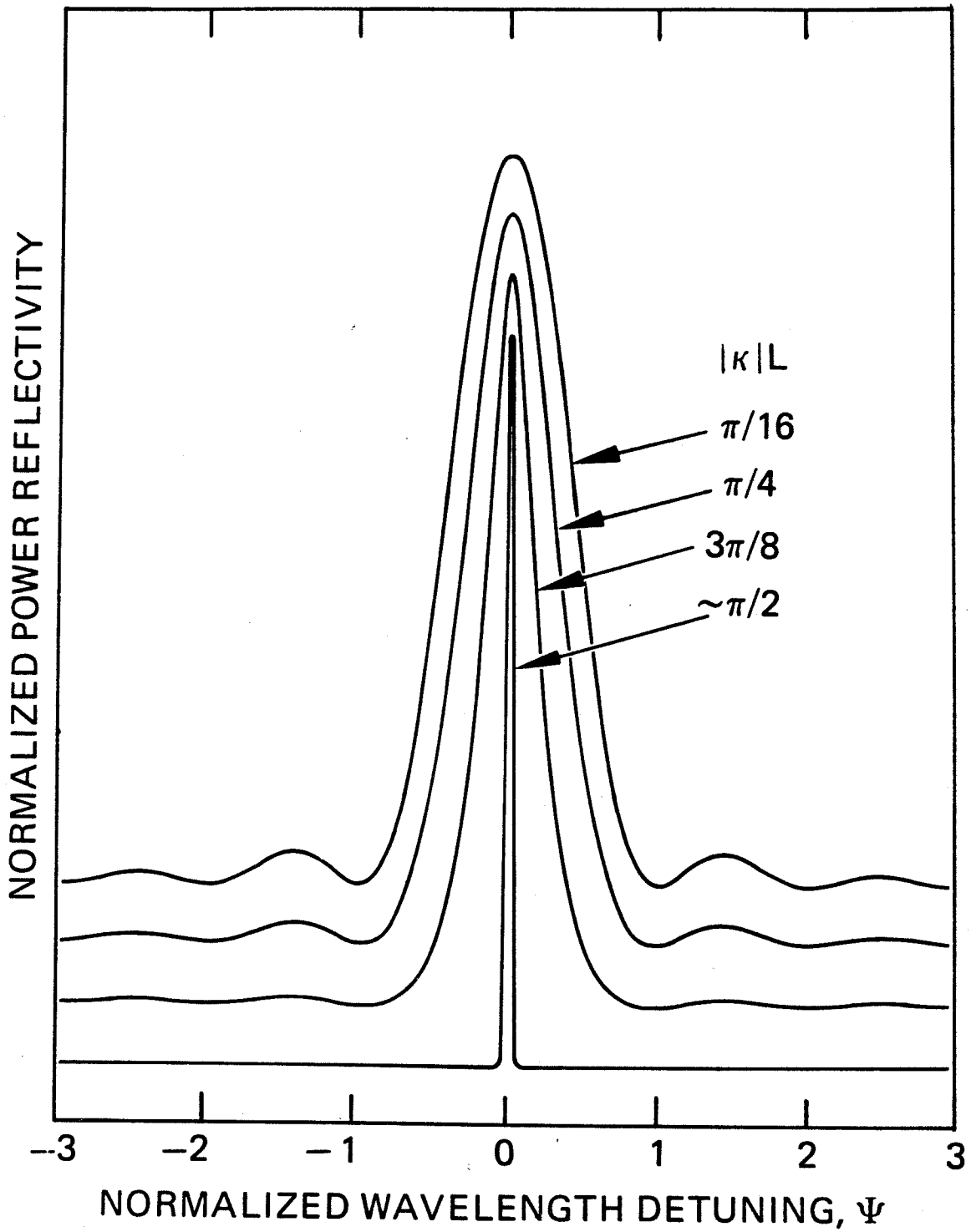

Fig. 6.3 Power reflectivity versus normalized wavelength detuning ψ for several values of the nonlinear gain $|\kappa|L$. All curves are normalized to unity to emphasize the frequency bandpass of the interaction.

condition is satisfied, the bandpass approaches zero, being limited ultimately by the linewidth and/or the coherence length of the pump sources.

The bandwidth (which we define to be the full-width at half maximum) characteristic of the filter as a function of the nonlinear gain ($|\kappa|L$) is shown explicitly (solid curve) in Figure 6.4. Also plotted in the figure for comparative purposes (dashed curve) is the normalized resolving power $\psi \equiv \delta\nu/\Delta\nu$ of a Fabry-Perot [11] (where $\delta\nu \equiv \mathcal{F}^{-1}\Delta\nu$, and $\mathcal{F}$ is the cavity finesse, given by $\mathcal{F} = \pi\sqrt{R}\exp(gL)/[1 - R\exp(2gL)]$; $\Delta\nu = c/2nL$, is the free spectral range of the cavity) as a function of the gain of an intracavity (nonsaturating) medium. We have (arbitrarily) chosen the Fabry-Perot parameters to be $(gL)_{th} = 1.13$, $R = .104$, $L = 1$ cm, and $n = 1.62$, so as to most closely resemble that of the corresponding four-wave mixing parameters. The characteristic to observe in the figure is the fact that both respective bandwidths decrease monotonically as the (nonlinear) gain increases. Of course, as the oscillation condition is approached, both the above theories need to be modified, as neither considers saturation mechanisms (e.g., pump depletion and stimulated emission for the respective cases).

It is of interest to note that at the oscillation condition ($|\kappa|L \sim \pi/2$), a slight phase mismatch ($|\Delta k|L > 0$) results in a drastic decrease of R, implying cessation of oscillation. Since the phase mismatch can in general be the result of either modifying the probe frequency and/or varying the direction of the pump beams with respect to each other (with the concomitant change in the interaction length), we can appreciate the sensitivity of the oscillation condition to the pump beam alignment.

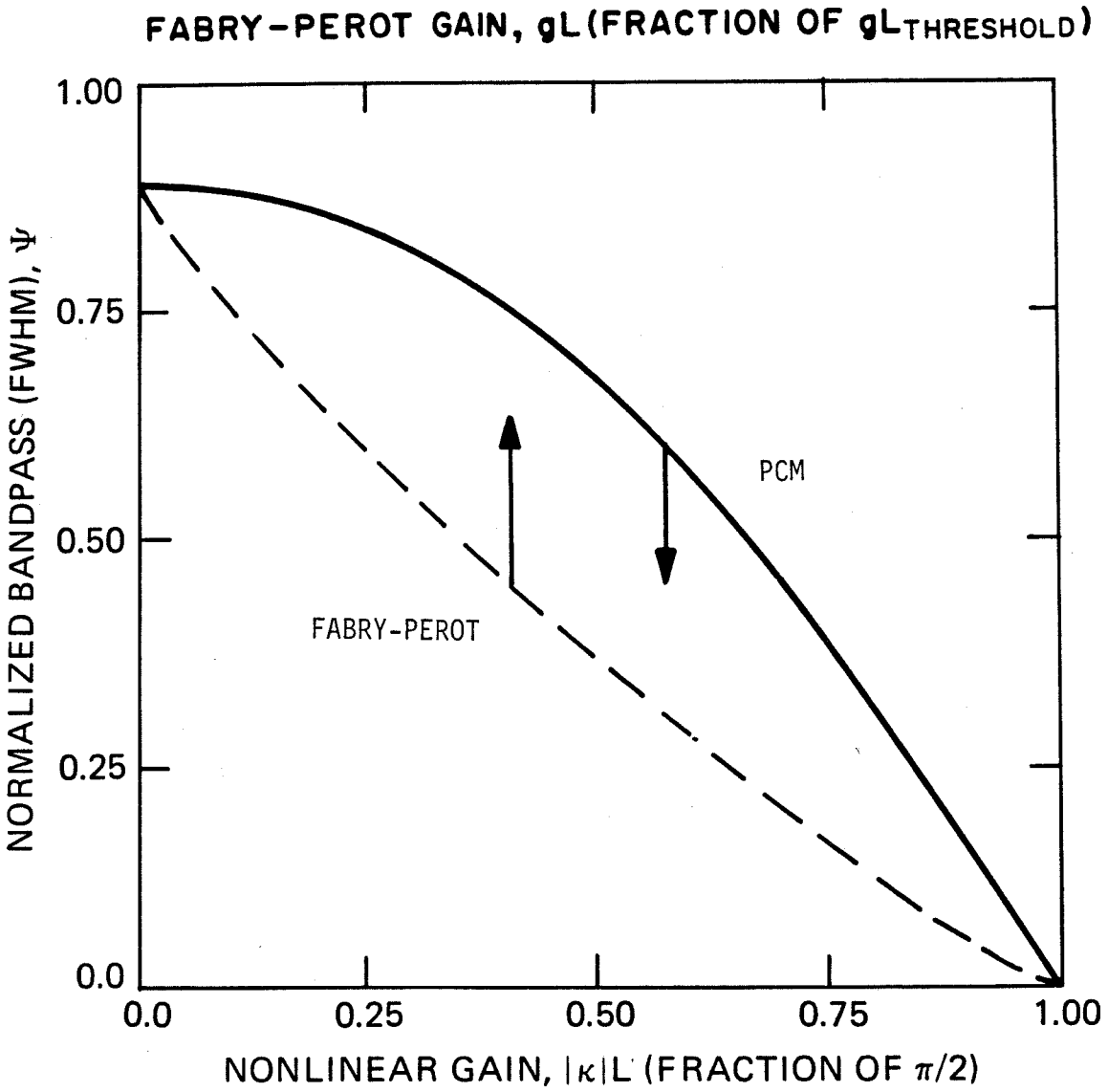

Fig. 6.4 Optical frequency bandpass (FWHM) of the filter versus nonlinear gain, $|\kappa|L$. For comparison, the normalized linewidth of a (nonsaturating) gain-filled Fabry-Perot resonator is shown versus gain. The bandpass approaches zero at the oscillation condition due to the assumed monochromaticity of the pump fields ($A_{1,2}$). For the parameters given in Figure 6.2, unity on the ordinate corresponds to $\Delta\nu$ = 9.26 GHz.

We note that since the four-wave interaction yields amplification of the forward-going wave (A_4), it too has a similar bandpass characteristic to that of its counterpropagating component, except that it is superimposed upon a unity transmission bandpass. The amplitude transmission coefficient is defined to be $t \equiv A_4(L)/A_4(0)$, and we have assumed again that $A_3(L) = 0$ (implying a single input probe field). Thus the "background" unity transmission bandpass, coupled with the lack of conjugacy of A_4, tends to limit the possibilities of filtering via the transmission mode.

We remark that (as opposed to the degenerate case; see Section 3.3) there <u>is</u> a net photon momentum transfer, $\vec{P}_{PCM}$, (or, equivalently, a non-zero radiation pressure) imparted to the PCM. It can be shown that $\vec{P}_{PCM} = (-2\delta\hbar n/c)\hat{k}_4$ per input probe photon (of frequency $\omega + \delta$), where we have neglected the (linear) dispersion of the PCM [i.e., $n(\omega \pm \delta) = n(\omega) \equiv n$].

We have shown how the process of nearly degenerate four-wave mixing can yield a real-time, active, narrow optical bandpass filter. The <u>interaction</u> has a large ($\sim 4\pi$) field of view and has a frequency response that depends on both the interaction length and pump intensity for a given medium. The actual field of view for a given <u>device</u> will, however, be limited by the specific optical detection scheme employed and the degree of spatial filtering. Spatial filtering of the time-reversed, phase-conjugate output wave can, however, be used to minimize noise sources. Finally, the filter is capable of yielding an amplified bandpass for large-enough nonlinear gains. Recent works have dealt with the filter properties in waveguides(see the discussion in Section 4.3 and reference 8), in resonantly enhanced media [9], and also the effect

of nonlinear phase changes upon the filter bandpass [10].

6.3 Compensation for Channel Dispersion by Nonlinear Optical Phase Conjugation

In this section we will discuss how the process of nonlinear optical phase conjugation can be utilized to compensate for the dispersion in optical communication channels, and hence to correct for temporal pulse broadening. Specifically, a four-wave nonlinear optical interaction is shown to achieve pulse renarrowing. Spectral bandwidth constraints of the input pulse are presented for typical phase conjugate interaction parameters.

In general, pulse spreading in an optical channel (e.g., an optical fiber communication link) limits the maximum modulation frequency or data rate possible (for a given channel length and at a given operating wavelength), and is thus undesirable [11,12]. This phenomenon arises from contributions such as frequency-dependent, waveguide [13], material [14], and modal dispersion [15]. (For reasons to be mentioned later, we will not consider the latter mechanism, and limit our treatment to single mode guides.) The result is that different frequency components of a given pulse propagate with differing phase and group velocities, leading to a temporal spreading as well as a "chirping" of the pulse at the output port of the channel. One possible technique to circumvent this problem is to frequency chirp the pulse (prior to insertion into the channel) such that the dispersive properties of the fiber essentially compress the pulse upon propagation through the channel [16]. That is, if one "arranges" the input pulse such that the slower

propagating frequency components enter the fiber prior to those components that propagate at greater group velocities, then the fiber dispersion characteristics will cause the latter frequency components to "catch-up" with the former components by the end of the link. As we will show below, the effect of the phase conjugate interaction does essentially this: Due to the frequency-flipping effect of the interaction (recall discussion of the last section), the output "instantaneous" frequency spectrum is inverted about the carrier frequency (i.e., the pump wave frequency). Hence, if this interaction were to take place midway along a dispersive channel, the resultant inversion of the spectrum, in conjunction with the conjugation operation (or phase reversal) would yield an undistorted temporal pulse shape at the output port of the link.

We now wish to explore theoretically what happens following conjugation to a short electromagnetic pulse which has traversed a dispersive channel. We find, reassuringly, that the group delay of the pulses is not time reversed, i.e., pulses retain their relative temporal order. The effect of group velocity dispersion, $dv_g/d\omega$, however, is time reversed to first order. This implies that pulses broadened in propagation can be renarrowed following conjugation by merely propagating through a second channel. We remark here that the concept of equalization or estimation and chirp techniques as applied to phase compensation due to pulse propagation is a well-known concept in data communication systems and in radar applications [17]. In addition, chirp compensation using four-wave mixing has been analyzed [18].

The model analyzed is shown in Figure 6.5. An input pulse

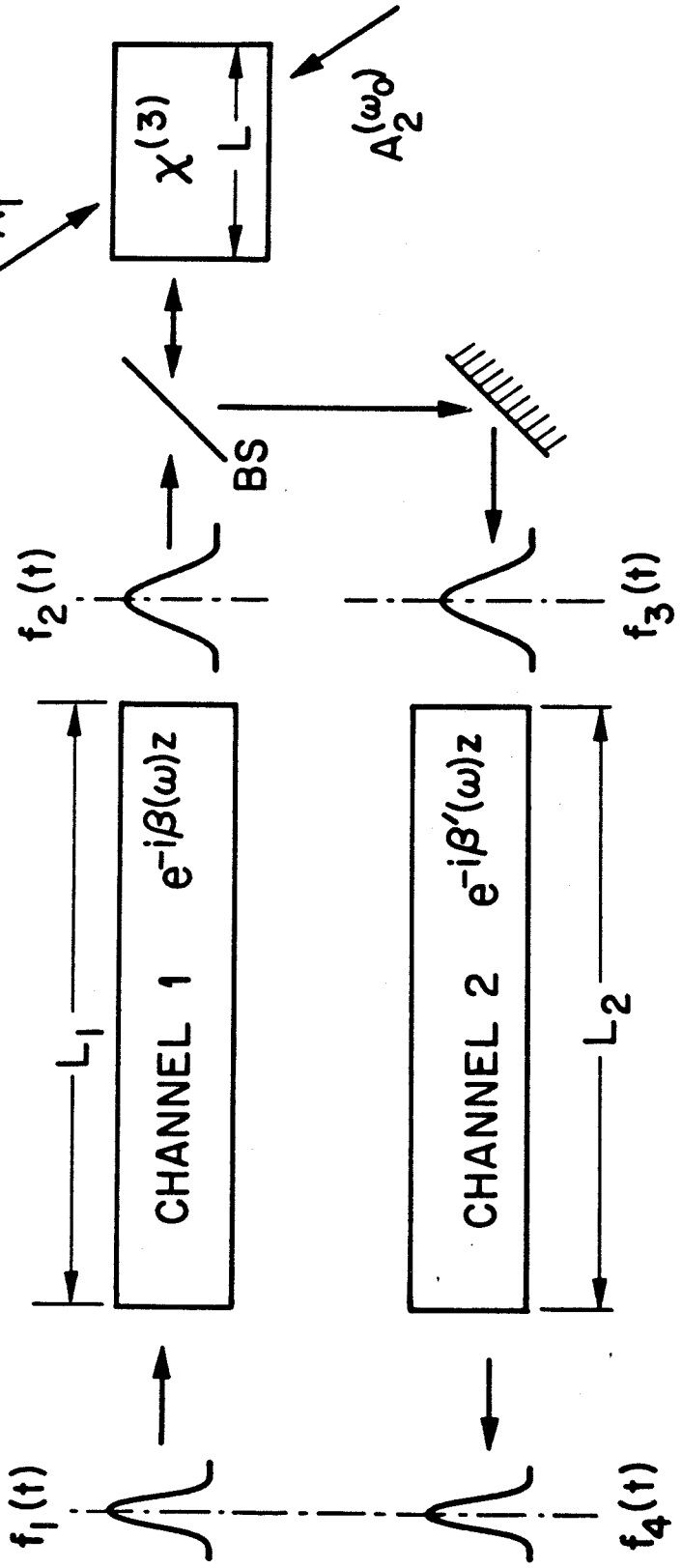

Fig. 6.5 Schematic diagram of pulse renarrowing scheme. The phase delay of channels 1 and 2 are given by $\beta(\omega)$ and $\beta'(\omega)$, respectively. The input pulse spectral envelope of $f_1(t)$ is assumed to be transform limited. BS is a beam splitter.

$$f_1(t) = g(t)\, e^{i\omega_0 t}$$

is incident on a dispersive channel. ω_0 is the optical carrier frequency, while the pulse envelope is $g(t)$. The Fourier transform of $g(t)$ is $F(\Omega)$

$$g(t) = \int_{-\infty}^{\infty} F(\Omega)\, e^{i\Omega t}\, d\Omega \qquad (6.3\text{-}1)$$

so that

$$f_1(t) = \int_{-\infty}^{\infty} F(\Omega)\, e^{i(\omega_0+\Omega)t}\, d\Omega \qquad (6.3\text{-}2)$$

Since the width of $g(t)$ is very large compared to the optical period $2\pi/\omega_0$, it follows that $\Omega << \omega_0$ over the region where $F(\Omega)$ is appreciable.

The propagation constant through the channel is $\beta(\omega)$ so that the output pulse $f_2(t)$ is

$$f_2(t) = \int_{-\infty}^{\infty} F(\Omega) e^{i[(\omega_0+\Omega)t - \beta(\omega_0+\Omega)L_1]}\, d\Omega \qquad (6.3\text{-}3)$$

where L_1 is the length of the channel.

Expanding $\beta(\omega)$ in a Taylor series near ω_0

$$\beta(\omega_0+\Omega) = \beta(\omega_0) + \frac{\partial\beta}{\partial\omega}\Omega + \frac{1}{2}\frac{\partial^2\beta}{\partial\omega^2}\Omega^2 + \ldots \qquad (6.3\text{-}4)$$

leads to

$$f_2(t) = e^{i(\omega_0 t - \beta_0 L_1)} \int_{-\infty}^{\infty} F(\Omega) e^{i[\Omega(t - \frac{\partial\beta}{\partial\omega}L_1) - \frac{1}{2}\frac{\partial^2\beta}{\partial\omega^2}\Omega^2 L_1]}\, d\Omega \qquad (6.3\text{-}5)$$

where $\beta_o \equiv \beta(\omega_o)$. The term $\frac{\partial\beta}{\partial\omega} L_1$ can be written as L_1/v_g, where $v_g = \partial\omega/\partial\beta$ is the group velocity. The term $\frac{\partial^2\beta}{\partial\omega^2}$ which can be written as $\left[-\frac{1}{v_g^2}\frac{\partial v_g}{\partial\omega}\right]$ corresponds to group velocity dispersion and causes $f_2(t)$ to be broader than $f_1(t)$, when $f_1(t)$ is a transform limited pulse.

The pulse $f_2(t)$ undergoes phase conjugation — the result being the pulse $f_3(t)$. To be specific, we will assume that the phase conjugation is achieved by four-wave mixing in a non-dispersive medium with two (essentially cw) pump waves, A_1 and A_2, at ω_o. We further assume that the response time of the non-linear interaction is shorter than the pulse duration. This causes [c.f. (6.2-2)] a Fourier component at $\omega_o + \Omega$ to be "reflected" at a frequency $\omega_o - \Omega$ so that the sum $2\omega_o$ of the pump frequencies is equal to the sum of the incident and reflected frequencies, as discussed in the last section. In general, an incident Fourier component $A \exp[i(\omega_o+\Omega)t]$ is reflected from the conjugator as $r(\Omega)\, e^{i\phi(\Omega)} A^* e^{i(\omega_o-\Omega)t}$ where $r(\Omega)\exp[i\phi(\Omega)]$ is the complex reflection coefficient of the conjugator at $\omega_o + \Omega$ (r is the magnitude of the reflectivity) given by equation (6.2-6). The total reflected wave is

$$f_3(t) = e^{i(\omega_o t+\beta_o L_1)} \int_{-\infty}^{\infty} r(\Omega) F^*(\Omega) e^{i[-\Omega(t-\frac{\partial\beta}{\partial\omega} L_1) + \frac{1}{2}\frac{\partial^2\beta}{\partial\omega^2}\Omega^2 L_1 + \phi(\Omega)]} d\Omega \qquad (6.3\text{-}6)$$

The wave $f_3(t)$ is incident on a medium of length L_2 whose propagation constant at $\omega_o - \Omega$ can be expanded as

$$\beta'(\omega_o-\Omega) = \beta_o' - \frac{\partial\beta'}{\partial\omega}\Omega + \frac{1}{2}\frac{\partial^2\beta'}{\partial\omega^2}\Omega^2 + \ldots. \qquad (6.3\text{-}7)$$

The output $f_4(t)$ is given by

$$f_4(t) = e^{i(\omega_o t + \beta_o L_1 - \beta_o' L_2)}$$

$$\times \int_{-\infty}^{\infty} r(\Omega)F^*(\Omega)e^{i[-\Omega(t - \frac{\partial\beta}{\partial\omega}L_1 - \frac{\partial\beta'}{\partial\omega}L_2) + \frac{1}{2}(\frac{\partial^2\beta}{\partial\omega^2}L_1 - \frac{\partial^2\beta'}{\partial\omega^2}L_2)\Omega^2 + \phi(\Omega)]}\, d\Omega \qquad (6.3\text{-}8)$$

The total group delay, $\frac{\partial\beta}{\partial\omega}L_1 + \frac{\partial\beta'}{\partial\omega}L_2$, is the sum of the individual channel delays. The group velocity dispersion term which involves the second order derivatives in (6.3-8) disappears, to first order, if

$$\frac{\partial^2\beta}{\partial\omega^2}L_1 = \frac{\partial^2\beta'}{\partial\omega^2}L_2 \qquad (6.3\text{-}9)$$

This requires that the sign of $\partial^2\beta/\partial\omega^2$ be the same in both channels. At the output of channel 2, the pulse is renarrowed. For maximum renarrowing, it is necessary that: (a) $r(\Omega)$ be a constant over the spectral range of the envelope function $F(\Omega)$; and (b), that $\phi(\Omega) = a + b$, where a and b are two real constants. Under these conditions the output from channel 2 is

$$f_4(t) = e^{i(\omega_o t + \beta_o L_1 - \beta_o' L_2 + a)}\, r(\omega_o) \int_{-\infty}^{\infty} F^*(\Omega)e^{i[-\Omega(t - \frac{\partial\beta}{\partial\omega}L_1 - \frac{\partial\beta'}{\partial\omega}L_2 - b)]}\, d\Omega \qquad (6.3\text{-}10)$$

Thus,

$$f_4(t) = r(\omega_o)\, e^{i\psi}[e^{i\omega_o t}\, g^*(t-t_g)] \qquad (6.3\text{-}11)$$

where

$$\psi = \beta_o L_1 - \beta_o' L_2 + a,$$

and

$$t_g = \frac{\partial\beta}{\partial\omega} L_1 + \frac{\partial\beta'}{\partial\omega} L_2 + b,$$

which corresponds to the total group delay; the nonlinear reflection coefficient magnitude $r(\omega_o)$ is assumed to be that evaluated at the center frequency, ω_o.

We find that in addition to conjugation and a reflection of the frequency spectrum from $\omega_o + \Omega$ to $\omega_o - \Omega$, the four-wave mixing process introduces a group delay of b. Under these conditions and neglecting higher orders in the expansion (6.3-4), the pulse at the output of channel 2 regains its original width.

To check the assumptions mentioned above concerning the phase conjugator, we plot in Figure 6.6 the calculated complex reflection coefficient $r(\Omega)\exp[i\phi(\Omega)]$ of a typical conjugator given by equation (6.2-6), divided by $A_4^*(0)$. We find that for $\Omega < 4$ GHz the deviation of $\phi(\Omega)$ from the requisite straight line dependence is very small compared to π so that pulses with a width of $\gtrsim 2 \times 10^{-10}$ seconds can be renarrowed by conjugation. Under these conditions, the constants a and b in the in the expansion of $\phi(\Omega)$ are $\phi_p - \pi/2$ and nL/c, respectively, where L and n are the interaction length and linear refractive index of the phase conjugator, and ϕ_p is the phase of the pump waves. Thus, the

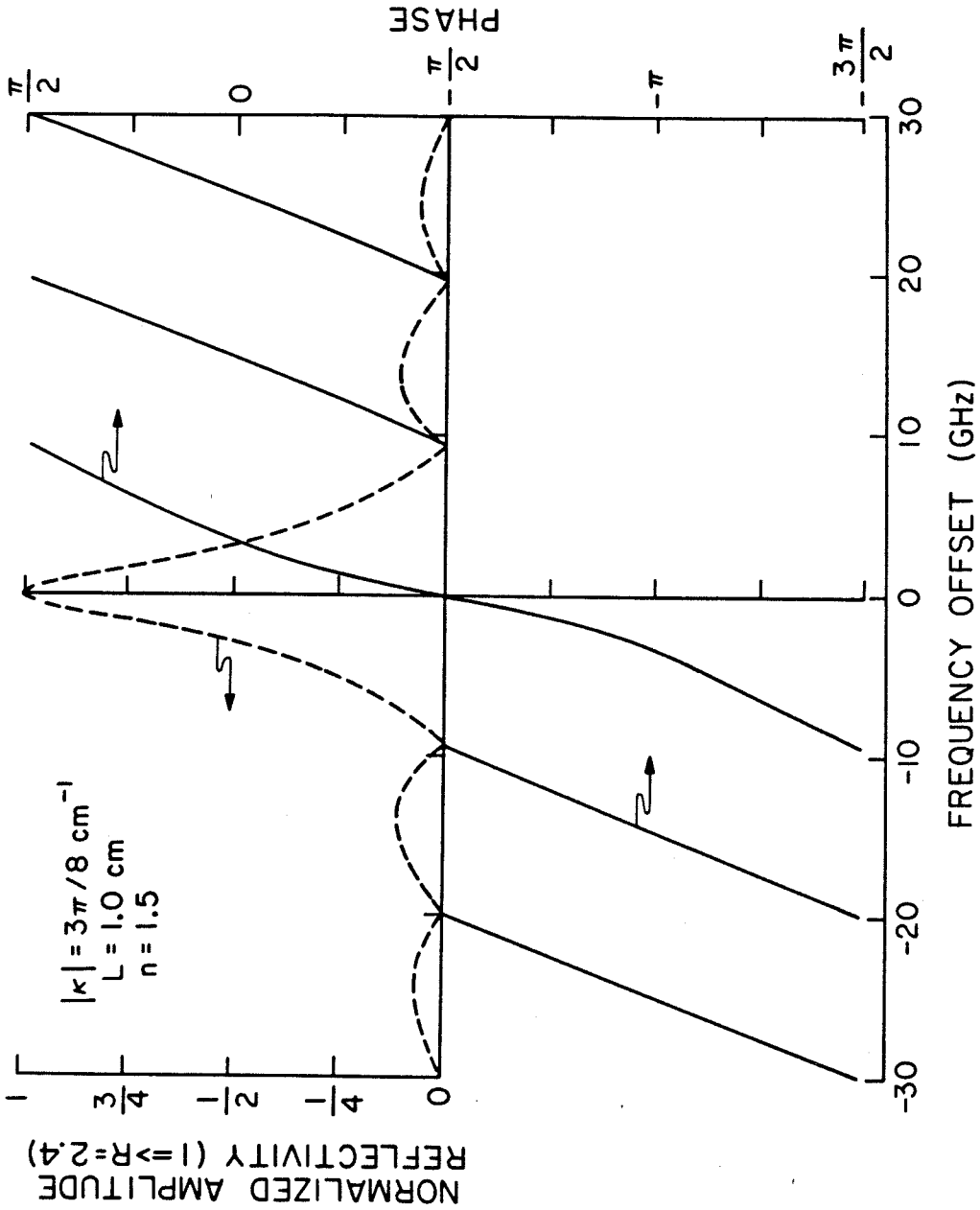

Fig. 6.6 Magnitude and phase of the complex reflection coefficient vs. frequency offset for typical four-wave phase conjugate parameters [from equation (6.2-6)].

additional group delay due to the four-wave interaction is given by $t_g' = nL/c$.

As a further check of the above formalism, we plot in Figure 6.7 the output amplitude from the conjugator versus time (solid curve) as calculated from equation (6.3-8). The input pulse to the conjugator is also shown (see dashed curve), and was chosen to have a (transform-limited) Gaussian time dependence and be of unity amplitude at line center.

The FWHM for this input pulse is 118 psec, corresponding to a bandwidth of $\sim$7.5 GHz. We note that from the preceding discussion the acceptable input bandwidth to the conjugator (given our parameters) was not to exceed 4 GHz (or FWHM to be greater than 200 psec) in order for the output pulse not to be distorted. Hence, the parameters of the input pulse used to generate Figure 6.7 clearly "stress" the system. The manifestation of this situation is apparent upon inspection of the output pulse shown in the figure. First, the output pulse is slightly broadened relative to the input pulse (viz. 160 psec output vs. 118 psec input FWHM). Next, the ouptput pulse is delayed in time somewhat more than predicted by the linear approximation to the frequency-dependent phase phase shift of the conjugator as discussed above. The linear model yields a delay of $t_g = nL/c \simeq 50$ psec, while the actual calculated output delay is seen to be 73 psec.

We also see that the peak amplitude of the output pulse is amplified ($R \sim 1.5$) relative to that of the input pulse. However, this value is less than that predicted for the steady-state case (i.e., $\tan(|\kappa|L) \sim 2.4$ for our parameters; see Figure 6.6). The reduction

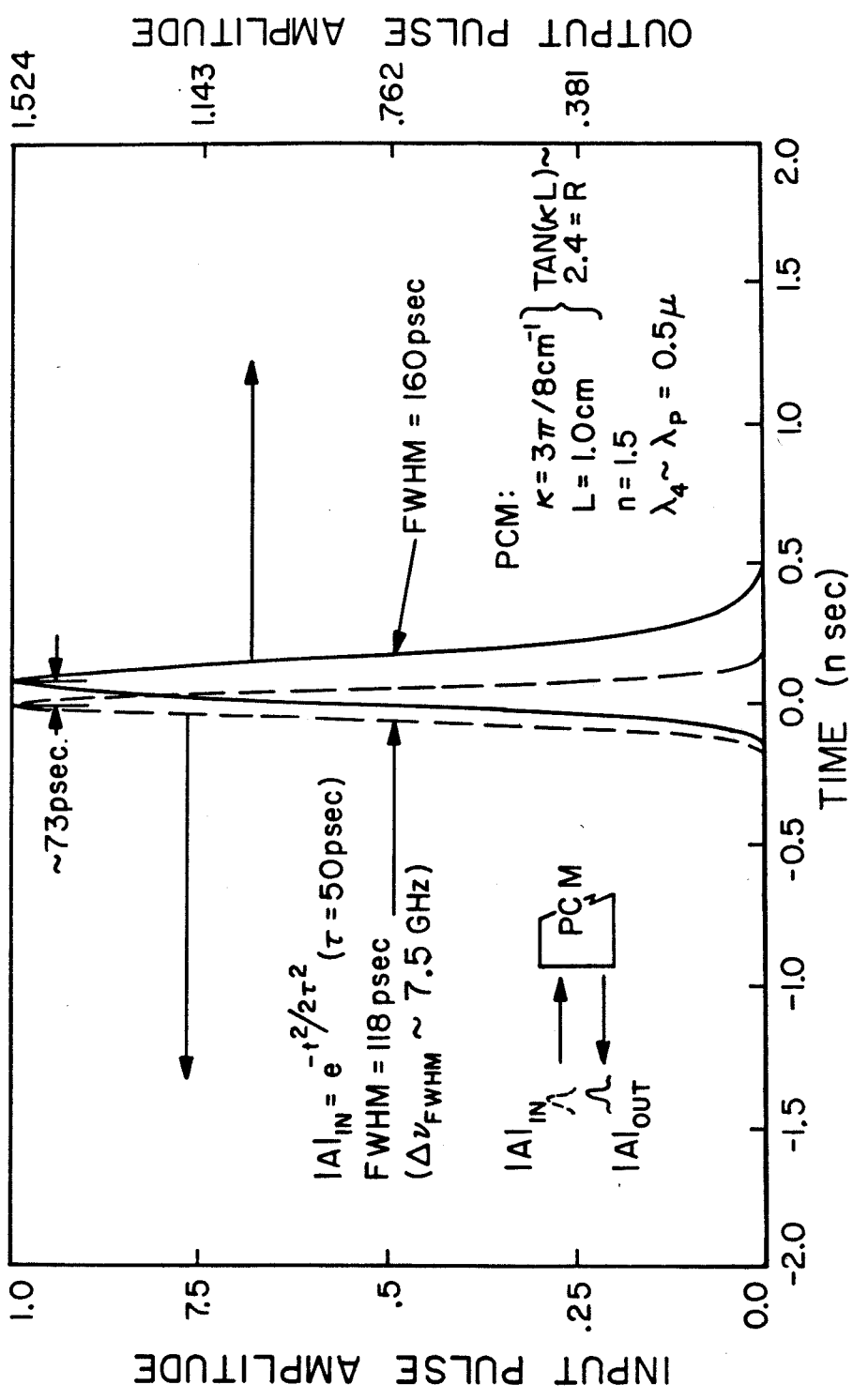

Fig. 6.7 Calculated response of a phase conjugator (parameters are those given in Figure 6.6) to a transform limited input pulse (dashed curve) of FWHM 118 ns. The output pulse amplitude (solid curve) is temporally delayed and slightly broadened due to the large input bandwidth.

of the amplitude of the PCM reflectivity is due to the fact that the input pulse bandwidth exceeds the acceptable value (for our parameters). In fact, upon inspection of the amplitude reflectivity (see Figure 6.6), we see that $\langle R \rangle \sim 1.5$ to 1.8 over a bandwidth range of $\sim$7.5 GHz centered at ω_o, which is in approximate agreement with the peak value of R = 1.524, plotted in Figure 6.7.

On the philosophical side, it is interesting to note that according to (6.3-11), the effect of conjugation plus the "flipping" of the frequency spectrum is to time-invert the effect of group velocity dispersion (and all additional terms in (6.3-4) that are even in powers of Ω), but not the group delay (along with other terms odd in powers of Ω). The group delays $(\partial\beta/\partial\omega)L_1$, and $(\partial\beta'/\partial\omega)L_2$ of the two legs are additive. The application of the term "time-inversion" to the conjugation process should thus be highly qualified.

We remark that the above scheme will <u>not</u> renarrow pulses which have temporally spread due to <u>modal</u> group velocity dispersion (occurring in multimode channels), since each mode is, in essence, an independent (or discrete) channel. The technique presented in this section can, however, compensate for other dispersive effects of each mode <u>separately</u>.

We note that for other nonlinear interactions which involve phase conjugation and frequency-flipping effects such as three-wave mixing [i.e., $\omega_{out} = 2\omega - (\omega + \Omega)$] and other forward-going conjugate generators (see, for example, Appendix 3A) can also give rise to pulse renarrowing, as described above. An analysis of the complex frequency-dependent transmission coefficient due to a three-wave mixing process and a forward-going,

four-wave interaction yields a constant phase factor similar to that given above. However, due to the copropagating nature of the input and output fields in these interaction geometries, the acceptable input frequency spectrum ($F(\Omega)$) depends primarily upon material dispersion, and, to first order in Ω, the medium does not introduce an additional overall group delay. Thus the acceptable bandwidth for pulse renarrowing should be greater in forward- vs. backward-wave conjugate interactions. In addition, the former scheme yields a conjugate wave that propagates in the forward direction, which may be desirable. Appendix 6A discusses the bandwidth limitations of the two schemes in more detail. We note that interactions that yield phase conjugate fields without frequency flipping (e.g., SBS or SRS) may also be useful in pulse renarrowing.

We emphasize that the interactions considered here do not compensate for overall group delays (as discussed above), and therefore do not violate the causal aspects of phase conjugate interaction. Thus, the notion of compensating for phase aberrations (recall Section 2.2 and Figure 2.2) does not violate causality, since that argument assumed monochromatic fields; the "bulges" shown in Figure 2.2 are equiphase fronts and do not imply temporal sequencing of energy flux. Temporal sequencing would imply the existence of nonmonochromatic signal fields and hence the analysis of this section would apply.

In conclusion, we have shown that nonlinear optical conjugation of a dispersion broadened pulse can be used to obtain a renarrowed pulse by subsequent traversal through a second channel. The input frequency bandwidth is essentially limited by the phase matching requirement of

the specific nonlinear mixing scheme for nondispersive media (additional linewidth-dependent constraints would apply for dispersive media) and for the case of small nonlinear gains (e.g., $\tan(|\kappa|L) \sim |\kappa|L$). The bandwidth decreases further as the nonlinear gain becomes larger (in a nonlinear fashion as does the filter bandpass discussed in Section 6.2 and shown in Figure 6.4). We note that the use of resonantly enhanced media would require the use of a highly frequency-dependent (complex) conjugator reflection coefficient [9] in equation (6.3-6).

6.4 Transient Two-Photon Spectroscopy via Phase Conjugate Optical Interactions

In this section we discuss an application of PCO in the field of nonlinear laser spectroscopy--that of probing Doppler-free, two-photon transitions [19] in atomic (or molecular) species on a transient basis (the steady state was considered in Section 3.11). We will use a time-dependent density matrix perturbation approach similar to that treated by Yariv and AuYeung [20], where the transient generation of phase conjugate wavefronts was analyzed. Specifically, we will limit our analysis to the so-called two-photon coherent state (TPCS) [21]. We will show that a probe photon which interacts with a TPCS gives rise to a conjugate wave [22,23] (i.e., a time-reversed replica) which may be useful for the many applications of PCO as outlined in this thesis. Further, by creating the TPCS in a transient sense (i.e., by using pulsed optical sources, for example), the temporal behavior of this state can provide one with information regarding various decay times that characterize the atomic system [22,23]. In addition, if one forms a TPCS in a nearly harmonic

system (e.g., via the rotation-vibration resonances of a molecule), the subsequent radiative decay of the state (known as the optical free-induction decay) after all the optical fields have been terminated results in amplitude fluctuations, the period of which is proportional to the degree of anharmonic contributions to the molecule's potential well. This latter technique is referred to as "α-beat spectroscopy" in the literature [24]. Prior to discussing the TPCS further, we begin by motivating two-photon Doppler-free spectroscopy (TPDFS). The application of TPDFS to phase conjugation has been discussed recently [22,23,25,26].

Consider an ensemble of atoms (or molecules) at low pressures in thermal equilibrium. If one desires to probe the natural linewidth $\delta\nu_N$ of a given transistion, the measured linewidth will be typically much greater than $\delta\nu_N$ due to, for example, Doppler-broadening [3] ($\delta\nu_D$). Hence, the determination of $\delta\nu_N$ would be obscured due to the thermally-induced broadening effects. One technique that can circumvent this problem is to employ TPDFS.

This technique eliminates Doppler shifts to first order, enabling one to probe linewidths on the order of $\delta\nu_N$. The method operates as follows. Assume an allowed two-photon transition to exist in the system at frequency ω_o. If one now irradiates the sample with a laser of frequency ω, such that $2\omega \simeq \omega_o$, then atoms can be promoted to the upper level if the selection rules are satisfied. In addition, the transition rate can be increased if a system is chosen so as to incorporate an (dipole-allowed) intermediate state having a resonance near ω. Now, assume that a geometry is chosen such that the sample is irradiated with counterpropagating beams, each of frequency ω. Assume further that the

polarization states of these two fields are chosen such that a two-photon transition requires one photon from each of the counterpropagating beams (as opposed to two photons from a single beam) in order to occur. For example, a $\Delta L_z = 0$ transition (e.g., nS → n'S) would require a RHCP (LHCP) photon from each beam; a $\Delta L_z = 2$ transition (e.g., S → D) on the other hand, would require a RHCP photon from one beam and a LHCP photon from the second beam (of course, 2 photons from either beam would induce a transition, but they only interact essentially with the zero velocity group of the atoms). It is easily seen that if the atom has a velocity component v in the direction of one beam, the atom will "see" a Doppler-upshifted photon (at frequency ω_+) from that beam; however, the same atom will "see" a Doppler-downshifted photon (at frequency ω_-) from the other beam, such that the frequency sum of the two photons corresponds to $\sim\omega_0$. Hence, to first order, the Doppler-shift is canceled. Specifically, the two photons have their frequencies modified (as viewed in the atoms rest frame) as

$$\omega_\pm = \omega\left[\frac{1 \pm \beta}{(1-\beta^2)^{1/2}}\right] = \omega\left(1 \pm \beta + \frac{1}{2}\beta^2 \pm \frac{1}{2}\beta^3 \cdots\right) \qquad (6.4\text{-}1)$$

where $\beta \equiv v/c$. The sum frequency is therefore

$$\omega_+ + \omega_- = 2\omega\left(1 + \frac{1}{2}\beta^2 + \frac{3}{8}\beta^4 + \cdots\right) \simeq \omega_0 \qquad (6.4\text{-}2)$$

Therefore, the Doppler-shift is effectively canceled to first (and all successive odd) order(s) in β. Since $\beta \sim 10^{-5}$ to 10^{-6} at typical tem-

peratures, the higher order Doppler-effects are seen to be negligible. Thus, the above scheme affords a large number of thermal atoms (i.e., nonzero velocity groups) to collectively participate in the interaction with a rather narrow (sub-Doppler) linewidth.

As a result of this Doppler-free transition, a TPCS is formed. The TPCS may be viewed as a zero-momentum, coherent superposition of the ground and upper states, which oscillates at $\omega_o \simeq 2\omega$. The state is one of zero momentum, since the linear momenta of the two counterpropagating laser photons which induced the transition cancel exactly. Further, all the atoms participate in the resonance, irrespective of their velocity.

By probing this TPCS one can make precise measurements of the resonance. This may be accomplished in the frequency domain by scanning the frequency of a probe laser, and hence measuring the linewidth of the interaction [19]. Alternatively, one may perform measurements in the time domain by investigating the transient response of the TPCS. Techniques such as quantum interference effects [27], spatially separated fields [28], Stark switching [29], saturation dips [30], and other broadband pulsed excitation techniques [22,23] have been used to this end. In these approaches, one can further investigate the various dephasing and other relaxation times [22,23] that characterize the TPCS through the use of varying temporal delays of the beams that create and/or probe the TPCS. Other coherent transient techniques such as the right angle photon echo [31] and the tri-level echo [32] have also been used to measure these relaxation times. Several reviews have been written that summarize both the techniques and the physics related to these transient effects (such

as optical free-induction decay, etc.) [33,34]. The technique of "α-beat spectroscopy,"as applied to ensembles of two-photon allowed transitions in atoms has been analyzed [24]. We will discuss below a specific application of the latter technique with respect to the determination of anharmonic contributions to molecular potentials. The elegance of this scheme is that since the spectroscopic information is obtained in the time domain, the need for highly stable, cw tunable lasers is obviated. Hence, one can use broadband, pulsed sources as well as Stark switching techniques (as referenced above).

The connection [22,23] between the probing of the TPCS and that of optical phase conjugation becomes apparent if one recognizes that the the two counterpropagating fields discussed above may be considered as being the two pump waves present in the standard four-wave mixing geometry (see Figure 3.1). The zero-momentum state of the TPCS now interacts with the probe photon so as to yield a backward-propagating (conjugate) photon. Now, by frequency scanning the probe wave (as discussed in the steady-state case of Section 3.9), or by investigating the transient behavior (to be discussed here) of the conjugate wave, the properties of the transition may be obtained (e.g., resonance structure, relaxation times, splittings, etc.). A major advantage of utilizing a conjugate-type interaction for this investigation is that the time-reversed propagation of the output photon may be exploited to yield a greater signal-to-noise ratio for the desired measurements. Thus by spatial filtering and/or polarization techniques, various background noise sources (such as fluorescence) may be reduced. Further, by creat-

ing the TPCS in a pulsed (transient) manner, the pump (or exciting) fields would be off during the actual generation of the conjugate wave.

We begin our analysis by considering the interaction of a sequence of three optical pulses with a three-level atomic (or molecular) system. The notation and relevant energy levels considered are shown in Figure 3.11a. (Most of the descriptions and notations presented here will follow those of Section 3.9). The atoms are subjected to

three pulses of duration δ of the same optical frequency ω, and propagate along arbitrary directions $\vec{k}_i$:

$$\vec{E}_i(\vec{r},t) = \frac{1}{2}\vec{E}_i(t)\exp[i(\omega t - \vec{k}_i\cdot\vec{r})] + \text{c.c.}, \quad i=1,2,4 \qquad (6.4\text{-}3)$$

The pulse envelopes are shown in Figure 6.8. The perturbing Hamiltonian, along with the (assumed) allowed dipole matrix elements, are the same as given in (3. 9-16). We assume for simplicity that only one field is incident upon the medium at a given time. Further, we neglect (i) atomic motion of the species, and (ii) saturation effects. With respect to the former approximation, we note that although the formation of the TPCS is independent of atomic motion, the subsequent probing of the TPCS will be dependent upon the velocity distribution (due to, for example, Doppler-induced nearly-degenerate four-wave mixing as viewed in the atom's rest frame). The latter approximation basically assumes that all the Rabi frequencies are smaller than any inverse relaxation times. The above assumptions enable us to use a velocity-independent, density matrix perturbation approach (as outlined in Section 3.9) to analyze the present problem.

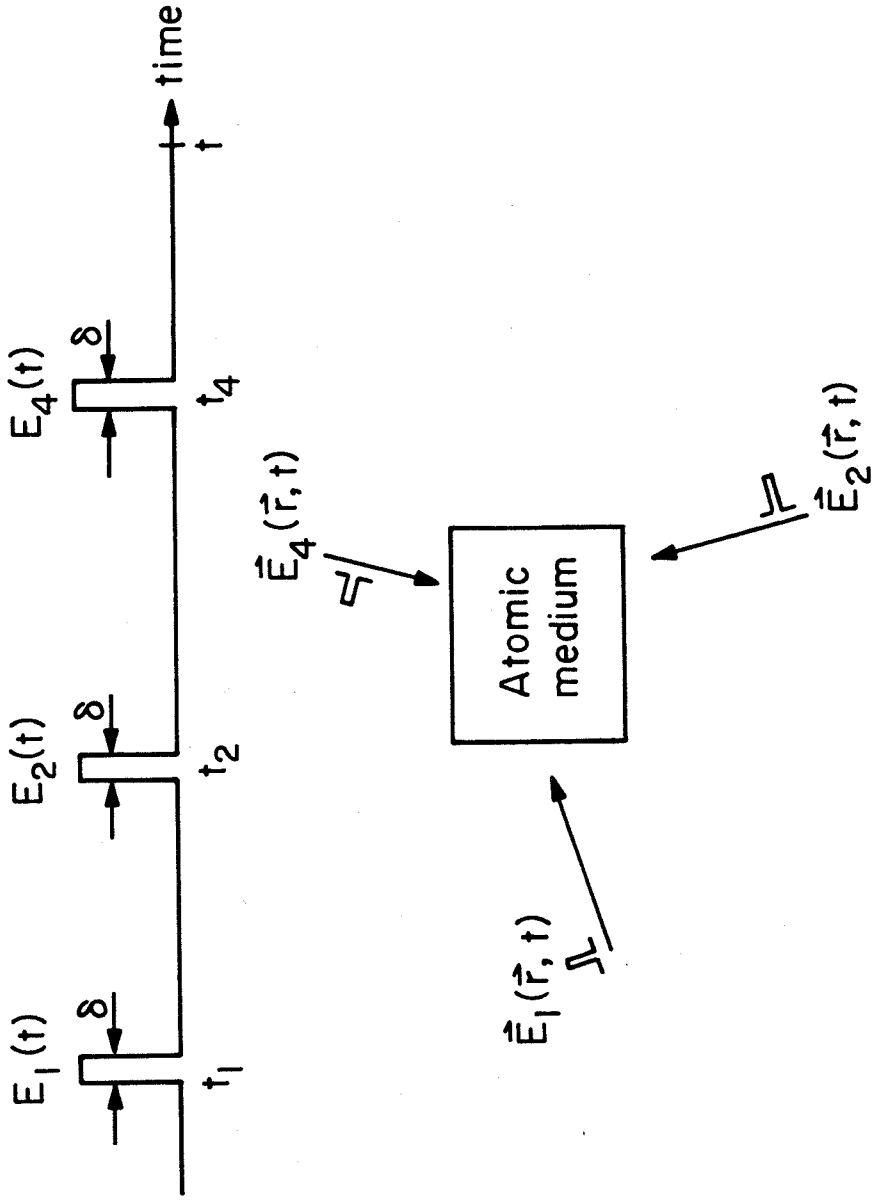

Fig. 6.8 The geometry for the interaction of a three-pulse sequence with an atomic (or molecular) medium.

We wish to evaluate the response of the atomic medium subsequent to the third (i.e., the last) optical pulse. Physically, the atomic oscillator is being driven sequentially, and we expect that this damped oscillator will relax (i.e., radiate) at its resonant frequency (or frequencies) after the external driving forces are off. This relaxation process is called the optical free-induction decay of the atomic system.

Returning to Figure 6.8, we want the first two pulses ($E_{1,2}$) to correspond to the pump waves and thus form the TPCS, with the last (probe) pulse (E_4) scattering off this state. Yariv and AuYeung [20] have analyzed a related scheme where the probe pulse was the first(second) pulse, with one of the pump waves being the second(first) pulse. These two fields were shown to give rise to a spatial modulation of the atomic population densities, which then decayed exponentially at the longitudinal decay rate (i.e., the spontaneous lifetime) of the system. If during this lifetime the third pulse (the other counterpropagating pump wave) was incident upon the medium, it was shown to scatter (diffract) off this spatially modulated "grating," yielding the desired conjugate wave. In their analysis [20], the first two pulses were required to possess nonzero, parallel polarization field vector components in order to realize conjugate wave generation.

In the present analysis, the probe pulse interacts lastly to yield the conjugate wave. Both Yariv's [20] scheme and the present temporal pulse sequence [22,23] follow from the different allowed density matrix "pathways" as shown in Figure 3.12. The pathways that yield second order diagonal density matrix elements (i.e., $\rho_{11}^{(2)}$ and $\rho_{22}^{(2)} \propto$

$E_i E_j^*$) imply a transfer of level populations and thus correspond to the holographic analogs of four-wave mixing as discussed in Section 3.10. These diagonal elements oscillate at zero frequency and decay as T_1. The remaining nonzero density matrix perturbation pathway involves the second order element $\rho_{13}^{(2)}$, otherwise known as the two-photon coherent state [21]. As we show below, it arises from products of fields of the form $E_i E_j$ (in our case, the two pump waves), and oscillates at $\omega_o \simeq 2\omega$ after excitation, thus forming a temporally modulated grating at that frequency. The TPCS decays at the dephasing rate of the system (i.e., T_2, or the transverse relaxation time). The subsequent scattering of the probe pulse off the TPCS, with the generation of the conjugate wave has no direct holographic analog (as discussed in Section 3.10). We note that experimentally the various density matrix pathways can be realized by the proper temporal sequencing and/or polarization states of the three interacting optical fields.

For the analysis we use the same density matrix perturbation scheme (in the rotating-wave approximation) whose solution is given by equation (3.9-18). We wish to obtain the expression for the induced third-order nonlinear dipole moment as given by (3.9-17) for the density matrix pathway (as shown in Figure 3.12) that involves $\rho_{13}^{(2)}$. The lower and upper limits of the integral are given by $t = t_i - \delta/2$ and $t = t_i + \delta/2$, respectively for $i = 1$, 2, and 4. We assume that the only nonzero unperturbed density matrix element is $\rho_{11}^{(0)}$ (as described in Section 3.9). Substitution of the commutator $[V(t'), \rho^{(0)}]$, given by (3.9-19) into (3.9-18) yields the following first order perturbed density matrix element

for ρ_{12} (as a result of the first pulse, E_1) for times after E_1:

$$\rho_{12}^{(1)}(t > t_1 + \tfrac{\delta}{2}) = (-\tfrac{1}{2\hbar}) \frac{\rho_{11}^{(0)}(\mu_{ab})_1 E_1 e^{i\omega_{ba}t - \gamma_{ab}t}}{(\omega_1 - \omega_{ba} - i\gamma_{ab})} \Lambda_{21} \qquad (6.4\text{-}4)$$

where $\Lambda_{21} = 2i\, e^{i\Omega_{21}t_1} \sin(\tfrac{\delta}{2}\Omega_{21})$

$$\Omega_{21} = \omega_1 - \omega_{ba} - i\gamma_{ab} \quad ,$$

and where $(\mu_{ij})_k$ is the component of the dipole moment $\vec{\mu}_{ij}$ which lies along the field $\vec{E}_k$; μ_{ij} connects states $|i>$ and $|j>$. We see that since $\omega_1 \simeq \omega_{ba}$, (6.4-4) is the major contribution to $\rho_{12}^{(1)}(t)$; other nonresonant terms have been neglected.

Substituting the above result into the commutator (3.9 -19) and evaluating the resultant integral (3.9 -18) over the second pulse (E_2) gives rise to the following expression for the second order density matrix element ρ_{13} (for times <u>after</u> the pulse E_2)

$$\rho_{13}^{(2)}(t > t_2 + \tfrac{\delta}{2}) = (-\tfrac{1}{2\hbar})^2 \frac{\rho_{11}^{(0)}(\mu_{ab})_1(\mu_{bc})_2 E_1 E_2 e^{i\omega_{ca}t - \gamma_{ac}t} \Lambda_{21}\Lambda_{32}}{[\omega_1 - \omega_{ba} - i\gamma_{ab}][\omega_2 - \omega_{cb} - i(\gamma_{ac} - \gamma_{ab})]} \qquad (6.4\text{-}5)$$

where

$$\Lambda_{32} = 2i\, e^{i\Omega_{32}t_2} \sin(\tfrac{\delta}{2}\Omega_{32})$$

and

$$\Omega_{32} = \omega_2 - \omega_{cb} - i(\gamma_{ac} - \gamma_{ab})$$

We see that $\rho_{13}^{(2)}$ corresponds to the two-photon coherent state [21] which is proportional to the product of the (pump) fields E_1 and E_2, oscillates at the two-photon transition frequency ω_{ca} (which is not necessarily the same as twice the pump frequency 2ω) and decays at the corresponding dephasing rate γ_{ac}. In arriving at (6.4-5), we again have retained the near resonant term (i.e., the rotating wave approximation).

We see from Figure 3.12 that there are two nonzero density matrix elements which occur as a result of the perturbation induced by the third (i.e., probe) pulse, E_4; the nonzero elements are $\rho_{12}^{(3)}$ and $\rho_{23}^{(3)}$. Since we are interested in probing the resonances (among other atomic parameters) of the atomic medium, we will evaluate the induced third order nonlinear dipole at times after all the pulses are off. In this way, the only fields detected will be a function of the atomic (or molecular) levels and not those of the exciting laser(s). This is called the optical free-induction decay of the medium. We therefore follow the same procedure as above and obtain the following expressions for the nonzero third order density matrix elements (again evaluated at times after the last pulse E_4):

$$\rho_{12}^{(3)}(t > t_4 + \tfrac{\delta}{2}) =$$

$$(-\tfrac{1}{2\hbar})^3 \frac{\rho_{11}^{(0)}(\mu_{ab})_1(\mu_{bc})_2(\mu_{cb})_4 E_1 E_2 E_4^* e^{i\omega_{ba}t-\gamma_{ab}t} \Lambda_{21}\Lambda_{32}\Lambda'_{23}}{[\omega_1-\omega_{ba}-i\gamma_{ab}][\omega_2-\omega_{cb}-i(\gamma_{ac}-\gamma_{ab})][\omega_{cb}-\omega_4-i(\gamma_{ab}-\gamma_{ac})]} \tag{6.4-6}$$

where $\Lambda'_{23} = 2ie^{i\Omega'_{23}t_4} \sin(\frac{\delta}{2}\Omega'_{23})$

$\Omega'_{23} = \omega_{cb} - \omega_4 - i(\gamma_{ab} - \gamma_{ac})$

and

$$\rho^{(3)}_{23}(t > t_4 + \frac{\delta}{2}) = (\frac{-1}{2\hbar})^3$$

$$\times \frac{\rho^{(0)}_{11}(\mu_{ab})_1 (\mu_{bc})_2 (\mu_{ba})_4 E_1 E_2 E_4^* e^{i\omega_{cb}t - \gamma_{bc}t} \Lambda_{21}\Lambda_{32}\Lambda'_{12}}{[\omega_1 - \omega_{ba} - i\gamma_{ab}][\omega_2 - \omega_{cb} - i(\gamma_{ac} - \gamma_{ab})][\omega_{ba} - \omega_4 - i(\gamma_{bc} - \gamma_{ac})]} \qquad (6.4\text{-}7)$$

where $\Lambda'_{12} = 2ie^{i\Omega'_{12}t_4} \sin(\frac{\delta}{2}\Omega'_{12})$

$\Omega'_{12} = \omega_{ba} - \omega_4 - i(\gamma_{bc} - \gamma_{ac})$

Now, forming the nonlinear polarization by using (6.4-6,7) in (3.9-17) and the definition $P_{NL} \equiv N\langle\mu\rangle$ (with $\rho^{(0)}_{11} \to 1$) yields

$$P^{(3)}_{NL}(t > t_4 + \frac{\delta}{2}) \to \frac{-\delta^3}{2\hbar^3} N|\mu_{ba}|^2 |\mu_{cb}|^2 E_1 E_2 E_4^* e^{-i(\vec{k}_1 + \vec{k}_2 - \vec{k}_4)\cdot\vec{r}}$$

$$\times e^{i\frac{\omega_{ca}}{2}t - \gamma_{ab}t} \sin(\frac{\Delta t}{2}) e^{-\gamma_{ab}(t_2 - t_1 + \frac{\delta}{2})} e^{-\gamma_{ac}(t_4 - t_2)} \qquad (6.4\text{-}8)$$

The polarization given by equation (6.4-8) radiates the conjugate wave if the pump waves are counterpropagating (i.e., $\vec{k}_1 + \vec{k}_2 \equiv 0$), and if $\omega_{ca}/2 \simeq \omega$. In arriving at (6.4-8) we have assumed the "small area" limit ($\Omega\delta/2 << 1$ for all Ω_{ij}), set all polarization vectors parallel for simplicity, assumed that $\gamma_{ab} \simeq \gamma_{bc} \equiv \gamma_{ab}$, added a factor of two in order to account for the permutation of E_1 with E_2, and included the spatial phase variation of the fields as given by (6.4-3). Further, we have assumed

near-resonant denominators (i.e., all Ω are pure imaginary, or equivalently, the γ_{ij} dominate over any frequency differences), and we defined $\Delta \equiv \omega_{ba}-\omega_{cb}$; thus Δ determines the anharmonic contribution of the potential (for a purely harmonic potential, $\Delta \to 0$). Recall that we have neglected atomic motion; in general, one must integrate a velocity-dependent nonlinear dipole moment over an assumed velocity distribution in order to yield the macroscopic nonlinear polarization.

Let us examine some features of (6.4-8). First, we see that if $\Delta \neq 0$, there exists an amplitude beat-frequency of roughly $\Delta/2$. This follows from the fact that there are two contributions to the third-order induced dipole, arising from the allowed transitions coupling levels a and b as well as levels b and c (given by the density matrix elements in (6.4-6) and (6.4-7), respectively). These two contributions interfere coherently in the time domain, thus giving rise to the amplitude beating. This effect has been termed "α-beat spectroscopy" by Levenson [24]. He applied the technique to an ensemble of two-level (dipole forbidden) atoms, of differing two-photon energy spacings. In our case, the observed beating in the time domain is a measure of the characteristics of a single atom; hence an ensemble of identical atoms could give rise to the beating.

The next aspect of our result, equation (6.4-8), that we will discuss relates to the overall decay rates of the polarization. We see that as a result of the specific density matrix sequence analyzed (which involves only off-diagonal matrix elements), the various decay times are those that correspond to the transverse, or dephasing lifetimes. It is seen from (6.4-8) that the amplitude of $P_{NL}^{(3)}$ is maximized

if the two pump photons overlap in time, and also if the probe photon is incident upon the TPCS at the time of its creation. Further, the conjugate wave decays as $\exp(-\gamma_{ab}t)$; thus, the temporal beating discussed above is damped by this decay rate. We see that one may infer the various dephasing rates by varying the time delay between the two pump waves, or between the creation of the TPCS and the subsequent scattering of the probe wave off this state [22,23]. We note that the other density matrix perturbation pathways (see Figure 3.12) involve both transverse and longitudinal decay rates [20].

We remark that if one wishes to determine the anharmonic contribution (Δ), the experimental region of interest for a given system is limited to $\gamma_{ab} < \Delta < \tau^{-1}$, where τ is the response time of the detection apparatus. These limits ensure that (i) a sufficient number of amplitude beats occur during the decay of the conjugate, optical free-induction decay; and (ii) the detection apparatus can respond fast enough to resolve these temporal beats. Levenson [24] has pointed out that the α-beat technique may be useful for splittings which are too large for quantum beats [19], yet too small for frequency-domain spectroscopy.

We emphasize that the generation of a conjugate wave by the interaction of a TPCS with a probe wave has no direct holographic analogs, since (in holographic terms) the reference and reconstruction beams (i.e., the pump waves) both interact with the system and even terminate prior to the incidence of the object wave. Further, the polarization vectors of the two pump waves need not be necessarily parallel to

the object wave (subject only to the selection rules of the atomic species) in order to realize the conjugate return field. Yet, despite this, a (near) pseudoscopic image is still generated, since all the phase information from the various interacting fields is retained in the interaction medium during the dephasing lifetime(s).

In conclusion, we have shown by using a time-dependent density matrix perturbation analysis that the scattering of a probe wave off a two-photon coherent state is capable of yielding a conjugate wave [22,23,35 36]. In addition, by investigating the temporal and amplitude decay of the conjugate field, one can infer various parameters that characterize the atomic (or molecular) medium such as the various dephasing lifetimes [22,23], as well as the degree of anharmonicity in nearly harmonic systems. Thus this scheme may be useful for wavefront reversal applications, as well as an interesting spectroscopic tool. The elegance of this scheme as a spectroscopic tool can be appreciated when one realizes the conjugate nature of the return wave. Hence, by utilizing the spatial, temporal, and polarization properties of the time-reversed wave, various undesirable background noise sources such as fluorescence and/or scattering of the input fields can be minimized--thus yielding a greater signal-to-noise ratio than is possible with many other spectroscopic techniques.

APPENDIX 6A

Acceptable Input Bandwidths for Group Velocity Dispersion Compensation Schemes

In this appendix we will investigate the maximum input bandwidth (and hence the shortest transform-limited pulse width, or maximum data rate) allowable for efficient group velocity dispersion compensation via optical phase conjugation. We will consider several cases of forward-going as well as backward-going conjugation geometries as discussed in Sections 3.2 and 3.3, and Appendix 3A. For brevity, we consider only the kinematical constraints or phase matching restrictions in arriving at the various bandwidth limitations. The dynamics for a given process involves a solution in terms of the amplitude evolution which may be obtained, for example , by using a coupled mode formalism similar to that presented in Section 3.3. Since the magnitude of the nonlinear gain can have a profound effect in terms of decreasing the bandpass for a given system (recall the arguments presented in Sections 6.2 and 6.3), one must ultimately consider this additional constraint. However, it was shown in Section 6.3 that the maximum acceptable bandpass is ultimately limited by the kinematical constraints. We therefore limit our discussion to this regime (equivalently, the small signal, or small nonlinear gain limit). Further we assume that the wavelengths involved are far from any material resonances characterizing the conjugator; thus, we take the nonlinear susceptibility to be a nondispersive, phenomenological constant.

A. Bandpass for Phase Conjugation via Forward-Going, Nearly Dengenerate Four-Wave Mixing

The geometry for this interaction is given in Figure 3A.1b, where

all four fields are assumed to be colinear and copropagating. We take the special case where the pump waves $E_2(\omega)$ and $E_3(\omega)$ are of the same frequency; that is, the degenerate case. The probe and conjugate fields are taken as $E_1(\omega+\delta)$ and $E_4(\omega-\delta)$, respectively, where $|\delta/\omega| << 1$. The field conventions are chosen to be consistent with that of the figure. We consider a nonlinear polarization of the form

$$P_{NL}^{(\omega_4)} = \frac{1}{2} \chi_{NL}^{(3)} E_2(\omega) E_3(\omega) E_1^*(\omega+\delta) + c.c. \qquad (6.A\text{-}1)$$

which gives rise to the conjugate wave. Photon energy conservation requires that the conjugate wave be of radian frequency $\omega_4 = \omega+\omega-(\omega+\delta) = \omega-\delta$. This "frequency flipping" property is the same as that discussed in Section 6.2 (for the backward-going conjugate scheme). The conservation of photon momentum results in the following phase mismatch

$$|\Delta\vec{k}|L = |\vec{k}_2(\omega) + \vec{k}_3(\omega) - \vec{k}_1(\omega+\delta) - \vec{k}_4(\omega-\delta)|L \qquad (6.A\text{-}2)$$

where L is the interaction length.

We see that due to the <u>copropagating</u> nature of the probe and conjugate fields, the vector sum of the pump wavevectors is nonzero. Therefore, aside from dispersive effects (to be discussed below), any increase in the probe wave vector magnitude (implying a frequency increase) results in a corresponding decrease in the conjugate field's wave vector, such that their sum is roughly equal to the total pump wavevector's magnitude. We therefore expect that, in general, for <u>copropagating</u> conjugate-wave schemes, the acceptable bandwidth will be <u>greater</u> than that of backward-wave (counterpropagating) conjugators. Of

course, the sacrifice to be made in the former case is that the scheme works most efficiently for one choice of propagation direction (i.e., there exist spatial-mode bandwidth limitations, as discussed in Chapter III).

To show the above bandwidth claim in more detail, we rewrite (6.A-2) as

$$|\Delta k| L = \left| \frac{\omega}{c} n(\omega) + \frac{\omega}{c} n(\omega) - \frac{(\omega+\delta)}{c} n(\omega+\delta) - \frac{(\omega-\delta)}{c} n(\omega-\delta) \right| L \qquad (6.A\text{-}3)$$

where $n(\omega)$ is the frequency-dependent linear refractive index.

If we assume that we are far from any material resonances, and that $|\delta/\omega| << 1$, we can expand the index of refraction about the pump wave frequency as

$$n(\omega \pm \delta) = n_o \pm n_o' \delta + \frac{1}{2!} n_o'' \delta^2 \pm \cdots \qquad (6.A\text{-}4)$$

where $n_o \equiv n(\omega)$; $n_o' \equiv \left.\frac{\partial n}{\partial \omega}\right|_\omega$; $n_o'' \equiv \left.\frac{\partial^2 n}{\partial \omega^2}\right|_\omega$; etc.

Using (6.A-4) in (6.A-3) yields

$$|\Delta k| L = \frac{\delta^2}{c} |2n_o' + \omega n_o''| L \qquad (6.A\text{-}5)$$

For efficient nonlinear coupling to take place (i.e. constructive interference of the distributed set of nonlinear dipoles in the medium), we require that $|\vec{\Delta k}| L \lesssim 2\pi$.

Hence, the filter bandpass subject to this condition becomes

$$\delta \lesssim \sqrt{\frac{2\pi c}{|2n_o' + \omega n_o''|L}} \qquad (6.A\text{-}6)$$

Using typical values for the dispersion of transparent media (e.g., glass) in (6.A-6) and neglecting the $\omega n_o''$ term yields a bandpass of $\sim 10^{13}$Hz or a pulse width of 0.1 psec for an interaction length of 1 cm at a wavelength of 0.5 μm. This technique therefore yields an acceptable temporal bandwidth which is nearly three orders of magnitude greater than that of the backward-going, four-wave mixing scheme considered in Section 6.3 (and to be discussed later in this appendix). The present scheme is limited, however, in its spatial-mode bandwidth.

B. Bandpass for Phase Conjugation via Forward-Going, Three-Wave Mixing

For this geometry, as shown in Figure 3A.1a, all three fields are again colinear and copropagating. The pump field complex amplitude is now given by $E_2(2\omega)$ and is at frequency 2ω, while the corresponding signal and conjugate amplitudes are given by $E_1(\omega+\delta)$ and $E_3(\omega-\delta)$. The nonlinear polarization at ω_3 for this case is given by

$$P_{NL}^{(\omega_3)} = \frac{1}{2}\chi_{NL}^{(2)} E_2(2\omega)\, E_1^*(\omega+\delta) + \text{c.c.} \qquad (6.A\text{-}7)$$

As discussed in Appendix 3A, a D.C. induced four-wave mixing geometry will yield a similar result.

Conservation of photon energy again yields a conjugate wave of frequency $\omega_3 = \omega-\delta$, and a corresponding phase mismatch as

$$|\Delta\vec{k}|L = |\vec{k}_2(2\omega) - \vec{k}_1(\omega+\delta) - \vec{k}_3(\omega-\delta)|L \qquad (6.A\text{-}8)$$

We see that since all waves are copropagating, we expect a large bandpass

for the same reasons as discussed above. However, since the pump wave is now at 2ω (as opposed to two separate pump waves each at ω), we expect the bandpass to be decreased somewhat, in general, due to dispersive effects.

Following the procedure above and using the same Taylor expansion for $n(\omega\pm\delta)$, we get the bandpass

$$\delta \lesssim \sqrt{\frac{(2\pi c/L) - 2\omega|n(2\omega) - n_o|}{|2n_o' + \omega n_o''|}} \qquad (6.A\text{-}9)$$

As expected, due to the difference in frequency of the pump and signal fields, we see a decrease in the bandpass due to the dispersion of the medium. However, this added term can be seen to vanish if the standard phase matching techniques used for three-wave nonlinear optical mixing schemes are invoked (e.g., angle or polarization tuning effects in birefringent uniaxial crystals, etc.). If this is done, then the bandwidth limitation of (6.A-6) is recovered.

C. Bandpass for Phase Conjugation via Backward-Going, Nearly Degenerate Four-Wave Mixing

For completeness, we now discuss the bandwidth limitations for the standard phase conjugate geometry as shown in Figure 3A.1c. The major difference in this approach relative to the two above schemes is that now the resultant wavevector magnitude for the pump waves is identically equal to zero. As discussed in Chapter III, it is this fact that makes this approach so attractive for phase conjugation applications, since signal waves of arbitrarily incident directions are time reversed equally (assuming an identical interaction length for all angles). However, in

terms of the filter bandpass, the zero resultant magnitude of pump wave vector considerably reduces the bandpass. This is due to the vector sum of the probe and conjugate wavevectors for this counterpropagating geometry being zero only for the degenerate case. Any deviation of the probe frequency from that of the pump waves' frequency yields a nonzero phase mismatch, even in the case of a nondispersive medium, since this phase mismatch is dependent upon the difference of the probe and conjugate wavevector magnitudes.

Recall that the phase mismatch is given by (see notation of Figure 3A.1c)

$$|\Delta\vec{k}|L = |\vec{k}_2(\omega) + \vec{k}_3(\omega) - \vec{k}_1(\omega+\delta) - \vec{k}_4(\omega-\delta)|L \qquad (6.A\text{-}10)$$

consistent with the conservation of photon energy and the desired nonlinear polarization (see Section 6.2). Since for our present geometry $\vec{k}_2 + \vec{k}_3 = 0$, equation (6.A-10) becomes

$$|\Delta k|L = \left|\frac{(\omega+\delta)}{c} n(\omega+\delta) - \frac{(\omega-\delta)}{c} n(\omega-\delta)\right|L \qquad (6.A\text{-}11)$$

Using the Taylor expansion for $n(\omega\pm\delta)$, we get

$$|\Delta k|L \simeq \frac{\delta}{c}\left|2(n_o + \omega n_o') + n_o''\delta^2\right|L \qquad (6.A\text{-}12)$$

If we (justifiably) neglect the last term in (6.A-12) we finally get the acceptable filter bandpass to be

$$\delta \lesssim \frac{\pi c}{L|n_o + \omega n_o'|} \qquad (6.A\text{-}13)$$

We therefore see that even in the absence of any material dispersion

($n_0' \rightarrow 0$), the acceptable filter bandpass is considerably less than the preceding two cases. The presence of material dispersion contributes only second order to the bandpass decrease. For the same conditions as given in the above two cases, the resultant bandpass is $\sim$9 GHz (see Section 6.2), yielding a minimum pulse width of $\sim$100 psec. This value corresponds to a data rate which is roughly three orders of magnitude less than the forward-going conjugate interactionsdiscussed above in terms of the potential use of the scheme for the compensation of channel dispersion. Recall, however, that we have considered only plane waves in this treatment. As alluded to earlier, the use of forward-going conjugate schemes can lead to spatial amplitude and phase distortions for nonplanar (i.e., multi-spatial mode) input fields. Hence, a system evaluation is necessary in order to establish the proper priorities (i.e., temporal bandwidth vs. spatial bandwidth).

Chapter VI - References

1. D. M. Bloom, P. F. Liao, and N. P. Economou, "Observation of amplified reflection by degenerate four-wave mixing in atomic sodium vapor," Opt. Lett. 2, 58 (1978).

2. D. M. Bloom, C. V. Shank, R. L. Fork, and O. Teschke, "Subpicosecond optical gating and wavefront conjugation by four-wave mixing," in Proceedings of the First Topical Meeting on Picosecond Phenomena, C. V. Shank, E. P. Ippen, and S. L. Shapiro, eds. (Springer-Verlag, Berlin, 1978).

3. A. Yariv, Quantum Electronics, 2nd ed. (Wiley, New York, 1975).

4. A. Yariv, "Four-wave mixing as real-time holography," Opt. Commun. 25, 23 (1978).

5. See, for example, F. Jenkins and H. White, Fundamentals of Optics (McGraw-Hill, New York, 1957), pp. 338-339.

6. R. P. Feynman, The Feynman Lectures in Physics (Addison-Wesley, Reading, Mass., 1963), Vol. I, pp. 30-36.

7. A. Yariv, California Institute of Technology, Pasadena, California, unpublished.

8. R. W. Hellwarth, "Four-wave mixing in optical waveguides," IEEE J. Quant. Electron. QE-15, 685 (1979).

9. J. Nilsen and A. Yariv, "Nearly degenerate four-wave mixing applied to optical filters," Appl. Opt. 18, 143 (1979); T. Y. Fu and M. Sargent III, "Effects of signal detuning on phase conjugation," Opt. Lett. 4, 366 (1979).

10. J. H. Marburger and J. R. Lam, "Effects of nonlinear index charges on degenerate four-wave mixing," Appl. Phys. Lett. 35, 249 (1979).

11. A. Yariv, Introduction to Optical Electronics, 2nd ed. (Holt, Winston, and Rinehart, New York, 1977).

12. See, for example, A. Kawasa, M. Kavachi, T. Miyasita, M. Saruwatsii, K. Asatari, J. Yamada, and K. Oe, "Pulse broadening in long-span

single-mode fibers around a material-dispersion-free wavelength," Opt. Lett. 2, 106 (1978), and references therein.

13. D. Gloge, "Propagation effects in optical fibers," IEEE Trans. Microw. Theory Tech. MTT-23, 106 (1975).

14. D. N. Payne and W. A. Gambling, "Zero material dispersion in optical fibers," Electron. Lett. 11, 177 (1975).

15. See, for example, D. Marcuse, Theory of Dielectric Optical Waveguides (Academic Press, New York, 1974).

16. T. Fukumoto and T. Suzuki, "Transmission characteristics of incoherent chirp pulses through a multimode optical fiber," Elect. & Commun. Japan 60-C, 97 (1977), and references therein.

17. See, for example, H. Bock, Network Analysis and Feedback Amplifier Design (D. Van Nostrand, New York, 1945); or F. G. Stremler, Introduction to Communication Systems (Addison-Wesley, Reading, Mass., 1977).

18. J. H. Marburger, "Optical pulse integration and chirp reversal in degenerate four-wave mixing," Appl. Phys. Lett. 32, 372 (1978).

19. For a recent review, see N. Bloembergen and M. D. Levenson in Topics in Applied Physics, Vol. 13: High Resolution Laser Spectroscopy, ed. by K. Shimoda (Springer-Verlag, Berlin, 1976).

20. A. Yariv and J. AuYeung, "Transient four-wave mixing and real-time holography in atomic systems,"IEEE J.Quant. Electron. QE-15, 224 (1979).

21. See, for example, R. G. Brewer, and E. L. Hahn, "Coherent two-photon processes: Transient and steady-state cases," Phys. Rev. A 11, 1641 (1975).

22. P. F. Liao, N. P. Economou, and R. R. Freeman, "Two-photon coherent transient measurements of Doppler-free linewidths with broadband excitation," Phys. Rev. Lett. 39, 1473 (1977).

23. D. G. Steel and J. F. Lam, "Two-photon coherent transient measurements of the nonradiative collisionless dephasing rates in SF_6 via

Doppler-free degenerate four-wave mixing," Phys. Rev. Lett. 43, 1588 (1979).

24. M. D. Levenson, "Optical beating spectroscopy of polarizabilities produced by two-photon absorption," Phys. Rev. A 13, 2314 (1976).

25. S. M. Jensen and R. W. Hellwarth, "Observation of the time-reversed replica of a monochromatic optical wave," Appl. Phys. Lett. 32, 166 (1978).

26. D. C. Haneisen, "Doppler-free two-photon spectroscopy using degenerate four-wave mixing," Opt. Commun. 28, 183 (1979).

27. M. M. Salour, "Quantum interference effects in two-photon spectroscopy," Rev. Mod. Phys. 50, 667 (1978).

28. See, for example, V. P. Chebotaev, A. V. Shishayev, B. Ya. Yurshin, and L. S. Vasilenko, "Observation of two-photon absorption resonance in spatially separated fields," Appl. Phys. 15, 43 (1978), and references therein; also, Nonlinear Laser Spectroscopy (Springer-Verlag, Berlin, 1977).

29. P. F. Liao, J. E. Bjorkholm, and J. P. Gordon, "Observation of two-photon optical free-induction decay in atomic sodium vapor," Phys. Rev. Lett. 39, 15 (1977).

30. M. D. Levenson, "Saturation dips in optical transient signals," Appl. Phys. 15, 13 (1978).

31. A. H. Zewail, T. E. Orlowski, K. E. Jones, and D. E. Godar, "Spontaneously detected photon echoes in excited molecular ensembles: A probe pulse laser technique for the detection of optical coherence of inhomogeneously broadened electronic transitions," Chem. Phys. Lett. 48, 256 (1977).

32. T. Mossberg, A. Flusberg, T. Kachru, and S. R. Hartmann, "Tri-level echoes," Phys. Rev. Lett. 48, 1523 (1978).

33. M.M.T. Loy, "Two-photon coherent transients," IBM J. Res. & Dev. 23, 504 (1979); also, in Laser Spectroscopy III, eds. J. L. Hall and J. L. Carlsten (Springer-Verlag, Berlin, 1977), p. 435.

34. R. G. DeVoe and R. B. Brewer, "Subnanosecond optical free-induction decays," IBM J. Res. & Dev. 23, 527 (1979).

35. We note that Juan F. Lam has subsequently analyzed PCO via a TPCS including both saturation as well as atomic motion effects. To be published in Phys. Rev. A.

36. H. P. Yuen and J. H. Shapiro, "Generation and detection of two-photon coherent states in degenerate four-wave mixing," Opt. Lett. 4, 334 (1979).

Chapter VII

THE PHASE CONJUGATE RESONATOR: A SPATIAL/TEMPORAL DOMAIN APPLICATION OF PHASE CONJUGATE OPTICAL INTERACTIONS

7.1 Introduction

In this chapter, we will focus upon an application of phase conjugate optics that realizes many of the major features of this interaction mentioned in the previous chapters. Specifically, we consider the case of laser oscillation in a resonator in which one of the mirrors is replaced by a phase conjugate reflector which utilizes four-wave mixing. There are several characteristics that make this resonator configuration especially attractive. The well-known "time-reversal" feature, and hence the spatial domain application(s) discussed earlier of the conjugator serves not only to compensate for various potential intracavity phase aberrating elements (e.g., gain medium phase and/or polarization distortion, poor quality optical components, etc.), but also gives rise to profound differences in the resonator stability criterion as compared to conventional Fabry-Perot laser resonators [1]. Further, the frequency filtering nature and the associated temporal domain features of the conjugator yields a type of "frequency locking" of the resonator output frequency to the frequency of the pump laser (which excited the conjugate mirror). It also renders the transverse modes present in the resonator to be degenerate in frequency, thus giving rise to a "transverse mode-locking" condition, which enables the mode volume in the resonator to "fit" into an aperture (subject to the limitations imposed on the angular acceptance range of the conjugate mirror). If the effective

aperture within the resonator is chosen to be the transverse gain profile, for example, then the use of a phase conjugate mirror can essentially "milk" the gain medium optimally for its stored energy. Finally, by temporally pumping the conjugate mirror, one can Q-switch this "phase conjugate resonator," PCR. In the next section, we present an analysis for this type of resonator which, using the Gaussian beam propagation formalism, considers resonator stability conditions, longitudinal and transverse mode spectra, and the frequency dependence of the phase conjugate mirror. This will be followed by a discussion of an experiment performed using a ruby laser as the pump source, and carbon disulfide as the conjugator's nonlinear medium. Laser oscillation was observed in a resonator configuration which was unstable in the conventional sense. Further, we observe a laser output energy that is comparable with that of a similar, conventional Fabry-Perot laser. Several additional observed aspects regarding the resonator will be discussed, including frequency locking of the oscillator output to the pump beams, and Q-switching properties due to the pulsed nature of the conjugate mirror.

Finally, in an appendix at the end of this chapter, we will discuss briefly a special, yet important case dealing with phase conjugate mirror geometries; that of the ray matrix for a phase conjugate mirror as generated by Gaussian spatially-dependent pump beams. The resultant "Gaussian tapered" reflectivity nature of the conjugate mirror has important consequences in terms of the modal characteristics when used in place of a conventional mirror that forms a laser resonator.

7.2 PCR Stability Criteria and Mode Spectra

In this section, we present a derivation of resonator stability criteria and mode spectra of a laser resonator in which one of the mirrors is replaced by a phase conjugate mirror, "PCM." The geometry of this phase conjugate resonator, "PCR," is shown in Figure 7.1. The PCM is assumed to be formed via a degenerate four-wave nonlinear optical interaction. The conjugate wave (of field E_i), E_r, is generated as a result of the simultaneous incidence of two counter-propagating plane waves, A_1 and A_2, with E_i onto a medium possessing a third-order nonlinear optical susceptibility, $\chi_{NL}^{(3)}$, all located within the PCM (as shown in Figure 7.1). In the analysis that follows, we neglect the depletion of the pump waves A_1 and A_2 as a result of the nonlinear interaction. We also neglect diffraction losses within the PCR, and self-focusing within the PCM. We further assume that the nonlinear medium is nondispersive, and is also capable of instantaneous response.

A. Matrix of the PCM (degenerate case)

We first discuss a matrix formalism that describes the operation of the PCM for the case where all the interacting fields are of the same radian frequency, ω. The stability criterion is then derived for both one and two round-trip self-consistent situations.

Consider a Gaussian field, E_i, propagating along the z-axis, to be

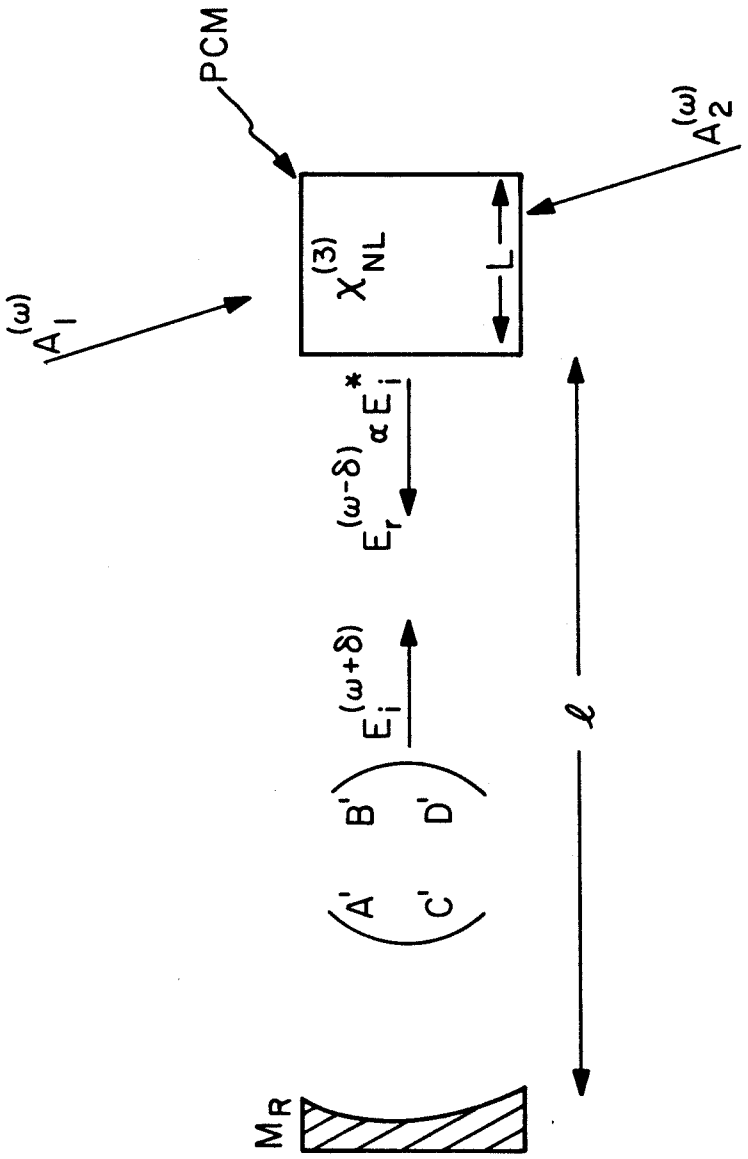

Fig. 7.1 The phase conjugate resonator (PCR). This general resonator is formed by surrounding some arbitrary optical components, denoted by an equivalent A'B'C'D' ray matrix, by a "real" mirror (of radius R) on one end, and a phase conjugate mirror (PCM) on the other end. For degenerate modes, $\delta = 0$.

incident upon the PCM. The beam field is described by [1]

$$E_i = \varepsilon_i(\vec{r}) \exp[i(\omega t - kz - \frac{kr^2}{2\rho(z)}) - \frac{r^2}{w^2(z)}] \qquad (7.2\text{-}1)$$

where $\varepsilon_i(\vec{r})$ is the complex amplitude of E_i (which may include any transverse mode dependence); ρ and w are the radius of curvature and the spot size of the incident field, respectively. This field can also be written as

$$E_i = \varepsilon_i(\vec{r}) \exp[i(\omega t - kz - \frac{kr^2}{2q_i})] \qquad (7.2\text{-}2)$$

The complex radius of curvature q_i is defined as

$$\frac{1}{q_i(z)} = \frac{1}{\rho(z)} - \frac{i\lambda}{\pi w^2(z)} \qquad (7.2\text{-}3)$$

The effect of the PCM is to "reflect" such an incident field so as to yield its conjugate replica as discussed in Chapter III, leaving the wave front and the spot size unchanged. The reflected field is thus

$$E_r \propto \varepsilon_i^*(\vec{r}) \exp[i(\omega t + kz + \frac{kr^2}{2\rho}) - \frac{r^2}{w^2}] \qquad (7.2\text{-}4)$$

which can also be expressed as

$$E_r \propto \varepsilon_i^*(\vec{r}) \exp[i(\omega t + kz - \frac{kr^2}{2q_r})] \qquad (7.2\text{-}5)$$

The reflected field complex radius of curvature subject to (7.2-3) and (7.2-4) is given by

$$\frac{1}{q_r} = -\frac{1}{\rho} - \frac{i\lambda}{\pi w^2} = -\frac{1}{q_i^*} \tag{7.2-6}$$

An observer traveling with the reflected beam will find the spot size unchanged, but will see an opposite sign for the curvature of the wave front.

If we introduce the ABCD matrix formalism [1,6], the (reflection) effect of the PCM can be represented by the matrix

$$\underset{\approx}{M} = \begin{pmatrix} A & B \\ C & D \end{pmatrix} = \begin{pmatrix} 1 & 0 \\ 0 & -1 \end{pmatrix} \tag{7.2-7}$$

with the output and input q-parameters related by

$$q_r = \frac{Aq_i^* + B}{Cq_i^* + D} \tag{7.2-8}$$

Note the conjugation operation upon q_i, as opposed to the conventional formalism [1] where the input field is not conjugated. We note that this matrix also describes the reflection of rays from the conjugate mirror. That this matrix (7.2-7) and the condition given by (7.2-8) satisfy the constraint (7.2-6) can be easily verified by substitution.

It follows directly that the ordinary ABCD formalism for treating the propagation of Gaussian beams through a sequence of lens-like media [6] can be applied also in the case when one of the elements is a PCM. The matrix representing the PCM is given by (7.2-7). The "q" parameter at any plane following the PCM is related to the input "q" by

$$q_{out} = \frac{A_T q_i^* + B_T}{C_T q_i^* + D_T} \tag{7.2-9}$$

where the subscript "T" implies that the matrix elements correspond to that of the resultant matrix for the given sequence of optical elements, including that of the PCM.

Since all the matrices thus far are assumed to be real, the conjugation operation imposed by (7.2-9) can be performed at any plane. We note that care must be taken when treating propagation through media described by matrices having complex elements. An example of such a matrix will be discussed (when considering Gaussian pump beams) in Appendix 7B. In this case, one must first evaluate the complex

q-parameter just prior to the PCM (using the conventional formalism), apply the operations given by (7.2-7 and 8) to describe the effect of the PCM, then finally evaluate the resultant q-parameter at the desired plane "after" the PCM.

B. Stability Condition for One Round Trip (degenerate case)

In this section, we will derive the stability condition for the PCR, assuming that one round trip of the field is required to define an eigenmode of the cavity. In this and the next section, we will restrict our discussion to the degenerate case. That is, all the interacting fields (viz. the pump, signal, and conjugate waves) are of the same radian frequency.

Consider the situation sketched in Figure 7.1. The resonator is bounded on one end by a mirror having a radius of curvature R, containing arbitrary intracavity optical components described collectively by an A'B'C'D matrix, $\underset{\approx}{M}'$, for optical propagation from left to right, and again by $\underset{\approx}{M}''$, for propagation from right to left. The resonator is bounded on the other end by a PCM. In order to investigate the stability criterion for such a cavity, we apply the standard self-consistent formalism in which we demand that the complex radius of curvature of the beam reproduce itself after one round trip. Choosing a plane to the immediate right of the real mirror, we trace a beam that propagates to the right and get, after one round trip, the following matrix product:

$$\underset{\approx}{M}_1 = \begin{pmatrix} A_1 & B_1 \\ C_1 & D_1 \end{pmatrix} = \begin{pmatrix} 1 & 0 \\ \frac{-2}{R} & 1 \end{pmatrix} \begin{pmatrix} A'' & B'' \\ C'' & D'' \end{pmatrix} \begin{pmatrix} 1 & 0 \\ 0 & -1 \end{pmatrix} \begin{pmatrix} A' & B' \\ C' & D' \end{pmatrix} \tag{7.2-10a}$$

$$= \begin{pmatrix} 1 & 0 \\ \frac{-2}{R} & 1 \end{pmatrix} \begin{pmatrix} 1 & 0 \\ 0 & -1 \end{pmatrix} \tag{7.2-10b}$$

where we have used the relation

$$\underset{\approx}{M''}\underset{\approx}{M} = \underset{\approx}{M}(\underset{\approx}{M'})^{-1} \tag{7.2-10c}$$

which can be shown straightforwardly, using the reciprocity property of the group of optical elements represented by $\underset{\approx}{M'}$ (or $\underset{\approx}{M''}$), where M is given by (7.2-7). The derivation of equation (7.2-10c) is sketched in Appendix 7A.

The above result [equation (7.2-10b)] is merely a reaffirmation of the fact that an arbitrary sequence of passive and lossless optical elements followed by a PCM is equivalent to the PCM alone. This is due to the time reversal occurring at the PCM and the reciprocity of the passive components.

Now we impose self-consistency; that is, we demand that the field be reproduced at the aforementioned plane after one round trip. Using (7.2-8) this condition is

$$\frac{1}{q} = \frac{C_1 + D_1/q^*}{A_1 + B_1/q^*} \tag{7.2-11}$$

The result of this constraint yields the following two conditions:

$$A_1 + D_1 = 0 \tag{7.2-12a}$$

and

$$B_1\left[\frac{1}{\rho^2} + \left(\frac{\lambda}{\pi w^2}\right)^2\right] + (A_1 - D_1)\frac{1}{\rho} - C_1 = 0 \tag{7.2-12b}$$

Using the values of A_1, B_1, C_1, and D_1 from (7.2-10) in equation (7.2-12), we get

$$\rho = -R \quad . \tag{7.2-13}$$

Hence, the radius of curvature of the Gaussian beam is equal to that of the real mirror at the real mirror's plane. This conclusion is also independent of the sign of the mirror's curvature. Also, there is no dependence of the stability conditions upon the cavity length or any other optical components within the cavity. In addition, there is no constraint on the spot size (w) of the resultant mode (subject to the angular acceptance limitations of the PCM). This freedom of spot size in conjunction with the frequency degeneracy of the transverse modes at the pump frequency (to be discussed later), leads to the concept of "spatial mode locking" of transverse modes. In Figure 7.2a, we sketch a typical Gaussian mode that is self-consistent for the one-round-trip, degenerate frequency case.

C. Stability Condition for Two Round Trips (degenerate case)

In conventional resonators, all allowed eigenmodes are obtained by demanding a single round trip self-consistent solution. However,

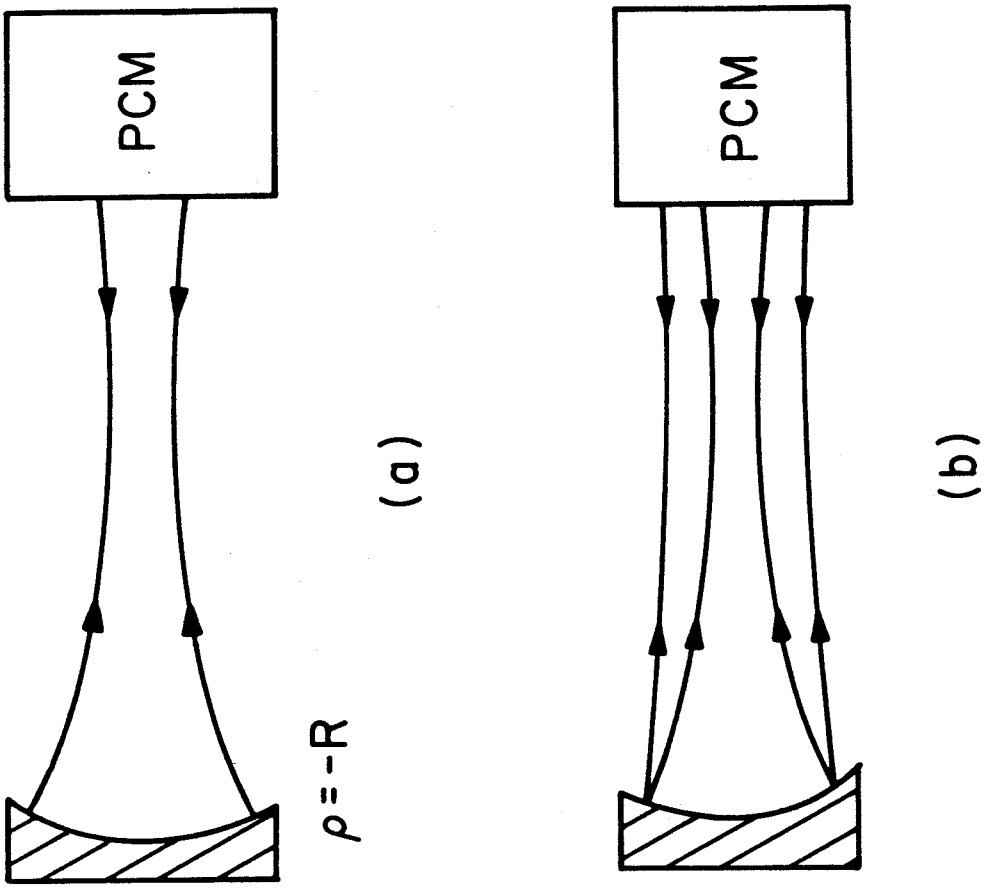

Fig. 7.2 Sketch of a typical allowed PCR Gaussian mode for the degenerate case and demanding self-consistent field solutions for one (a) and two (b) round trips.

for the case of a PCR, it is possible to have allowed modes which will reproduce themselves after two round trips. Furthermore, by simple ray tracing, it can be shown that, due to the time-reversing nature of the PCM, these rays will reproduce themselves after two round trips. Thus, for two round trips, and for the case of degenerate fields, we can use the matrix from the preceding section, forming the resultant matrix as

$$\begin{aligned} \underset{\approx}{M}_2 &= (\underset{\approx}{M}_1)^2 \\ &= \underset{\approx}{I} \end{aligned} \tag{7.2-14}$$

where $\underset{\approx}{I}$ is the identity matrix. We note that, since for a two round-trip situation, we have encountered the PCM twice, the q-parameters have been conjugated two times and thus remain unchanged. Hence, in contrast to the single round trip constraints, any complex radius of curvature, (i.e., both ρ and w) at the initial plane (at the real mirror) will yield a self-consistent solution. We therefore conclude (as was the case for the one-round-trip constraint) that the PCR is stable for any real mirror, regardless of its radius of curvature or sign, and is stable regardless of the cavity length or the intracavity optical components. In Figure 7.2b, we sketch an allowed Gaussian mode that satisfies the two-round-trip degenerate frequency case.

We thus see that there exists a large range of Gaussian beam parameters that satisfy the self-consistency criterion for both the one- and two-round trip cases. This multitude of acceptable solutions follows from the very nature of the PCM. Since we have specified only one constraint within the resonator (in this case the radius of curvature of the real mirror), and realizing that the action of

the PCM is to replicate any field incident upon its surface, there exists no unique set of ρ and w within the resonator. This is in contrast to conventional resonators, where, in general, the curvature is specified at two planes in space, which determines uniquely the complex beam radius everywhere in space.

We have not taken into account any additional constraints within the PCR, which can be due to several sources; one can, for example, place an aperture within the resonator. In addition, the PCM itself can possess an effective aperture due to, for example, the spatial extent of the pump beams. This latter point will be considered in Appendix 7B. Another possibility can be the "effective aperture" introduced by the gain medium (i.e., the transverse gain profile). We note that in this case, the action of the PCM is to form a mode volume within the resonator that interacts with as much of the gain medium as possible, while still being above threshold. Hence, in this configuration, the PCR can be capable of most efficiently extracting the stored laser energy within a given gain medium.

D. Ray Matrix for the PCM (nondegenerate case)

We now treat the self-consistency requirement for one and two round trips within the PCR for the case of nondegenerate fields. Knowledge of the stability condition for nondegenerate fields is relevant to analyzing PCR "modes" that are not at the pump frequency (to be considered later). We consider the case where the pump waves

exciting the PCM are both at radian frequency, ω, while the PCR field incident upon the PCM is at radian frequency $\omega+\delta$, where δ can be greater than or less than 0. Due to the frequency flipping nature of the PCM as discussed in Section 6.2, the conjugate field is at frequency $\omega-\delta$. The phase matching constraint requires that each plane wave component of a given signal field incident upon the PCM give rise to a "conjugate replica" whose $\vec{k}$-vector is antiparallel to that of the input plane wave component considered. This applies to both the degenerate (see Section 3.3) and the nondegenerate (see Section 6.2) cases. Thus, the ray matrix given by (7.2-7) can also be used to describe the effect of the PCM for each plane wave component (or ray) for the nondegenerate case. However, for the nondegenerate case of an arbitrary incident wavefront, the "reflected" field no longer exactly retraces the path of the input wave, due to their difference in frequency.

This problem can be treated formally by decomposing the input field into its plane wave components, using (7.2-7) for the effect of the PCM for each of these components, changing $\omega+\delta$ to $\omega-\delta$, then finally forming the resultant superposition.

In what follows, we show that for the special case of Gaussian beams, one can form a frequency-dependent ABCD "ray" matrix that properly describes the effects of the PCM. Consider an incident Gaussian beam of the form [1,6]

$$E_i = \varepsilon(\vec{r}) \exp\{i[(1 + \frac{\delta}{\omega})\omega t - (1 + \frac{\delta}{\omega})kz - (1 + \frac{\delta}{\omega}) \frac{kr^2}{2q_i}]\}, \quad (7.2\text{-}15)$$

where $k = \omega n/c$.

The "reflected" field from the PCM (located at z = 0) is given by

$$E_r \propto \varepsilon^*(\vec{r})\exp\{i[(1 - \tfrac{\delta}{\omega})\omega t + (1 - \tfrac{\delta}{\omega})kz - (1 + \tfrac{\delta}{\omega})\frac{kr^2}{2(-q_i^*)}]\} \quad . \quad (7.2\text{-}16)$$

This can be rewritten as

$$E_r \propto \varepsilon^*(\vec{r})\ \exp\{i[(1 - \tfrac{\delta}{\omega})\omega t + (1 - \tfrac{\delta}{\omega})kz - (1 - \tfrac{\delta}{\omega})\frac{kr^2}{2q_r}]\} \quad . \quad (7.2\text{-}17)$$

This reflected field is thus recognized as being a Gaussian beam at frequency $\omega(1 - \frac{\delta}{\omega})$, having a complex radius of curvature, q_r, which can be related to q_i by

$$q_r = -q_i^* \frac{(1 - \delta/\omega)}{(1 + \delta/\omega)} \quad . \quad (7.2\text{-}18)$$

The "ray" matrix that relates q_i to q_r which satisfies equations (7.2-15 to 18) can be represented by

$$\underset{\approx}{M} = \begin{pmatrix} 1 - \frac{\delta}{\omega} & 0 \\ 0 & -(1 + \frac{\delta}{\omega}) \end{pmatrix} \quad , \quad (7.2\text{-}19)$$

where the operation given in equation (7.2-8) is to be used. We note that as $\delta \to 0$, equation (7.2-19) reduces to the degenerate-case matrix, given by equation (7.2-7). It can be shown that the effect of the PCM is to change the radius of curvature (at the output boundary of the PCM) while leaving the spot size unchanged (this

follows from the frequency-flipping effect of the PCM). As discussed above, we remark that equation (7.2-19) applies to Gaussian beams and not to rays (since applying (7.2-19) to a ray changes the "reflected" slope magnitude, which violates the phase matching constraint discussed at the beginning of this subsection).

E. Stability Condition for One Round Trip (nondegenerate case)

Following the discussion given for the degenerate case, we can now solve for the self-consistency constraint for the nondegenerate situation. Demanding replication after one round trip, we now consider an explicit resonator configuration. For the ease of calculation, we set the M' and M" matrices of Section 7.2B to represent cavity spacing of length ℓ. That is [1,6]

$$\underset{\approx}{M}' = \underset{\approx}{M}'' = \begin{pmatrix} 1 & \ell \\ 0 & 1 \end{pmatrix} \tag{7.2-20}$$

For this choice of the cavity matrix, the total single round trip matrix evaluated at the real mirror plane is given by

$$M_1 = \begin{pmatrix} 1 & 0 \\ -\frac{2}{R} & 1 \end{pmatrix}\begin{pmatrix} 1 & \ell \\ 0 & 1 \end{pmatrix}\begin{pmatrix} 1-\frac{\delta}{\omega} & 0 \\ 0 & -(1+\frac{\delta}{\omega}) \end{pmatrix}\begin{pmatrix} 1 & \ell \\ 0 & 1 \end{pmatrix}$$

$$= \begin{pmatrix} 1-\frac{\delta}{\omega} & -2\ell\frac{\delta}{\omega} \\ -\frac{2}{R}(1-\frac{\delta}{\omega}) & \frac{\delta}{\omega}(\frac{4\ell}{R}-1)-1 \end{pmatrix} \tag{7.2-21}$$

The self-consistency criterion, equation (7.2-11), yields the

same conditions [equations (7.2-12a,b)] as for the degenerate case. Using the resultant matrix [equation (7.2-21)] in first condition [equation (7.2-12a)] gives the constraint $\ell = R/2$. Substitution of this result into the second condition [equation (7.2-12b)] does yield a range of (ρ,w) pairs which satisfy the equation. However, due to the frequency-flipping nature of the PCM, any (ρ,w) pair at frequency $\omega+\delta$ will not replicate itself after a second round trip, i.e., at frequency $\omega-\delta$. That is, there is no common (ρ,w) pair that satisfies the self-consistency requirement for both $\pm\delta$ frequency components.

We thus conclude that no stable mode exists for the one-round-trip, nondegenerate case.

F. Stability Condition for Two Round Trips (nondegenerate case)

In considering the nondegenerate two-round-trip stability condition, we cannot simply take the square of the single-round-trip matrix, equation (7.2-21) (as was done in the degenerate frequency case). This is due to the frequency-flipping nature of the PCM. That is, upon each "reflection" off the PCM, the field changes frequency. Hence, the total two-round-trip matrix, using equation (7.2-20) to describe the intracavity propagation, becomes

$$\underset{\approx}{M}_2 = \begin{pmatrix} A_2 & B_2 \\ C_2 & D_2 \end{pmatrix} = \begin{pmatrix} 1+\frac{\delta}{\omega} & 2\ell\frac{\delta}{\omega} \\ -\frac{2}{R}\left(1+\frac{\delta}{\omega}\right) & -\frac{\delta}{\omega}\left(\frac{4\ell}{R}-1\right)-1 \end{pmatrix} \begin{pmatrix} 1-\frac{\delta}{\omega} & -2\ell\frac{\delta}{\omega} \\ -\frac{2}{R}\left(1-\frac{\delta}{\omega}\right) & \frac{\delta}{\omega}\left(\frac{4\ell}{R}-1\right)-1 \end{pmatrix} \tag{7.2-22}$$

where the second matrix has $\delta \to -\delta$, consistent with the above remark.

We note that since we have encountered the PCM twice, the conjugation operation is effectively cancelled. Thus, the applicable self-consistency criterion corresponds to that of conventional resonators [1,6], and is given by

$$\frac{1}{q} = \frac{D_2 - A_2}{2B_2} \pm i \sqrt{-\left(\frac{D_2 - A_2}{2B_2}\right)^2 - \frac{C_2}{B_2}} \qquad (7.2\text{-}23)$$

Substituting the resultant matrix [equation (7.2-22)] into the self-consistency condition, equation (7.2-23), yields $\rho = -R$; i.e., the Gaussian beam curvature at the mirror is equal to that of the real mirror radius of the curvature at each round trip, and is independent of the frequency offset, δ. However, the spot size (evaluated at the real mirror) does depend on the frequency offset and can be shown to be

$$w = \sqrt{\frac{c}{\pi(\omega+\delta)}} \left\{ \frac{1}{R}\left(\frac{1}{R} - \frac{1}{\ell}\right) \left[\frac{1 - \frac{\delta}{\omega}\left(1 - \frac{2\ell}{R}\right)}{1 + \frac{\delta}{\omega}\left(1 - \frac{2\ell}{R}\right)} \right] \right\}^{-1/4} . \qquad (7.2\text{-}24)$$

From equation (7.2-24) we get the following condition for stable modes to exist

$$\begin{aligned} &\ell > R \ ; && \text{for } R > 0 \\ &\text{all } \ell \ ; && \text{for } R < 0 \end{aligned} \qquad (7.2\text{-}25)$$

We thus conclude that for nondegenerate fields, the PCR is stable for two round trips only over limited ranges of cavity length (for a given mirror radius). Furthermore, the radius of curvature of the

mode always matches that of the real mirror; however, the spot size alternates between two values for each round trip [by using $\pm\delta$ in equation (7.2-24)].

In Figure 7.3 we sketch a typical stable Gaussian mode for the nondegenerate, two-round-trip, self-consistent condition.

We note that when $\delta = 0$, equation (7.2-24) is no longer valid since the matrix element $B_2 = 0$ [see equation (7.2-23)]. In this limit, the discussion presented in Section 7.2C applies.

G. Longitudinal and Transverse PCR Mode Spectra

In this section, we derive the PCR longitudinal and transverse mode spectra for Gaussian beams. Due to the frequency-flipping nature of the PCM, a given frequency component (e.g., at $\omega+\delta$) requires two round trips to return to its initial frequency. Alternatively, if we assume two fields to co-exist (i.e., at $\omega\pm\delta$) we can then superpose these fields and thus require that this superposition repeat only after one round trip. Referring to Figure 7.1, we assume that the PCR is of length and linear index, ℓ and n_c, respectively; the PCM is of length and linear index, L and n, respectively.

We represent the p,qth transverse mode of the total field at the real mirror (located at the $z = z_1$ plane) as the following superposition (of the $\omega\pm\delta$ frequency components) of the well-known Hermite-Gaussian eigenmodes [1,6]

$$E_{p,q}(x,y,z=z_1) = \sum_{\pm} E_o \left(\frac{w_o}{w(z)}\right)_{\pm} H_p\left(\frac{\sqrt{2}\,x}{w(z)}\right)_{\pm} H_q\left(\frac{\sqrt{2}\,y}{w(z)}\right)_{\pm} \tag{7.2-26}$$

$$\times \exp\left[i(\omega\pm\delta)t - \frac{x^2+y^2}{w_{\pm}^2(z)} - \frac{ik_{\pm}(x^2+y^2)}{2R_{\pm}(z)} - ik_{\pm}z + i(p+q+1)\tan^{-1}\left(\frac{z_1}{z_o}\right)_{\pm}\right]$$

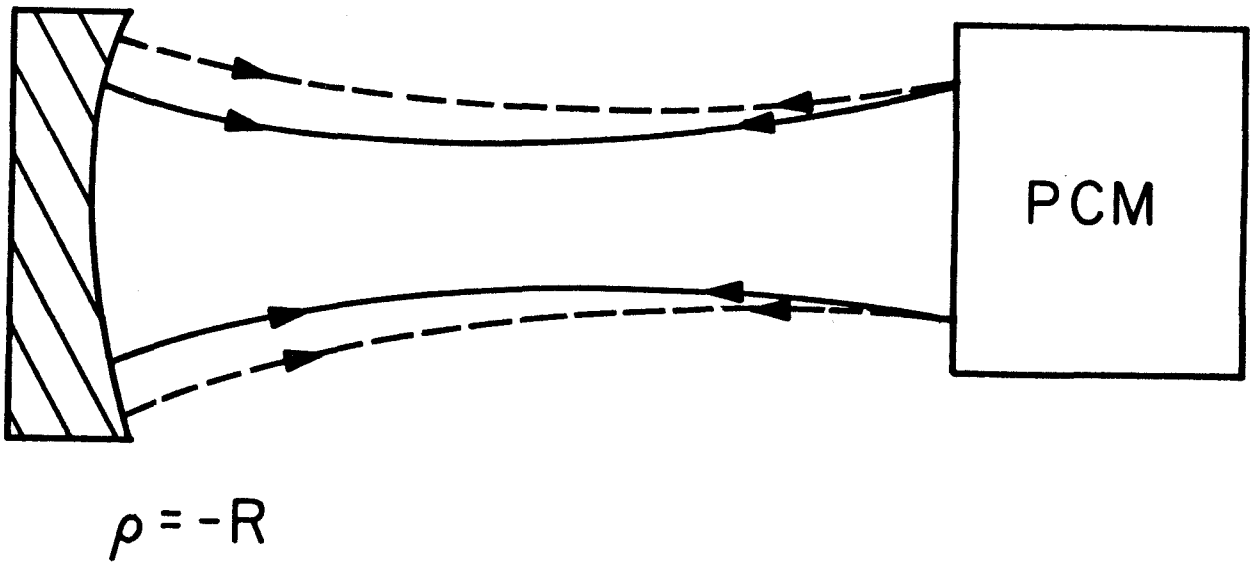

Fig. 7.3 Sketch of a typical allowed PCR Gaussian mode for the nondegenerate case. The solid and dashed lines correspond to a positive ($\delta > 0$) and negative ($\delta < 0$) frequency offset, respectively. Note that at the real mirror end, $\rho(\delta > 0) = \rho(\delta < 0)$; while at the PCM, $w(\delta > 0) = w(\delta < 0)$, consistent with a two-round-trip, self-consistent solution. Recall that for the nondegenerate case, there does not exist a solution which satisfies the single-round-trip constraint

The summation is taken over the two frequencies, $\omega \pm \delta$.

In (7.2-26) H_p is the Hermite polynomial of order p, and [1,6]

$$w^2(z) = w_o^2\left(1 + \frac{z^2}{z_o^2}\right)$$

$$R(z) = z\left(1 + \frac{z_o^2}{z^2}\right) \qquad (7.2\text{-}27)$$

and

$$z_o = \frac{\pi w_o^2 n_c}{\lambda}$$

$w(z)$ and $R(z)$ are the z dependent beam spot size and radius of curvature, respectively. Equation (7.2-26) can be rewritten as

$$E(z=z_1) = \sum_{\pm} A_{\pm} \exp\{i(\omega \pm \delta)t + i\theta_{\pm}\} \qquad (7.2\text{-}28)$$

where we have dropped the p,q mode labels for convenience and the summation implies that the upper (lower) signs correspond to the $+\delta(-\delta)$ components of the total field.

This total Gaussian field is now propagated to the right by a distance ℓ, and is incident upon the PCM, located at the plane $z = z_2$.

The effect of the PCM (in addition to the previously mentioned properties) is to multiply the field by a complex frequency-dependent reflectivity, $R_{\pm} e^{i\phi_{\pm}}$ given by [see equation (6.2-6)]

$$R_{\pm} = \frac{2\pi}{nc}(\omega \mp \delta)\left|\chi_{NL}^{(3)} A_1 A_2 \tan(\beta L)\right| \left\{\beta^2 + \left(\frac{n\delta}{c}\right)^2 \tan^2(\beta L)\right\}^{-1/2} \qquad (7.2\text{-}29a)$$

and

$$\phi_{\pm} = -\frac{\pi}{2} + \eta \pm \tan^{-1}\left[\frac{n\delta}{c\beta}\tan(\beta L)\right] \quad , \tag{7.2-29b}$$

where

$$\beta = \left\{\left(\frac{2\pi}{nc}\right)^2 \left|\chi^{(3)}_{NL} A_1 A_2\right|^2 (\omega^2-\delta^2) + \left(\frac{n\delta}{c}\right)^2\right\}^{1/2} \tag{7.2-30}$$

and η is the phase of $\chi^{(3)}_{NL} A_1 A_2 \tan(\beta L)$. In equation (7.2-29) the $(\pm)$ subscript implies that the field incident upon the PCM is of radian frequency $\omega\pm\delta$, while the "reflected" field is of radian frequency $\omega\mp\delta$, where ω is the pump frequency (of fields $A_{1,2}$), as derived in Section 6.2.

The resultant field after "reflection" from the PCM (at $z=z_2$) is given by

$$E(z=z_2) = \sum_{\pm} R_{\mp} A_{\mp} \exp\left\{i(\omega\pm\delta)t + i\phi_{\mp} - i\theta_{\mp} + i(\omega\mp\delta)n_c\ell/c \right.$$
$$\left. -i(p+q+1)\left[\tan^{-1}\left(\frac{z_2}{z_0}\right)_{\mp} + \tan^{-1}\left(\frac{z_1}{z_0}\right)_{\mp}\right]\right\} \tag{7.2-31}$$

This field is now propagated back to the left, reflected off the real mirror, represented by a complex reflectivity $re^{i\gamma}$, and then evaluated again at the initial plane, $z=z_1$. The resultant field is

$$E(z=z_1) = \sum_{\pm} r\, R_{\mp} A_{\mp} \exp\Big\{ i(\omega \pm \delta)t + i\phi_{\mp} - i\theta_{\mp} + i\gamma$$

$$+ i(\omega \mp \delta)\, n_c \ell/c - i(\omega \pm \delta) n_c \ell/c$$

$$- i(p+q+1)\left[\tan^{-1}\left(\frac{z_2}{z_o}\right)_{\mp} + \tan^{-1}\left(\frac{z_1}{z_o}\right)_{\mp} - \tan^{-1}\left(\frac{z_2}{z_o}\right)_{\mp} - \tan^{-1}\left(\frac{z_1}{z_o}\right)_{\pm}\right]\Big\}$$

(7.2-32)

We now impose the self-consistency requirement, which states that the total phase shift acquired by each given frequency component of the field (relative to its respective initial phase) be equal to an interger times 2π. From equations (7.2-28 and 7.2-32), this condition implies that

$$\theta_{\pm} - \phi_{\pm} + \theta_{\mp} - \gamma - [(\omega \mp \delta) - (\omega \pm \delta)]\, n_c \ell/c$$

$$+ (p+q+1)\left[\tan^{-1}\left(\frac{z_2}{z_o}\right)_{\mp} + \tan^{-1}\left(\frac{z_1}{z_o}\right)_{\mp} - \tan\left(\frac{z_2}{z_o}\right)_{\mp} - \tan^{-1}\left(\frac{z_1}{z_o}\right)_{\pm}\right]$$

$$= 2\pi m_{\pm} \qquad (7.2\text{-}33)$$

where m_+ and m_- are (in general) two different integers. Now, subtracting the $(-\delta)$ component (lower sign) from the $(+\delta)$ component (upper sign) in (7.2-33), setting $m_+ - m_- \equiv m$, and substituting the expressions for $\phi_{\pm}$ from (7.2-29) into the resultant expression yields the following self-consistency condition upon the PCR mode spectra

$$\tan^{-1}\left\{\frac{2\pi n\Delta\nu_m}{c\beta_m}\tan(\beta_m L)\right\} + \frac{4\pi n_c \ell\,\Delta\nu_m}{c}$$

$$+ (p+q+1)\tan^{-1}\left\{\frac{\frac{4\pi\Delta\nu_m \ell}{\omega R}\sqrt{1-\frac{R}{\ell}}}{\left[1-\left(\frac{2\pi\Delta\nu_m}{\omega}\right)^2\left(1-\frac{2\ell}{R}\right)^2\right]^{1/2}}\right\} = m\pi \qquad (7.2\text{-}34)$$

where $\Delta\nu_m = \delta/2$, (p,q) corresponds to the transverse mode indices of the Gaussian beam [1,6], and m is an integer.

The resultant set of PCR modes [corresponding to a mode set (m,p,q)] of frequency $\omega/2\pi + \Delta\nu_{m,p,q}$ is thus given by the solutions to equation (7.2-34). We first see that for m=0 (i.e., $\Delta\nu_m = 0$) <u>all</u> the transverse modes (p,q) are at the <u>same</u> frequency (i.e., equal to the pump frequency,ω). Thus, in contrast to conventional resonators (where for a given longitudinal mode each transverse mode has a different frequency) the PCR transverse modes (for m=0) are <u>degenerate</u> in frequency. This gives rise to the possibility of a"spatial transverse mode locking condition." If a number of transverse modes (i.e., modes with different values of p,q) exist, all with m=0, then the resulting spatial field distribution due to the superposition of these modes will be stationary in time. The possibility of an oscillation field made up of a superposition of degenerate transverse modes with arbitrary waists and waist locations affords a great deal of flexibility for the mode to assume spatial distributions which will optimally milk a given gain medium or avoid an obstruction, even under dynamic conditions.

This result is consistent with the fact that the conjugate mirror enables one to "time-reverse" a given field at ω; we have merely expressed a general field as a superposition of transverse Gaussian modes. Alternatively, one can view the PCM as compensating for the phase accumulated at frequency $\tilde{\omega}$ after each half of a round trip. The notion of this "supermode" fitting itself through any intracavity aperture (as mentioned earlier) easily follows from the above PCR arguments.

We next point out that this m = 0 longitudinal "mode" does not have any analog to conventional Fabry-Perot modes. This follows since, by equation (7.2-34), the m=0 mode always exists and is thus stable regardless of any cavity parameters (e.g., mirror radius or cavity length), corresponding to a frequency equal to that of the pump beam frequency. The "frequency-locking" feature of the PCR fields (for m = 0) to the pump waves follows directly from this fact.

Another property resulting from equation (7.2-34) is that the transverse modes (p,q pairs) belonging to higher order PCR longitudinal modes (i.e., $m \neq 0$) are no longer degenerate in frequency. Thus, the "mode-locking" property of the PCR holds only for m=0. This follows from the nonvanishing phases that are accumulated as a result of the frequency shift property of the PCM for different p and q (except, of course, for the "accidental degeneracy" of p,q pairs where p+q = constant).

We further note that due to the filter character of the PCM (i.e., the phase-matching requirement), higher order longitudinal modes will experience a smaller nonlinear reflection coefficient, thus decreasing

the cavity Q for these nondegenerate modes. Thus, even if $\ell > R$, which would allow higher order modes to exist [see equation (7.2-25)], the filter character will discriminate against their presence. The result is that these higher order modes ($m \neq 0$) are far less likely to oscillate. Hence, one expects essentially single frequency operation of the PCR (i.e., $m = 0$) given monochromatic pump waves.

In Figure 7.4, we plot the allowed longitudinal modes [i.e., the roots of equation (7.2-34)], along with the nonlinear reflection coefficient of the PCM for typical PCR conditions ($|\kappa| \sim \pi/4L$, $L = 40$ cm, $\ell = 25$ cm, $n_c = 1.0$, and $n = 1.62$). These quantities, which correspond to our measured experimental parameters (to be discussed in the next section), yield a (degenerate frequency) nonlinear reflection coefficient of $\sim 100\%$. There exist two longitudinal modes that satisfy equation (7.2-34) for each nonzero value of m. We also note that the modes are not uniformly spaced, and that the higher order longitudinal modes have reflectivities down by almost two orders of magnitude relative to that of the $m = 0$ mode. These higher order transverse modes (i.e., p,q pairs for $m = 0$), which are <u>not</u> degenerate in frequency, cannot be resolved in the figure due to their close spacing (of order $10^{-4}\ \Delta\nu_m$), while the higher order transverse modes (p,q pairs) corresponding to $m = 0$ are <u>all</u> degenerate.

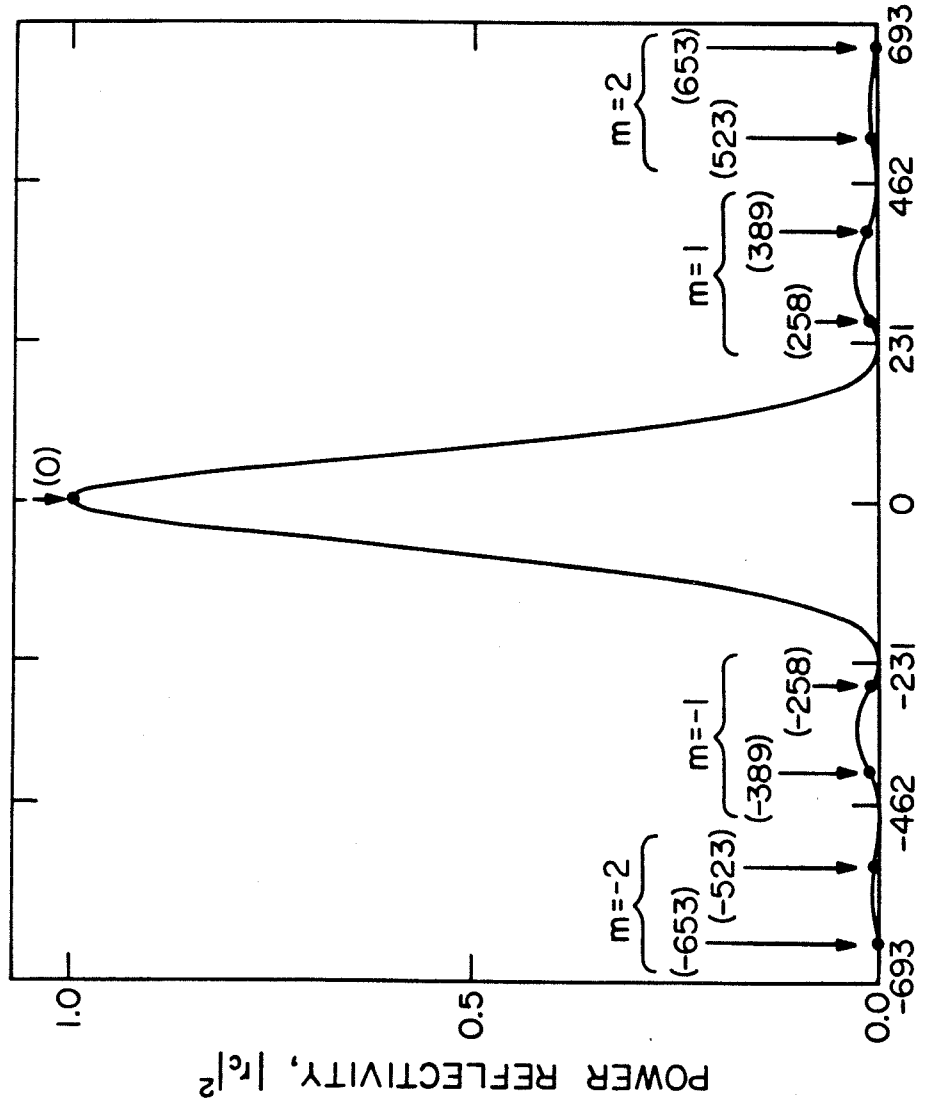

Fig. 7.4 PCR axial mode structure, indicated by arrows, and phase conjugating mirror (PCM) power reflectivity $|r_c|^2$ [after (6.2-6)] vs. $\Delta\nu$, for a value of $|\kappa|L = \pi/4$. $\Delta\nu = 0$ corresponds to the pump frequency of the PCM. Values in parentheses indicate the frequency offset relative to the pump frequency (in MHz) of several PCR modes [roots of eq. (7.2-34)]. The transverse mode spectra (which are degenerate for $m = 0$, and nondegenerate for $m \neq 0$) are unresolvable, and hence are not shown.

We now wish to investigate the relevance of the phase shifts introduced by the PCM upon the PCR mode spectra. Note that had we neglected any phase shifts due to the PCM, and neglected any transverse modal structure, the first and third terms of (7.2-34) would vanish, with the resultant free spectral range

$$\Delta\nu_m \to \frac{mc}{4n_c\ell} \tag{7.2-35}$$

This makes physical sense by virtue of the fact that any ray within a PCR will retrace itself after <u>two</u> round trips. One can view this geometry as being equivalent to a conventional resonator having twice the length of the PCR. Thus, the mode spacing would be one-half that of a conventional resonator of length ℓ (recall that $\Delta\nu = c/2n_c\ell$ for conventional resonators); therefore, (7.2-35) follows. As we will show below, however, the PCM phase shifts can have profound effects upon the PCR mode spacing.

Upon substitution of the cavity parameters used in the plot shown in Figure 7.4 into (7.2-35), a set of longitudinal modes having equal spacing of 300 MHz results (of course with no constraint upon the center frequency corresponding to the pump wave frequency). We see that these values do not coincide with those obtained from the numerical solution of (7.2-34).

For the next level of approximation for the mode spectra, we will approximate the PCM phase shift in the linear regime and for the case of small nonlinear gains. Recall that these approximations were also used in estimating the phase shifts and delay times for pulses reflected

from a PCM (see Section 6.3).

Applying these approximations to (7.2-34), we obtain the following longitudinal mode spectra

$$\Delta\nu_m \rightarrow \frac{mc}{2nL + 4n_c\ell} \tag{7.2-36}$$

where we have again neglected the transverse modal structure. Substitution of the same parameters used above into (7.2-36) yields a set of longitudinal modes having an equal spacing of 130.5 MHz. If we assume that the m = 0 mode coincides at the pump wave frequency, we obtain the following mode set: (0, 130.5, 261, 391.5, 522, 652.5, ... MHz), as compared with the mode set (0, 258, 389, 523, 653 ... MHz) as seen from Figure 7.4. We see that except for the absence of the first "approximate" mode, the other modes from (7.2-36) are in close agreement with those calculated numerically from (7.2-34). We therefore see that the phase shifts introduced by the PCM have profound effects upon the PCR longitudinal mode structure. We note that the expression (7.2-36) applies to the mode spectrum of a resonator having a length of 2ℓ+L. Thus, applying the concept of the PCR to replicate a ray after two round trips plus considering a round trip through the PCM at once leads to (7.2-36). We remark that from (7.2-36) the propagation time through the PCM, given by nL/c, is consistent with the pulse "reflection" PCM delay time given in Section 6.3.

7.3 Experimental Demonstration of a Phase Conjugate Resonator

A. Description

A sketch of the experiment designed to check some of the theoretical results is shown in Figure 7.5. It consists of a "resonator" (of length ℓ = 25 cm) containing a ruby gain medium (of length ℓ' = 5.08 cm), bounded on one end by a "real" mirror, M_R, and on the other end by a "phase conjugate mirror," PCM, (of length L = 40 cm) employing CS_2 as the nonlinear medium. Three different real mirror configurations were used in order to examine various aspects of the PCR, which will be discussed below. In order to obtain the largest PCM nonlinear reflection coefficient, the PCM interaction length (L) was maximized using a colinear pump signal scheme similar to that considered in Section 4.2; polarization discrimination was used to separate the PCR fields from the pump waves. The pump waves ($A_{1,2}$ in Figure 7.5) were derived from a separate, Q-switched ruby laser ($\sim$ 18 mj in 15 ns) operating in both a single transverse (TEM_{00}) and longitudinal mode. An optical delay path of $\sim$10 m separated the pump laser from the experimental apparatus, thus avoiding the retro-reflected pump wave (A_2) from interfering with the pump laser during the experimental measurements. The PCM was bounded by glan laser prisms to confine the PCR fields (s-polarized) within the CS_2, while passing the pump waves (π-polarized). The rear glan prism (P_3) coupled out s-polarized (PCR) fields which then passed through the ruby gain medium and reflected off M_R. The ruby gain medium within the PCR was aligned such that its c-axis was orthogonal to the s-polarized fields (thus maximizing the ruby gain coefficient for this polarization).

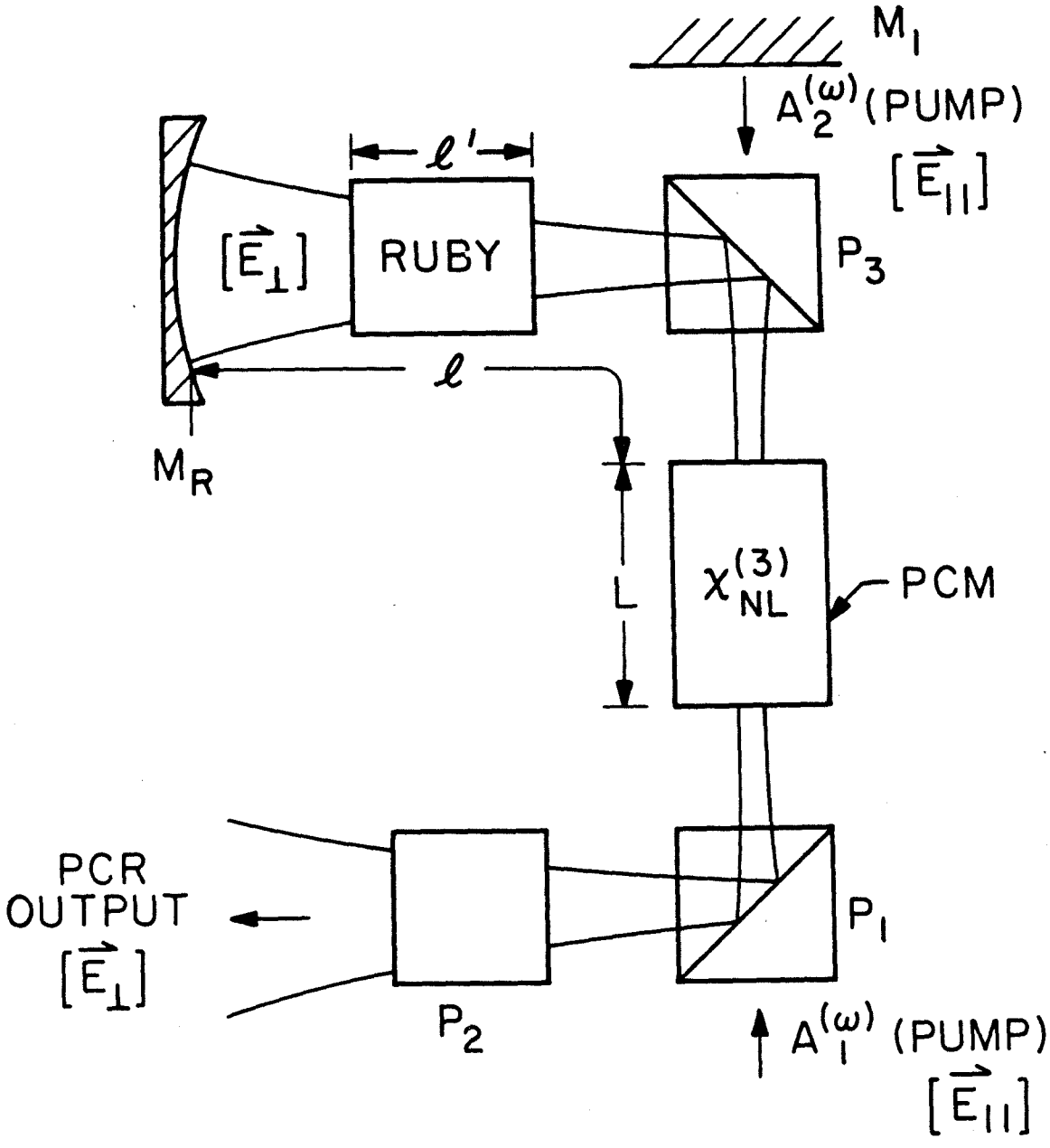

Fig. 7.5

Schematic diagram of the experimental PCR set-up. The counterpropagating pump beams, A_1 and A_2, can in principle be along any arbitrary direction relative to the PCR optic axis; in the experiment, a colinear geometry was chosen to maximize the interaction length.

The PCR output was monitored either from the PCM via the front glan prism (P_1) or from a partially transmitting mirror, M_R. This output field then passed through a third glan prism, which was used to eliminate any stray-reflected π-polarized fields. The total polarization rejection ratio for the PCR output calcite glan laser prisms (which were AR coated and wedged), P_1 and P_2, was measured to be $\sim 10^{-12}$, thus ruling out detection of stray π-polarized fields (e.g., the pump waves). When the flash-lamp pumping the gain medium within the PCR was properly synchronized with the PCM pump fields, an intense s-polarized pulse was detected. No output was observed when either (i) the counterpropagating pump beam, A_2, was blocked (or misaligned); or (ii) the rear mirror, M_R, was blocked (or misaligned). The latter test ruled out spurious effects such as self-oscillation within the PCM and regenerative amplification of depolarized or fluorescent fields; the former test ruled out ellipse rotation effects, and residual birefringence of both the optics and the CS_2 cell windows.

B. Resonator Stability

In the first experiment, the real mirror, M_R, (having a 2m radius of curvature and being totally reflecting) was inverted, thus forming an unstable resonator in the conventional sense. In this configuration we observed oscillation of the PCR (with the PCR output coupled out from the PCM, as discussed above). The nonlinear reflection coefficient of the PCM was measured (in a similar way as discussed in Section 4.2) to be $\sim$100% for this experiment. The PCR output energy was measured to be $\sim$0.72 mj. This value is quite reasonable, as will

be discussed below. This lends support to the theoretical result that due to the "time-reversing" nature of the PCM, the PCR should be stable regardless of the parameters of the real mirror or of the cavity length (at the degenerate frequency).

C. PCR Energy Output

In another experiment we compared the PCR output energy with that of an "equivalent" conventional Fabry-Perot laser. For this measurement the real mirror of the PCR was oriented to be concave with respect to the PCR fields, with the PCR output coupled out from the PCM end of the resonator. The nonlinear reflectivity of the PCM was again measured to be $\sim$100%. Under these conditions, the output energy was measured to be 1.62 mJ. This value correlates well with a measured value of 2 mJ obtained from the same gain medium when operated in a conventional laser resonator configuration, with the same (2m radius) real mirror as used above, output etalon (60% reflectivity), 1.0 mm intracavity Mendenhall aperture, and passive Q-switch (cryptocyanine in methanol). The effective aperture of the PCM results from the (transverse) spatial overlap of the (TEM_{00}) pump beams within the PCM, which had an intensity spot size measured to be 2.2 mm in diameter. In fact, when the pump laser oscillated in a higher order transverse mode, the PCR output was observed to have a similar transverse character. The greater output of the PCR using a concave, as opposed to a convex real mirror (i.e., 1.62 mJ vs. 0.72 mJ) is attributed to the fact that the former geometry sampled a greater mode volume within the ruby gain medium (as a result of the ef-

fective aperture of the PCM, due to the transverse Gaussian spatial distribution of the pump beams).

D. PCR Frequency Spectra

We mentioned in Section 7.2F that, for $\ell < R$ (which corresponds to our experimental parameters), higher order longitudinal modes do not exist. Hence, the PCR output should be frequency locked to the pump wave's frequency. (Recall that, even if $\ell > R$, the filter character of the PCM should also yield this frequency-locking property). In order to verify this conjecture, the frequency spectrum of the PCR output was measured with a Fabry Perot and compared with the pump-wave spectrum. Within the resolution of our Fabry-Perot ($\sim$ 150 MHz), both signals were degenerate in frequency, thus experimentally confirming the above claim. The PCR Fabry-Perot spectrum also yielded no additional spectral structure. Therefore, other nonlinear processes, such as stimualted Brillouin or Raman scattering were not present.

E. PCR Temporal Structure

We now investigate the temporal output of the PCR. Since the pump laser is operated on a pulsed basis (i.e., Q-switched), the conjugate mirror is only "on" during the temporal overlap of the pump waves. Hence, the PCM effectively Q-switches the PCR. The temporal output of the PCR is given in Figure 7.6a. The left pulse is that of the pump laser; the right pulse, delayed due to the 10 m delay path discussed earlier, is that of the PCR output (the amplitude of each of these pulses has been attenuated differently

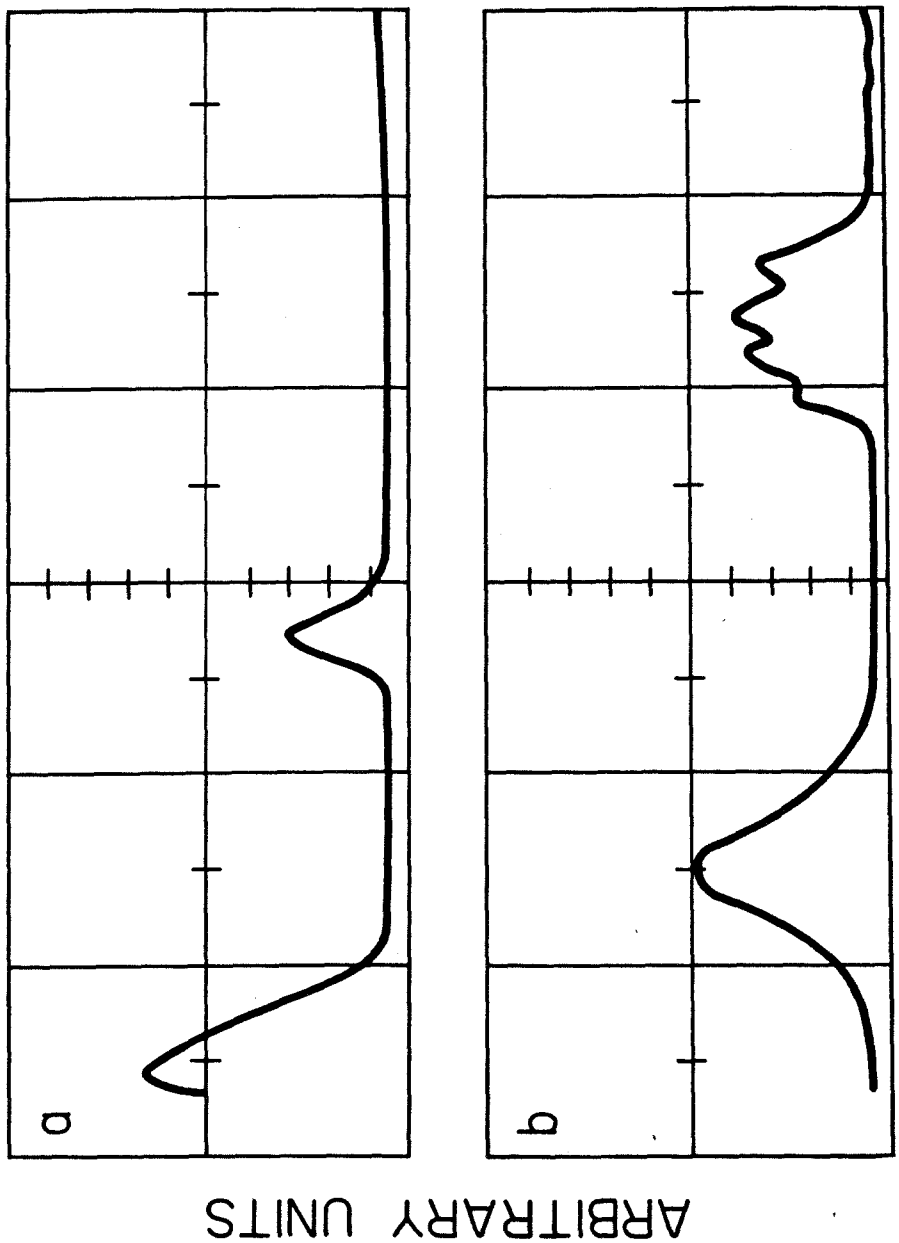

Fig. 7.6 Temporal evolution of the PCR output (right pulse in each trace) for a PCM power reflectivity of ∿25% (a), and ∿ 100% (b). Note for a large reflectivity (b), the PCR output is on for a longer time interval, and also exhibits a relaxation oscillation behavior. The left pulse in each trace is that of the pump laser output.

for visual purposes). For this measurement, the PCM reflection coefficient was measured to be ∿25%. Increasing the PCM reflectivity to ∿100% yields the results shown in Figure 7.6b. We note that the output pulse is on for a time longer than that corresponding to the former case. This follows from the fact that the temporal overlap of the pump beams within the PCM, which yields a time dependent PCM reflectivity, will satisfy the PCR oscillation condition for a longer time period than that of a PCR with a smaller nonlinear gain. (For several of these measurements, the PCR output was derived from the "real" mirror end of the PCR.)

We see that the large PCM reflectivity case yields a temporal structure upon the output (Figure 7.6b) which is not present in the former case (Figure 7.6a). We thus speculate that the temporal structure of the PCR output is attributable probably not to mode beating, but to a form of relaxation oscillation. (We note that the effect could also be due to a self-focusing phenomenon [7].) Recall that theory does not predict higher order modes for our experimental parameters (which may occur for larger PCM reflection coefficients). Pump depletion within the PCM due to interaction with the PCR circulating intensity, in conjunction with the temporal population density variation within the PCR's ruby gain medium, apparently gives rise to such oscillations. To verify this conjecture experimentally, the temporal evolution of the pump beam (A_1) was monitored after passage through the CS_2, and was seen to also exhibit temporal fluctuations which were not present when the counterpropagating pump beam of the PCM (A_2) was misaligned, thus preventing the PCR from oscillating.

F. Conclusions

We note that several (independent) reports [2,3] in the literature have recently considered the properties of the PCR from a Fox and Li [8] type approach, where a numerical solution to a scalar diffraction formulation of the problem is discussed. In the analysis presented in Section 7.2, we recall that a paraxial (or ray) approximation was utilized which implicitly assumed that diffraction losses (due to finite apertures, optical elements, etc.) were negligible; this implies essentially infinite resonator Fresnel [1] numbers (i.e., $F \equiv a^2/\lambda\ell \to \infty$, where a and ℓ correspond to the mirror radius and cavity length, respectively). We also note that distributed feedback effects in parametric interactions have been treated [5]. Finally, the consideration of Gaussian apertures and quadratic gain media has been discussed recently [4]. In Appendix 7B, we describe briefly the modifications necessary for the ABCD matrices (as derived in Section 7.2) when considering spatially-dependent, Gaussian distributed pump beams.

In conclusion, we have analyzed the stability criterion, longitudinal and transverse mode structure, and have demonstrated stable laser action in a novel resonator bounded by a nonlinear phase conjugating "reflective" element. The concept of frequency and spatial mode-locking of the transverse modes was discussed, which, among other features, should enable one to fully extract the stored energy within a gain medium or equivalently "fit" a mode volume through an arbitrary intracavity aperture. Several interesting properties of this device, such as the spatial, temporal, and spectral output, were shown to be consistent with those expected from such an interaction. An unstable

resonator configuration in the usual sense was seen to exhibit stability and a substantial output energy. Also, time-dependent saturation effects of the PCM have been observed. Finally, the PCR output energy was measured and shown to be comparable with that of a conventional resonator.

The use of a phase conjugate mirror, in addition to the above-mentioned aspects, has the property of correcting for both static and dynamic phase and polarization distortions or aberrations within the resonator. Hence by coupling the PCR output from the real mirror end of the cavity, or by using a two-PCM resonator, one can thus increase the efficiency of and therefore decrease the stringent requirements for the optical components comprising the cavity.

APPENDIX 7A

Derivation of the Matrix Relationship $\underset{\approx}{M}''\underset{\approx}{M} = \underset{\approx}{M}(\underset{\approx}{M}')^{-1}$

In this appendix, we shall prove that equation (7.2-10c)

$$\underset{\approx}{M}''\underset{\approx}{M} = \underset{\approx}{M}(\underset{\approx}{M}')^{-1} \tag{7.A-1}$$

is valid, and thus demonstrate that a sequence of lossless, passive optical elements followed by a PCM is equivalent to just the PCM alone. This fact makes sense on physical grounds due to the time-reversal nature of the PCM coupled with the reciprocity aspects of an arbitrary sequence of optical elements.

We start by forming the resultant ray vector $\vec{r}_2$ (a two-element column vector containing the position r_2 and slope r_2' of a given ray) as a result of the propagation of a ray $\vec{r}_1$ from the left to the right through a sequence of optical element(s) described by a ray matrix product, $\underset{\approx}{M}'$:

$$\begin{pmatrix} r_2 \\ r_2' \end{pmatrix} = \underset{\approx}{M}' \begin{pmatrix} r_1 \\ r_1' \end{pmatrix} \tag{7.A-2}$$

Now, due to the reciprocity nature of typical optical elements, we expect that if we merely "reverse" the output ray (given by changing $r_2' \rightarrow -r_2'$) and propagate this ray back through the same sequence of optical elements, from right to left (given by the ray matrix product, $\underset{\approx}{M}''$), we should obtain the same input ray vector ($\vec{r}_1$) except that its slope is now opposite to its initial slope (due to its reversed direction of propagation).

We therefore demand that

$$\begin{pmatrix} r_1 \\ -r_1' \end{pmatrix} = \underset{\approx}{M''} \begin{pmatrix} r_2 \\ r_2' \end{pmatrix} \tag{7.A-3}$$

Now, premultiplying each side of (7.A-3) by the matrix $\underset{\approx}{M}$ given by equation (7.2-7) , we get

$$\begin{pmatrix} 1 & 0 \\ 0 & -1 \end{pmatrix} \begin{pmatrix} r_1 \\ -r_1' \end{pmatrix} = \begin{pmatrix} 1 & 0 \\ 0 & -1 \end{pmatrix} \underset{\approx}{M''} \begin{pmatrix} r_2 \\ -r_2' \end{pmatrix} \tag{7.A-4}$$

The lefthand side is seen to be equal to $\begin{pmatrix} r_1 \\ r_1' \end{pmatrix}$. We premultiply each side of (7.A-4) by $\underset{\approx}{M}(\underset{\approx}{M''})^{-1}\underset{\approx}{M}$ and obtain

$$\underset{\approx}{M}(\underset{\approx}{M''})^{-1}\underset{\approx}{M} \begin{pmatrix} r_1 \\ r_1' \end{pmatrix} = \underset{\approx}{M}(\underset{\approx}{M''})^{-1} \underset{\approx}{M}\,\underset{\approx}{M}\,\underset{\approx}{M''} \begin{pmatrix} r_2 \\ -r_2' \end{pmatrix} \tag{7.A-5}$$

Since the matrix $\underset{\approx}{M}$ is self-inverse(i.e., $\underset{\approx}{M} = \underset{\approx}{M}^{-1}$; or $\underset{\approx}{M}\underset{\approx}{M} = I$, where I is the identity matrix) we get

$$M(M'')^{-1}M \begin{pmatrix} r_1 \\ r_1' \end{pmatrix} = M(M'')^{-1} M'' \begin{pmatrix} r_2 \\ -r_2' \end{pmatrix} = \begin{pmatrix} r_2 \\ r_2' \end{pmatrix} \tag{7.A-6}$$

where we have used the fact that $\underset{\approx}{M}\begin{pmatrix} r_i \\ \\ -r_i' \end{pmatrix} = \begin{pmatrix} r_i \\ \\ r_i' \end{pmatrix}$

for i = 1,2 and that $(\underset{\approx}{M}'')^{-1}\ \underset{\approx}{M}'' = I$. Substituting equation (7.A-2) for the right side of equation (7.A-6), results in

$$\underset{\approx}{M}(\underset{\approx}{M}'')^{-1}\underset{\approx}{M}\begin{pmatrix} r_1 \\ \\ r_1' \end{pmatrix} = \underset{\approx}{M}'\begin{pmatrix} r_1 \\ \\ r_1' \end{pmatrix} \tag{7.A-7}$$

Since equation (7.A-7) holds for any arbitrary $\vec{r}_1$, we have

$$(\underset{\approx}{M}'')^{-1}\ \underset{\approx}{M} = \underset{\approx}{M}\ \underset{\approx}{M}' \tag{7.A-8}$$

or equivalently

$$\underset{\approx}{M} = \underset{\approx}{M}''\ \underset{\approx}{M}\ \underset{\approx}{M}' \quad . \tag{7.A-9}$$

Therefore, from equation (7.A-9) we see that any arbitrary sequence of optical elements described collectively by $\underset{\approx}{M}'$ (for propagation from left to right) followed by a PCM (described by $\underset{\approx}{M}$) yields, upon subsequent propagation back through the same train of optical elements described collectively by $\underset{\approx}{M}''$ (for propagation from right to left), the matrix that describes the PCM itself (i.e., the matrix $\underset{\approx}{M}$).

APPENDIX 7B

PCM RAY MATRIX ASSUMING SPATIALLY-DEPENDENT GAUSSIAN PUMP BEAMS

In this section, we discuss the necessary modifications for the PCM ray matrix when we assume spatially-dependent Gaussian pump beams. We expect any spatial dependence of the pump wave amplitudes to be manifested in a corresponding PCM spatially-dependent reflectivity. Recall that the previous discussions assumed that the pump beams were infinite plane waves. This is a reasonable approximation when the spatial extent of the pump beams is large compared to other transverse dimensions present in a given PCR geometry. In the following analysis, we extend the treatment by Yariv and Yeh [9] of Gaussian tapered real mirrors for conventional resonators to that of a Gaussian tapered PCM as applied to a PCR. For simplicity, we consider the degenerate case (i.e., all interacting fields to be of the same radian frequency), and a colinear pump/probe geometry.

We begin our discussion by assuming that the small nonlinear gain approximation holds. That is, the reflection coefficient behaves as

$$\tan(|\kappa|L) \approx |\kappa|L \quad . \tag{7.B-1}$$

Therefore, the nonlinearly reflected field (at z=0) becomes,

$$A_3 \propto \chi^{(3)} L\, A_1\, A_2\, A_4^* \tag{7.B-2}$$

We assume that the pump waves have a Gaussian dependent

spatial distribution, given by

$$A_{1,2}(r) = A_{1,2}(0)\exp(-r^2/b^2) \tag{7.B-3}$$

where b is the (field) spot size.

Assuming that the input signal wave is of the form given by (7.2-1), we obtain using (7.B-3) the following conjugate wave

$$A_3 \propto [A_1(0)\exp(-r^2/b^2)]\,[A_2(0)\exp(-r^2/b^2)]$$

$$\times A_4^* \exp\left[i\left(\omega t + kz + \frac{kr^2}{2\rho_i}\right) - \frac{r^2}{w_i^2}\right] \tag{7.B-4}$$

In what follows, we assume that the curvatures of the pump waves are such that the fields are phase matched for all spatial modes. We further neglect "cross coupling" of these spatial modes (as discussed in Section 3.7B).

Using the definition of the complex radius of curvature given by (7.2-3) , the corresponding reflected (output) complex curvature can be written as

$$\frac{1}{q_r} = \frac{-1}{\rho_i} - \frac{i\lambda}{\pi}\left(\frac{1}{w^2} + \frac{2}{b^2}\right) = \frac{-1}{q_i^*} - \frac{i\lambda}{\pi a^2} \quad , \tag{7.B-5}$$

where

$$a^2 = b^2/2.$$

The "reflected" field thus has its radius of curvature reversed (i.e., the phase fronts are conjugated), with the reflected spot size decreased. The reflected q-parameters are given from (7.B-5) as

$$\rho_r = -\rho_i \qquad (7.B\text{-}6)$$

and

$$w_r = \frac{aw_i}{\sqrt{w_i^2 + a^2}} < w_i \quad \text{(positively-tapered PCM)} \qquad (7.B\text{-}7a)$$

We define a positively-tapered PCM as being a conjugator formed by pump waves having a Gaussian taper of the form (7.B-3); that is, $A_{1,2}$ are maximum for r=0.

From (7.B-7) we see that $w_r < w_i$, implying that the conjugate wave will diverge at a greater rate than that reflected off a non-tapered PCM.

We note that for a negatively-tapered PCM (i.e., where the pump beam's amplitude increases radially with a Gaussian dependence), the "reflected" spot size can be greater than the incident beam waist as follows

$$w_r^2 = \frac{a^2 w_i^2}{a^2 - w_i^2} \qquad \text{(negatively-tapered PCM)} \qquad (7.B\text{-}7b)$$

The reflected curvature is the same as that of the previous case (7.B-6). This results in a reflected field of smaller divergence than that of a

nontapered PCM for $0 < w_i/a < 1$. The output beam has a negative taper for $w_i/a > 1$, and is undefined for $w_i/a = 1$.

From the transformation relating the input and output q-parameters for conjugate mirrors in terms of the ray matrix elements [given by equation (7.2-8)], we can represent (7.B-5) by the ABCD matrix

$$\underset{\approx}{M} = \begin{pmatrix} A & B \\ C & D \end{pmatrix} = \begin{pmatrix} 1 & 0 \\ \dfrac{-i\lambda}{\pi a^2} & -1 \end{pmatrix} \tag{7.B-8}$$

Equation (7.B-8) reduces correctly to the nontapered PCM matrix (7.2-7) in the limit of $a \to \infty$.

This matrix can now be applied to evaluating the PCR stability and mode spectra as was discussed in Section 7.2. Without actually deriving these results, we wish to point out several basic differences in the analysis. First, since the PCM matrix has a complex element, the matrix identity given in (7.2-10c) no longer holds; that is, a sequence of lossless optical elements followed by a Gaussian tapered PCM and then followed by the same (reversed) sequence of elements no longer can be replaced by the PCM matrix itself due to its tapered function. Physically this is due to the fact that the tapered nature of the PCM changes the spot size of the "reflected" field, thus not strictly generating a time-reversed replica even for the degenerate frequency case considered here. This results in a resonator mode having a different spatial profile for left-to-right as compared to right-to-left propagation. Yariv and Yeh obtained similar results for Gaussian tapered, real-mirror resonators [9]. Next, by virtue of

the complex element in the PCM matrix, care must be taken when evaluating a resultant q-parameter after a given sequency of optical elements [recall the discussion regarding equation (7.2-9)].

The effect of the Gaussian tapered PCM also results in a different self-consistency constraint. For example, the generalization of the condition given in (7.2-11) becomes, for complex matrix elements

$$\frac{1}{q_R}(A_R - D_R) - \frac{1}{q_I}(A_I + D_I) + \frac{1}{|q|^2} B_R - C_R = 0 \qquad (7.B\text{-}9a)$$

and

$$\frac{1}{q_R}(A_I - D_I) + \frac{1}{q_I}(A_R + D_R) + \frac{1}{|q|^2} B_I - C_I = 0 \qquad (7.B\text{-}9b)$$

where q_R and q_I are the real and imaginary parts of the complex radius of curvatures as defined in (7.2-3); the real and imaginary parts of the ABCD one-round trip, resultant matrix elements are denoted by the subscripts R and I, respectively. Equations (7.B-9) reduce properly to the conditions of (7.2-12) in the limit of the ABCD elements being purely real.

As an example of the above formalism, we consider the case of a resonator of length ℓ, bounded by a real mirror of radius R on the left and by a Gaussian tapered PCM on the right. The radius of curvature at the immediate right of the real mirror, upon substitution of the resultant matrix in the conditions (7.B-9), is given by

$$\rho = \frac{-R\sqrt{h}\,[\sqrt{h} \pm g(\ell - R)]}{1 - Rg^2(R - 2\ell)} \qquad (7.B\text{-}10)$$

where $h = 1 + \ell^2 g^2$ and $g = \frac{-\lambda}{\pi a^2}(1 - \ell/R)$. The curvature alternates between two values, which is consistent with the qualitative features discussed above. We note that for the nontapered PCM condition, $g \to 0$ and $h \to 1$; hence $\rho \to -R$, in accordance with the results of Section 7.2B.

From the conditions (7.B-9) the spot size (at the immediate right of the real mirror) is given by

$$w = \frac{\lambda}{\pi a}\sqrt{\frac{\ell(1-\ell/R)}{\frac{1}{\rho} + \frac{1}{R}}} \qquad (7.B\text{-}11)$$

where the two values of ρ obtained from (7.B-8) are to be used in evaluating w with the condition that w be real. We see that for the nontapered case ($\rho \to -R$), w becomes undefined, also in accordance with the results of Section 7.2B.

We note that the small nonlinear gain approximation given by (7.B-1) which led to the analytical expressions and results presented in this appendix need not hold in general in order to obtain physical results. This follows from the fact that for high nonlinear gains [and for the negatively-tapered pump waves given in (7.B-3)], the the approximation (7.B-1) becomes valid for radial distances satisfying $r \gtrsim a$, due to the strong radial exponential dependence of

the pump waves. This results(in the high nonlinear gain, on-axis limit) in the formation of a tapered PCM having a more sharply peaked nonlinear reflection coefficient for $r < a$ than that given by (7.B-4), which rapidly approaches the Gaussian dependence of (7.B-4) as $r \gtrsim a$. Thus the qualitative argument presented here should apply to this case.

In conclusion, we have discussed the case of a PCM possessing a Gaussian tapered, radial dependent nonlinear reflectivity. The degenerate frequency case was treated for simplicity. We found that as a result of the taper, the conjugate reflected wave was seen to have a different spot size, and hence a differing diffractive character. The properties of this PCM were recast in the form of a complex ABCD matrix, and applied to analyze a typical phase conjugate resonator (PCR). Several profound features regarding the resultant PCR stability criterion and modal constraints were obtained that differed considerably from that of a PCR formed by a non-tapered PCM. We found that the freedom from arbitrary beam waist parameters was removed in the case of a PCR employing a tapered PCM. This result follows intuitively upon realization of the fact that the present resonator now has two specified constraints or boundary conditions (viz., the curvature of the real mirror and the tapering character of the PCM), thus uniquely defining the resultant mode (in terms of both the radius of curvature and the spot size throughout space). Further, the complex radius of curvature was seen to alternate between two values, due to the fact that the PCM modifies the spot size upon each nonlinear "reflection" (as a result of the

PCM tapering function). All the above results were seen to reduce properly to those of a PCR employing a nontapered PCM in the limit of $b \to 0$. We finally note that the stability criteria for both one- and two-round-trip conditions, as well as the longitudinal/transverse mode spectra (which involves the treatment of the nondegenerate frequency case) follows from the analysis described herein.

Chapter VII - References

1. See, for example, A. Yariv, Quantum Electronics, 2nd ed. (Wiley, New York, 1975); or A. E. Siegman, An Introduction to Lasers and Masers (McGraw-Hill, New York, 1971).

2. I. M. Bel'dyugin, M. G. Galushkin, and E. M. Zemskov, "Properties of resonators with wavefront-reversing mirrors," Kvant. Elektron. (Moscow) 6, 38 (1979) [Sov. J. Quant. Electron. 9, 20 (1979)].

3. J. F. Lam and W. P. Brown, "Optical resonators with phase conjugate mirrors," submitted to Opt. Lett.

4. P. A. Belanger, A. Hardy, and A. E. Siegman, "Resonate modes of optical cavities with phase-conjugate mirrors," submitted to Appl. Opt.

5. S. A. Akhmanov, G. A. Lyakhov, and N. V. Suyazov, "Distributed feedback in lasers due to parametric interaction: transient effects and nonlinear conditions," Kvant Elektron. (Moscow) 4, 556 (1977) [Sov. J. Quant. Eletron. 7, 308 (1977)].

6. A. Yariv, Introduction to Optical Electronics, 2nd ed. (Holt, Rinehart, and Winston, New York, 1976).

7. J. H. Marburger, "Self-focusing: Theory," Prog. Quant. Electron. 4, 35 (1975).

8. See, for example, the review by H. Kogelnik and T. Li, "Laser beams and resonators," Proc. IEEE 54, 1312 (1966), and references 4, 5, and 6, therein.

9. A. Yariv, and P. Yeh, "Confinement and stability in optical resonators employing mirrors with Gaussian reflectivity tapers," Opt. Commun. 13, 370 (1975).